# FTIR study of zeolites: the nature, concentration and accessibility of the acid sites

**Cátia Manuela Antunes da Silva Freitas**

Thesis submitted for the degree of Doctor of Philosophy

June 2020

Keele University

## Abstract

Zeolites represent one of the most important groups of industrial heterogeneous catalysts with large-scale applications in refining, petrochemistry and increasing potential in environmental catalysis and synthesis of fine chemicals. This broad range of catalytic applications comes from their unique set of acidic properties; it is therefore, vital to understand these properties.

The main aim of this doctoral thesis is the further study of the acidity properties of a variety of zeolite materials using *in situ* infrared spectroscopy (FTIR) in combination with different probe molecules. The focus of the work will be on the generation of accurate quantitative and qualitative analysis, and the development of new methodologies for the application of various probe molecules with different kinetic diameters and basicity. The approaches developed in this research expand upon the characterisation of the nature, number, accessibility and strength of acid sites in medium-, large- and mixed pore zeolites subject to different synthesis methods and post-synthesis modifications.

This work demonstrates the importance of cross-validation of data between characterisation techniques and significance of utilising different approaches to understand interactions between acid site and different probe molecules. This study also provides a detailed investigation on the textural, structural and acidity properties in different zeolite structures and relevant catalytic materials. The methodologies for the use of various probe molecules with FTIR presented offer a better understanding of the acid sites and their properties, in a great variety of zeolites and relevant catalytic materials.

**Acknowledgements**

I am most grateful to my supervisor, Dr Vladimir Zholobenko, for his guidance, patience and support (and chocolate) throughout these years of research and most importantly for creating this amazing opportunity and trusting me with his research ideas. I would also like to thank my industrial supervisor, Dr Edward Abram, for his advice and expertise, all the feedback (especially during final writing stage) and for the assistance and hospitality during my visits to Johnson Matthey.

I gratefully acknowledge Johnson Matthey PLC and Keele University (ACORN-2015 grant) for their support and funding provided for this work. My special thanks to all the people of the Johnson Matthey team involved in this project: Dr Gordon Kelly, Dr Rhys Lloyd, Dr Nathan Barrow, Rob Fletcher, Dr Alessandro Turrina, Dr Ming-Feng Hsieh, Dr John West, Dr Raquel García, Dr Steve Bailey and Dr John Casci, for their help, support, advice and assistance throughout my visits and meetings at the Johnson Matthey PLC sites. I also would like to thank all the colleagues from LCS Laboratories in Normandy University and Manchester University for the support on this work.

Moreover, I would love to express my appreciation to all people from the Birchall Centre, a special thanks to Martin, Aqeel, Isabel, Emma and Matt for their great friendship, help and support throughout this journey.

I am especially grateful to my mother and sister, who always believed in me and wanted the best for me. Thank you for encouraging me in all of my pursuits and inspiring me to follow my dreams giving me the strength needed to achieve my goals.

## Papers and presentations resulting from this Doctoral Thesis

C. Freitas, V. Zholobenko, E. Abram and G. Kell**y.** Acid sites in zeolites: their nature, concentration, strength and accessibility. Johnson Matthey Science Forum 2019 - Presentation.

C. Freitas, V. Zholobenko, E. Abram and G. Kelly. Acid sites in zeolites: their nature, concentration, strength and accessibility. Johnson Matthey Academic Conference (JMAC'18), 2018- Presentation.

**Chapter 2**

C. Freitas, V. Zholobenko, E. Abram and S. Bailey. *Molar absorption coefficients of Py-B and Py-L complexes in acidic zeolites: an FTIR study*. Johnson Matthey Academic Conference (JMAC'17), 2017- Poster presentation.

V. Zholobenko, C. Freitas, M. Jendrlin, P. Bazin, A. Travert and Frederic Thibault-Starzyk. *Probing the acid sites of zeolites with pyridine: quantitative AGIR measurements of the molar absorption coefficients.* J. Catal., 2020, 385, 52-60.

**Chapter 3**

C. Freitas, S. Ginnell and V. Zholobenko. *Stability of thermally treated zeolites Beta and ZSM-5.* 40$^{th}$ Annual Meeting of the British Zeolite Association (BZA meeting), 2017- Poster presentation.

**Chapter 4**

C. Freitas, N. S. Barrow and V. Zholobenko. *Accessibility and location of acid sites in zeolites as probed by Fourier transform infrared spectroscopy and magic angle spinning nuclear magnetic resonance.* Johnson Matthey Technol. Rev., 2018, 62, (3), 279-290.

C. Freitas, V. Zholobenko, E. Abram and G. Kelly. *FTIR study of Brønsted acid sites accessibility in zeolitic structures.* 41$^{st}$ Annual Meeting of the British Zeolite Association (BZA meeting), 2018 and 19$^{th}$ International Zeolite Conference (IZC'19), 2019 - Poster presentations.

A. Al-Ani, C. Freitas and V. Zholobenko. *Nanostructured large-pore zeolite: the enhanced accessibility of active sites and its effect on the catalytic performance*. Micropor. Mesopor. Mat., 2020, 293, 109805.

## Table of contents

## List of Figures

## List of tables

## Abbreviations

AGIR- Analysis by gravimetry and infrared

a.u.- Arbitrary units

BAS- Brønsted acid sites; Py-$H^+$

BEA- Zeolite beta

BET- Brunauer-Emmett-Teller

Coll-2,4,6-trimethylpyridine; Collidine

DTBPy-2,6-di-tert-butylpyridine

EDS- Energy-dispersive X-ray spectroscopy

EFAl- Extra-framework aluminium

FAl- Framework aluminium

FAU- Faujasite

FER- Zeolite ferrierite

FTIR- Fourier Transform Infrared Spectroscopy

IE- Ion exchange

IM- Impregnation

IR-Infrared spectroscopy

IZA- International Zeolite Association

LAS- Lewis acid sites; Py-L

LF- Low frequency peak

LTA- Zeolite linde type A

Lut- 2,6-dimethylpyridine; Lutidine

MAS- Magic angle spinning

MAZ- Zeolite mazzite

MOR- Zeolite mordenite

NMR- Nuclear Magnetic Resonance

Py- Pyridine

SEM- Scanning electron microscopy

TGA- Thermogravimetric analysis

TPD- Temperature-programmed desorption

XPS- X-ray photoelectron spectroscopy

XRD- X-ray diffraction

XRF- X-ray fluorescence

ZSM-5- Zeolite socony mobil-5

# Chapter 1 Literature Overview

## 1.1 Zeolites

### 1.1.1 From discovery to synthesis

Zeolites were discovered in cavities and vugs of basalts more than 250 years ago. The Swedish mineralogist Axel F Crønstedt was the first scientist to describe a distinctive property of these materials; upon heating in a blow-pipe flame, the mineral released a substantial amount of water, which it adsorbed again from the atmosphere on cooling without any noticeable change [1]. From this unique behaviour, it was given the designation of zeolite, by using the Greek words *Zeo* ("boiling") and *Lithos* (stone or rock) [2].

There are many naturally occurring zeolites, such as analcime, clinoptilolite, erionite, heulandite, laumontite and mordenite, which have valuable properties as sorbents and catalysts [3]. Such zeolites, however, often have faults and irregularities in their structures and do not meet the huge industry demands [4,5]. The development of synthetic zeolites made it possible to adjust their properties, such as pore size and chemical composition. The first synthetic zeolites (X, Y and A) started to be used in the industry as adsorbents, ionic-exchangers (laundry detergents) and, mainly, as heterogeneous catalysts [6,7]. Since then, the development of this field was mainly to formulate new materials (e.g. aluminophosphates, mesoporous materials) and to improve the characterisation techniques [8-10].

Having recognised the importance of optimising the size and shape of pores for catalytic applications, the number of synthetic zeolites has increased exponentially over the last decades. Up to 2018, the International Zeolite Association (IZA) had accepted more than 240 types of zeolitic structures [11]. Using electron diffraction, X-ray diffraction and specific software, numerous zeolites and related materials have been identified, by describing the connectivity of the tetrahedral units ($TO_4$). Each framework is identified by a three-letter mnemonic code, according to IZA [12], the three-letter code comes normally

from the name of the zeolite or "type of material", for example, FAU from the mineral faujasite, LTA from Linde Type A. The IZA association is responsible for listing different arrangements, regulating and assigning the classification of the different zeolite structures.

### 1.1.2 Definition and structure

Zeolites are crystalline solids with a well-defined microporous structure consisting of molecular scale pores and channels (0.3-2 nm). Their primary units $TO_4$ ($SiO_4$ or $AlO_4$) tetrahedra are linked by oxygen (O) atoms at their vertices (Figure 1.1). The angle formed by the T-O-T (inter-tetrahedrons) varies in a broad interval (130º-180º) [13], creating a variety of known zeolite structures [12,14]. The $AlO_4$ units in the zeolite impart a negative charge within the framework which is normally balanced by cationic species (e.g $H^+$, $Na^+$ or $K^+$).

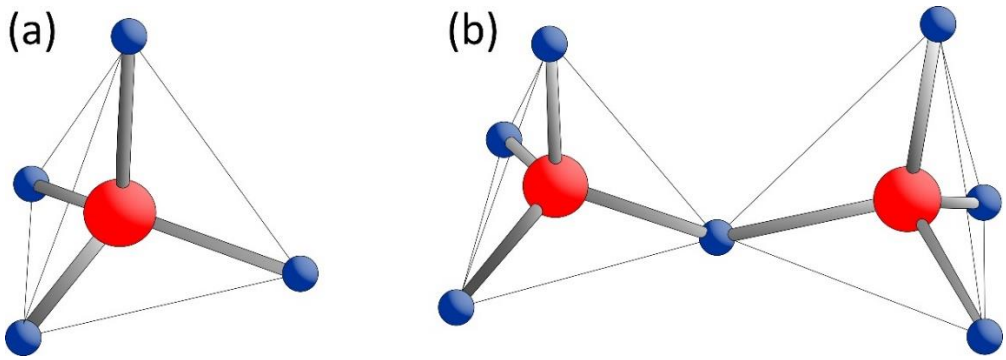


**Figure 1.1. (a)** $TO_4$ tetrahedron **(b)** $TO_4$ tetrahedra sharing a common O vertex.

The cations, along with water molecules, occupy the intra-crystalline space of the aluminosilicates. These cationic species are retained by steric effects and electrostatic interactions and can be exchanged with other cations, making zeolites highly valuable as cation-exchangers [5,15,16].

The typical chemical composition of the zeolite crystal framework has the following empirical formula (Equation 1.1):

$$(M^{m+})_{y/m}\,(SiO_2)_x \cdot\ (AlO_2^-)_y \cdot zH_2O \qquad \textbf{Equation 1.1}$$

Where *m* is the valence of the cation M, *x* and *y* are the total number of tetrahedra of Si and Al per unit cell respectively, *x/y* represents the atomic Si/Al ratio and *z* is the number of water molecules per cell unit [16].

The 'aluminium avoidance' rule (Löwenstein rule) states that whenever two tetrahedra are linked by an O bridge if the centre of one is occupied by an Al atom, the other must be occupied by Si atom [17]. This rule, therefore, prohibits –Al–O–Al– linkages from occurring within zeolites, restricting the minimum Si/Al ratio of any zeolite to unity. Conversely, recent investigations into zeolites synthesised at high temperatures have shown non-Löwenstein distributions in the various protonated zeolites [18].

Different zeolite structural types have been recognized by varying in size, shape and connectivity of their channels [14,19]. Due to this variation of the pore size, zeolites can be divided into three major groups (Figure 1.2): small-pore zeolites with 8 membered-ring pore apertures (e.g. zeolite FER), medium-pore zeolites with 10 membered-ring pore apertures (e.g. zeolites MFI or MEL) and large-pore zeolites with 12 membered-ring pore apertures (e.g. zeolite BEA or FAU) [19]. Recently, zeolites with extra-large pores (14- 16, 18-, 20-, 28-, and 30 membered-rings) were also synthesised [5,10]. For all the zeolite topologies, the primary arrangements of T atoms are the same and it is possible to build different zeolite topologies by assembling different geometric arrangements of $SiO_4$ and $AlO_4$ tetrahedra (Secondary Building Units, SBU).

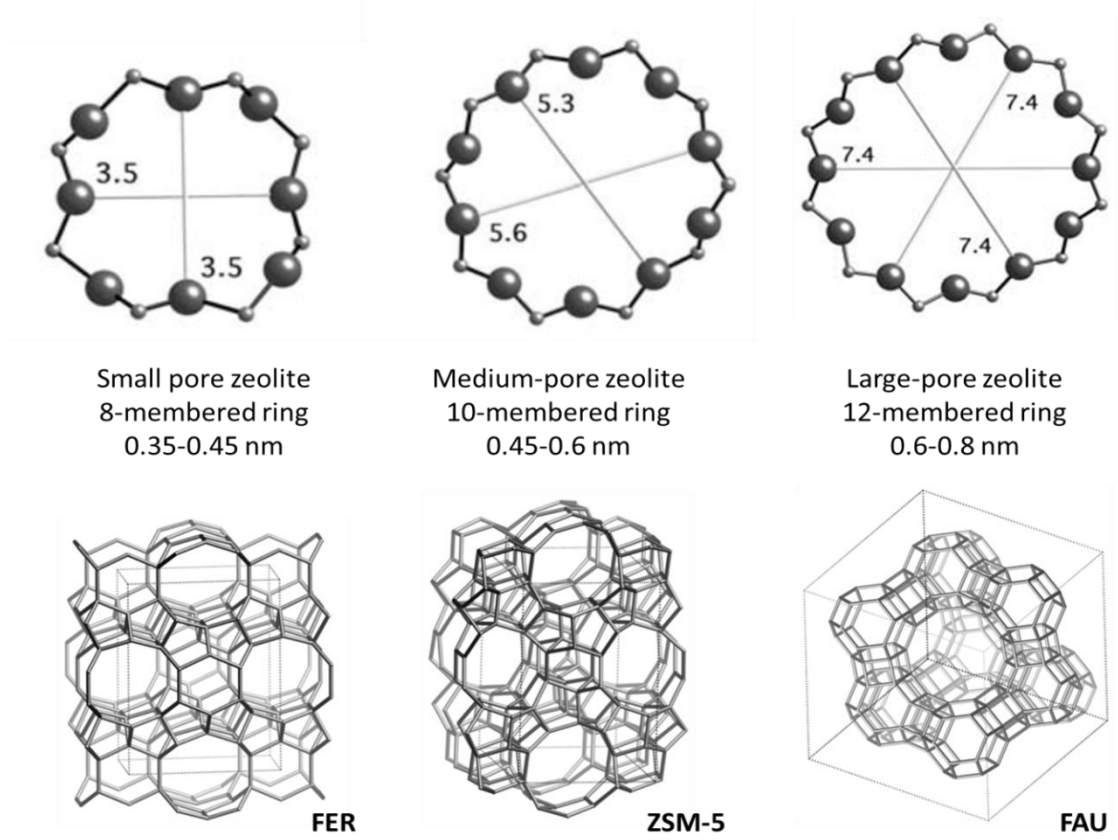


**Figure 1.2.** Classification of zeolites according to their membered-ring openings [12].

Medium- and large-pores zeolites are the most commonly used in a great number of catalytic reactions [6,20]. However, small-pore systems are particularly efficient in the conversion of methanol into olefins, due to the small size of the reactants and products [6,21-23]. Additionally, the development the extra-large microporous zeolites not only enrich the structural chemistry of these materials but also enlarged the potential applications of zeolites in catalysis and sorption–separation [10].

### 1.1.3 Properties and applications

Synthetic zeolites have been used for decades in adsorption and separation [24,25], ion exchange [26] and catalysis [7,6,14,20] with new emerging applications in microelectronics, medicine and sensor fabrication [27]. The success of these materials is the result of their unique set of properties such as high adsorption capacity, intrinsic acidity, hydrothermal stability and shape selectivity. Furthermore, they have a good cost/benefit ratio and allow clean and ecological processes. Their microporous framework can act as reaction channels

in which activity and selectivity are improved through the introduction of active sites. The existence of strong electric fields and controllable adsorption properties within the pores produce an exceptional characteristic for their use in catalysis and therefore they can be considered as catalytic micro-reactors [15].

Zeolites with their regular well-defined pore dimensions can discriminate reactants and products by size and shape when they present significant differences in diffusivity through a given pore channel system [15]. This shape-selective property is very important, as most of the active sites are located inside the intra-crystalline pore structure (where catalytic reactions mainly occur) [28], which constrains the formation of transition states, reaction intermediates and the diffusion of both reactants and products molecules. The size and shape of both molecules and zeolite pores influences the diffusion rate inside a zeolitic system [15]. For this reason, zeolites can permit or reject the entry of molecules into their pores, restrict the formation of some molecules within themselves or prevent their exit [15,29].

Another important parameter that applies a strong influence in zeolites is their chemical composition. These materials can be synthesised over a range of Si/Al ratios which directly affect properties such as maximum ion-exchange capacity, thermal and hydrothermal stability, hydrophobicity, concentration and strength of acid sites and the unit cell dimensions of a zeolite [16]. The ion-exchange capacity of a zeolite is related to its Al content, a lower Si/Al ratio (high in Al) results in a higher ion-exchange capacity [16]. A great deal of attention has been devoted to post-synthesis methods such as hydrothermal, acid leaching treatments and extraction or insertion of Al, able to change the framework Si/Al ratio [5,30-32]. However, many elements other than Si and Al can also be incorporated in the zeolitic structure; materials containing phosphorous, titanium, vanadium, iron and other transition metals in the framework have recently attracted interest as catalysts for selective oxidations [33-34].

The acidic nature of the zeolites has always been a major source of interest and is the key property for their successful applications; many processes in refinery, petrochemistry [20,35-38], fine chemicals [39,40] and environment protection [24,41] require a highly efficient solid acid catalyst. These applications are based on the nature, concentration, location, accessibility and strength of the acid sites. A detailed description of the acidic nature of zeolites will be addressed in Section 1.2.

The advances in zeolite catalyst technology have changed the nature of the refinery and petrochemical processes, requiring less separation, less energy, smaller reactors and simple process configurations.

## 1.2 Acidity characterisation of zeolite materials

Several experimental techniques, such as calorimetric measurements [42,43] temperature-programmed desorption (TPD) of basic molecules [43-45], $^{1}H$, $^{13}C$, and $^{27}Al$ solid-state nuclear magnetic resonance (NMR) [43,46-48], theoretical studies [45,49,50] infrared (IR) [43,51-54] and Raman vibrational spectroscopies [55-57] are employed to characterise the acidic behaviour of zeolites.

### 1.2.1 Infrared spectroscopy - basis concepts

The infrared (IR) corresponds to a specific variation of the electromagnetic spectrum (from 12000 to about 20 $cm^{-1}$), where its interaction with a specific molecule produces changes in their vibrational and rotational behaviour. This changes can provide information about molecular vibrations and can discriminate the different geometrical distortions of the molecules according to the adsorption state on a site [52].

Based on an approximation to the simple harmonic oscillator, each normal mode of vibration of a polyatomic molecule acts as an independent oscillator (without interaction). On the other hand, each normal mode of vibration has a fundamental characteristic, $\nu_j$:

$$\nu_j = \frac{1}{2\pi}\left(\frac{k}{\mu}\right)^{1/2} \qquad \textbf{Equation 1.2}$$

where $\nu_j$ is the frequency of vibration ($s^{-1}$), $k$ is the force constant ($Kg \cdot s^{-2}$) and $\mu$ is the reduced mass (Kg), this equation shows that the frequency is directly proportional to the force constant and indirectly proportional to the mass of the atoms involved in the vibration. The variation of μ is successfully used to identify functional groups [58,59].

An IR spectrum is displayed as a plot of the energy of the infrared radiation (usually expressed in wavenumbers) versus the percentage of light transmitted by the compound. The spectrum of the molecule appears as a series of broad absorption bands or peaks of variable intensity; each provides structural information. Each absorption band or peak in the spectrum corresponds to a vibrational transition within the molecule and gives a measure of the frequency at which the vibration occurs. However, for a particular vibrational mode to absorb infrared radiation, the vibrational motion associated with that mode must lead to a change in the dipole moment of the molecule.

IR spectroscopy is commonly divided into three groups: near-IR ($\nu$ > 3000 $cm^{-1}$), mid-IR ($\nu$ = 4000–400 $cm^{-1}$) and far-IR ($\nu$ < 300 $cm^{-1}$) [59]. For zeolite science, the mid-IR region provides information on OH groups, adsorbed molecules and framework vibrations. The integration and position of particular peaks and bands in the IR spectrum can estimate the acidity of zeolite materials in terms of type, concentration, location, accessibility and strength. Although the IR technique is versatile for those structures and surfaces, not all information can be obtained by direct spectral analysis and in many cases probe molecules with specific vibrational spectroscopic properties need to be used (Section 1.2.4).

Being a very sensitive technique, IR spectroscopy also allows the detection of impurities on the surface of zeolites, such as water, carbonates (formed by catalyst contact with ambient atmosphere), organics and other residual species after synthesis [52]. These impurities may inhibit the adsorption of probe molecules or interfere with data collection. It is therefore fundamental a thermal activation step in the removal of the molecules capable of perturbing the O-H stretching [52,53,60]. The preparation of zeolite samples as thin self-supported discs with a thickness of about 10 mg $cm^{-2}$ is usually required.

### 1.2.2 Hydroxyl groups

The direct evaluation of the wavenumber associated with the stretching vibration frequency of hydroxyl groups ν (OH), can identify different types of hydroxyl groups in the zeolitic material (Figure 1.3). These stretching vibrations can be observed in the region between 3800 and 3500 $cm^{-1}$ and are normally responsible for the existence of Brønsted acidity. At lower frequencies (> 3400 $cm^{-1}$) are typically detected hydroxyl groups originated by hydrogen bonding interactions.

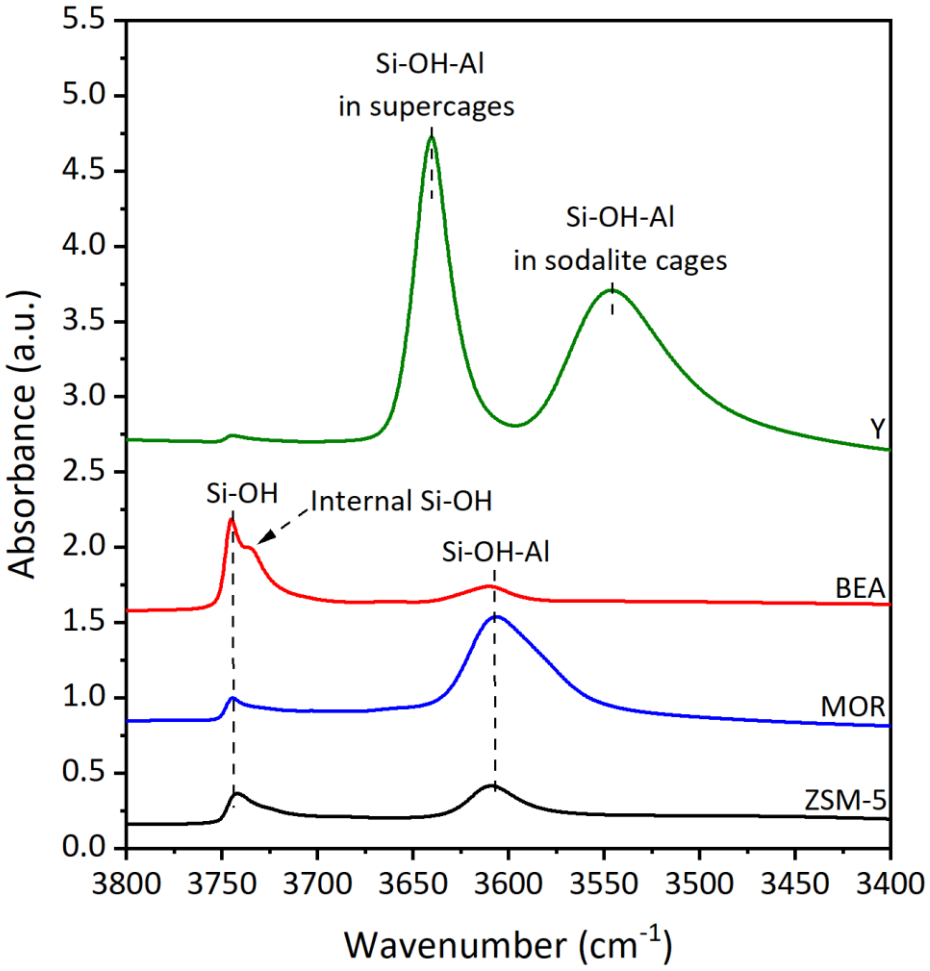


**Figure 1.3.** FTIR spectra the main hydroxyl groups of several activated zeolites.

At higher frequencies, zeolites exhibit two peaks at ~3745 $cm^{-1}$ and ~3735 $cm^{-1}$ corresponding to silanol groups (Si-OH) located on the external and internal surfaces, respectively (Figure 1.3) [60]. The intensity of the external silanols peak is strongly affected by the zeolite particle size; where small sizes are related to higher peak intensities (e.g BEA zeolite) [61].

In the frequency range of 3650-3600 $cm^{-1}$ it can be observed the region of bridging hydroxyl groups (Si-OH-Al) or also called framework aluminium (FAl). These Si-OH-Al groups are typically associated with the strong protonic acidity of the zeolite (Brønsted acid sites, BAS) and are formed by the bonding of a proton to a framework O atom connecting two tetrahedrally coordinated Si and Al atoms [44] (Figure 1.4). Any perturbation of the Si-OH-Al groups can lead to a peak shift to lower wavenumbers [60]. The structure type, framework Si/Al ratio, the nature of the trivalent ion, the location of the OH groups and the existence of extra-framework cations are some of the many factors that can influence the position of the Si-OH-Al peak [43,60,61].

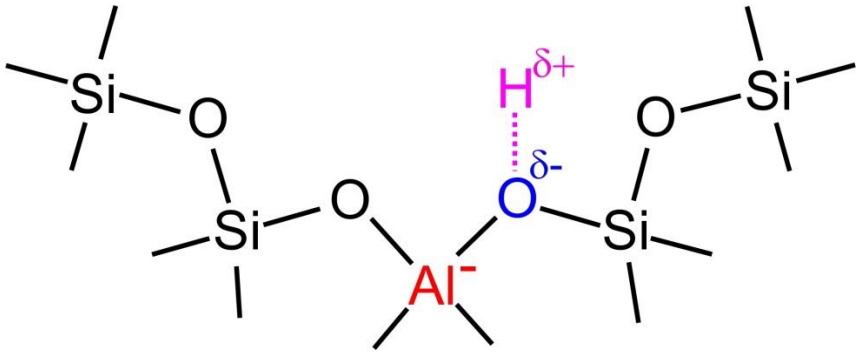


**Figure 1.4.** Bridging Si-OH-Al groups associated to Brønsted acidity.

Aluminium hydroxyls groups (Al-OH) are also observed in some zeolites; Al-OH not in framework positions is normally observed at 3670-3660 $cm^{-1}$ and ~3782 $cm^{-1}$ [60]. However, the appearance of these peaks depends on their structure, synthesis and treatment conditions [60].

The stretching vibrational frequency ν (OH), is normally related to the strength of the OH bond: the lower the stretching frequency, the weaker the OH bond and therefore the higher the acid strength. However, this simple approach cannot be applied to zeolites with different types of bridging Si-OH-Al groups. One good example is Y zeolite; this zeolite displays two different bridging Si-OH-Al groups: OH groups hosted in the supercages (at 3640 $cm^{-1}$) and OH groups located in the sodalite cages of zeolite Y (at 3545 $cm^{-1}$) (Figure 1.3). The bond between the hydrogen and the framework oxygen in the sodalite cage is

considered strong due to the small size of the cage, indicating that the acid strength of bridging OH groups in this zeolite cannot be measured by the frequency of the IR peak [44,53].

### 1.2.3 Brønsted and Lewis acid sites

Brønsted acid sites (BAS), the most important catalytic sites in acid catalysis, are related to Si-OH-Al groups being typically found inside the pores of the zeolite (Figure 1.2). The presence of these protons (and any extra-framework cations) is a consequence of the overall negative charge of $AlO_4$ tetrahedra [15,16]. It has been suggested that the maximum number of BAS equals the number of Al atoms in the framework (FAl). In reality, however, the number of BAS may be lower than the number of FAl species as a result of an incomplete exchange or dihydroxylation and dealumination phenomena [43].

Lewis acid sites (LAS), are electron-acceptor sites and the majority originate from extra-framework $Al^{3+}$ (EFAl), which are normally the result of dealumination caused by mild steaming or calcination, and Al structural defects caused by dihydroxylation of BAS as a consequence of dehydration of the structure at high temperatures [42,43]. These acid sites can also be created by the presence of charge-balancing extra-framework cations ($Na^+$, $Mg^{2+}$, $La^{2+}$, $Ca^{2+}$) and heteroatoms substituted at framework T positions [53]. LAS can become extremely important in catalytic reactions that involve redox steps [41,62,63]. Depending on the structure, synthesis and post-synthesis treatments, the surfaces of zeolites can exhibit BAS, LAS and also a combination of both.

### 1.2.4 Probe molecules in the determination of zeolite acidity

As discussed above IR spectroscopy deals with the direct vibrational mode of hydroxyl groups and BAS, but Lewis acidity can only be determined with the help of suitable probe molecules [64]. The adsorption of a base probe molecule allows the characterisation of the zeolite acidity; these molecules with particular properties (e.g. basicity, kinetic diameter) interact with acid sites present in these materials producing characteristic adsorption signals.

By considering the electronic or geometrical distortion of the probe molecule induced by adsorption, or the chemical modification, it is possible to gain information in terms of number, strength, type, accessibly and location of the acid sites [47]. To be an applicable probe, the molecule should accomplish several requirements, summarised in several review articles [43,52,53,60,64-66]:

(i) The probe molecule should be basic enough to interact with strong and weak acid sites.

(ii) The interaction should be selective to a particular type of acid site. The resulting spectrum should allow the discrimination of protonic and non-protonic sites (different types of acid sites).

(iii) The probe molecule should be sensitive to acidity strength. Acid-base interaction induces displacements in certain peaks which can be used to measure acid site strength.

(iv) The reactivity of the probe molecules in the experimental conditions should be low or none; not causing any chemical modification of the zeolite. Decomposing probes, however, can be used when the temperature and the mechanism of the decomposition are known and reveal additional and necessary information [43].

(v) The size of the probe molecule should be related to the accessibility of the acid sites. Small probe molecules are often used to allow access even to acid sites located in the narrow pores and channels (e.g. adsorption of $NH_3$ on MOR zeolites). Some bulky probes can also be utilised to characterise only acid sites located on the external surface of the zeolite (e.g. substituted pyridines).

However, no probe can be universally utilised and each interaction reveals a particular property of the zeolite acidity in terms of the probe under use. The variety of commonly used probe molecules (ammonia, acetonitrile, benzene, substituted benzenes, pyridine, substituted

pyridines, carbon monoxide and hydrogen) provides a large range of chemical reactivity and steric hindrance. Each probe molecule has different basicity, dimensions and limitations and therefore requires different experimental conditions.

Pyridine is considered a standard probe [45,51-53,60,67,68]; this molecule is thermally stable, with a kinetic diameter of 5.4 Å and interacts with the BAS forming pyridinium ions (Py-$H^+$ complexes, i.e. protonated Py) and H-bonded complexes (strong and weak acidity, respectively) and LAS (Py-L complexes). The interaction produces characteristic adsorption signals allowing the discrimination between the different types of acid sites (Figure 1.5). Two peaks at ~1545 ($\nu_{19b}$) and 1637 ($\nu_{8a}$) $cm^{-1}$ due to pyridinium ions resulting from Py protonation on Brønsted acid sites two peaks assigned to Py coordinated to Lewis acid sites at ~1456 ($\nu_{19b}$) and 1622 ($\nu_{8a}$) $cm^{-1}$ and the signals of Py on Lewis and Brønsted acid sites at ~1491 ($\nu_{19a}$) $cm^{-1}$.

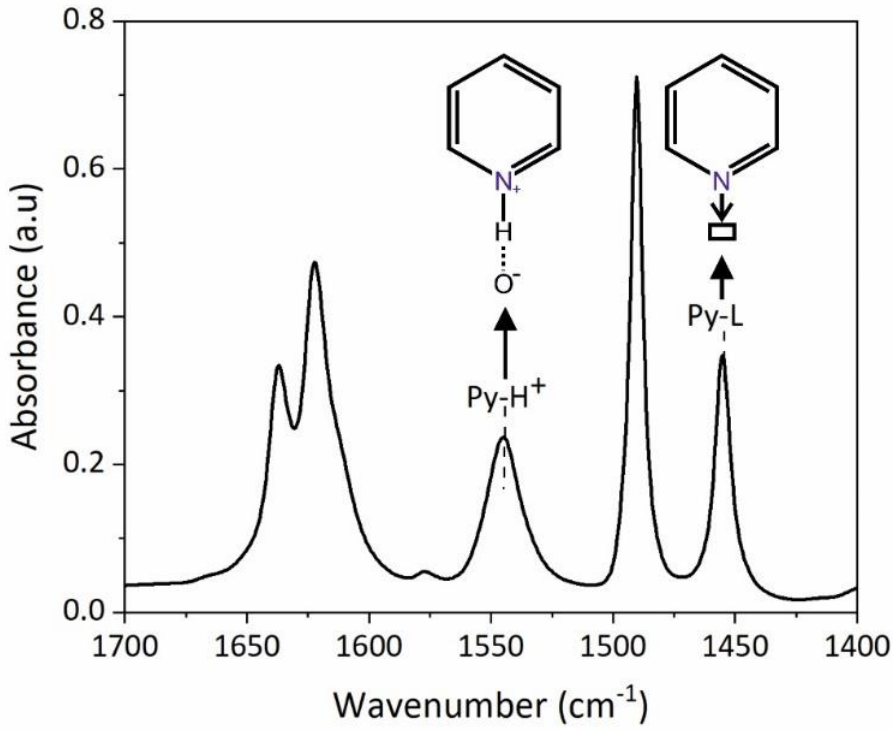


**Figure 1.5.** FTIR spectrum following Py adsorption at 150°C of zeolite BEA (12.5).

As a probe molecule, Py is normally used to obtain the overall number of acid sites existing in medium- (e.g. ZSM-5) and large-pore zeolites (e.g. BEA), while the kinetic diameter is too large to access all acid sites in small-pore zeolites. To achieve accurate results

using Py as a probe molecule, it is important to consider the experimental details, in particular weakly adsorbed species (physisorbed Py). The standard procedure is to adsorb the Py at 150°C at a vacuum pressure of $10^{-6}$ Torr to allow the diffusion of Py vapours into the pores and ensure that weakly adsorbed species are removed [60].

Bulky alkylpyridines such as, 2,6-di-tert-butylpyridine [69-72], 2,6-dimethylpyridine [69,73-76] and 2,4,6-trimethylpyridine [77-80] have been recently used for accessibility characterisation. These substituted pyridines allow the discrimination between acid sites located on the internal and external surfaces since they are too bulky to enter the internal pores and channels of most zeolite structures [81]. The location of acid sites and how easy it is to access them is important for the understanding of the relationship between acidity and catalytic performance [16,60].

The adsorption of weak bases is typically adopted to characterise the acid site strength of the hydroxyl group. Probe molecules such as carbon monoxide [51,82,83], hydrogen [84], benzene [85,86] or acetonitrile [87,88], form a H-bond with the acidic OH group resulting in a downward shift of the O-H stretching modes. The magnitude of the shift is a measure of the acid site strength and is proportional to the proton affinity of the surface groups [43,61]; since the larger the shift the stronger the interaction. The apparent strength of acid sites can also be obtained by desorbing Py at increasing temperatures, where the stronger sites retain the pyridine at higher temperatures.

## 1.3 Complementary characterisation techniques

Fundamental characterisation techniques are inevitable to study the zeolite properties and catalytic activity. The influence of structural, chemical, morphological and textural information in their applications makes characterisation essential to the understanding of these materials. In this work, a broad characterisation of the zeolite materials was also performed to obtain a better understanding of their properties and changes. The complementary techniques used were: powder X-ray diffraction (XRD), scanning electron

microscopy with an EDX analytical system (SEM-EDX), argon (Ar) physisorption, X-ray photoelectron spectroscopy (XPS), X-ray fluorescence (XRF) and aluminium ($^{27}$Al) and phosphorous ($^{31}$P) solid-state nuclear magnetic resonance ($^{27}$Al and $^{31}$P NMR).

***Powder X-ray diffraction (XRD)***

X-ray diffraction is based on constructive interference of monochromatic X-rays and crystalline material. The X-rays are generated by a cathode tube, filtered to produce monochromatic radiation, collimated to concentrate and directed toward the sample. The interaction of the incident X-rays with the material creates constructive interference (and a diffracted X-ray) when the conditions satisfy the Bragg's Law ($n\lambda=2d\sin\theta$). This law relates the wavelength of electromagnetic radiation to the diffraction angle and the lattice spacing in a crystalline material. The diffracted X-rays are then detected, processed and counted. By scanning the sample through a range of 2θ angles, all possible diffraction directions of the lattice are found due to the random orientation of the powdered material. Conversion of the diffraction peaks to d-spacings allows identification of the material because each material has a set of unique d-spacings. Typically, this is accomplished by comparison of d-spacings with standard reference patterns [89,90].

XRD allows the examination of the long-range atomic structure of crystalline zeolitic materials, this includes the framework topology and the positions of extra-framework cations and adsorbed molecules [91]. The XRD patterns of known zeolite structures are compiled in *Collection of Simulated XRD Patterns for zeolites* [92].

***Argon physisorption at 87 K***

Gas adsorption occurs whenever an adsorbable gas (adsorptive) is brought into contact whit the surface of the solid (adsorbent), calculating the amount of the adsorbate gas bound by relatively weak forces (Van der Waals forces) to a monomolecular layer on the surface [93,94]. The amount of gas adsorbed can be measured by volumetric or continuous flow procedure. For microporous materials, such as zeolites, argon (Ar) at 87 K seems to be the

adequate adsorbable gas, due to the absence of the quadrupole moment (in contrast to nitrogen) and the high temperature of the experiments. The cross-section area of Ar is less sensitive to differences in the structure of the microporous surfaces and at 87 K this molecule allows a straightforward correlation between the pore filling pressure and the confinement effect, which is particularly important in zeolitic materials [94].

The knowledge of the textural parameters (surface areas, pore volumes and sizes) obtained by this technique contributes to the understanding of the behaviour of a zeolite since the material surface can be determinant for an efficient distribution of catalytically active sites, while the type of porosity can affect the accessibility and the diffusion process of reactant and product molecules through the porous structure [95]. Parameters such as pore volume and pore-size distribution are also crucial for shape selectivity catalysts [95].

***Scanning electron microscopy (SEM)***

Scanning electron microscopy (SEM) is a method for determining the size and morphology of zeolites crystals, this method can obtain three-dimensional backscatter images of the surface of a wide variety of heterogeneous materials in a nanometre (nm) and micrometre (μM) range. During the analysis, an electron gun produces an electron beam that is focused into a fine spot as small as 1 nm in diameter on the sample surface. This beam is scanned in a rectangular raster over the specimen and the intensities of various signals created by interactions between the beam electrons and the specimen are measured and stored in computer memory. The stored values are then mapped as variations in brightness on the image display. The *secondary electron* (*SE*) signal is the most frequently used signal and it varies with the topography of the sample surface [96,97]. Because zeolites are not electrically conductive in the SEM, it is advantageous to disperse large aggregates into smaller fragments that can have better contact with a conductive surface.

***Energy-dispersive X-ray spectroscopy (EDS)***

Energy-dispersive X-ray spectroscopy (EDX) is an analytical technique were element-specific radiation is used for chemical characterisation of a material surface and it is normally coupled with SEM, transmission electron microscopy (TEM) and scanning transmission electron microscopy (STEM) [96]. When combined with SEM, provides elemental analysis on areas as small as nanometres in diameter.

This technique is based on the collection of X-rays generated as incident electrons impinge upon the sample [96]. When the interaction energy between the incident electron and an atom of the sample is high enough, an electron in the inner shell (lower energy shell) of the sample is ejected, creating a vacancy [96,98]. An electron from an outer shell (higher-energy shell) then fills this vacancy, and the difference in energy between the higher-energy shell and the lower energy shell is released in the form of an X-ray. The number and energy of the X-rays emitted from a sample are then measured by an energy-dispersive spectrometer [98].

***X-ray fluorescence (XRF)***

X-ray fluorescence spectrometry (XRF) is a relatively effective quantitative technique to determine the elemental composition of any material [89]. XRF is often used to verify the XRD data and vice versa. The sample is excited by a primary high-energy X-ray, emitting characteristic X-rays (so-called secondary X-rays or X-ray fluorescence) from the sample, with energy lower than the incident X-rays. These fluorescent X-rays are used to determine the elements, while the intensity of these rays is proportional to the abundance of the elements present in the sample [89]. This technique is used for routine and non-destructive bulk chemical analyses, however, it cannot distinguish between isotopes of an element and ions of the same element in different valence states.

***X-ray photoelectron spectroscopy (XPS)***

X-ray photoelectron spectroscopy (XPS) is a widely used surface analysis technique and is useful in the determination of the chemical composition and the oxidation state of the elements present in the solid materials. This technique works by exciting the sample with mono-energetic Al kα x-rays leading to the emission of photoelectron from the sample surface. An electron energy analyser is utilised to measure the energy of the emitted photoelectrons. From the binding energy and intensity of a photoelectron peak, it is possible to identify and quantify an element and their chemical state [89].

***Magic angle spinning nuclear magnetic resonance (MAS NMR)***

Solid-state NMR spectroscopy is largely used to obtain important information on the structural properties of solids and demonstrate high sensitivity for chemical bonds in the local structure of the resonating nuclei, such as of framework atoms, extra-framework species, surface sites, and adsorbate complexes in zeolites [42,43].

The most important technique for solid-state nuclear magnetic resonance is the magic angle spinning (MAS), as it averages the nuclear interactions in solids. This technique consists in quickly spinning the entire sample at a rotation of thousands of revolutions per second, to minimize the effects of the immobility of the molecules and the anisotropic interactions. This spinning is executed at an angle of 54.74° with the magnetic fields to withdraw the effect of the dipole-dipole interactions.

The understanding of zeolite acidity using MASNMR can be achieved by exploiting several magnetically active nuclei such as $^{29}$Si, $^{27}$Al, $^{1}$H, $^{17}$O, $^{15}$N, $^{31}$P. These analyses have become essential in the study of zeolite chemistry, giving distinctive information about the nature and concentration of acid sites. $^{29}$Si and $^{27}$Al enable the determination of the acid sites concentration, while the $^{1}$H, $^{17}$O, $^{15}$N, and $^{31}$P can give information on the acid strength of BAS [44,47]. For this purpose, zeolite samples dehydrated at elevated temperatures in vacuum are filled in gas-tight magic-angle spinning (MAS) rotors or sealed in glass inserts.

## 1.4 Objectives and thesis outline

The main focus of this PhD thesis is to further develop characterisation of zeolite based catalysts in terms of their acid-site type, accessibility, concentration and strength, by improving the use of *in situ* infrared spectroscopy (FTIR) in combination with different probe molecules. Particular emphasis is given to the development of efficient quantitative analysis and the expansion of methodologies using a diverse range of probe molecules with different basicity and kinetic diameters. In addition, this knowledge will be applied to characterise a great diversity of zeolite structures and important catalytic materials. An extensive characterisation of the zeolite materials was also carried out using a wide range of techniques such as XRD, SEM-EDX, Ar physisorption, $^{27}$Al solid-state NMR, $^{31}$P solid-state NMR, XPS and XRF. The insights gained in this research should improve future characterisation of acidity, help in the cross-validation of different characterisation techniques and obtain a better understanding of catalytic performances using zeolite based catalysts.

This thesis is organised into six chapters. This introductory chapter is Chapter 1 and the main results of this thesis are described in Chapters 2 to 6.

Accurate determination of molar adsorption coefficients for Py species adsorbed on Brønsted and Lewis acid sites in various zeolitic structures and the improvement of quantitative analysis by FTIR spectroscopy using Py as a probe molecule are described in Chapter 2. A study of the validity of the Beer-Lambert law for FTIR studies of zeolite materials is also included.

In Chapter 3 an investigation of the stability of thermally treated and cation-containing zeolites was carried out, to obtain information on their textural, structural and acidic properties. This study focuses on quantitative measurements of the different types of active sites in the two zeolitic structures (BEA and ZSM-5). A combination of different techniques is used to described the changes after the post-synthesis modifications and evaluate the stability of both structures.

An extensive FTIR investigation of accessibility and location of acid sites in medium- (ZSM-5), large- (BEA) and mixed-pore (MOR and MAZ) zeolites is presented in Chapter 4. The interaction between the zeolite Brønsted acid sites and different probe molecules are studied to optimise the experimental procedures for the application of a combination of probe molecules in FTIR spectroscopy.

Chapter 5 describes the acidic properties of two sets of P/H-ZSM-5 zeolites prepared by different methods. A detailed evaluation of the effects of the incorporation of phosphorous on the number, location and accessibility of the acid sites in ZSM-5 zeolite is examined.

Finally, Chapter 6 summarises and integrates the main conclusions withdrawn from this research project.

## 1.5 Reference

[1] A. F. Crønstedt., *Academies Handlingar Stockholm.*, 1756, 17, 120-123, translated into English. *On the unknown mineral-species called zeolites* in *Proceedings from the ninth international zeolite conference*., Butterworth-Heinemann, 1993, 3-9.

[2] C. Colella and A. F. Gualtieri. *Crønstedt's zeolite*. Micro Meso Mater., 2007, 105 (3), 213-221.

[3] E. Passaglia and R. A. Sheppard. *Crystal structures of natural zeolites* in *natural zeolites: Occurrence, properties, applications*. Eds: D. L. Bish and D. W. Ming. Walter de Gruyter GmbH & Co KG, 2018, 1-69.

[4] E. M. Flanigen. *Zeolites and molecular sieves. An historical perspective* in *Introduction to zeolite science and practice.* Eds: H. van Bekkum, E. M. Flanigen, P.A. Jacobs and J. C. Jansen. Elsevier, 2001, 11-37.

[5] R. Xu, W. Pang, J. Yu, Q. Huo, and J. Chen. *Structural chemistry of microporous materials* in *Chemistry of zeolites and related porous materials: synthesis and structure*. John Wiley & Sons, 2007, 345-383.

[6] G. Busca. *Zeolites and other structurally microporous solids* in *Heterogeneous catalytic materials: Solid-state chemistry, surface chemistry and catalytic behaviour*. Elsevier., 2014, 198-241.

[7] P. M. M. Blauwhoff, J. W. Gosselink, E. P. Kieffer, S. T. Sie and W. H. J. Stork. *Zeolites as catalysts in industrial processes* in *Catalysis and zeolites: Fundamentals and applications.* Eds: J. Weitkamp and L. Puppe. Springer, 2013, 437-538.

[8] C. S. Cundy and P. A. Cox. *The hydrothermal synthesis of zeolites: history and development from the earliest days to the present time.* Chem. Rev, 2003, 103 (3) 663-701.

[9] A. Taguchi and F. Schüth. *Ordered mesoporous materials in catalysis*. Microporous Mesoporous Mater., 2005, 77, 1-45.

[10] J. Li, A. Corma and J. Yu. *Synthesis of new zeolite structures*. Chem. Soc. Rev., 2015, 44, 7112-7127.

[11] E. Koohsaryan and M. Anbia. *Nanosized and hierarchical zeolites: A short review.* Chin. J. Cat., 2016, 37, 447-467.

[12] C. Baerlocher, L. B. McCusker and D. H. Olson. *Atlas of zeolite framework types*. 2007, Elsevier.

[13] T. Maesen, *The zeolite scene - An overview* in *Introduction to zeolite science and practice.* Eds: J. Čejka, H. van Bekkum, A. Corma and F. Schüt. Stud. Surf. Sci. Catal., 2007 168, 1-12.

[14] J. Čejka, G. Centi, J. Perez-Pariente and W. J Roth. *Zeolite-based materials for novel catalytic applications: Opportunities, perspectives and open problems.* Catal. Today., 2012, 179 (1), 2-15.

[15] A. Corma. *State of the art and future challenges of zeolites as catalysts*. J. Catal., 2003, 216 (1-2), 298-312.

[16] J. Weitkamp. *Zeolites and catalysis*. Solid State Ionics., 2000, 131 (1-2), 175-188.

[17] W. Löwenstein. *The distribution of aluminium in the tetrahedra of silicates and aluminates*. Am. Mineral., 1954, 39 (1-2), 92-96.

[18] R. E. Fletcher, S. Ling and B. Slater. *Violations of Löwenstein's rule in zeolites*. Chem. Sci., 2017, 8, 7483-7491.

[19] L. B. McCuster and C. Baerlocher. *Zeolite structures* in *Introduction to zeolite science and practice.* Eds: H. van Bekkum, E. M. Flanigen, P. A. Jacobs and J. C. Jansen. Elsevier. 2001, 37-69.

[20] M. Kubůa, R. Millini and N. Žilkováa. *10-ring zeolites: Synthesis, characterization and catalytic applications*. Catal. Today, 2019, 324, 3-14.

[21] E. V. Gallego, C. Li, C. Paris, N. Martín, J. Martinez-Triguero, M. Boronat, M. Moliner and A. Corma. *Making nanosized CHA zeolites with controlled Al distribution for optimizing methanol-to-olefin performance*. Chem. Eur. J., 2018, 24, 14631-14635.

[22] N. A. Khan, D. K. Yoo, B. N. Bhadra, J. W. Junb, T-W. Kim, C-U. Kim, S. H. Jhung. *Preparation of SSZ-13 zeolites from beta zeolite and their application in the conversion of ethylene to propylene.* Chem. Eng. J., 2019, 377, 119546.

[23] M. Dusselier and M. E. Davis. *Small-pore zeolites: synthesis and catalysis*. Chem. Rev., 2018, 118, 5265-5329.

[24] M. Tagliabuea, D. Farrusseng, S. Valencia, S. Aguado, U. Ravon, C, Rizzoa, A. Corma and C. Mirodatos. *Natural gas treating by selective adsorption: Material science and chemical engineering interplay.* Chem. Eng. Sci., 2009,155, 553-566.

[25] B. Sreenivasulu, P. Suresh, I. Sreedhar, and K. V. Raghavan. *Development trends in porous adsorbents for carbon capture.* Environ. Sci. Technol., 2015, 49, 12641-12661.

[26] S. Cinar and B. Beler-Bayka. *Ion exchange with natural zeolites: an alternative for water softening.?* Water. Sci. Technol., 2005, 51, 71-77.

[27] L. Bacakova, M. Vandrovcova, I. Kopova and I. Jirka. *Applications of zeolites in biotechnology and medicine - a review.* Biomater. Sci., 2018, 6, 974-989.

[28] C. R. Marcilly. *Where and how shape selectivity of molecular sieves operates in refining and petrochemistry catalytic processes*. Top. Catal., 2000, 13, 357-366.

[29] J. Kärger and D. M. Ruthven. *Diffusion in zeolites and other microporous solids.* Wiley, 1992, 1-605.

[30] H. K. Beyer. *Dealumination techniques for zeolites* in *Post-synthesis modification I. Molecular sieves*. Eds: H. G. Karge and J. Weitkamp. Springer, 2002, 204-248.

[31] M-C. Silaghi, C, Chizallet and P. Raybaud. *Challenges on molecular aspects of dealumination and desilication of zeolites.* Microporous Mesoporous Mater., 191, 2014, 82-96.

[32] G. Cruciani. *Zeolites upon heating: Factors governing their thermal stability and structural changes*. J. Phys. Chem. Solids., 67, 2006, 1973-1994.

[33] H. E. van der Bij and B. M. Weckhuysen. *Phosphorus promotion and poisoning in zeolite-based materials: synthesis, characterisation and catalysis*. Chem. Soc. Rev., 2015, 44, 7406-7428.

[34] M. H. Mahyuddin, Y. Shiota and K. Yoshizawa. *Methane selective oxidation to methanol by metal-exchanged zeolites: A review of active sites and their reactivity.* Catal. Sci. Technol.**,** 2019, 9, 1744-1768.

[35] E. T. C. Vogt and B. M. Weckhuysen. *Fluid catalytic cracking: recent developments on the grand old lady of zeolite catalysis.* Chem. Soc. Rev., 2015, 44, 7342-7370.

[36] A. Primo and H. Garcia. *Zeolites as catalysts in oil refining*. Chem. Soc. Rev., 2014, 43, 7548-7561.

[37] W. Vermeiren and J-P. Gilson. *Impact of zeolites on the petroleum and petrochemical industry.* Top. Catal., 2009, 52, 1131-1161.

[38] A. Feliczak-Guzik. *Hierarchical zeolites: Synthesis and catalytic properties.* Microporous Mesoporous Mater., 2018, 259, 33-45.

[39] D. E. de Vos and P. A. Jacobs. *Zeolite effects in liquid phase organic transformations.* Microporous Mesoporous Mater., 2005, 82, 293-304.

[40] M. J. Climent, A. Corma and S. Iborra. *Heterogeneous catalysts for the one-pot synthesis of chemicals and fine chemicals.* Chem. Rev. 2011, 111, 1072-1133.

[41] R. Zhang, N. Liu, Z. Lei and B. Chen. *Selective transformation of various nitrogen-containing exhaust gases toward $N_2$ over zeolite catalysts*. Chem. Rev., 2016, 116, 3658-3721.

[42] E. G. Derouane, J. C. Védrine, R. R. Pinto, P. M. Borges, L. Costa, M. Lemos, F. Lemos and F. R. Ribeiro. *The acidity of zeolites: Concepts, measurements and relation to catalysis: A review on experimental and theoretical methods for the study of zeolite acidity.* Cat. Rev., 2013, 55 (4), 454-515.

[43] L-E. Sandoval-Díaz, J-A. González-Amaya, C-A. Trujillo. *General aspects of zeolite acidity characterisation*. Microporous Mesoporous Mater., 2015, 215, 229-243.

[44] M. Boronat and A. Corma. *Factors controlling the acidity of zeolites.* Catal. Lett., 2015, 145, 162-172.

[45] M. Niwa, N. Katada and K. Okumura. *Characterization and design of zeolite catalysts: solid acidity, shape selectivity and loading properties.* Springer, 2010, 1-184.

[46] A. Zheng, S-B. Liu and F. Deng. *Acidity characterization of heterogeneous catalysts by solid-state NMR spectroscopy using probe molecules*. Solid. State. Nucl. Mag., 2013, 55-56, 12-27.

[47] G. Paul, C. Bisio, I. Braschi, M. Cossi, G. Gatti, E. Gianotti, and L. Marchese. *Combined solid-state NMR, FT-IR and computational studies on layered and porous materials.* Chem. Soc. Rev., 2018, 47, 5684-5739.

[48] A. Zheng, S-J. Huang, Q. Wang, H. Zhang, F. Deng and S-B, Liu. *Progress in development and application of solid-state NMR for solid acid catalysis.* Chin. J. Catal., 2013, 34 (3), 436-491.

[49] M. Boronat, and A. Corma. *What is measured when measuring acidity in zeolites with probe molecules?* ACS Catal., 2019, 9 (2), 1539-1548.

[50] D. Zhai, Y.Liu, H. Zheng, L. Zhao, J. Gao, C. Xu and B. Shen. *A first-principles evaluation of the stability, accessibility, and strength of Brønsted acid sites in zeolites.* J. Catal., 2017, 352, 627–637.

[51] G. Busca. A*cidity and basicity of zeolites: A fundamental approach.* Microporous Mesoporous Mater., 2017, 254, 3-16.

[52] A. Vimont, F. Thibault-Starzyk and M. Daturi. *Analysing and understanding the acid site by IR spectroscopy.* Chem. Soc. Rev., 2010, 39, 4928-4950.

[53] S. Bordiga, C. Lamberti, F. Bonino, A. Tavert and F. Thibault-Starzyk. *Probing zeolites by vibrational spectroscopies.* Chem. Soc. Rev., 2014, 44, 7262-7341.

[54] C. Lamberti, A. Zecchina, E. Groppob and S. Bordiga. *Probing the surfaces of heterogeneous catalysts by in situ IR spectroscopy.* Chem. Soc. Rev., 2010, 39, 4951-5001.

[55] F. Fan, Z. Fenga and C. Li. *UV Raman spectroscopic study on the synthesis mechanism and assembly of molecular sieves.* Chem. Soc. Rev., 2010, 39, 4794-4801.

[56] Ö. Attila, H. E. King, F. Meirer and B. M. Weckhuysen. *3-D Raman spectroscopy of large zeolite ZSM-5 crystals.* Chem. Eur. J., 2019, 25 (29), 7158-7167.

[57] S. Jin, Z. Feng, F. Fan and C. Li. *UV Raman spectroscopic characterization of catalysts and catalytic active sites*. Catal. Lett, 2015, 145, 468-481.

[58] E. M. Flanigen. *Infrared and raman spectroscopy for characterizing zeolites* in *Introduction to zeolite science and practice.* Eds: H. van Bekkum, E. M. Flanigen, P.A. Jacobs and J. C. Jansen. Elsevier, 2001, 435-476.

[59] X. Liu. *Infrared and Raman Spectroscopy* in *Zeolite characterization and catalysis A tutorial.* Eds: A. W. Chester and E. G. Derouane. Springer, 2009, 435-476.

[60] K. Hadjiivanov. *Identification and characterization of surface hydroxyl groups by infrared spectroscopy*. Adv. Catal., 2014, 57, 99-318.

[61] A. Jentys and J. A. Lercher. *Techniques of zeolite characterization*. Stud. Surf. Sci. Catal., 2001, 137, 345-386.

[62] H. Y. Luo, J. D. Lewis and Y. Roman-Leshkov. *Lewis acid zeolites for biomass conversion: Perspectives and challenges on reactivity, synthesis, and stability*. Annu. Rev. Chem. Biomol. Eng. 2016, 7, 663-692.

[63] P. Y. Dapsens, C. Mondelli and J. Pérez-Ramírez. Design of Lewis-acid centres in zeolitic matrices for the conversion of renewables. Chem. Soc. Rev., 2015, 44, 7025-7043.

[64] J. A. Lercher, C. Gründling and G. Eder-Mirth. *Infrared studies of the surface acidity of oxides and zeolites using adsorbed probe molecules*. Catal.Today., 1996, 27(3-4), 353-376.

[65] E. A. Paukshtis and E. N. Yurchenko. *Study of the acid-base properties of heterogeneous catalysts by infrared spectroscopy.* Russ. Chem. Rev., 1983, 52, 242-258.

[66] H. Knözinger and S. Huber. *IR spectroscopy of small and weakly interacting molecular probes for acidic and basic zeolites.* J. Chem. Soc., Faraday. Trans., 1998, 94 (15), 2047-2059.

[67] T. Barzetti, E. Selli, D. Moscotti and L. Forni. *Pyridine and ammonia as probes for FTIR analysis of solid acid catalysts*. J. Chem. Soc., Faraday. Trans., 1996, 92 (8), 1401-1407.

[68] F. Jin and Y. Li. *A FTIR and TPD examination of the distributive properties of acid sites on ZSM-5 zeolite with pyridine as a probe molecule*. Catal. Today., 2009,145, 101-107.

[69] N. S. Nesterenko, F. Thibault-Starzyk, V. Montouillout, V. V. Yuschenko, C. Fernandez, J-P. Gilson, F. Fajula and I. I. Ivanova. *Accessibility of the acid sites in dealuminated small-port mordenites studied by FTIR of co-adsorbed alkylpyridines and CO*. Microporous Mesoporous Mater., 2004, 71, (1-3), 157-166.

[70] V. V. Ordomsky, V. Y. Murzin, Yu. V. Monakhova, Y. V. Zubavichus, E. E. Knyazeva, N. S. Nesterenko and I. I. Ivanova. *Nature, strength and accessibility of acid sites in micro/mesoporous catalysts obtained by recrystallization of zeolite BEA*. Microporous Mesoporous Mater., 2007, 105, (1-2), 101-110.

[71] A. Corma, V. Fornés, L. Forni, F. Márquez, J. Martínez-Triguero and D. Moscotti. *2,6-di-tert-butylpyridine as a probe molecule to measure external acidity of zeolites*. J. Catal., 1998, 179, (2), 451-458.

[72] K. Góra-Marek, K. Tarach and M. Choi. *2,6-di-tert-butylpyridine sorption approach to quantify the external acidity in hierarchical zeolites.* J. Phys. Chem. C., 2014, 118, (23), 12266-12274.

[73] T. Onfroy, G. Clet and M. Houalla. *Quantitative IR characterization of the acidity of various oxide catalysts.* Microporous Mesoporous Mater., 2005, 82, (1-2), 99-104.

[74] L. Oliviero, A. Vimont, J-C. Lavalley, F. R. Sarria, M. Gaillard and F. Maugé. *2,6-dimethylpyridine as a probe of the strength of Brønsted acid sites: study on zeolites. Application to alumina*. Phys. Chem. Chem. Phys., 2005, 7, (8), 1861-1869.

[75] A. Corma, C. Rodellas and V. Fornes. *Characterization of acid surfaces by adsorption of 2,6-dimethylpyridine*. J. Catal., 1984, 88, (2), 374-381.

[76] T. Armaroli, M. Bevilacqua, M. Trombetta, A. G. Alejandre, J. Ramirez and G. Busca. *An FT-IR study of the adsorption of aromatic hydrocarbons and of 2,6-lutidine on H-FER and H-ZSM-5 zeolites*. Appl. Catal., A., 2001, 220, (1-2), 181-190.

[77] N. S. Nesterenko, F. Thibault-Starzyk, V. Montouilliout, V. V. Yushchenko, C. Fernandez, J. P. Gilson, F. Fajula and I. I. Ivanova, Kinet. Katal., 2006, 47, (1), 45; translated into English. *The use of the consecutive adsorption of pyridine bases and carbon monoxide in the IR spectroscopic study of the accessibility of acid sites in microporous/mesoporous materials*. Kinet. Catal., 2006, 47, (1), 40-48.

[78] K. Barbera, F. Bonino, S. Bordiga, T. V. W. Janssens and P. Beato. *Structure–deactivation relationship for ZSM-5 catalysts governed by framework defects.* J. Catal., 2011, 280, (2), 196-205.

[79] S. M. T. Almutairi, B. Mezari, E. A. Pidko, P. C. M. M. Magusin and E. J. M. Hensen. *Influence of steaming on the acidity and the methanol conversion reaction of HZSM-5 zeolite.* J. Catal., 2013, 307, 194-203.

[80] M. S. Holm, S. Svelle, F. Joensen, P. Beato, C. H. Christensen, S. Bordiga and M. Bjørgen. *Assessing the acid properties of desilicated ZSM-5 by FTIR using CO and 2,4,6-trimethylpyridine (collidine) as molecular probes.* Appl. Catal., A., 2009, 356, (1), 23-30.

[81] F. Thibault-Starzyk, I. Stan, S. Abelló, A. Bonilla, K. Thomas, C. Fernandez, J-P. Gilson and J. Pérez-Ramírez. *Quantification of enhanced acid site accessibility in hierarchical zeolites – The accessibility index.* J. Catal., 2009, 264, (1), 11-14.

[82] C. O. Areán. *Probing Brønsted acidity of protonic zeolites with variable-temperature infrared spectroscopy.* Ukr. J. Phys., 2018, 63 (6), 538-545.

[83] P. Rejmak, J. Datka and E. Broclawik. *Identity of two types of strong Brønsted acid sites in mazzite revealed by CO probe: IR study and periodic DFT modelling*. Int. J. Quantum. Chem., 2019, 119, 2-7.

[84] M. A. Makarova, V. L. Zholobenko, K. M. Al-Ghefaili, N. E. Thompson, J. Dewing and J. Dwyer. *Brønsted acid sites in zeolites. FTIR study of molecular hydrogen as a probe for acidity testing.* J. Chem. Soc., Faraday. Trans.,1994, 90, 1047-1054.

[85] M. Trombetta, A. G. Alejandre. J. R. Solis and G. Busca. *An FT-IR study of the reactivity of hydrocarbons on the acid sites of HZSM5 zeolite*. Appl. Catal., A., 2000, 198, 81-93.

[86] K. Chakarova and K. Hadjiivanov. *Interaction of benzene with hydroxyl groups in zeolites: A FTIR study of $C_6H_6$ and $C_6D_6$ adsorption on H-ZSM-5 and D-ZSM-5.* Microporous Mesoporous Mater., 2011, 143, (1), 180-188.

[87] W. Daniell, N-Y. Topsøe and H. Knözinger. *An FTIR study of the surface acidity of USY zeolites: Comparison of CO, $CD_3CN$, and $C_5H_5N$ probe molecules*. Langmuir., 2001, 17, 6233-6239.

[88] T. Montanari, M. Bevilacqua and G. Busca. *Use of nitriles as probe molecules for the accessibility of the active sites and the detection of complex interactions in zeolites through IR spectroscopy*. Appl. Catal. A., 2006, 307, (1), 21-29.

[89] G. Busca. *Characterization of real catalytic materials: An overview* in *Heterogeneous catalytic materials: Solid-state chemistry, surface chemistry and catalytic behaviour*. Elsevier., 2014, 23-34.

[90] R. E. Morris and P. S. Wheatley. *Diffraction techniques applied to zeolites* in *Introduction to zeolite science and practice.* Eds*: J. Čejka, H. van Bekkum, A. Corma and F. Schüt. Stud. Surf. Sci. Catal.*, 2007, 168, 375-401.

[91] A. W. Burton. *Powder diffraction in zeolite science: An introductory guide* in *Zeolite characterization and catalysis: A tutorial.* Eds: A. W. Chester and E. G. Derouane. Springer, 2010, 1-64.

[92] M. M. Treacy and J. B. Higgins. *Collection of simulated XRD powder patterns for zeolites*. Elsevier. 2007.

[93] J. Rouquerol, F. Rouquerol, P. Llewellyn, G. Maurin and K. S. W. Sing. *Adsorption by powders and porous solids: principles, methodology and applications.* Academic press 2013, 1-646.

[94] M. Thommes, K. Kaneko, A. V. Neimark, J. P. Olivier, F. Rodriguez-Reinoso, J. Rouquerol and K. S. W. Sing. *Physisorption of gases, with special reference to the evaluation of surface area and pore size distribution (IUPAC Technical Report).* Pure Appl. Chem. 2015, 87 (9-10), 1051-1069.

[95] S. Storck, H. Bretinger, W. F Maier. *Characterization of micro-and mesoporous solids by physisorption methods and pore-size analysis.* App. Catal. A: Gen, 1998, 174,137-146.

[96] C. E. Kliewer. *Electron Microscopy and Imaging* in *Zeolite characterization and catalysis: A tutorial.* Eds: A. W. Chester and E. G. Derouane. Springer, 2010, 1-64.

[97] J. I. Goldstein, D. E. Newbury, P. Echlin, D. C. Joy, Charles E. Lyman, E. Lifshin, L. Sawyer and J. R. Michael. *The SEM and its modes of operation* in *Scanning electron microscopy and X-ray microanalysis.* Springer, 2003, 21-60.

[98] J. I. Goldstein, D. E. Newbury, P. Echlin, D. C. Joy, Charles E. Lyman, E. Lifshin, L. Sawyer and J. R. Michael. *Generation of X-Rays in the SEM Specimen* in *Scanning electron microscopy and X-ray microanalysis.* Springer, 2003, 271-296.

# Chapter 2 Molar absorption coefficients of Py-$H^+$ and Py-L complexes in acidic zeolites

## 2.1 Introduction

Infrared spectroscopy (IR) is an important and well-developed tool to carry out quantitative analysis of acidity in zeolite-based catalysts. The key to quantitative measurements is the use of the Beer-Lambert law (Equation 2.1), which requires the knowledge of molar absorption coefficients (ε). These coefficients are relevant to determine the amount of probe molecule that interacts with the solid material and the number of adsorption sites (acidic, basic and accessible metallic sites). The accuracy of the quantitative measurements strongly depends on the precise determination or choice of the ε values.

$$A = \varepsilon \times c \times l \qquad \textbf{Equation 2.1}$$

Where *A* is absorbance or intensity of the peak, *c* is the molar concentration of probe molecule introduced in the IR cell and *l* is the pathlength. Pyridine (Py) is the most commonly used probe molecule to quantify acidity (Chapter 1 Section 1.5), and there are a wide range of ε values published in the literature (Table 2.1) for Py species adsorbed onto Brønsted (Py-$H^+$ or BAS) and Lewis acid sites (Py-L or LAS). However, significant differences are observed between the values reported by the different laboratories; the values vary by six orders of magnitude (Table 2.1) suggesting that ε reported may be associated with significant errors [1]. The lack of a good description of the experimental approach is one of the factors leading to these discrepancies [2]. Furthermore, the geometry and physical properties of the sample (thickness of the disc, pressure used to prepare the disc, particle size etc.) [3] and all experimental parameters (resolution, temperature, vacuum system or in gas flow) may have a large influence on the ε values obtained by different researchers.

**Table 2.1.** Molar absorption coefficients (ε) values for Py adsorb5ed on BAS and LAS reported in the literature.

| Material | $\varepsilon_{BAS}$ | Units | $\varepsilon_{LAS}$ | Units | $\varepsilon_{BAS}/\varepsilon_{LAS}$ | Resolution $cm^{-1}$ | Temperature °C | Year | Ref |
|---|---|---|---|---|---|---|---|---|---|
| **Silica-alumina** | - | - | - | - | 8.8 ± 15% | 2 or 4 | - | 1964 | [4] |
| **Silica-alumina** | - | - | - | - | 6.0±9 | - | - | 1966 | [5] |
| **$NH_4Y$** | 3.03±0.13 | cm $\mu mol^{-1}$ | 3.26±0.13 | cm $\mu mol^{-1}$ | 0.93 | - | 150 | 1967 | [6] |
| **MOR** | - | - | - | - | 2.61 | - | - | 1968 | [7] |
| **MOR** | - | - | - | - | 1.54 | 4 | - | 1971 | [8] |
| **NaY** | 0.059 ±0.004 | $\mu mol\ cm^{-2}$ | - | - | - | - | 150 | 1980 | [9] |
| **NaHY** | 0.059±0.004 | $cm^2\ \mu mol^{-1}$ | 0.084±0.003 | $cm^2\ \mu mol^{-1}$ | 0.70 | - | - | 1981 | [10] |
| **ZSM-5** | $1.3\times10^{-6}$ | cm $\mu mol^{-1}$ | $1.5\times10^{-6}$ | cm $\mu mol^{-1}$ | 0.87 | - | 150 | 1986 | [11] |
| **$Al_2O_3$, Y** | 0.73 | cm $\mu mol^{-1}$ | 1.11 | cm $\mu mol^{-1}$ | 0.66 | 2 | 200 | 1992 | [12] |
| **MOR, ZSM-5, Y** | 1.67±0.12 | cm $\mu mol^{-1}$ | 2.22±0.21 | cm µmol | 0.75 | 1 | 150 and 350 | 1993 | [13] |
| **BEA** | $1.3\times10^{-6}$ | cm $\mu mol^{-1}$ | $1.5\times10^{-6}$ | cm $\mu mol^{-1}$ | 0.87 | - | 30 | 1994 | [14] |
| **HY** | 1.8±0.1 | cm $\mu mol^{-1}$ | 1.5 | cm $\mu mol^{-1}$ | 1.2 | - | - | 1994 | [2] |
| **Y**<br>**EMT** | 1.1<br>1.6 | cm $\mu mol^{-1}$<br>cm $\mu mol^{-1}$ | -<br>- | -<br>- | -<br>- | 2 | 30<br>30 | 1995 | [15] |
| **MOR** | 1.8 | cm $\mu mol^{-1}$ | - | - | - | 2 | 30 | 1995 | [16] |
| **MOR , Y** | 0.078±0.004 | $cm^2\ \mu mol$ | 0.269±0.01 | $cm^2\ \mu mol$ | 0.29 | - | 145 | 1996 | [17] |
| **MOR, $Al_2O_3$** | 1.13 | cm $\mu mol^{-1}$ | 1.28 | cm $\mu mol^{-1}$ | 0.88 | - | n.a | 1997 | [18] |
| **Y** | 0.085±0.005 | $cm^2\ \mu mol$ | - | - | - | - | 145 | 1997 | [19] |
| **MAZ** | 1.13 | cm $\mu mol^{-1}$ | 1.28 | cm $\mu mol^{-1}$ | 0.88 | - | - | 1998 | [20] |
| **MCM-41** | 1.47 | cm $\mu mol^{-1}$ | 1.98 | cm $\mu mol^{-1}$ | 0.74 | - | 150 | 1999 | [21] |
| **BEA, MOR, Y, Silica-alumina** | 0.73±0.04 | cm $\mu mol^{-1}$ | 0.64±0.04 | cm $\mu mol^{-1}$ | 1.14 | 2 | 150 | 1999 | [22] |

| | | | | | | | | | |
|---|---|---|---|---|---|---|---|---|---|
| **Y** | 1.36±0.03 | cm $\mu mol^{-1}$ | - | - | - | 4 | 200 | 2004 | [23] |
| **HMCM-41, $Al_2O_3$** | 0.070 | cm $\mu mol^{-1}$ | 0.100 | cm $\mu mol^{-1}$ | 0.70 | 2 | 150 | 2005 | [24] |
| **BEA, VBEA** | 0.070 | cm $\mu mol^{-1}$ | 0.100 | cm $\mu mol^{-1}$ | 0.70 | 2 | 150 | 2006 | [25] |
| **MCM-48, MCM-68** | 0.078 | cm $\mu mol^{-1}$ | 0.165 | cm $\mu mol^{-1}$ | 0.47 | 2 | 170 | 2010 | [26] |
| **Silica-alumina** | 0.57 | cm $\mu mol^{-1}$ | 1.5 | cm $\mu mol^{-1}$ | 0.38 | - | - | 2010 | [27] |
| **SBA-15** | 1.67±0.12 | cm µmol | 2.22±0.21 | cm µmol | 0.75 | 4 | 30 | 2010 | [28] |
| **Silica-alumina** | 1.67±0.12 | cm µmol | 2.22±0.21 | cm µmol | 0.75 | 4 | 150 | 2012 | [29] |
| **HY**<br>**SnBEA** | 1.95±0.13<br>- | cm $\mu mol^{-1}$<br>- | 1.45±0.10<br>1.42±0.30 | cm $\mu mol^{-1}$<br>cm $\mu mol^{-1}$ | 1.34<br>1.37 | 2 | 150 | 2016 | [30] |
| **SAPO-34** | 0.06 | $cm^2$ $\mu mol^{-1}$ | - | - | - | 4 | - | 2017 | [31] |
| **ZSM-5** | 0.07 | $cm^2$ $\mu mol^{-1}$ | 0.10 | $cm^2$ $\mu mol^{-1}$ | 0.70 | 2 | 170 | 2017 | [32] |
| **BEA, ZSM-5, Y** | 1.98±0.16<br>2.98±0.49<br>2.55±0.28 | mmol/$g_{cat}$/area | 2.53±0.38<br>~2.2<br>2.27±0.41 | mmol/$g_{cat}$/area | 0.78<br>1.35<br>1.12 | 4 | 30 | 2018 | [33] |

For other probe molecules, there is a lack of ε values in the literature, however, some reports have been published on the calculation of these coefficients for ammonia, quinoline, acetonitrile and substituted pyridines [34-38].

Important advances in new tools for the determination of ε values have been made in the last few years [23,39-40], such as the combination of high-precision thermogravimetry and FTIR (AGIR-Analysis by Gravimetry and IR). This technique, in which a microbalance is integrated with an FTIR *in situ* cell in a single set-up, allows simultaneous monitoring of the weight changes of the sample along with its IR spectra during adsorption or desorption of probe molecules, and consequently, highly accurate quantitative data (e.g. the molar absorption coefficient values, can be obtained directly). The method was successfully used to investigate ε values for water and ammonia on FAU zeolites and demonstrated the importance of the conditions in which the experiments are carried out [40].

The aim of this work was to carry out accurate quantitative analysis of the number of acid sites in different zeolites and to determine the role of experimental conditions that are essential for the reliable characterisation of the acidic properties of zeolite based catalysts. This study also examines the validity of the Beer-Lambert law in solids materials. The molar absorption coefficients of Py adsorbed on Brønsted, $\varepsilon(\text{Py-H}^+)$, and Lewis, $\varepsilon(\text{Py-L})$, acid site have been determined using the *in situ* FTIR experiments and the AGIR technique. Overall, the optimisation of the experimental procedures is imperative for the successful quantitative evaluation of different types of acid sites in zeolitic materials. With the new level of instrumentation available now, this work sets a benchmark for the quantitative acidity measurements in zeolites and related materials.

## 2.2 Experimental

### 2.2.1 Materials

Ammonium forms of zeolites BEA (CP814E, Zeolyst International, Si/Al=12.5), BEA (CP814C, Zeolyst International, Si/Al=19) ZSM-5 (CBV8014, Zeolyst International,

Si/Al=40), MOR (Crossfield, Si/Al=7.0), FAU (Crossfield, Si/Al=2.6), fumed silica ($SiO_2$, Sigma-Aldrich, 99.8%) and ɤ-alumina (Puralox, Sasol) were obtained in powder form. The materials were either used as received or calcined ex situ at 450C-900ºC in a muffle furnace for 5 hours. This procedure gives materials with the same type of zeolite framework but with the different BAS/LAS ratios necessary for molar absorption coefficient measurements using *in situ* FTIR experiments.

### 2.2.2 Beer-Lambert law studies

Preliminary studies were carried out to verify the validity of the Beer-Lambert law in solid materials and to evaluate the influence of different parameters on quantitative measurements using FTIR spectroscopy. For this preliminary work scanning electron microscopy (SEM) and Py-FTIR spectroscopy analyses were performed. The selected materials (fumed silica, BEA and ZSM-5 zeolites) were pressed into 1.3 cm self-supporting discs with a cross-section area of (S) 1.3 $cm^2$ using a hydraulic bench press. The discs were made with different mass (~2-40 mg), load (0, 1, 2, 5 and 8 tonnes) and time under load (1, 3, 5 and 120 sec). The discs from SEM measurements were fixed to 15 mm stubs by sticky carbon tabs and the SEM micrographs were collected on a Hitachi TM3000 scanning microscope equipped with an EDX analytical system and heat beam of 15 keV. FTIR experiments were performed according to the description below (Section 2.2.3 *In situ* experiments).

### 2.2.3 Molar absorption coefficients calculations

#### *In situ experiments*

The experiments were carried out at Keele University using an *in situ* IR cell attached to a vacuum system and the analysis was monitored by a Thermo iS10 spectrometer, equipped with a DTGS detector, at a spectral resolution of 1-8 $cm^{-1}$ (Figure 2.1). Prior to FTIR studies, the zeolites were pressed into self-supporting discs (1.3 cm in diameter, S=1.3 $cm^2$, ~2.6-40 mg) and pre-treated in an *in situ* IR cell at 450°C under vacuum ($10^{-5}$ Torr) for

5 h. Small portions of Py were admitted into the cell by injection at 150ºC until no changes in the peaks under investigation were observed in the spectra. Physisorbed molecules were subsequently removed by evacuation at adsorption temperature. The obtained infrared spectra were analysed (including integration, subtraction, and determination of peak positions) using specialised Thermo software, Omnic. All the spectra presented in this chapter were normalised and offset for clarity. The *in situ* FTIR measurements were carried out on different zeolitic structures with different Si/Al ratios and subject to different calcination temperatures: BEA (12.5), BEA (19), ZSM-5 (40), MOR (7) and Y (2.6), where the values in brackets refer to Si/Al ratios.

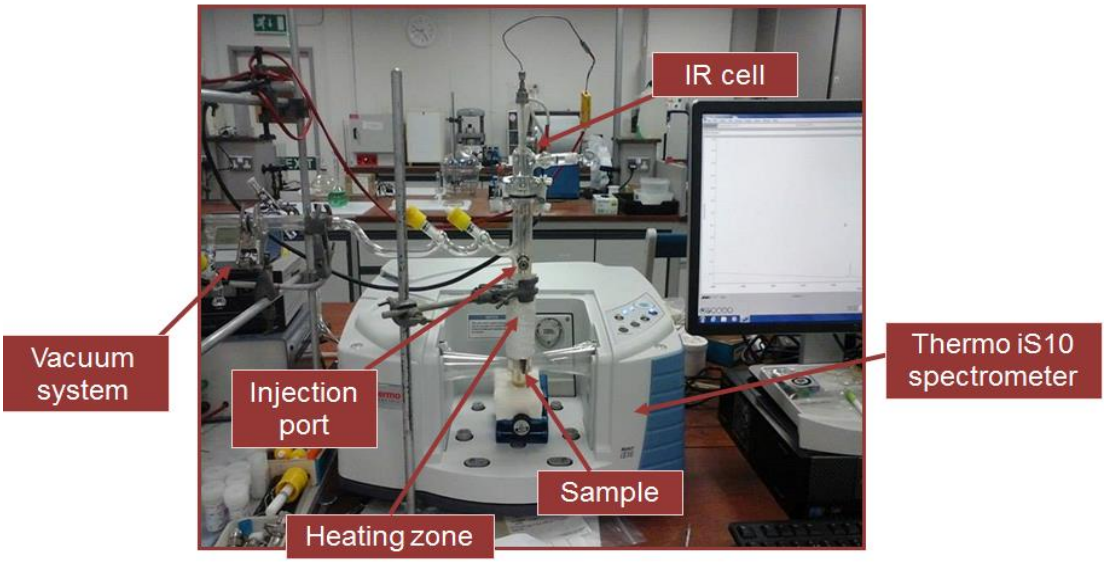


**Figure 2.1.** *In situ* FTIR spectroscopy equipment at Keele University.

The modified Beer-Lambert law (Equation 2.2) allows the calculation of the ε values when knowing the total amount of Py introduced and the intensity of the peak under investigation.

$$A = \varepsilon \frac{n_{total}}{S} \qquad \textbf{Equation 2.2}$$

Where $n_{total}$ is the number of Py species in the sample disc and $S$ is the cross-section area of the zeolite disc (S=1.3 $cm^2$ for studies with the *in situ* IR cell). As zeolites often have more than one type of acid sites (BAS and LAS) and Py interacts with both of these acid

sites, the relationship between the amount of Py that interacts with each type of acid site and the molar absorption coefficients values are given by the following equations:

$$n_{total}^{Py} = n_{BAS}^{Py} + n_{LAS}^{Py} \quad \textbf{Equation 2.3}$$

$$n_{BAS}^{Py} = \frac{A_{BAS} \times S}{\varepsilon_{BAS}} \quad \textbf{Equation 2.4}$$

$$n_{LAS}^{Py} = \frac{A_{LAS} \times S}{\varepsilon_{LAS}} \quad \textbf{Equation 2.5}$$

$$n_{total}^{Py} = \frac{A_{BAS} \times S}{\varepsilon_{BAS}} + \frac{A_{LAS} \times S}{\varepsilon_{LAS}} \quad \textbf{Equation 2.6}$$

To obtain $n_{total}^{Py}$, small and known amounts of Py are injected into the *in situ* IR cell and the changes of the IR peaks under investigation (~1454 $cm^{-1}$ for Py-$H^+$ and ~1445 $cm^{-1}$ for Py-L) were monitored. In the first injections, there is a linear relationship between the amount of Py introduced and the changes in the peak intensities. When all sites are saturated, Py is no longer absorbed on the acid sites and a plateau is observed (e.g Figure 2.2).

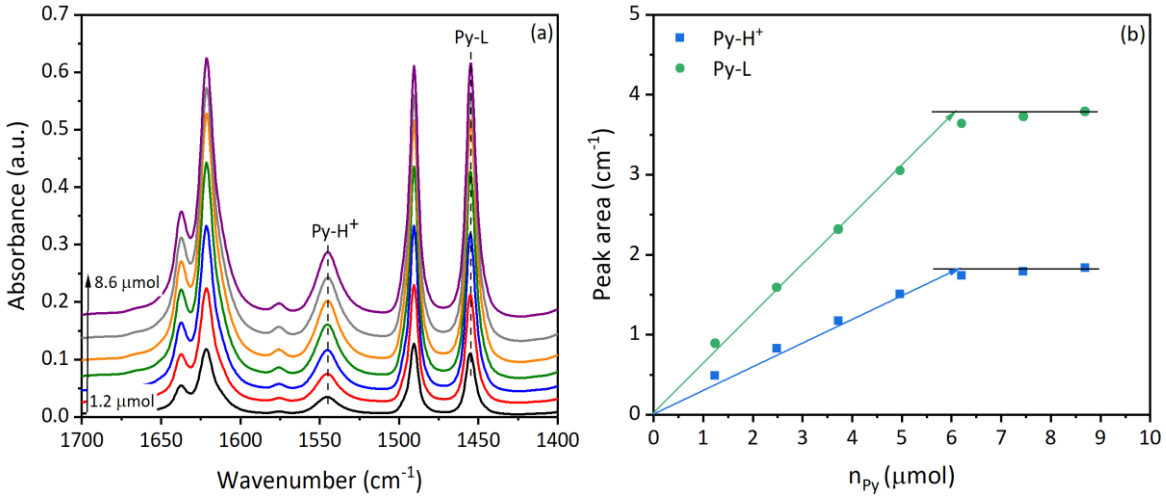


**Figure 2.2.** Titrations of increasing amounts of Py at 150°C on zeolite BEA (12.5) calcined at 600°C. **(a)** Difference spectra of Py region following Py adsorption at 150°C. **(b)** Integrated areas of the Py-$H^+$ and Py-L peaks over the $n_{total}$ (Py) added.

However, Equation 2.6 still contains two unknown parameters ($\varepsilon_{BAS}$ and $\varepsilon_{LAS}$) and in a single experiment, it is impossible to determine the two parameters. It is, therefore, necessary to use zeolitic materials with different BAS/LAS ratios (calcined zeolites). The

calculation of both $\varepsilon_{BAS}$ and $\varepsilon_{LAS}$ were achieved using Equation 2.7, which is a rearrangement of Equation 2.6.

$$\frac{A_{BAS} \times S}{n_{total}^{Py}} = -\frac{\varepsilon_{BAS}}{\varepsilon_{LAS}} \times \frac{A_{LAS} \times S}{n_{total}^{Py}} + \varepsilon_{BAS} \qquad \textbf{Equation 2.7}$$

By plotting Equation 2.7 both $\varepsilon_{BAS}$ and $\varepsilon_{LAS}$ can be determined from the gradient and the y-intercept of the trendlines.

***AGIR experiments***

The experiments using the AGIR set-up were carried out in the Laboratoire Catalyse et Spectrochimie (LCS) at Normandie University. In this set-up, the mass (and therefore the number of adsorbed molecules) and IR spectra of the sample can be measured simultaneously in real-time *operando* conditions in a gas-flow system at a temperature between 30-500°C (Figure 2.3).

**Figure 2.3.** AGIR set-up at LCS laboratories, Caen, France.

The analyses were carried out on self-supporting discs (~20 mg, 1.6 cm in diameter S=2.0 $cm^2$) and pre-treated in the IR reactor cell at 450°C under a flow of Ar for 5 h. IR spectra of the samples were recorded at every 300 secs with a Nicolet 6700 spectrometer equipped with an MCT detector, at a spectral resolution of 4 $cm^{-1}$. In parallel, the weight

changes were continuously monitored by a SETSYS-B Setaram microbalance and the outlet gas flow composition was observed by a MS analyser (Pfeiffer Omnistar GSD301). All the spectra presented in this chapter were normalised and offset for clarity. Measurements were carried out on different zeolitic structures: BEA (12.5), ZSM-5 (40), MOR (7) and Y (2.6), ɤ-alumina and Na-ZSM-5 (40), where the values in brackets refer to Si/Al ratios.

## 2.3 Beer-Lambert law studies

Preliminary work in selected materials (fumed silica, ZSM-5 (40) and BEA (12.5) zeolites) was carried out to check the validity of the Beer-Lambert in solids for the FTIR characterisation and to illustrate the effects of the preparation procedure in quantitative measurements. As an example, Figure 2.4 presents two SEM micrographs collected to obtain thickness data. Thickness of the discs decreases with increasing loads for all selected materials and this effect is more noticeable for heavier discs (40 mg) (Figure 2.5). The changes are also observed when the discs are pressed at a different time under load, especially for the 40 mg discs. There are no significant changes in the thickness in lower weight discs (10 mg) mainly after 5 seconds under pressure. These conclusions are similar for all materials selected for this part of the study.

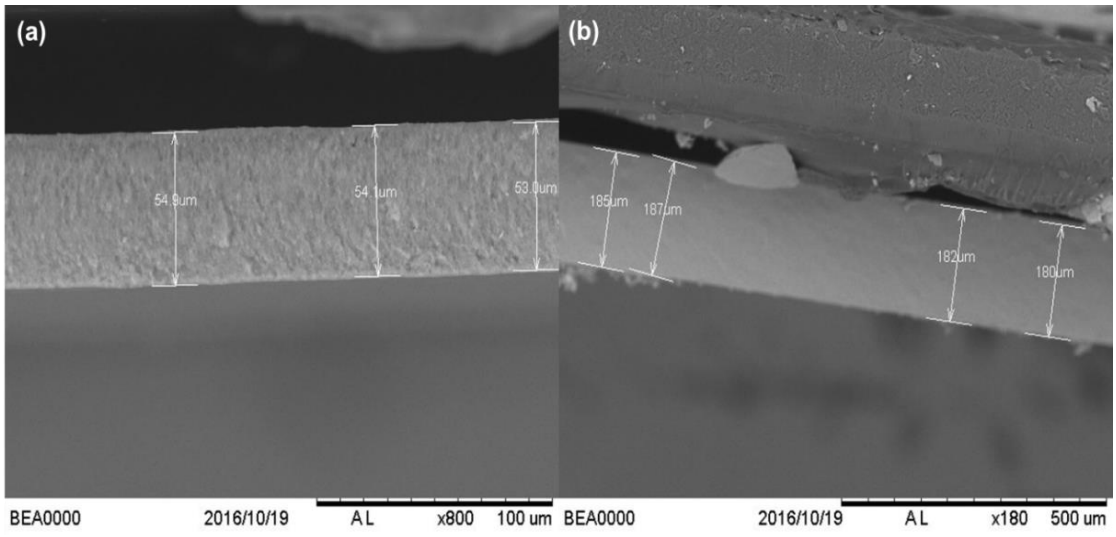


**Figure 2.4** SEM micrograph of self-supported BEA (12.5) discs at different magnifications. **(a)** 10mg BEA (12.5) prepared at an 8 tonne load for 1 sec and **(b)** 40 mg BEA (12.5) prepared at an 8 tonne load for 1 sec.

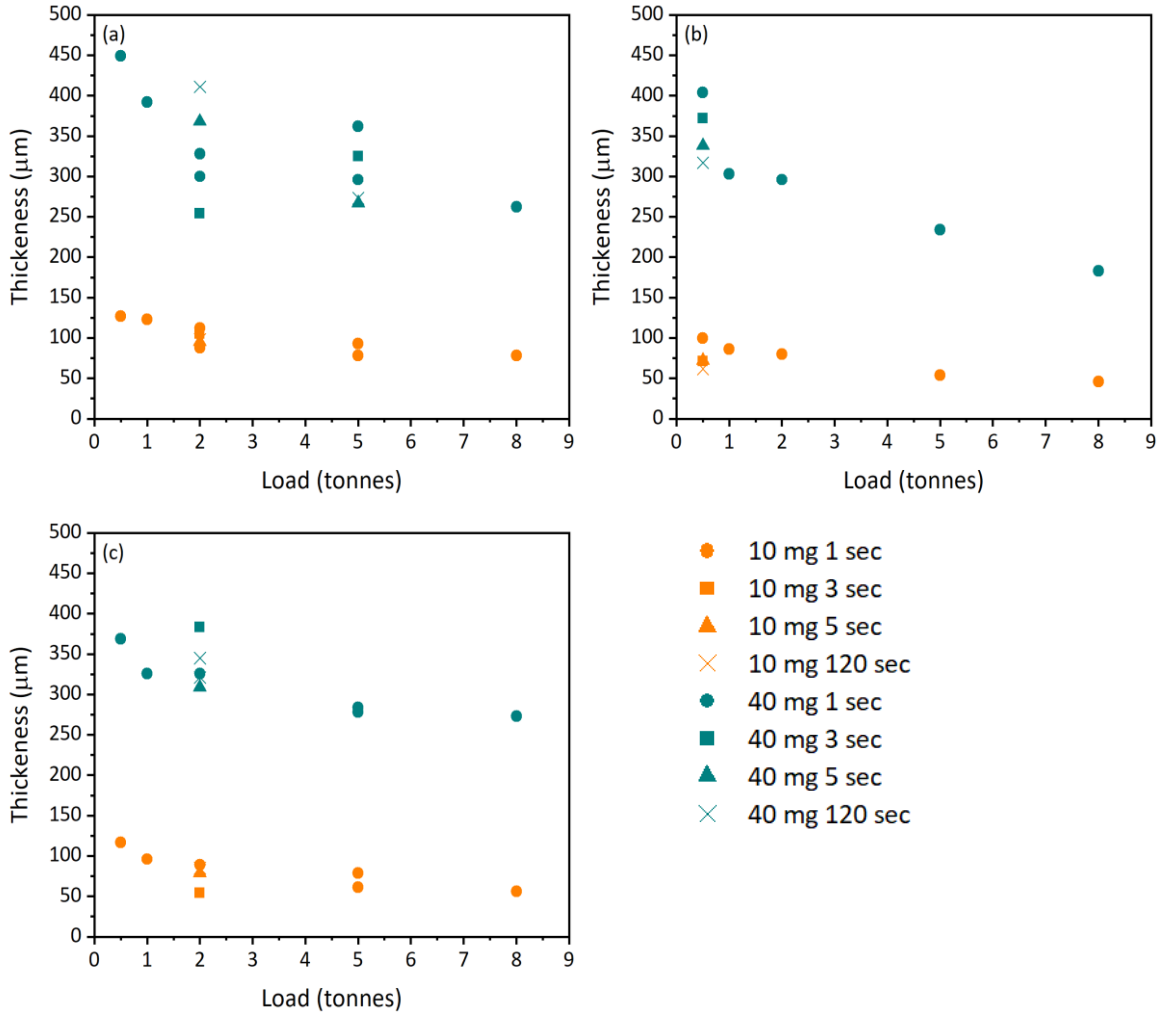


**Figure 2.5.** Thickness of the self-supporting discs prepared with different mass, load and time under load. **(a)** Fumed silica, **(b)** BEA (12.5), **(c)** ZSM-5 (40) zeolites.

The influence of the different preparation parameters (mass and load) in quantitative measurements using FTIR spectroscopy was also evaluated (e.g. Figures 2.6, 2.7 and 2.8). FTIR spectra of BEA zeolite show two major peaks at 3745 $cm^{-1}$, with a shoulder at ~3735 $cm^{-1}$, and 3610 $cm^{-1}$ (Figure 2.6 a). The peak at 3610 $cm^{-1}$ is assigned to acidic bridging Si-OH-Al groups and the peaks at ~3745 and ~3735 $cm^{-1}$ are attributed to the external and internal Si-OH groups, respectively. The interaction of Py with the zeolites gives rise, in the range of 1400-1700 $cm^{-1}$, to the following sets of peaks: two peaks at 1545 and 1637$cm^{-1}$ due to pyridinium ions (Brønsted acid sites, Py-$H^{+}$), two peaks assigned to Py coordinated to Lewis acid sites (Py-L) at 1456 and 1622 $cm^{-1}$ and the signals of Py on Lewis and Brønsted acid sites at 1491 $cm^{-1}$ (Figure 2.6 b). The intensities of the peaks of Si-OH-Al (~3610 $cm^{-}$

$^{-1}$), Si-OH (~3745 cm$^{-1}$) groups, BAS (~1545 cm$^{-1}$) and LAS (~1456 cm$^{-1}$) increase with disc mass (Figures 2.6). These data show a clear linear relationship between absorbance and the mass of the discs (which is used by proxy for the effective sample pathlength), demonstrating that the Beer-Lambert law is valid for solid materials in IR spectroscopy (Figure 2.7), although, some noticeable deviation from it is observed for samples heavier than 25 mg (20 mg/cm$^2$). For practical FTIR measurements, the sample size between 5 and 15 mg/cm$^2$ should be recommended.

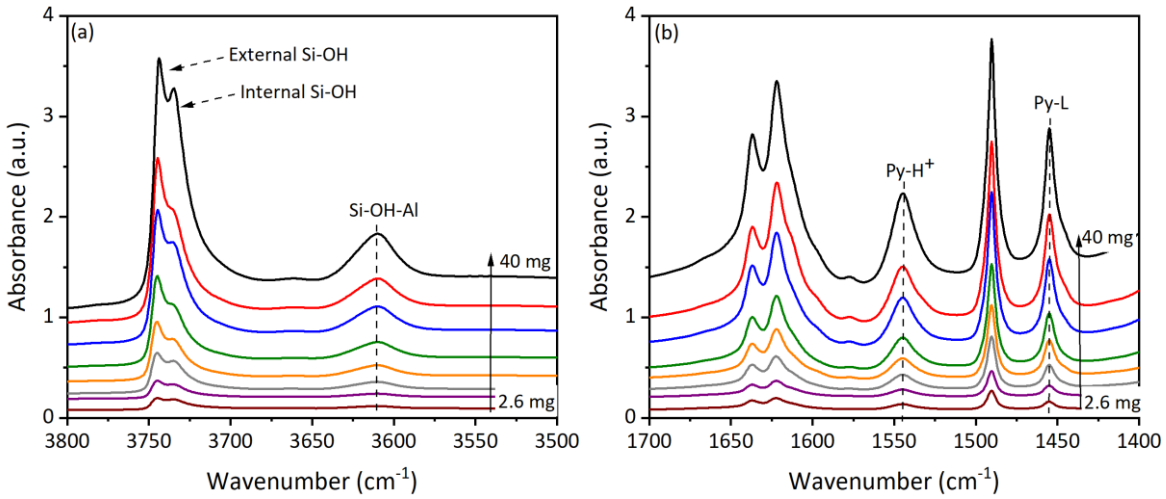


**Figure 2.6. (a)** FTIR spectra of the hydroxyl region following Py adsorption at 150°C of BEA (12.5) discs with different mass (~2-40 mg). **(b)** Difference spectra Py region following Py adsorption at 150°C of BEA (12.5) discs with different mass (~2-40 mg).

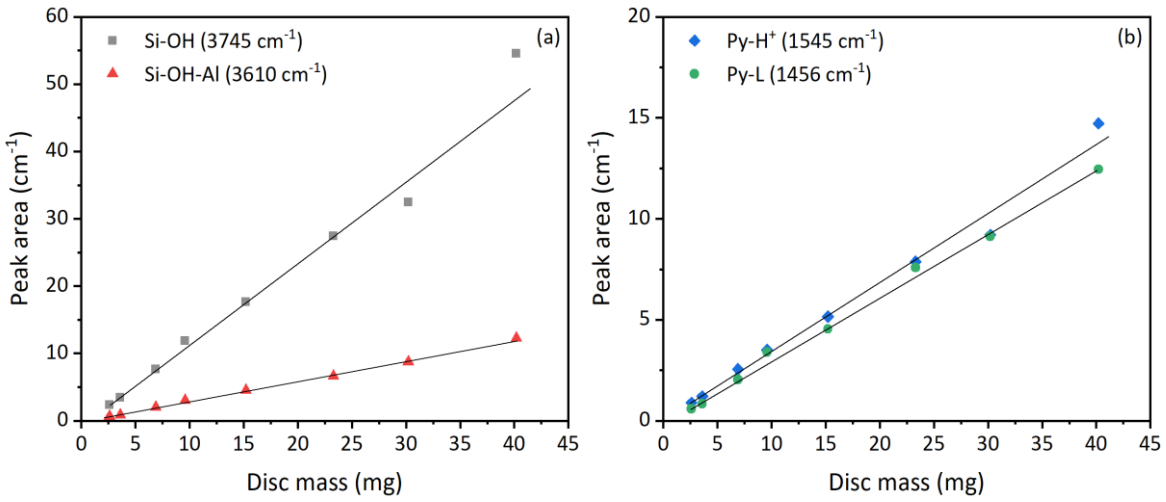


**Figure 2.7.** Linear relationship between the zeolite disc mass and the integrated absorbance of the IR bands of OH groups and Py adsorbed on BAS and LAS in BEA (12.5).

The increasing load (0.5-8 tonnes) used to prepare the discs leads to a decrease in the intensity of the peak at ~3610 $cm^{-1}$ corresponding to Si-OH-Al groups and in consequence the peak related to BAS (~1545 $cm^{-1}$). This decrease is due to residual ammonia still present in the zeolite disc, which results from an incomplete activation during the pre-treatment step especially for discs prepared at excessive high loads. These results are observed not only for discs with higher mass (40 mg) as shown in Figure 2.8 but also for discs with lower mass (10 mg). The preparation conditions of the discs must be carefully controlled since zeolites are sensitive and their structure can be altered. The intensity of the transmitted light significantly depends on the optical path.

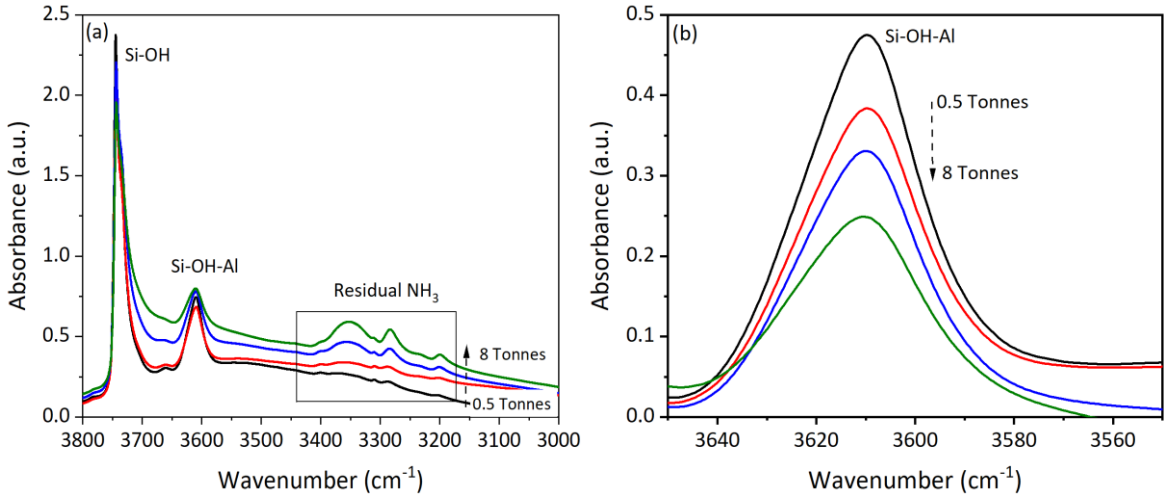


**Figure 2.8. (a)** FTIR spectra of the hydroxyl region following Py adsorption at 150°C of 40 mg BEA (12.5) discs prepared with different load (0.5-8 tonnes) **(b)** FTIR spectra of the Si-OH-Al peak at ~3610 $cm^{-1}$ of 40 mg BEA (12.5) discs prepared with different load (0.5-8 tonnes).

The results demonstrate that sample preparation and activation procedure needs to be carefully controlled to obtain quantitative data. Although the experimental data confirm the validity of Beer-Lambert law for solid materials, these experiments have been performed with BEA zeolite, which is a zeolite with low scattering at the mid-IR range. For materials with stronger scatter IR radiation, the sample density used for the measurements should be limited to 10 $mg/cm^2$ to ensure both good quality and quantitative nature of the FTIR measurements. Additionally, the pressure applied while making the self-supported discs

should be kept to a minimum, below 0.5 tonne/cm$^2$, as a higher pressure can lead to the incomplete sample activation and structural damage in extreme cases. To obtain accurate measurements of ε values using the Beer-Lambert law it is essential the carefully design of the experimental conditions.

## 2.4 Calculation of molar absorption coefficients using in situ FTIR spectroscopy

Quantitative addition of Py was performed for all samples to obtain the amount of Py necessary to saturate all acid sites ($n_{total}$) in each sample, as shown in Figure 2.2. The integrated areas of the peaks corresponding to Py adsorbed on BAS (Py-$H^+$) and LAS (Py-L) and $n_{total}$, for each sample under investigation, were plotted in Figure 2.9, according to Equation 2.7. Three or four data points for each zeolite were obtained using zeolites calcined at different temperatures, which allow the investigation of the same structure but with samples with different BAS/LAS ratios. The $\varepsilon_{BAS}$ and $\varepsilon_{LAS}$ were evaluated from the plotted trendlines where $-\frac{\varepsilon_{BAS}}{\varepsilon_{LAS}}$ is the gradient and $\varepsilon_{BAS}$ is the y-intercept, being expressed in cm/μmol (Table 2.2).

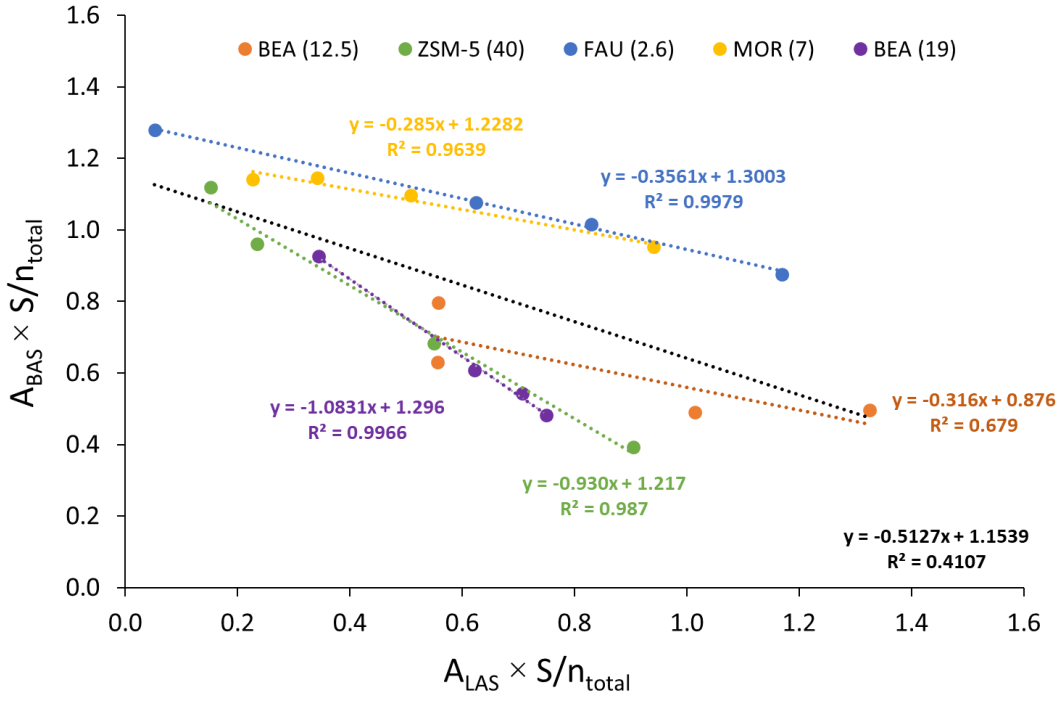


**Figure 2.9.** Determination of molar absorption coefficients for Py in BAS and LAS on various zeolites obtained by *in situ* FTIR experiments.

**Table 2.2**. Summary of the molar absorption coefficients for Py in BAS and LAS on various zeolites obtained by *in situ* FTIR experiments.

| Zeolites | $\varepsilon_{BAS}$ (cm/μmol) | $\varepsilon_{LAS}$ (cm/μmol) | $\varepsilon_{BAS}/\varepsilon_{LAS}$ |
|---|---|---|---|
| **BEA (12.5)** | 0.88 | 2.77 | 0.32 |
| **BEA (19)** | 1.30 | 1.20 | 1.08 |
| **ZSM-5 (40)** | 1.22 | 1.31 | 0.93 |
| **MOR (7)** | 1.23 | 4.31 | 0.29 |
| **Y (2.6)** | 1.30 | 3.65 | 0.36 |
| **Average** | 1.18 | 2.65 | - |
| **StDev** | 0.18 | 1.39 | - |

Both $\varepsilon_{BAS}$ and $\varepsilon_{LAS}$ values are different for different zeolites; this indicates that ε values are dependent on the zeolite structure, which disagrees with the assumptions of Emeis [13] and Gould et al. [33]. The $\varepsilon_{BAS}$ value obtained for BEA (12.5) is much lower than the values for other zeolites. This is probably due to the presence of a high number of LAS and weakly acidic groups (most likely Si-OH groups) in this zeolite structure. The value of $\varepsilon_{LAS}$ varies from 1.20 to 3.87 cm/μmol, which could be due to the different nature of LAS existing in the different zeolite materials and a significant experimental error.

Although both $\varepsilon_{BAS}$ and $\varepsilon_{LAS}$ values can be calculated from FTIR *in situ* experiments, the values are strongly dependent on the zeolite, the nature of the acid sites and the presence of weak acid sites such as Si-OH and Al-OH groups. The assumption that one type of BAS and one type of LAS is present within the zeolite structure must be made when considering Equation 2.7. However, in practice, this is not true in the majority of cases. For instance, a significant number of defect sites are present in zeolite BEA, such as Si-OH and Al-OH groups with weak or moderately strong Brønsted acidity, while the nature of Lewis acidity is still under discussion. Another limitation with this method is the lack of knowledge of the real amount of Py which is chemisorbed on the zeolite disc. An unknown amount of Py can be adsorbed on the walls of the IR cell at the same time as it is chemisorbed, leading to an

inaccurate determination of the amount of probe molecule interacting with each type of acid site (BAS and LAS) and strongly affecting the calculations [40,42]. Therefore, it is ideal to obtain a direct measurement of disc mass changes and IR analysis (AGIR set up) during the adsorption of the probe molecule to allow the evaluation of a more precise $\varepsilon_{BAS}$ and $\varepsilon_{LAS}$ values.

## 2.5 Calculation of molar absorption coefficients using AGIR

The new combination technique offers the possibility to measure the quantitative relationship between the amount of adsorbed species and the intensities for its characteristic adsorption bands (Figures 2.10). Adsorption of Py at 150°C (Figure 2.10 a and b) using the AGIR system on BEA (12.5) zeolite leads to the formation of peaks at 1545 and 1456 $cm^{-1}$ corresponding to Py-$H^+$ and (pyridinium ions, BAS) and Py-L (coordinated to LAS), respectively.

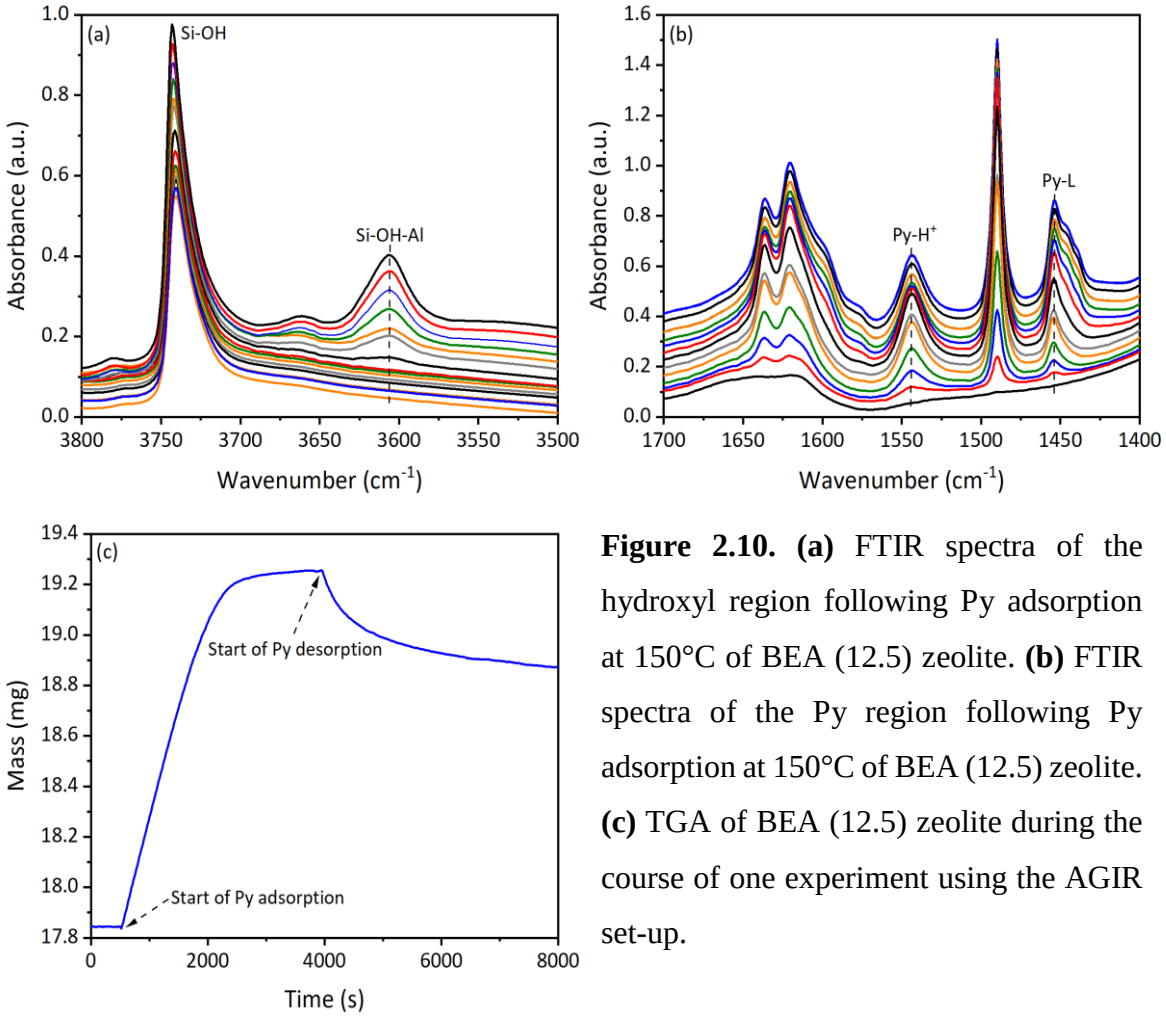


**Figure 2.10. (a)** FTIR spectra of the hydroxyl region following Py adsorption at 150°C of BEA (12.5) zeolite. **(b)** FTIR spectra of the Py region following Py adsorption at 150°C of BEA (12.5) zeolite. **(c)** TGA of BEA (12.5) zeolite during the course of one experiment using the AGIR set-up.

The increase of the amount of Py in the system increases the intensity of Py-$H^+$ and Py-L peaks until saturation is achieved (no changes in the peaks is observed). The IR data acquired using this set-up is in agreement with spectral observations obtained by *in situ* FTIR spectroscopy. The mass of the sample disc is monitored during the course of the experiment (Figure 2.10 c). An increase of the disc mass can be observed over time due to Py species formation. This parallel increase of disc mass and the intensity of IR peaks with the Py amount allow a direct calculation of ε values.

### 2.5.1 Effect of physisorbed Py species

Py adsorption on zeolites is typically performed at 30-150°C followed by the removal of physisorbed Py species, which are held on the zeolite surface by weak hydrogen-bonding and van-der-Waals interactions giving rise to the peaks at 1585-1595 and 1438-1445 $cm^{-1}$ [1,43]. The effect of physisorbed Py on the intensity of the IR bands is exemplified by the spectra obtained for BEA zeolite after Py desorption at 150°C (Figure 2.11).

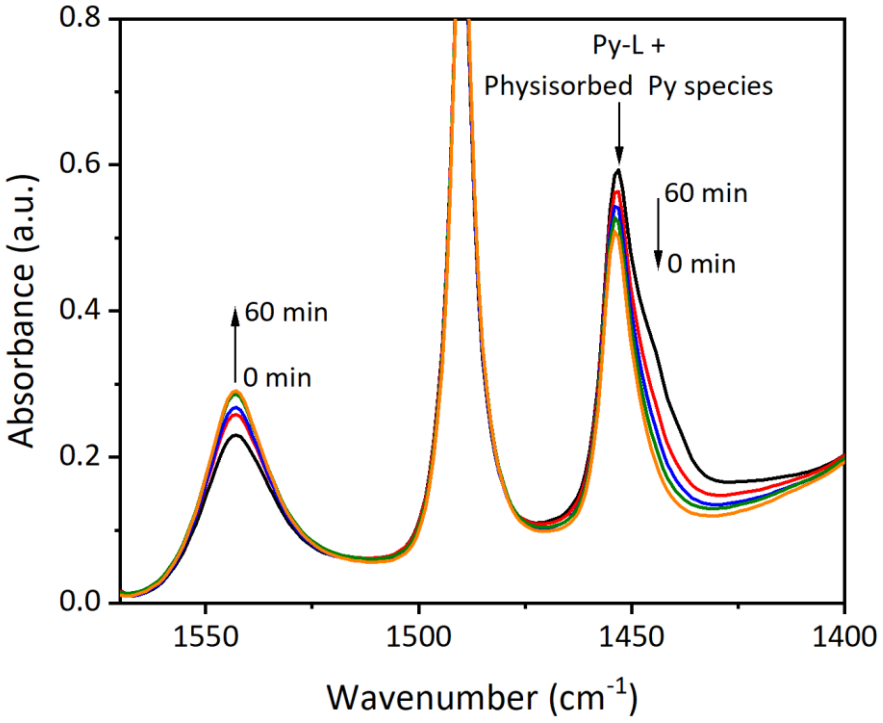


**Figure 2.11.** Difference FTIR spectra of Py region following Py adsorption at 150°C on BEA (12.5) zeolite after desorption over 60 min.

Over ~60 minutes, the intensity of the peak shoulder at ~1440 $cm^{-1}$ decreases, indicating that the physisorbed Py species are being removed at 150°C. At the same time, the TG signal shows a ~27% decrease (from 850 to 615 μmol/g), but the intensity of the peak corresponding to Py-$H^+$ species at ~1545 $cm^{-1}$ increases by ~25%. These observations can be explained by a "solvent" effect, as weakly bound Py molecules reduce the transient dipole moment of the protonated Py-$H^+$ species (probably, by forming Py···Py-$H^+$ complexes, in which the N-atom of the Py molecule forms a H-bond with the pyridinium ion) that would cause a decrease in the value of $\varepsilon_{BAS}$. These data demonstrate that the removal of physisorbed Py species should be conducted at 150-200°C (depending on the zeolite) by purging or evacuating the system and should be monitored to ensure the accuracy of acidity measurements and the one-to-one interaction between Py and BAS.

### 2.5.2 Effect of the resolution

Table 2.1 shows the significant differences in the experimental approaches described by different laboratories, especially the resolution at which the IR spectra are collected. The usual resolution used is 4 $cm^{-1}$, however, depending on the research laboratory, the values utilised vary from 1 to 4 $cm^{-1}$ or are not mentioned (Table 2.1) and this could be one of the factors leading to discrepancies in the literature values.

The effect of the use of different resolutions on both Py-$H^+$ and Py-L peaks was studied using BEA (19) zeolite after adsorption of Py at 150°C (Figure 2.12). The main differences can be observed in the shape of both peaks of Py-$H^+$ and Py-L. However, this effect is more pronounced in the intensity of the Py-L peak for spectra collected at higher resolutions (Table 2.3).

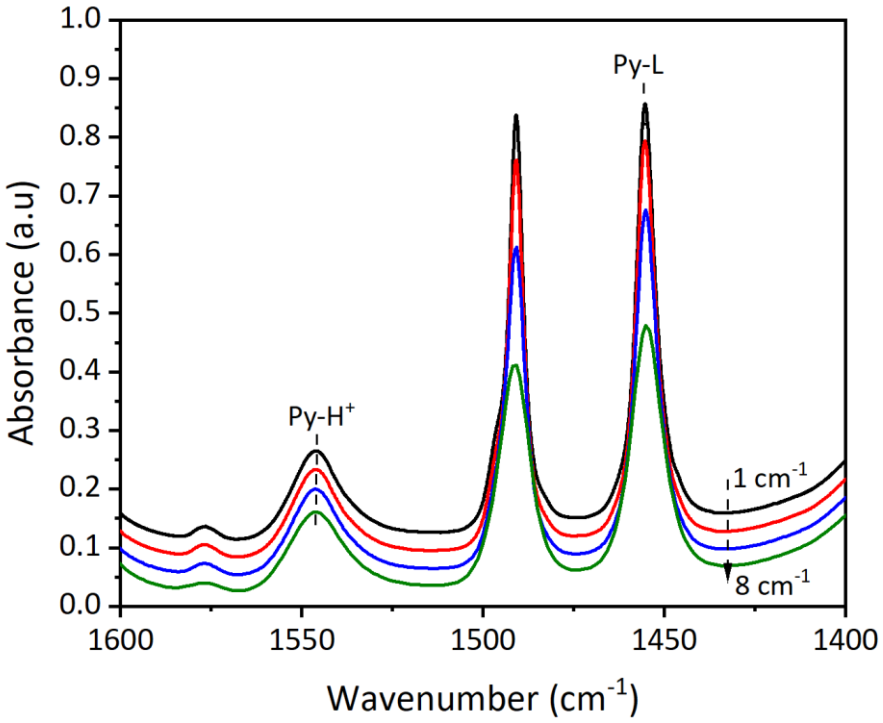


**Figure 2.12.** Difference spectra of Py region following Py adsorption at 150°C of BEA (19). Spectra collected at different resolutions (1-8 $cm^{-1}$).

**Table 2.3.** Integration of the peaks areas and heights of Py-$H^+$ and Py-L (at ~1545 and at ~1456 $cm^{-1}$, respectively) of BEA (19). Spectra collected at different resolutions from 1 to 8 $cm^{-1}$.

| **Resolution** | **Peak Area** | | **Peak height** | |
|---|---|---|---|---|
| **$cm^{-1}$** | **BAS** | **LAS** | **BAS** | **LAS** |
| **1** | 2.52 | 5.40 | 0.15 | 0.70 |
| | - | - | - | - |
| **2** | 2.51 | 5.30 | 0.14 | 0.67 |
| | 0.6% | 1.9% | 0.7% | 4.7% |
| **4** | 2.50 | 5.08 | 0.14 | 0.58 |
| | 0.6% | 5.9% | 2.8% | 17.1% |
| **8** | 2.43 | 4.63 | 0.13 | 0.41 |
| | 3.5% | 14.3% | 10.3% | 41.3% |

Integration of both peaks (Table 2.3) shows noticeable experimental errors associated with the spectroscopic data collected at different resolutions, especially when the measurements are done by the peak height (~17% for Py-L at 4 $cm^{-1}$ of resolution). It is best

to compare results obtained under the same conditions, but when this is not possible it is better to use measurements obtained by peak area instead of peak height.

### 2.5.3 Effect of the temperature

The temperature of the measurements has a very significant effect on the calculation of ε values (Figure 2.13). With the increase in the temperature of the measurements (temperature of the sample in the IR cell), both peaks of Py-$H^+$ and Py-L become boarder and their peak intensity decreases. As the temperature increases by 100°C the Py-$H^+$ peak shifts by 2 $cm^{-1}$ and Py-L peak shifts by 1 $cm^{-1}$.

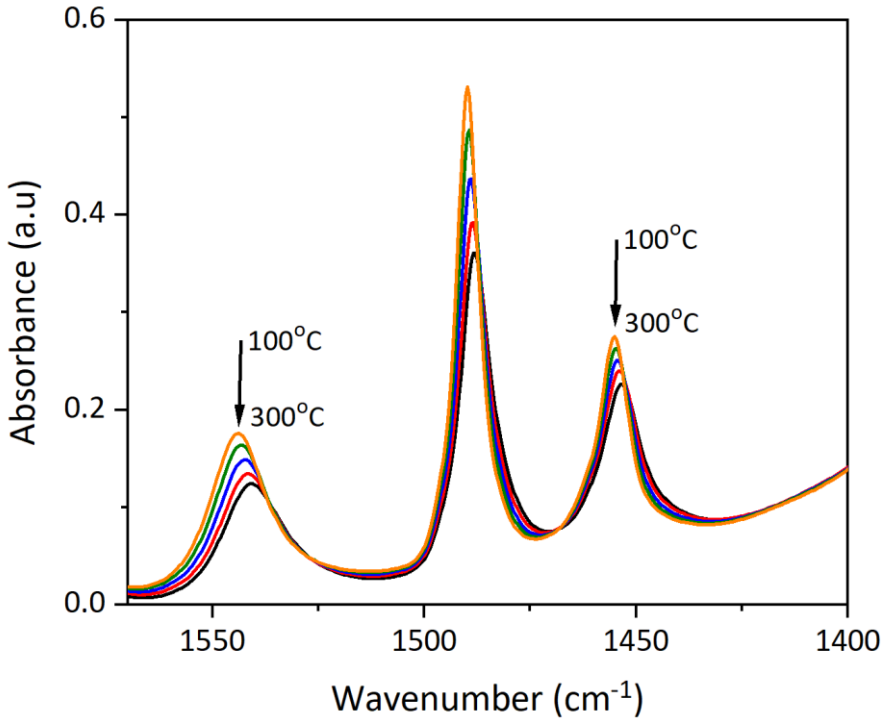


**Figure 2.13.** Difference spectra of Py region following Py adsorption at 150°C of BEA (12.5) after desorption at increasing temperatures (100-300°C).

These results are evidence that $\varepsilon_{BAS}$ and $\varepsilon_{LAS}$ values obtained will be different depending on the temperature of the measurements, which disagrees with previous assumptions [13]. Furthermore, as indicated in Table 2.1, the experimental temperature used for adsorption of Py is often not specified in many published reports, which can introduce another source of error in the calculation of the number of acid sites using this literature data of the molar adsorption coefficients.

### 2.5.4 Molar absorption coefficients

The integrated areas of the peaks corresponding to Py adsorbed on BAS and LAS and $n_{total}$ (obtained by TGA), for each material under investigation, were used to calculate $\varepsilon_{BAS}$ and $\varepsilon_{LAS}$ values according to the Beer-Lambert law (Equation 2.1). The obtained values at different temperatures were plotted (e.g. Figure 2.14).

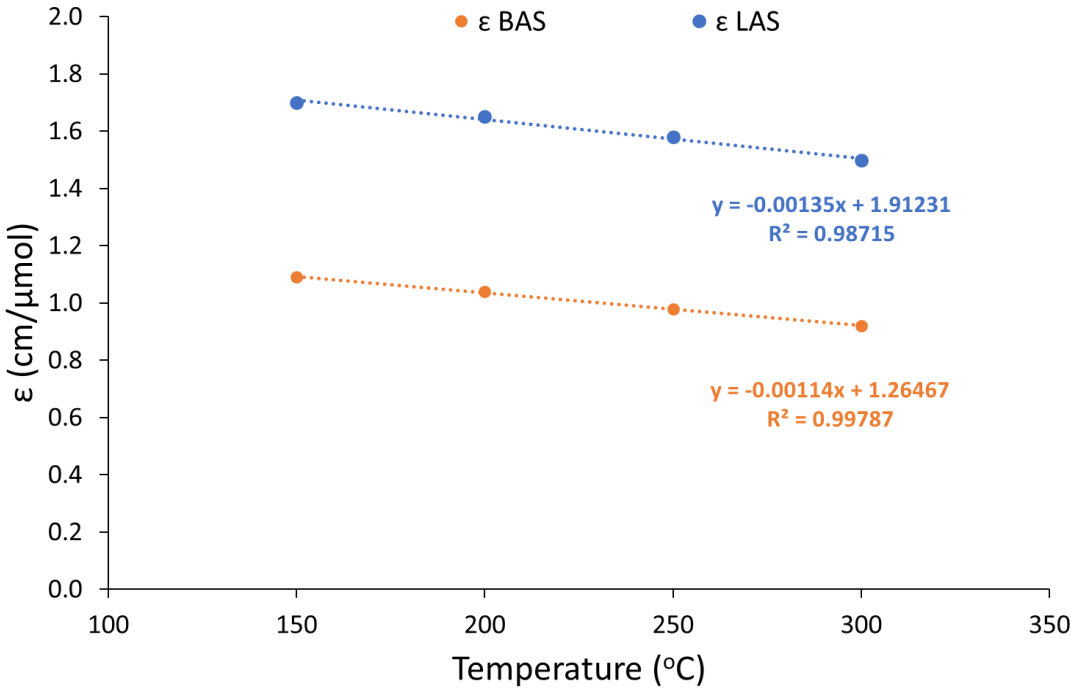


**Figure 2.14.** Molar absorption coefficients for Py on BAS and LAS on ZSM-5 (40) zeolite obtained using AGIR experiments.

The ε values for other zeolite materials were also obtained using the same approach, (Table 2.4). As the presence of both BAS and LAS in the same sample can interfere with the calculations, to obtain ε values directly and minimise experimental errors, measurements of $\varepsilon_{BAS}$ and $\varepsilon_{LAS}$ values were carried out separately. Zeolites with only BAS (e.g. ZSM-5 (40)) were used to calculate $\varepsilon_{BAS}$ and zeolites with only LAS were used to calculate $\varepsilon_{LAS}$ (e.g. ϒ-alumina).

**Table 2.4.** Summary of the molar absorption coefficients extrapolated to 90°C for Py on BAS and LAS on various zeolites obtained by AGIR experiments.

| Zeolites | $\varepsilon_{BAS}$ (cm/μmol) | $\varepsilon_{LAS}$ (cm/μmol) |
|---|---|---|
| **ZSM-5 (40)** | 1.16±0.08 | - |
| **BEA (12.5)** | 1.19±0.16 | - |
| **MOR (7)** | 1.38±0.04 | - |
| **Y (2.6)** | 1.64±0.15 | - |
| **ɣ-alumina** | - | 1.87±0.1 |
| **Na/ZSM-5 (40)** | - | 1.88±0.2 |

The $\varepsilon_{BAS}$ values vary from 1.16 to 1.64 cm/μmol confirming the dependence of these values on the zeolitic structure. The Si/Al ratios, confinement effects and the number and nature of both BAS and LAS are expected to influence the calculations and be responsible for the differences in the values. The discrepancies in the values are lower when compared with the results obtained by *in situ* FTIR experiments (Section 2.4). $\varepsilon_{LAS}$ values are less affected by these factors, as the values obtained for $Al_2O_3$ and Na/ZSM-5 are very similar.

The values obtained in this section were used on the quantitative measurements of acid sites presented in the following chapters of this thesis.

## 2.6 Summary

In this study, a method was developed for calculating more accurate $\varepsilon_{BAS}$ and $\varepsilon_{LAS}$ values for Py species adsorbed onto a different range of zeolitic structures. Studies on the Beer-Lambert law confirmed that this law is valid for IR studies of zeolites and made evident that to obtain precise measurements, it is necessary to carefully design and give attention to the experimental details. The quantitative measurements using *in situ* FTIR experiments demonstrated the dependency of the calculations on the zeolitic structure and the importance of knowing the exact amount of Py chemisorbed on the sample disc. The quantitative measurements using the AGIR system allowed a more precise and direct determination of both $\varepsilon_{BAS}$ and $\varepsilon_{LAS}$ values for different zeolitic structures. The Si/Al ratio, confinement

effects, number and nature of both BAS and LAS, adsorption temperature, physisorbed species and experimental set-up are the most important factors which can affect the calculations of these values.

Despite the significant progress made in the calculation of ε values, this work could be further extended to the evaluation of other zeolite materials containing different types of BAS and LAS and studies about the effect of acid site strength on the values of ε. The experimental $\varepsilon_{BAS}$ and $\varepsilon_{LAS}$ values obtained in this project should expand the accuracy of the quantitative analysis of acid sites of different zeolite-based catalysts using IR spectroscopy.

## 2.7 References


[1] K. Hadjiivanov. *Identification and characterization of surface hydroxyl groups by infrared spectroscopy*. Adv. Catal., 2014, 57, 99-318.

[2] S. Khabtou, T. Chevreau and J. C. Lavalley. *Quantitative infrared study of the distinct acidic hydroxyl groups contained in modified Y zeolites.* Microporous Mater., 1994, 3, 133-148.

[2] C. Morterra, G. Magnacca and V. Bolis. *On the critical use of molar absorption coefficients for adsorbed species: the methanol/silica system.* Catal. Today., 2001, 70, 2001, 43-58.

[3] M. R. Basila, T. R. Kantner and K. H. Rhee. *The nature of the acidic sites on a silica-alumina. Characterization by infrared spectroscopic studies of trimethylamine and pyridine chemisorption.* J. Phys. Chem, 1964, 68 (11), 3197-3207.

[4] M. R. Basila and T. R. Kantner. *The nature of the acidic sites on silica-alumina. A revaluation of the relative absorption coefficients of chemisorbed pyridine*. J. Phys. Chem., 1966, 70 (6) 1681-1682.

[5] T. R. Hughes and H. M. White. *Study of the surface structure of decationized Y zeolite by quantitative infrared spectroscopy.* J. Phys. Chem., 1967, 71 (7), 2192-2201.

[6] F. R. Cannings. *Acidic sites on mordenite. An infrared study of adsorbed pyridine*. J. Phys. Chem., 1968, 72 (13) 4691-4693.

[7] M. Lefrancois and G. Malbois. *The nature of the acidic sites on mordenite. Characterization of adsorbed pyridine and water by infrared study*. J. Catal., 1971, 20, 350-358.

[8] J. Datka. *Transformations of but-1-one molecules adsorbed in NaHY zeolites studied by infrared spectroscopy.* J.C.S Faraday I., 1980, 76, 2437-2447.

[9] J. Datka. *Dehydroxylation of NaHY zeolites studied by infrared spectroscopy.* J. Chem. Soc., Faraday Trans., 1, 1981, 77, 2877-2881.

[10] J. Take, T. Yamaguchi, K. Miyamoto, H. Ohyama, and M. Misono, *Brønsted site population on external and on internal surface of shape-selective catalysts*. Stud. Surf. Sci. Catal., 1986, 28, 495-502.

[11] J. Datka, A. M. Turek, J. M. Jehng and I. E. Wachs. *Acidic properties of supported niobium oxide catalysts: An infrared spectroscopy investigation.* J. Catal., 1992, 135 (1), 186-199.

[12] C. A. Emeis. *Determination of integrated molar extinction coefficients for infrared adsorption bands of pyridine adsorbed on solid acid catalysts.* J. Catal., 1993, 141 (2), 347-354.

[13] I. Kiricsi, C. Flego, G. Pazzuconi, W. O. Jr. Parker, R. Millini, C. Perego and G. Bellussi. *Progress toward understanding zeolite β acidity: An IR and $^{27}$Al NMR spectroscopic study.* J. Phys. Chem., 1994, 98, 4627-463.

[14] M. A. Makarova, K. Karim and J. Dwyer. *Limitation in the application of pyridine for quantitative studies of Brønsted acidity in relatively aluminous zeolites.* Microporous Mater., 1995, 4, 243-246.

[15] M. Maache, A. Janin, J. C. Lavalley and E. Benazzi. *FT infrared study of Brønsted acidity of H-mordenites: heterogeneity and effect of dealumination.* Zeolites., 1995, 15, 507-516.

[16] J. Datka, B. Gil and A. Kubacka. *Heterogeneity of OH groups in H-mordenites: Effect of dihydroxylation.* Zeolites., 1996, 17, 428-433.

[17] M. Guisnet, P. Ayrault, C. Coutanceau, M. F. Alvarez and J. Datka. *Acid properties of dealuminated beta zeolites studied by IR spectroscopy.* J. Chem. Soc., Faraday Tran., 1997, 93 (8), 1661-1665.

[18] B. Sulikowski, J. Datka, B. Gil, J. Ptaszynski and J. Klinowski. *Acidity and catalytic properties of realuminated zeolite Y.* J. Phys. Chem. B, 1997, 101, 6929-6932.

[19] M. Guiset, P. Ayrault and J. Datka, *Acid properties of mazzite zeolites studied by IR spectroscopy.* Microporous Mesoporous Mater., 1998, 20, 283-291.

[20] A. Taouli, A. Klemt, M. Breede and W. Reschetilowski. *Acidity investigations and determination of integrated molar extinction coefficients for infrared adsorption bands of ammonia adsorbed on acidic sites of MCM-41*. Stud. Surf. Sci. Catal., 1999, 125, 307-314.

[21] E. Selli and L. Forni. *Comparison between the surface acidity of solid catalysts determined by TPD and FTIR analysis of pre-adsorbed pyridine.* Microporous Mesoporous Mater., 1999, 31, 129-140.

[22] F. Thibault-Starzyk, B. Gil, S. Aiello, T. Chevreau and J. P Gilson. *In situ thermogravimetry in an infrared spectrometer: an answer to quantitative spectroscopy of adsorbed species on heterogeneous catalysts.* Microporous Mesoporous Mater., 2004, 67, 107-112.

[23] K. Góra-Marek, M. Derewinski, P. Sarv and J. Datka. *IR and NMR studies of mesoporous alumina and related aluminosilicates.* Catal. Today, 2005, 101, 131-138.

[24] K. Góra-Marek, J. Datka, S. Dzwigaj and M. Che. *Influence of V content on the nature and strength of acidic sites in VSiβ zeolite evidenced by IR spectroscopy.* J. Phys. Chem. B., 2006, 110, 6763-6767.

[25] B. Gil, G. Kosová and J. Cejka, *Acidity of MCM-58 and MCM-68 zeolites in comparison with some other 12-ring zeolites.* Microporous Mesoporous Mater., 2010, 129, 256-266.

[26] I. S. Pieta, M. Ishaq, R. P. K. Wells and J. A. Anderson. *Quantitative determination of acid sites on silica–alumina.* Appl. Catal. A., 390 (2010) 127-134.

[27] J. M. R. Gallo, C. Bisio, G. Gatti, L. Marchese and H. O. Pastore. *Physicochemical characterization and surface acid properties of mesoporous [Al]-SBA-15 obtained by direct synthesis*. Langmuir., 2010, 26 (8), 5791-5800.

[28] E. J. M Hensen, D. G. Poduval, V. Degirmenci, D. A. J. M. Ligthart, W. Chen, F. Maugé, M. S. Rigutto and J. A. Rob van Veen. *Acidity characterization of amorphous silica-alumina.* J. Phys. Chem. C., 2012, 116, 21416-21429.

[29] J. W. Harris, M. J. Cordon, J. R. Di Iorio, J. C. Vega-Vila, F. H. Ribeiro and R. Gounder. *Titration and quantification of open and closed Lewis acid sites in Sn-Beta zeolites that catalyze glucose isomerization.* J. Catal., 2016, 335, 141-154.

[30] I. Miletto, G. Paul, S. Chapman, G. Gatti, L. Marchese, R. Raja and E. Gianotti. *Mesoporous silica scaffolds as precursor to drive the formation of hierarchical SAPO-34 with tunable acid properties*. Chem. Eur. J., 2017, 23, 9952-9961.

[31] K. A. Tarach, K. Góra-Marek, J. Martinez-Triguero and I. Melián-Cabrera, *Acidity and accessibility studies of desilicated ZSM-5 zeolites in terms of their effectiveness as catalysts in acid-catalyzed cracking processes.* Catal. Sci. Technol., 2017, 7, 858-873.

[32] N. S. Gould and B. Xu. *Quantification of acid site densities on zeolites in the presence of solvents via determination of extinction coefficients of adsorbed pyridine*. J. Catal., 2018, 358, 80-88.

[33] N. S. Nesterenko, F. Thibault-Starzyk, V. Montouilliout, V. V. Yushchenko, C. Fernandez, J. P. Gilson, F. Fajula and I. I. Ivanova. *The use of the consecutive adsorption of pyridine bases and carbon monoxide in the IR spectroscopic study of the accessibility of acid sites in microporous/mesoporous materials*. Kinet. Katal., 2006, 47, (1), 45; translated into English in Kinet. Catal., 2006, 47, (1), 40-48.

[34] K. Góra-Marek, K. Tarach and M. Choi. *2,6-di-tert-butylpyridine sorption approach to quantify the external acidity in hierarchical zeolites.* J. Phys. Chem. C, 2014, 118, (23), 12266-12274.

[35] T. Onfroy, G. Clet and M. Houalla. *Quantitative IR characterization of the acidity of various oxide catalysts.* Microporous Mesoporous Mater., 2005, 82, (1-2), 99-104.

[36] B. Wichterlová, Z. Tvarkuzová, Z. Sobalík and P. Sarv. *Determination and properties of acid sites in H-ferrierite. A comparison of ferrierite and MFI structures*. Microporous Mesoporous Mater., 1998, 24, 223-233.

[37] A. A. Gabrienko, I. G. Danilova, S. S. Arzumanov, L.V. Pirutko, D. Freude, and A. G. Stepanov. *Direct measurement of zeolite Brønsted acidity by FTIR spectroscopy: Solid-State $^{1}H$ MAS NMR approach for reliable determination of the integrated molar absorption coefficients.* J. Phys. Chem. C., 2018, 122, 25386-25395.

[38] P. Bräuera, P. L. Nga, O. Situmoranga, I. Hitchcock and C. D'Agostino. *Effect of Al content on number and location of hydroxyl acid species in zeolites: A DRIFTS quantitative protocol without the need for molar extinction coefficients*. RSC Adv., 2017, 7, 52604-52613.

[39] P. Bazin, A. Alenda and F. Thibault-Starzyk. *Interaction of water and ammonium in NaHY zeolite as detected by combined IR and gravimetric analysis (AGIR).* Dalton Trans., 2010, 39 (36), 8432-8436.

[40] S. Bordiga, C. Lamberti, F. Bonino, A. Travert and F. Thibault-Starzyk. *Probing zeolites by vibrational spectroscopies*. Chem. Soc. Rev., 2015, 44 (20), 7262-7341.

[41] V. Bolis, G. Magnacca, G. Cerrato and C. Monterra. *Microcalorimetric and IR-spectroscopic study of the room temperature adsorption of $CO_2$ on pure and sulphated t-ZrO2*. Themochim. Acta, 2001, 379, 147-161.

[42] A. Popov, E. Kondratieva, J. M. Goupil, L. Mariey, P. Bazin J-P. Gilson, A. Travert and F. Maugé. *Bio-oils hydrodeoxygenation: Adsorption of phenolic molecules on oxidic catalyst supports.* J. Phys. Chem. C., 2010, 114, 15661- 15670.

[43] L. M. Parker, D. M. Bibby and G. R. Burns. *Fourier-transform infrared study of pyridine sorbed on zeolite HY*. J. Chem. Soc. Faraday Trans., 1991, 87 (19), 3319-3323.

# Chapter 3 Thermal stability of ZSM-5 and BEA zeolites

## 3.1 Introduction

The diversity of reactions catalysed by zeolites relates to their acid-base character, indeed H-form zeolites represent one of the most important classes of materials applied in industry as catalysts [1-3]. Recently, there has been a great deal of interest in the development of solid Lewis acid catalysts for processes involving biomass conversion [4,5], isomerisation [6] and gaseous ozone elimination [7]. One of the developments in zeolite catalysis has come from the recognition that metal-containing zeolites are highly active and stable catalysts. Zeolites containing transition metals find applications as redox catalysts [8,9], while zeolites containing alkali metals and alkaline earth metals are used as industrial adsorbents for gas purification [10-13], production of membranes for gas separation [14] and as ion exchangers for water softening [15]. Cationic zeolites can also be used in heterogeneous catalysis as stable supports for other catalytic active phases [16-18] and more recently in biomass conversion [19-21].

The acid-base characteristics and structural properties of zeolites are very much dependent on the type and severity of post-synthesis modifications. These modifications tune the physicochemical and acidity characteristics favourable for a particular application and are important steps in the preparation of a stable and active catalyst. Thermal treatment is one of the most common post-synthesis modification methods [22,23] and for this reason, the understanding of zeolite behaviour upon heating is of particular importance since sorptive, catalytic and molecular sieve properties are often altered during calcination and under operating conditions [24]. Additionally, zeolite activation and regeneration requires thermal treatments, which can cause their structural degradation and the loss of catalytic activity and selectivity. Thermal treatment often leads to a removal of aluminium (Al) atoms from the zeolite framework (dealumination) accompanied by the formation of Lewis acid sites (LAS, extra-framework Al species), resulting in a change in the number and strength

of the acid sites [25,26]. This post-synthesis modification is the main cause of the formation of framework defects and silanol groups (Si-OH). Besides changes in the acidic properties, dealumination by calcination also affect the zeolite pore network resulting in a gradual collapse of the structure and pore blockage by aggregated forms of Al [27-30]. Cation introduction into zeolites may also require a thermal treatment, which leads to the decomposition of the salts used and redistribution of cationic species in the cavities of the zeolite [16]. It is essential to verify the thermal stability of the zeolite under investigation, knowing that these properties are significantly dependent on the framework topology, Si/Al ratio, Al distribution and the nature and number of the cation [22,25]. Thermal stability of zeolites is generally very high, and in the absence of water vapour, many zeolites can be heated to temperatures of 800°C without loss of crystallinity or recrystallisation to denser phases. Typically high-silica zeolites (e.g. ZSM-5), are more stable than low-silica zeolites (e.g. USY) [24,25,29,31]. Higher thermal stability of a zeolite structure can be achieved through ion exchange with multivalent cations.

Systematic quantitative studies that explore how thermal treatment affects the properties of commercial and cation-containing zeolites are rare. In this work, a detailed investigation of the thermal stability of thermally treated and cation-containing zeolites was carried out by combining different characterisation techniques. The main goal was to obtain information on their structural, textural, and acidic properties, with particular emphasis on quantitative measurements of the different types of active sites in two zeolitic structures, BEA and ZSM-5 containing common metal cations ($Na^+$, $K^+$, $Ca^{2+}$, and $Mg^{2+}$). The results should provide new insights into ZSM-5 and BEA structural stability and acidity changes at temperatures relevant to different catalytic reactions and zeolite regeneration.

## 3.2 Experimental

### 3.2.1 Zeolite modification

***Thermal treatment***

Ammonium forms of zeolites BEA (CP814E, BEA framework, Si/Al=12.5) and ZSM-5 (CBV8014, MFI framework, Si/Al=40) were obtained from *Zeolyst International* in powder form. The two zeolite structures were calcined at different temperatures (450ºC, 600ºC, 700ºC, 800ºC and 900ºC) in a muffle furnace for 5 hours. The samples are reported in Table 3.1 and the calcination profile is shown in Figure 3.1.

**Table 3.1.** BEA and ZSM-5 zeolites prepared using different temperature.

| **Calcination temperature (°C)** | **BEA (12.5) samples** | **ZSM-5 (40) samples** |
|---|---|---|
| **-** | BEA | ZSM-5 |
| **450** | BEA 450ºC | ZSM-5 450ºC |
| **600** | BEA 600ºC | ZSM-5 600ºC |
| **700** | BEA 700ºC | ZSM-5 700ºC |
| **800** | BEA 800ºC | ZSM-5 800ºC |
| **900** | BEA 900ºC | ZSM-5 900ºC |

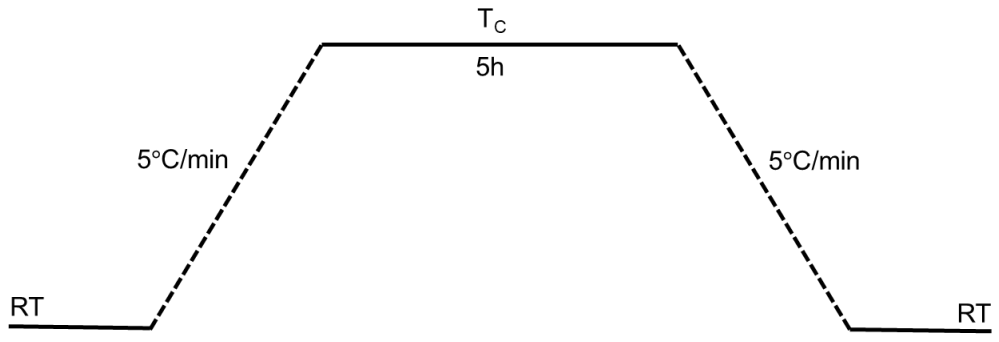


**Figure 3.1.** Calcination temperature profile.

***Incipient wetness impregnation***

Cation-containing zeolites modified by incipient wetness impregnation were prepared at Keele University. The impregnation was performed with aqueous solutions of potassium nitrate ($KNO_3$, Alfa Aesar, 99%), sodium nitrate ($NaNO_3$, Alfa Aesar, 98%), calcium nitrate ($Ca(NO_3)_2\,4H_2O$, Lancaster Synthesis, 99%) and magnesium nitrate ($Mg(NO_3)_2\,6H_2O$, Alfa Aesar, 98%). The cation-containing zeolites were prepared from aqueous solutions of nitrate salt with a ratio 1mL/1g ZSM-5 and 1.5mL/1g BEA. The solution concentrations were calculated so that different quantities of cations would be incorporated (25, 50 and 100% of cation per Al atom; e.g. 1 K/BEA sample would contain 100% of $K^+$ or 1:1 K/Al). 4g of zeolite was introduced into a 50 mL beaker, and the aqueous solution of one of the nitrates was added dropwise at room temperature. The mixture was stirred for 15min and subsequently dried at 60ºC overnight. Finally, the cation-containing zeolites were calcined at the desired temperature (450ºC or 800ºC). The impregnation and subsequent calcinations were repeated for each parent zeolite using the same experimental conditions.

A "blank" impregnation was also completed with ammonium nitrate ($NH_4NO_3$, BHR, 99%) in order to evaluate the effect of the nitrate on both zeolitic structures. These experiments did not show any differences in the thermal stability between the parent and zeolites impregnated with $NH_4NO_3$. Tables 3.2 and 3.3 summarise the cation-containing zeolites prepared by impregnation.

**Table 3.2.** Cation-containing BEA zeolites prepared by impregnation followed by thermal treatment.

| Zeolite | Salt | $T_{calcination}$ (ºC) | Cation $_{Target}$ (%) | Cation/Al (EDX) | Zeolite ID |
|---|---|---|---|---|---|
| BEA | $KNO_3$ | 450 | 25 | 0.2 | 0.25 K/BEA-IM 450ºC |
| | | | 50 | 0.3 | 0.5 K/BEA-IM 450ºC |
| | | | 100 | 0.4 | 1 K/BEA-IM 450ºC |
| | | 800 | 25 | 0.2 | 0.25 K/BEA-IM 800ºC |
| | | | 50 | 0.3 | 0.5 K/BEA-IM 800ºC |
| | | | 100 | 0.4 | 1 K/BEA-IM 800ºC |
| | $NaNO_3$ | 450 | 25 | 0.2 | 0.25 Na/BEA-IM 450ºC |
| | | | 50 | 0.4 | 0.5 Na/BEA-IM 450ºC |
| | | | 100 | 0.5 | 1 Na/BEA-IM 450ºC |
| | | 800 | 25 | 0.2 | 0.25 Na/BEA-IM 800ºC |
| | | | 50 | 0.4 | 0.5 Na/BEA-IM 800ºC |
| | | | 100 | 0.5 | 1 Na/BEA-IM 800ºC |
| | $Ca(NO_3)_2\,4\,H_2O$ | 450 | 25 | 0.6 | 0.25 Ca/BEA-IM 450ºC |
| | | | 50 | 0.8 | 0.5 Ca/BEA-IM 450ºC |
| | | | 100 | 1.7 | 1 Ca/BEA-IM 450ºC |
| | | 800 | 25 | 0.6 | 0.25 Ca/BEA-IM 800ºC |
| | | | 50 | 0.8 | 0.5 Ca/BEA-IM 800ºC |
| | | | 100 | 1.7 | 1 Ca/BEA-IM 800ºC |
| | $Mg(NO_3)_2\,6\,H_2O$ | 450 | 25 | 0.3 | 0.25 Mg/BEA-IM 450ºC |
| | | | 50 | 0.9 | 0.5 Mg/BEA-IM 450ºC |
| | | | 100 | 1.7 | 1 Mg/BEA-IM 450ºC |
| | | 800 | 25 | 0.3 | 0.25 Mg/BEA-IM 800ºC |
| | | | 50 | 0.9 | 0.5 Mg/BEA-IM 800ºC |
| | | | 100 | 1.7 | 1 Mg/BEA-IM 800ºC |

**Table 3.3.** Cation-containing ZSM-5 zeolites prepared by impregnation followed by thermal treatment.

| Zeolite | Salt | $T_{calcination}$ (ºC) | $Cation_{Target}$ (%) | Cation/Al (EDX) | Zeolite ID |
|---|---|---|---|---|---|
| ZSM-5 | $KNO_3$ | 450 | 25 | 0.2 | 0.25 K/ZSM-5-IM 450ºC |
| | | | 50 | 0.4 | 0.5 K/ZSM-5-IM 450ºC |
| | | | 100 | 1.0 | 1 K/ZSM-5-IM 450ºC |
| | | 800 | 25 | 0.2 | 0.25 K/ZSM-5-IM 800ºC |
| | | | 50 | 0.4 | 0.5 K/ZSM-5-IM 800ºC |
| | | | 100 | 1.0 | 1 K/ZSM-5-IM 800ºC |
| | $NaNO_3$ | 450 | 25 | 0.3 | 0.25 Na/ZSM-5-IM 450ºC |
| | | | 50 | 0.6 | 0.5 Na/ZSM-5-IM 450ºC |
| | | | 100 | 0.8 | 1 Na/ZSM-5-IM 450ºC |
| | | 800 | 25 | 0.3 | 0.25 Na/ZSM-5-IM 800ºC |
| | | | 50 | 0.6 | 0.5 Na/ZSM-5-IM 800ºC |
| | | | 100 | 0.8 | 1 Na/ZSM-5-IM 800ºC |
| | $Ca(NO_3)_2$ 4 $H_2O$ | 450 | 25 | 0.3 | 0.25 Ca/ZSM-5-IM 450ºC |
| | | | 50 | 0.4 | 0.5 Ca/ZSM-5-IM 450ºC |
| | | | 100 | 0.9 | 1 Ca/ZSM-5-IM 450ºC |
| | | 800 | 25 | 0.3 | 0.25 Ca/ZSM-5-IM 800ºC |
| | | | 50 | 0.4 | 0.5 Ca/ZSM-5-IM 800ºC |
| | | | 100 | 0.9 | 1 Ca/ZSM-5-IM 800ºC |
| | $Mg(NO_3)_2$ 6 $H_2O$ | 450 | 25 | 0.2 | 0.25 Mg/ZSM-5-IM 450ºC |
| | | | 50 | 0.6 | 0.25 Mg/ZSM-5-IM 800ºC |
| | | | 100 | 0.8 | 0.5 Mg/ZSM-5-IM 450ºC |
| | | 800 | 25 | 0.2 | 0.25 Mg/ZSM-5-IM 800ºC |
| | | | 50 | 0.6 | 0.5 Mg/ZSM-5-IM 800ºC |
| | | | 100 | 0.8 | 1 Mg/ZSM-5-IM 800ºC |

***Ion exchange***

Cation-containing zeolites modified by ion exchange were prepared at Keele University. The modification was carried out with aqueous solutions of potassium nitrate ($KNO_3$, Alfa Aesar, 99%), sodium nitrate ($NaNO_3$, Alfa Aesar, 98%), calcium nitrate ($Ca(NO_3)_2$ $4H_2O$, Lancaster Synthesis, 99%) and magnesium nitrate ($Mg(NO_3)_2$ $6H_2O$, Alfa Aesar, 98%). 4g of the zeolite were added to 20 mL of an aqueous solution of each nitrate salt at room temperature, where different quantities of cations were incorporated (25, 50 and 100% of cation per Al atom; e.g. 1 K/BEA contains 100% of $K^+$ or 1:1 K/Al). The mixture was stirred for 24h followed by centrifugation to separate the solid, washed with deionised

water and dried in an oven at 80°C for 24h. Subsequently, the cation-containing zeolites were calcined at the desired temperatures (450ºC and 800ºC). The ion exchange and subsequent calcinations were repeated for each parent zeolite using the same experimental conditions.

### 3.2.2 Zeolite characterisation

A comprehensive structural characterisation of selective materials was carried out using powder X-ray diffraction (XRD), scanning and transmission electron microscopy with an EDX analytical system (SEM-EDX), argon (Ar) physisorption, $^{27}$Al solid-state NMR and FTIR spectroscopy using pyridine (Py) as probe molecule.

Py-FTIR experiments and SEM-EDX analyses are detailed described in Chapter 2. For the quantification of the zeolite acidic properties using adsorption of Py, the values of the molar absorption coefficients applied were those obtained in Chapter 2. The quantification of cationic species was obtained by deconvolution of the peaks in the range 1460-1420 cm$^{-1}$ using a mixed Gaussian-Lorentzian function in OMNIC software and the molar absorption coefficients value for LAS. The error margin of the quantification was estimated as ± 5%. X-ray diffraction patterns were recorded by a Bruker D8 Advance diffractometer with nickel-filtered CuKα radiation scanning in the range of 5-60º (2θ) and at an angular rate of 0.3º/min with a step size of 0.01º. The estimated relative crystallinities (%) were calculated using the areas of several peaks in the range of 15-35º (2θ) and using the respective parent material (ZSM-5 and BEA uncalcined) as a reference. Physisorption experiments were performed with a Micromeritics 3Flex using Ar as the adsorbate at -185°C. The zeolites were pre-treated under vacuum for 1h at 90ºC and subsequently at 300ºC for 16h. The apparent surface areas ($S_{BET}$) were calculated by applying the Brunauer-Emmett-Teller (BET) equation, while the external surface area ($S_{ext}$), micropore area ($S_{micro}$) and micropore volume ($V_{micro}$) were calculated by the t-method. The solid-state MAS NMR spectra were acquired at a static magnetic field strength of 9.4 T ($v_0(^1H)$ =400MHz) on a Bruker Avance III console using TopSpin 3.1 software. The probe used for $^{27}$Al solid-state MAS NMR was tuned to

104.27 MHz and referenced to yttrium aluminium garnet (YAG) at 0.0 ppm. Prior to the experiments, the zeolites were stored overnight in a humid environment before being packed into a zirconia MAS rotor with Kel-F caps and the sample mass was recorded. All solid-state NMR and Ar physisorption experiments were performed at Johnson Matthey PLC.

## 3.3 Effect of thermal treatment

### 3.3.1 Structural and textural properties

The morphology of BEA zeolite demonstrates agglomerates of crystals about 40-50 nm in size (Figure 3.2 a), which is in agreement with the dimension of BEA zeolite mentioned in the literature [30,32]. ZSM-5 zeolite shows a typical morphology of an MFI structure with individual particles forming larger and irregular aggregates. Therefore, it is difficult to determine the mean size of the primary particles from the SEM image (Figure 3.2 b). All thermally treated zeolites maintain the Si/Al ratio of the parent zeolite being ~12 for BEA and ~32 for ZSM-5 (Table 3.4). This demonstrates that after thermal treatment even at high temperatures, all Al species remain in the zeolite structure (as framework and extra-framework Al).

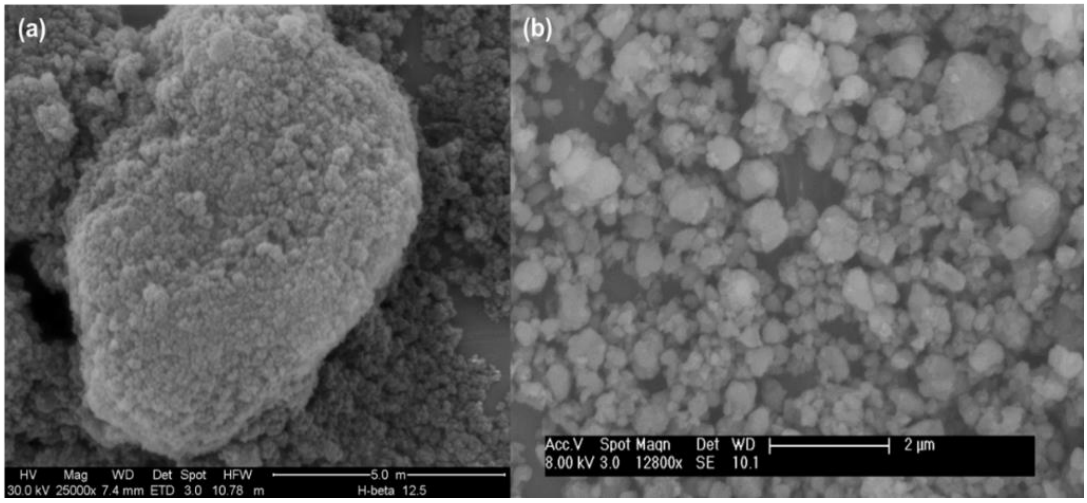


**Figure 3.2.** SEM micrographs of the parent zeolites. **(a)** BEA and **(b)** ZSM-5 at different magnifications.

According to XRD, all parent and thermally treated zeolites are well-crystallised materials with low background, which is indicative of the absence of an amorphous phase

(Figure 3.3). The XRD patterns of BEA zeolites suggest that this structure is a material of ~60% of polymorph A and 40% of polymorph B [33]. The XRD patterns of ZSM-5 zeolites are ascribed to the typical structure characteristic of the MFI framework (Figure 3.3 b) [33]. Although the XRD patterns show no significant changes in the zeolite's structure, the estimated values for the relative crystallinities gradually decrease (Table 3.4), indicating a loss of crystal structure with the increasing calcination temperature. This loss can be attributed to dealumination caused by thermal treatment, which could lead in extreme cases to a collapse of the structure.

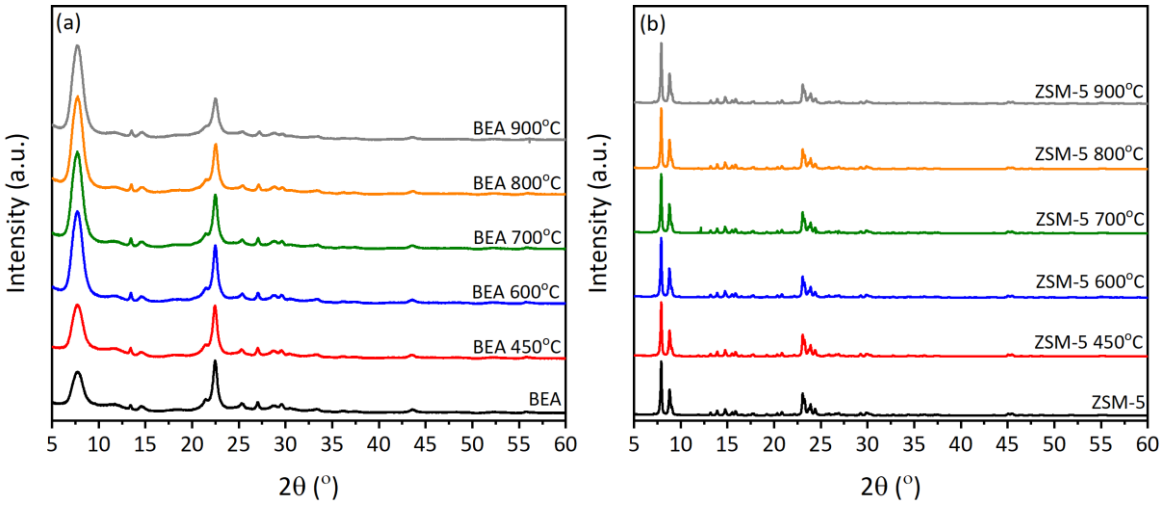


**Figure 3.3.** X-ray diffraction patterns obtained for **(a)** BEA and **(b)** ZSM-5 zeolites.

**Table 3.4.** Structural and textural properties of parent and thermally treated BEA and ZSM-5 zeolites.

| Zeolite | Si/Al (EDX) | Relative crystallinity (%)[a] | Apparent $S_{BET}$ ($m^2/g$) | $S_{ext}$ ($m^2/g$) | $S_{micro}$ ($m^2/g$) | $V_{micro}$ $cm^3/g$ |
|---|---|---|---|---|---|---|
| **BEA** | 11.9 | 100 | 604 | 214 | 390 | 0.15 |
| **BEA 450°C** | 11.7 | 90 | 580 | 217 | 364 | 0.14 |
| **BEA 600°C** | 11.6 | 85 | 550 | 217 | 333 | 0.13 |
| **BEA 700°C** | 11.0 | 81 | 527 | 191 | 336 | 0.13 |
| **BEA 800°C** | 12.1 | 63 | 525 | 186 | 342 | 0.13 |
| **BEA 900°C** | 11.4 | 62 | 418 | 166 | 251 | 0.10 |
| **ZSM-5** | 32.0 | 100 | 450 | 57 | 392 | 0.15 |
| **ZSM-5 450°C** | 32.1 | 99 | 459 | 55 | 404 | 0.15 |
| **ZSM-5 600°C** | 32.3 | 97 | 460 | 57 | 402 | 0.15 |
| **ZSM-5 700°C** | 31.6 | 94 | 442 | 55 | 387 | 0.14 |
| **ZSM-5 800°C** | 31.4 | 90 | 445 | 58 | 387 | 0.14 |
| **ZSM-5 900°C** | 32.1 | 85 | 448 | 58 | 389 | 0.14 |

The increase in the temperature of the thermal treatment also leads to a gradual decrease in the textural properties of BEA zeolite (apparent $S_{BET}$, $S_{micro}$, $S_{ext}$ and $V_{micro}$) especially when the zeolite is calcined at temperatures above 700°C (Table 3.4). In contrast, there are no remarkable changes in the textural parameters of ZSM-5 zeolite, not even when calcined at higher temperatures (Table 3.4), which is in agreement with previous reports [34]. The parent and thermally treated ZSM-5 zeolites display a type-I isotherm, which is typical of solids with a microporous structure having relatively small external surfaces (Figure 3.4 b) [35] while BEA thermally treated zeolites show a mix between type-I and IV isotherm (Figure 3.4 a) [35]. The shape of adsorption and desorption isotherms for both sets of zeolites are very similar within each group, even after high calcination temperatures.

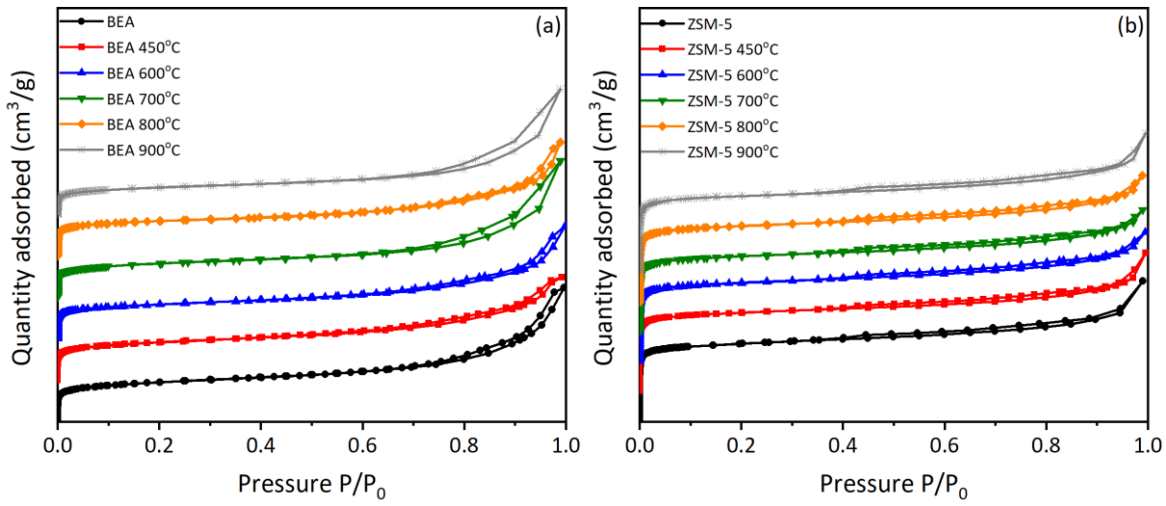


**Figure 3.4**. Ar adsorption-desorption isotherms for parent and thermally treated zeolites. **(a)** BEA **(b)** ZSM-5.

Thermal treatment promotes changes in the relative crystallinities of both zeolites and in the textural properties of zeolite BEA. The modification in this zeolite properties are more pronounced than in ZSM-5 zeolite; changes in the structural and textural properties of BEA zeolite occur at low calcination temperatures (450°C), which agrees with other reports [36,37]. The literature on the structural stability of this zeolite is inconsistent and studies have already shown a structural collapse at 900ºC [38,39]. However, in the set of thermally treated BEA zeolites studied in this work, there is only a partial degradation of the structure (~62%).

From these results there is no evidence of structural collapse in ZSM-5 zeolite, but structural alterations are observed in samples calcined (450-900ºC), in similarity to previous studies [34,40,41]. It has been shown that ZSM-5 is more resistant to dealumination during thermal treatments than other zeolites [31,42], such as BEA, MOR and FAU with a high amount of Al, which are less stable against dealumination at high temperatures [25,43] Additionally, the flexibility in the coordination sphere of the Al atoms in the 12-MR system of zeolite BEA [44,45], makes it more susceptible to dealumination, while ZSM-5 zeolite is more resistant to high temperature treatment.

### 3.3.2 Acidic properties

FTIR spectra of parent zeolites BEA and ZSM-5 show two major peaks at 3610 $cm^{-1}$ and 3745 $cm^{-1}$, with a shoulder at ~3735 $cm^{-1}$ (Figures 3.5 and 3.6). The peak at 3610 $cm^{-1}$ corresponds to acidic bridging Si-OH-Al groups. The peaks at 3745 and 3735 $cm^{-1}$ are attributed to external and internal silanol groups (Si-OH), respectively. The separation of external and internal Si-OH peaks is more noticeable in the spectra of the BEA zeolites, which is a result of the relatively small crystal dimensions of this material (Figure 3.5) [32]. Thermal treatment causes a decrease in intensity of the peak of Si-OH-Al groups at 3610 $cm^{-1}$ in both sets of zeolites. This peak completely disappears after calcination at high temperatures (for BEA at 700-900ºC and for ZSM-5 at 900ºC). This decrease results from the breaking of Si-O-Al bonds during the thermal treatment and is accompanied by the formation of extra-framework aluminium species (EFAl) and hydroxyl nests [25,26] (Figures 3.5 a and 3.6 a). The breaking of Si-O-Al bonds is dependent on the calcination temperature; a higher calcination temperature leads to a greater degree of dealumination, complete removal of Si-OH-Al groups (BEA 700-900ºC and ZSM-5 900ºC) and partial collapse of the zeolitic structure. BEA 450C-900ºC and ZSM-5 600-800ºC samples display two additional peaks at 3782 $cm^{-1}$ and 3662 $cm^{-1}$ assigned to Al-OH groups formed through the dealumination of Al from the framework [46]. The Al-OH groups with a peak at 3782 $cm^{-1}$ is associated to Lewis acidity, similar to Al-OH groups observed in alumina, while the peak at 3662 $cm^{-1}$ is related to weak Brønsted acidity (BAS). With the breaking of the Si-O-Al bonds more defects are generated in the structure, which are associated with the small increase in the intensity of the peak at ~3745 $cm^{-1}$ (terminal Si-OH groups) and the appearance of the Al-OH peaks at 3782 and 3662 $cm^{-1}$.

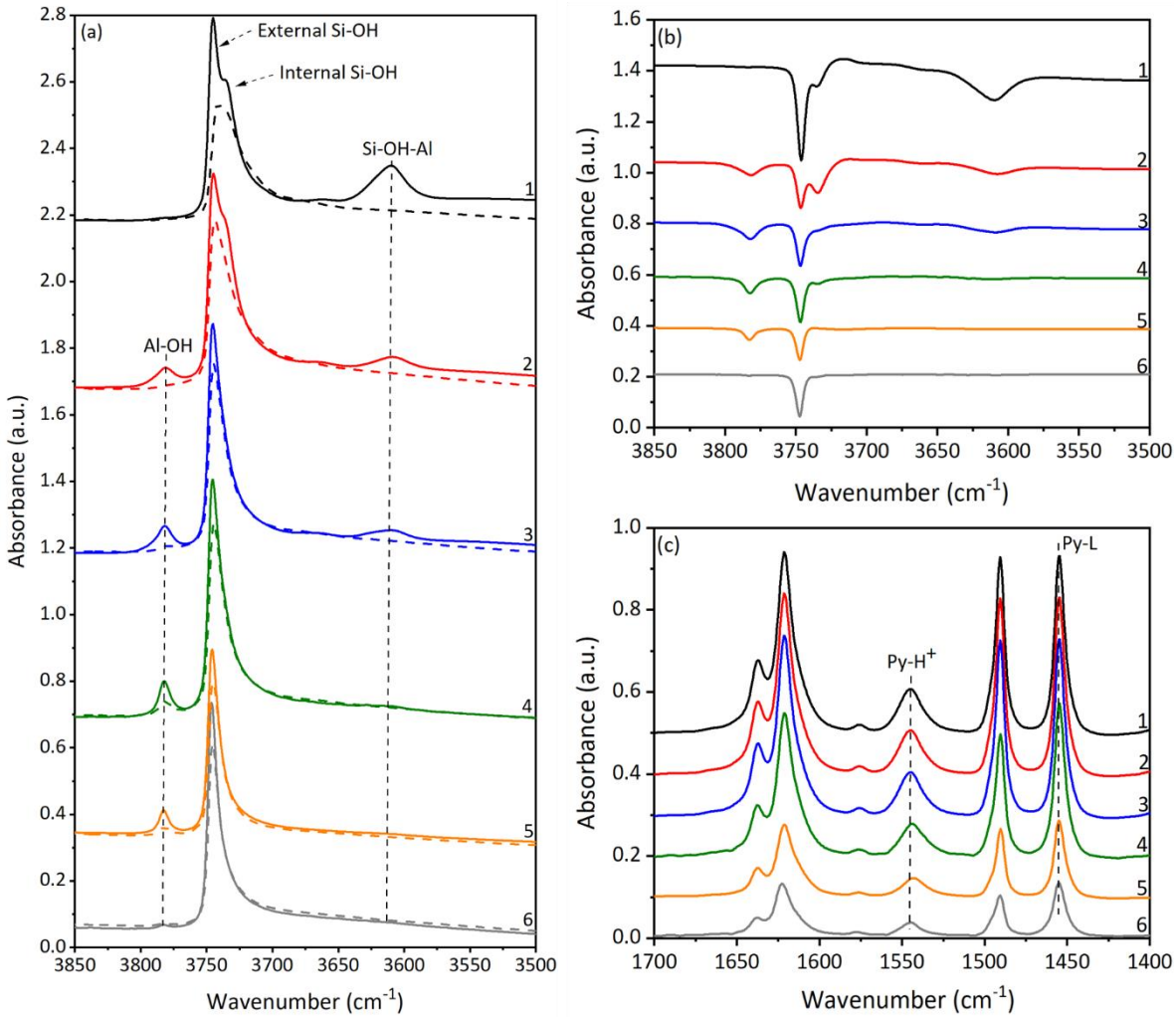


**Figure 3.5**. FTIR spectra of hydroxyl groups of BEA parent and thermally treated zeolites **(a)** before (solid lines) and after Py adsorption at 150ºC (dashed lines). **(b)** Difference spectra of the hydroxyl groups following Py adsorption at 150ºC. **(c)** Difference spectra of the Py region following Py adsorption at 150ºC. **(1)** Parent BEA zeolite, **(2)** BEA 450ºC, **(3)** BEA 600ºC, **(4)** BEA 700ºC, **(5)** BEA 800ºC and **(6)** BEA 900ºC.

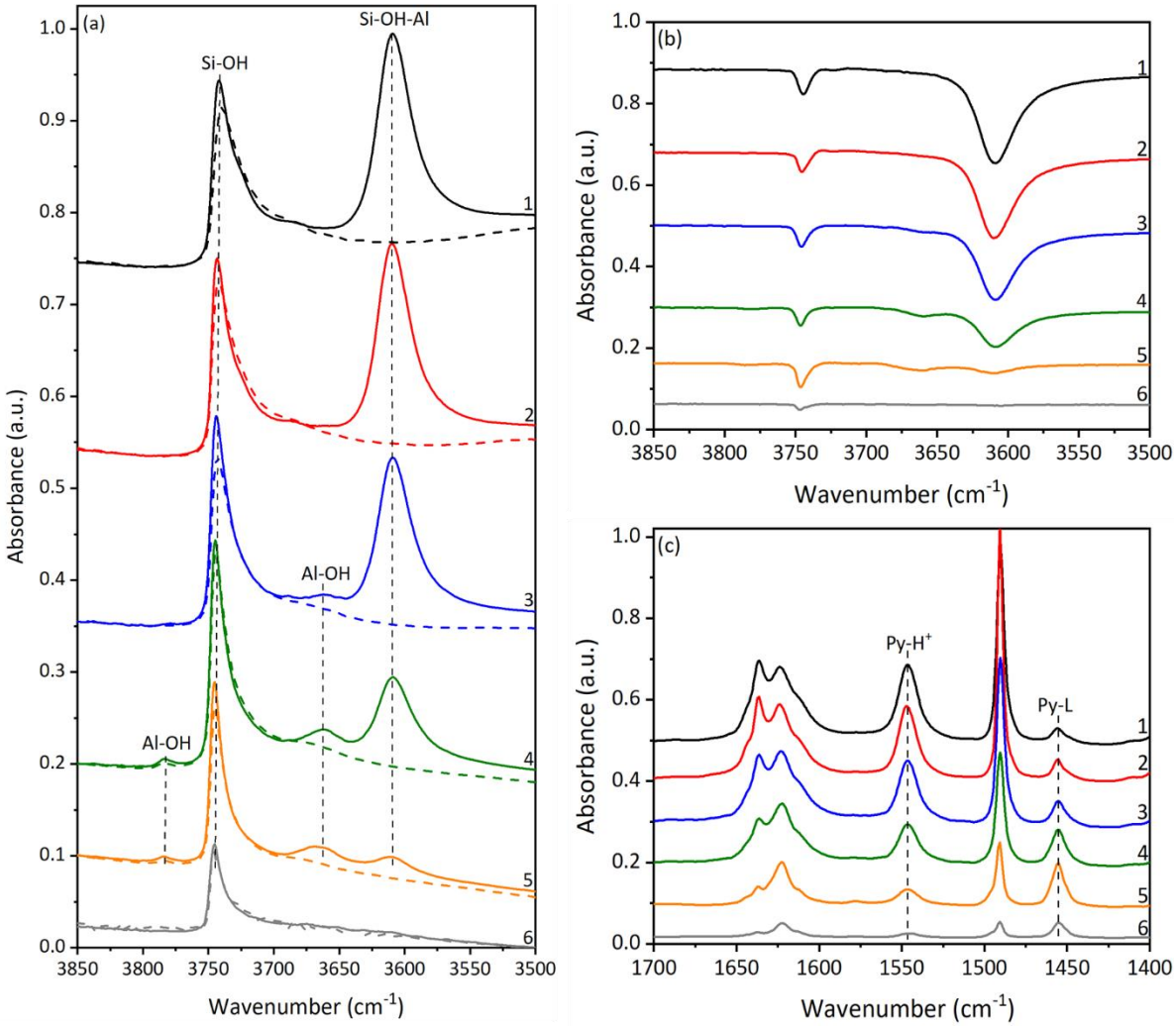


**Figure 3.6.** FTIR spectra of hydroxyl groups of ZSM-5 parent and thermally treated zeolites **(a)** before (solid lines) and after Py adsorption at 150ºC (dashed lines). **(b)** Difference spectra of the hydroxyl groups following Py adsorption at 150ºC. **(c)** Difference spectra of the Py region following Py adsorption at 150ºC. **(1)** Parent ZSM-5 zeolite, **(2)** ZSM-5 450ºC, **(3)** ZSM-5 600ºC, **(4)** ZSM-5 700ºC, **(5)** ZSM-5 800ºC and **(6)** ZSM-5 900ºC.

The interaction of Py with ZSM-5 and BEA zeolites (Figures 3.5 and 3.6) results in a complete disappearance of the peaks at 3610 $cm^{-1}$ and 3662 $cm^{-1}$ corresponding to bridging Si-OH-Al groups and Al-OH groups. A decrease in the intensity of the Si-OH peak at ~3745 $cm^{-1}$ is also observed. The reduction in the intensity of the Si-OH-Al and Al-OH peaks demonstrates the acidic character of these hydroxyl groups. The decrease in the intensity of the Si-OH peak shows that part of Si-OH groups interacts with Py; these groups are probably located close to LAS. The remaining Si-OH groups not interacting with Py are usually attributed to non-acidic terminal species in the framework or extra-framework positions

distant from LAS [47]. The Al-OH peak at 3782 $cm^{-1}$ in BEA 450-900ºC and ZSM-5 600-800ºC also decrease in intensity after adsorption of Py, which according to [48] are non-acidic OH groups similar to Al-OH groups observed in alumina.

In the range of 1400-1700 $cm^{-1}$, chemisorbed Py is revealed by the following sets of peaks: two peaks at 1545 and 1637 $cm^{-1}$ due to pyridinium ion (Py-$H^+$ or BAS), two peaks at 1456 and 1622 $cm^{-1}$ assigned to Py coordinated to Lewis acid sites (Py-L or LAS) and the peak at 1491 $cm^{-1}$ corresponding to the signal of Py on Lewis and Brønsted acid sites (Figures 3.5 c and 3.6 c). ZSM-5 zeolite shows a lower total concentration of acid sites when compared with BEA zeolite (Table 3.5). That is explained by the lower amount of Al in ZSM-5 structure, Si/Al=~ 40 for ZSM-5 vs Si/Al=~12.5 for BEA.

**Table 3.5** Concentration of acid sites for BEA and ZSM-5 parent and thermally treated zeolites in quantitative experiments using Py adsorption monitored by FTIR.

| Zeolite | BAS (µmol/g) | LAS (µmol/g) | Total amount (µmol/g) | BAS/LAS |
|---|---|---|---|---|
| **BEA** | 352 | 195 | 547 | 2.0 |
| **BEA 450°C** | 224 | 328 | 552 | 0.7 |
| **BEA 600°C** | 207 | 291 | 498 | 0.7 |
| **BEA 700°C** | 144 | 251 | 395 | 0.6 |
| **BEA 800°C** | 83 | 129 | 212 | 0.6 |
| **BEA 900°C** | 48 | 96 | 144 | 0.5 |
| **ZSM-5** | 338 | 25 | 363 | 13.3 |
| **ZSM-5 450°C** | 304 | 31 | 335 | 9.7 |
| **ZSM-5 600°C** | 263 | 45 | 308 | 5.9 |
| **ZSM-5 700°C** | 166 | 71 | 237 | 2.3 |
| **ZSM-5 800°C** | 55 | 78 | 133 | 0.7 |
| **ZSM-5 900°C** | 15 | 28 | 43 | 0.6 |

The number of BAS in both set of samples gradually decreases with the increasing calcination temperature. This decrease is directly related to the breaking of the Si-O-Al bonds resulting in the increase of the number of LAS attributed to the formation of EFAl species. Thermal treatment affects more strongly the acidic properties of BEA zeolite. After

calcination at 450°C BEA zeolite losses ~46% of the total number of BAS, while ZSM-5 only losses 10% total number of BAS. Zeolites BEA 800-900ºC and ZSM-5 900ºC (Figures 3.5 a and 3.6 a) display a total loss of Si-OH-Al groups, however the $^{27}$Al NMR (Figure 3.7) shows the presence of tetrahedral Al (δ ~60ppm) related to Si-OH-Al groups. This indicates that the breaking of the Si-O-Al bonds leads to the formation of cations such $[Al=O]^+$, acting as contour ions to neutralise the change, which are still visible in the $^{27}$Al NMR spectra at δ ~60-54 ppm. The presence of BAS in some of the zeolites after the loss of the majority of the Si-OH-Al groups confirms the existence of weak protonic sites (weak BAS), not related to Si-OH-Al groups but weakly acidic hydroxyl groups such as Al-OH (3662 $cm^{-1}$) and Si-OH groups (3745 $cm^{-1}$ and ~3735 $cm^{-1}$) perturbed by EFAl species (which are LAS interacting with weak Si-OH groups and therefore increasing their acid strength, which leads to an increased number of BAS) (Table 3.5).

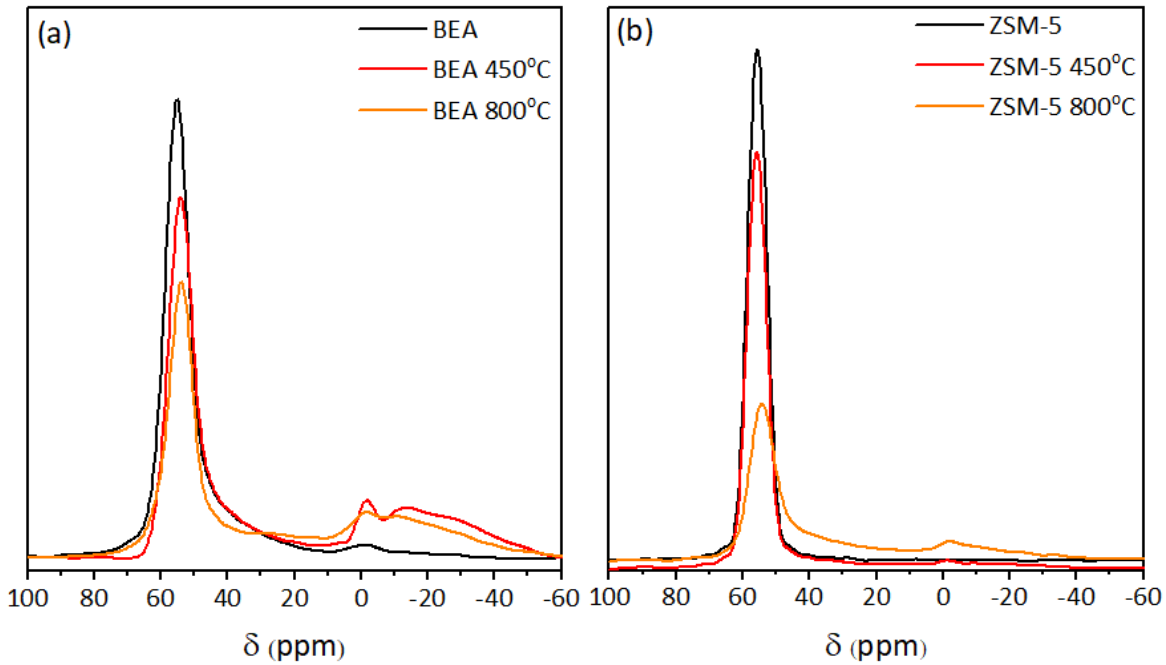


**Figure 3.7.** Normalised $^{27}$Al solid-state MAS NMR spectra of selected **(a)** BEA and **(b)** ZSM-5 zeolites.

The changes in the number of Si-OH-Al groups and BAS for ZSM-5 zeolite (Figure 3.8 b) at different calcination temperatures are very similar. This indicates that no more weak acidic hydroxyl groups are formed in this structure; the ratio between strong/weak BAS

remains the same for all thermally treated ZSM-5 zeolites. For BEA, the changes in the number of Si-OH-Al groups and BAS do not coincide, suggesting the contribution of Si-OH groups affected by EFAl species to the Brønsted acidity of this zeolite (Figure 3.8 a). BEA zeolite shows a higher number of LAS than ZSM-5 zeolite (Table 3.5). The concentrations of this type of acidic sites are clearly dependent on the zeolitic structure (and its Si/Al ratio) and calcination temperature. The number of LAS increases with thermal treatment, which can be explained by the framework Al removal. At calcination temperatures of 600ºC for BEA and 800ºC for ZSM-5 a decrease in the number of LAS can be observed (Table 3.5 and Figure 3.8). This decrease is a result of the agglomeration of EFAl species or alumina-like clusters ($Al_2O_3$), and coincides with the loss of crystallinity of the structures as the calcination temperature increases (Table 3.4).

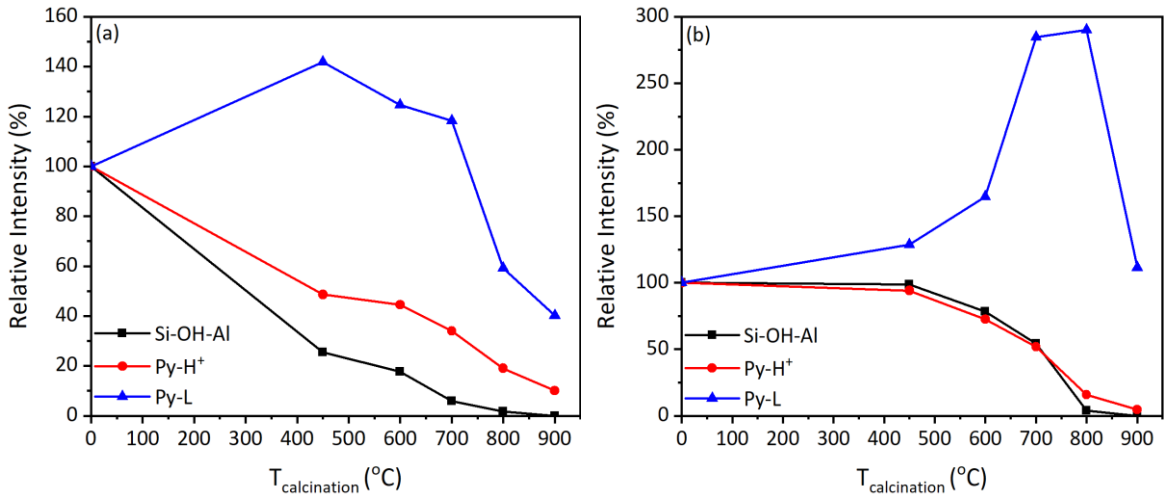


**Figure 3.8.** Evolution of intensities of the peaks of OH groups and acid sites of thermally treated zeolites in the difference spectra following Py adsorption at 150°C. **(a)** BEA (12.5). **(b)** ZSM-5 (40).

Various mechanisms can produce LAS during thermal treatment (Figure 3.9). The first two mechanisms, shown below in equations 1 and 2, produce a one-to-one BAS-to-LAS ratio and are indistinguishable from one mechanism to another as silanol groups are not quantifiable. For these mechanisms to successfully occur there should be no loss in the total number of acid sites as the temperature increases.

$$\text{Si-OH + Si-OH-Al} \rightarrow \text{LAS (EFAl)} + H_2O \qquad 1\ \text{BAS} \rightarrow 1\ \text{LAS} \qquad (1)$$

$$2\ \text{Si-OH-Al} \rightarrow 2\ \text{LAS (EFAl)} \qquad 2\ \text{BAS} \rightarrow 2\ \text{LAS} \qquad (2)$$

For the mechanism 3 to operate, as the calcination temperature increases, the total number of 2 BAS + 1 LAS should remain constant (and approximate the same as the initial concentration) and the experimental lines should be parallel to the x-axis.

$$2\ \text{Si-OH-Al} \rightarrow \text{LAS (EFAl)} + H_2O \qquad 2\ \text{BAS} \rightarrow 1\ \text{LAS} \qquad (3)$$

For the mechanism 4 to be valid, as the calcination temperature increases, the total number of 2 BAS + 1 LAS should remain constant (and approximate the same as the initial concentrations) and the experimental lines should be parallel to the x-axis.

$$\text{Si-OH + Si-OH-Al} \rightarrow \text{LAS (EFAl)} + \text{LAS} (\equiv Si) + H_2O \qquad 1\ \text{BAS} \rightarrow 2\ \text{LAS} \qquad (4)$$

According to the experimental data (Figure 3.9), mechanism 3 can be excluded (red lines). For the zeolites calcined at lower temperatures (< 600ºC), the loss of one Si-OH-Al group with the formation of one (Figure 3.9 mechanisms 1 or 2 black lines) or the loss of two Si-OH-Al group with the formation of one LAS (Figure 3.9 mechanism 4 blue lines) are more likely to take place in both ZSM-5 and BEA zeolite structures. Above this calcination temperature, none of these mechanisms is valid due to the significant reduction in the number of acid sites. This is probably due to agglomeration of $Al_2O_3$-like species, forming large clusters, in which some of the Al is not accessible to Py.

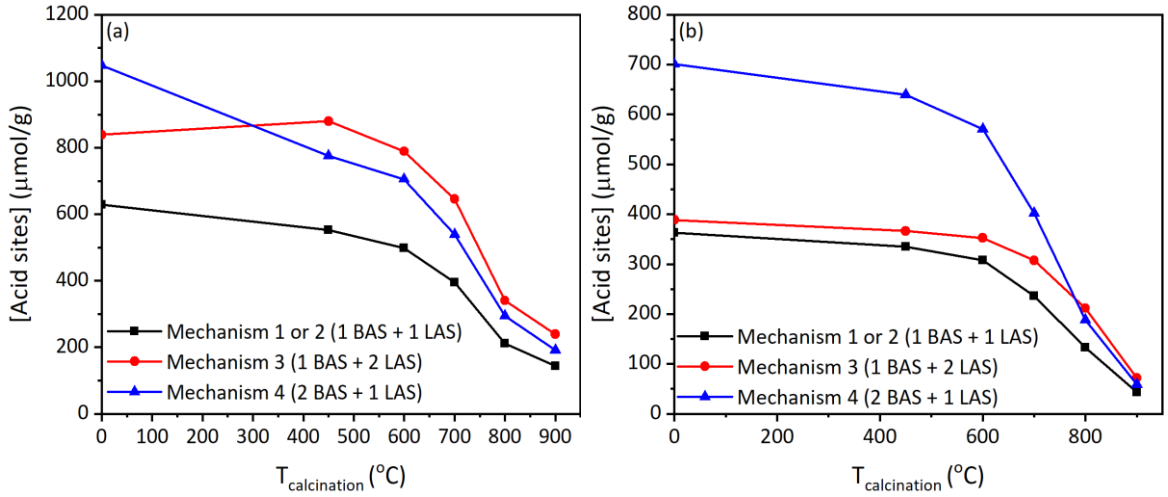


**Figure 3.9.** Number of acid sites reflecting possible mechanisms for LAS formation in **(a)** BEA (12.5) and **(b)** ZSM-5 (40) zeolites.

Calcination of BEA zeolite leads to an increase in the amount of octahedral EFAl species with a chemical shift δ~0 ppm (Figure 3.7 a), agreeing with the increase of the number of LAS obtained by Py-FTIR (Figure 3.8 a). In addition, BEA zeolites show a noticeable broad signal for the framework Al species (δ ~60-54 ppm), which is indicative of the increasing disorder of the local Al environment resulting from the thermal treatment [49] (Figure 3.7 a). From the comparison of $^{27}$Al MAS NMR and FTIR data, it can be concluded that Py molecules producing Py-L complexes observed in the infrared spectra may interact with these distorted tetrahedral Al species. Thermal treatment at 450ºC did not cause the formation of octahedral EFAl species at δ~0 ppm in ZSM-5 zeolite and the bulk of Al remains in tetrahedrally coordinated framework positions (Figure 3.7 b). At higher calcination temperatures (800ºC) is observed an increase in the amount of octahedral EFAl species at δ~0 ppm and a noticeable signal boarding for the framework Al species (δ~60-54 ppm). These $^{27}$Al MAS NMR results are in agreement with the changes demonstrated by acid site quantification obtained by Py-FTIR for thermally treated ZSM-5 zeolites (Table 3.5 and Figure 3.8 b).

The effect of Py desorption temperature on the Si-OH-Al peak intensities and peaks corresponding to adsorbed Py species (deduced from the difference between spectra, before Py adsorption and after thermodesorption) was also examined for both sets of zeolites

(Figures 3.10 and 3.11). Figure 3.10 shows difference IR spectra of the parent BEA zeolite in the OH and Py regions whereas Figures 3.11 summarise the quantitative changes in the relative intensities of the bands corresponding to Si-OH-Al, Py-$H^+$ and Py-L species for all zeolites. The relative intensity of the Si-OH-Al peak remains constant up to 300ºC gradually decreasing at higher desorption temperatures for all zeolites that still present Si-OH-Al groups. After desorption at 450ºC, a significant number of Si-OH-Al groups still interact with Py, for samples calcined at temperature below 700ºC (e.g. 74% for the parent ZSM-5 and 79% for parent BEA). A small restoration of the Si-OH-Al peak, represented by the decrease in the intensity of the negative peak of the Si-OH-Al in Figure 3.10 a, is observed in all samples during the Py desorption.

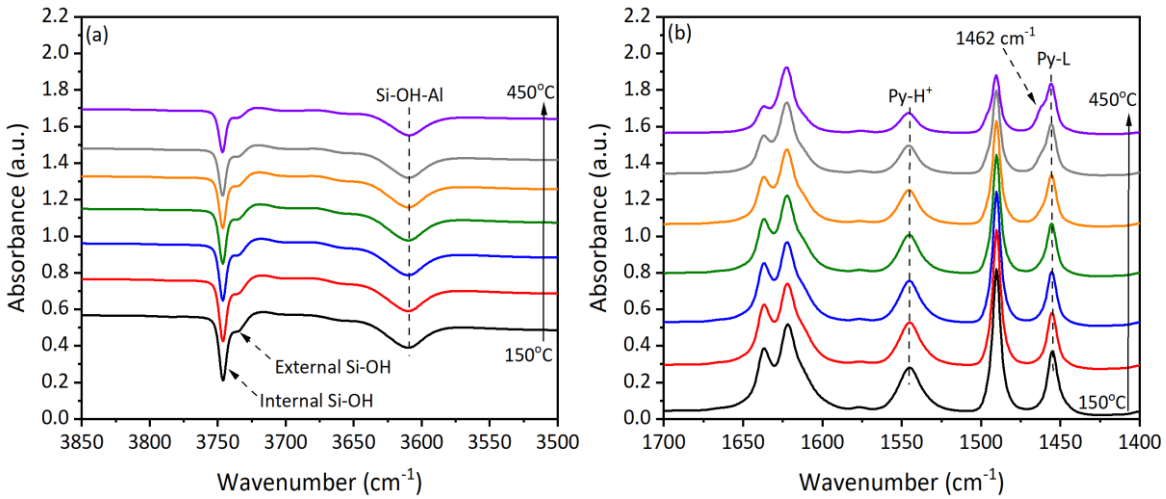


**Figure 3.10.** Difference spectra of the **(a)** hydroxyl region and **(b)** Py region of BEA parent zeolite following Py desorption at increasing temperatures (150°C- 450°C).

The relative intensity of the Py-$H^+$ peak decreases for all samples, following desorption above 150ºC (Figure 3.11 b and e). This confirms the presence of relatively weak BAS interacting with Py (weaker than Si-OH-Al, which retain Py up to desorption temperatures of 300ºC), such as Al-OH and Si-OH groups. The results demonstrate a significant decrease in the apparent strength of BAS in both structures especially when calcined at high temperatures. This decrease in apparent strength is explained by the decrease in the number of bridging Si-OH-Al groups (strong BAS), resulting in fewer Py desorption-

readsorption cycles ('travel' of Py along the zeolite channels), which can be observed as a lower desorption temperature required to remove Py.

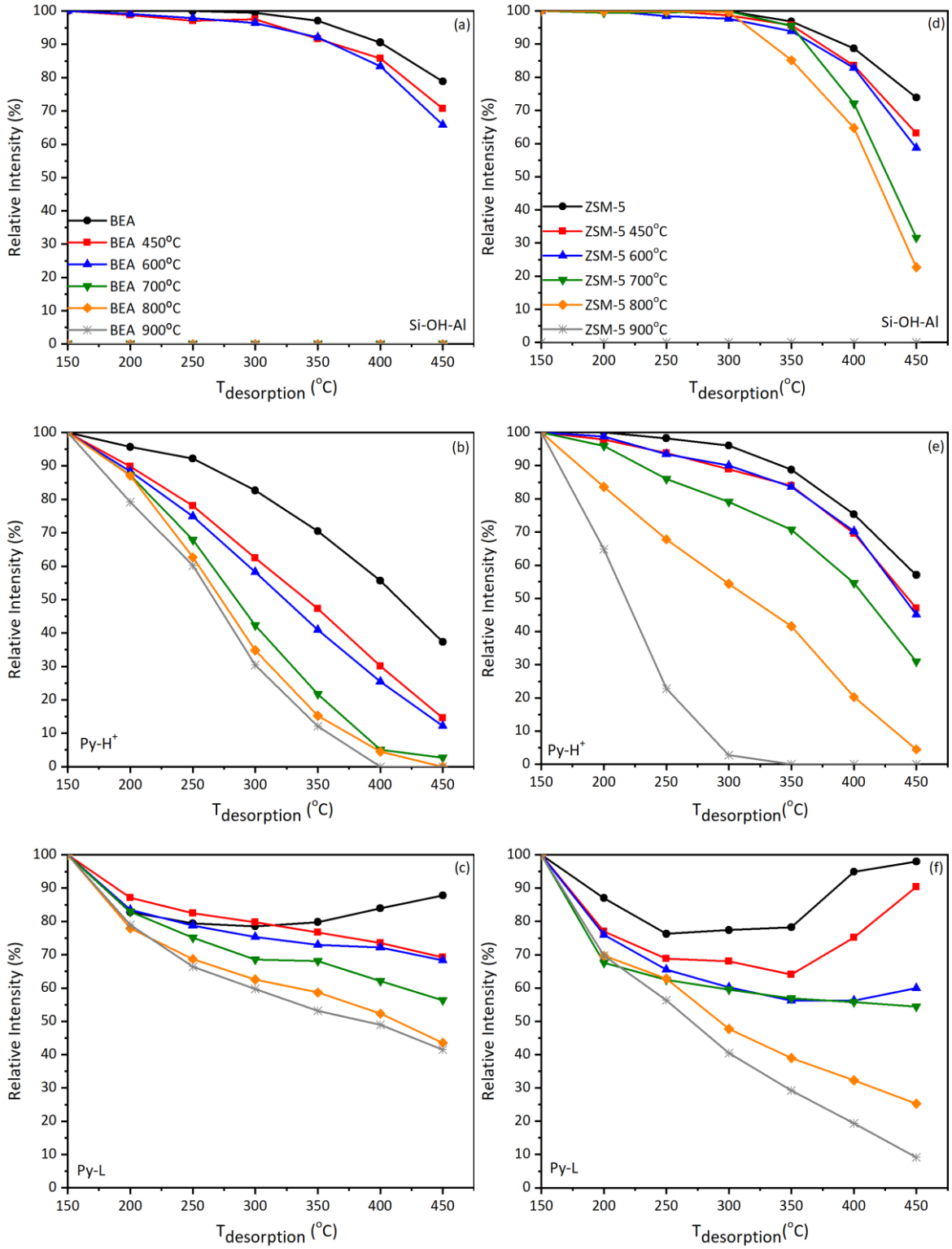


**Figure 3.11.** Quantitative changes in relative intensities of the peaks corresponding to Si-OH-Al groups, Py-$H^+$ and Py-L species after desorption of Py at increasing temperatures (150-450ºC). **(a-c)** BEA (12.5) and (**d-f)** ZSM-5 (40) zeolites.

The relative intensities of the Py-L peak vary to a lesser degree with the increasing of desorption temperature, when compared with the Py-$H^+$ peak. Parent and thermally treated zeolites calcined at lower temperatures (450-600°C) show a small increase in the Py-L relative intensities. This increase is due to the appearance of a shoulder at ~1462 $cm^{-1}$ (e.g. Figures 3.10 b) at desorption temperatures above 350ºC. The peak is assigned to iminium ions, which are possibly Py molecules coordinated to Lewis in EFAl positions and at the same time interacting through an H-bond with BAS [30] and have been already studied in BEA [46,50] and MAZ zeolites [51].

## 3.4 Effect of cation incorporation by impregnation

### 3.4.1 Structural and textural properties

All cation-containing zeolites obtained after the impregnation method show XRD patterns which are very similar to those of the respective calcined zeolites (e.g. Figure 3.12). Evidence of a broad feature in the patterns of 1 Ca/BEA 800°C and 1 Mg/BEA 800°C samples impregnated with higher amounts of $Ca^{2+}$ and $Mg^{2+}$ can be observed, which indicates the presence of an amorphous material. No extra diffraction peaks assigned to different phases (e.g. hydroxides) or significant changes in the peak positions have been observed. The absence of additional peaks, even in the presence of high amounts of cations suggests a good dispersion of the species through the zeolitic structure.

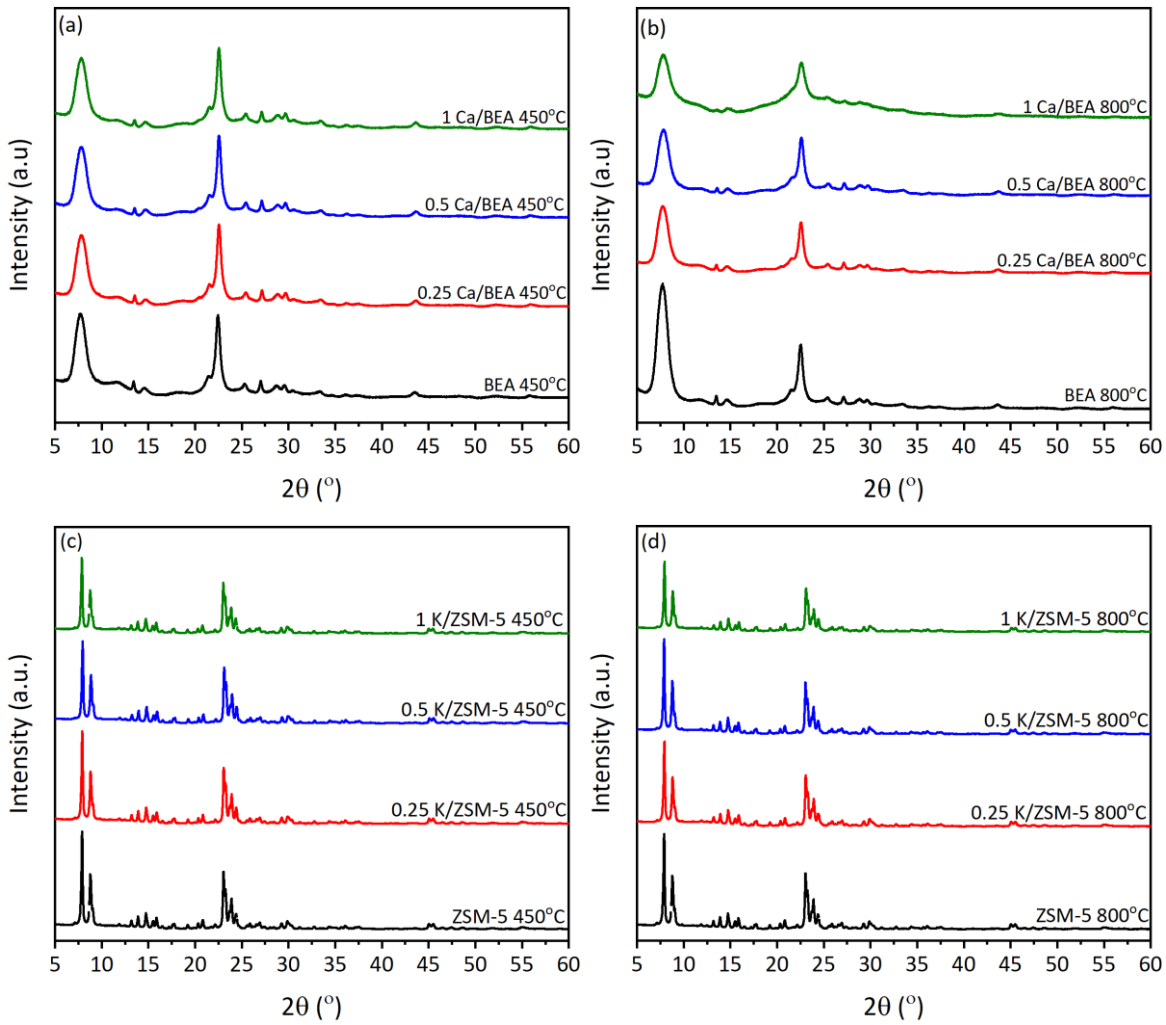


**Figure 3.12.** X-ray diffraction patterns obtained for **(a)** Ca/BEA 450ºC **(b)** Ca/BEA 800ºC **(c)** K/ZSM-5 450ºC **(b)** K/ZSM-5 800ºC zeolites.

The estimated relative crystallinities decrease with the increase of the cation content and calcination temperature (Tables 3.6 and 3.7). The impregnation of BEA zeolite with $Ca^{2+}$ and $Mg^{2+}$ cations affects significantly the framework of BEA, especially followed by thermal treatment at 800°C. There is a decrease in the estimated crystallinity to 36% for 1 Mg/BEA 800°C and 22% to 1 Ca/BEA 800°C with the increasing cation content (Table 3.6). This decrease in the crystallinity is typically ascribed to partial damage of zeolite framework during thermal treatment [21]. The observation is supported by the decrease in both apparent $S_{BET}$ and $S_{micro}$ areas obtained by Ar physisorption for 1 Ca/BEA 800°C and 1 Mg/BEA 800°C zeolites (Figure 3.13), indicating the possible partial blockage to the zeolite pores resulting in lower adsorption capacity or the formation of amorphous phases. These results

can be explained by the excess of $Ca^{2+}$ and $Mg^{2+}$ cations existing in zeolite BEA (Table 3.6), which could lead to an excessive formation of oxide clusters especially during thermal treatment at high temperatures (800°C). Normally, the incorporation of solvated cations followed by calcination leads to the formation of metal oxide particles occluded in the cavities of the zeolite and the excess of these clusters promotes pore blockage and structural degradation of the zeolite framework [16].

**Table 3.6.** Structural properties of parent and cation-containing BEA zeolites prepared by impregnation.

| Zeolite ID | Si/Al (EDX) | Cation/Al (EDX) | Relative Crystallinity (%) |
|---|---|---|---|
| BEA | 11.9 | - | 100 |
| BEA 450ºC | 11.7 | - | 90 |
| BEA 800ºC | 12.1 | - | 73 |
| 0.25 K/BEA-IM 450ºC | 11.9 | 0.2 | 100 |
| 0.5 K/BEA-IM 450ºC | 12.1 | 0.3 | 97 |
| 1 K/BEA-IM 450ºC | 12.0 | 0.4 | 94 |
| 0.25 K/BEA-IM 800ºC | 11.9 | 0.2 | 92 |
| 0.5 K/BEA-IM 800ºC | 12.1 | 0.3 | 90 |
| 1 K/BEA-IM 800ºC | 12.0 | 0.4 | 81 |
| 0.25 Na/BEA-IM 450ºC | 11.6 | 0.2 | 100 |
| 0.5 Na/BEA-IM 450ºC | 11.6 | 0.4 | 96 |
| 1 Na/BEA-IM 450ºC | 11.1 | 0.5 | 90 |
| 0.25 Na/BEA-IM 800ºC | 11.6 | 0.2 | 94 |
| 0.5 Na/BEA-IM 800ºC | 11.6 | 0.4 | 91 |
| 1 Na/BEA-IM 800ºC | 11.1 | 0.5 | 87 |
| 0.25 Ca/BEA-IM 450ºC | 12.2 | 0.6 | 100 |
| 0.5 Ca/BEA-IM 450ºC | 11.7 | 0.8 | 95 |
| 1 Ca/BEA-IM 450ºC | 12.0 | 1.7 | 77 |
| 0.25 Ca/BEA-IM 800ºC | 12.2 | 0.6 | 91 |
| 0.5 Ca/BEA-IM 800ºC | 11.7 | 0.8 | 64 |
| 1 Ca/BEA-IM 800ºC | 12.0 | 1.7 | 22 |
| 0.25 Mg/BEA-IM 450ºC | 11.8 | 0.3 | 100 |
| 0.5 Mg/BEA-IM 450ºC | 12.0 | 0.9 | 92 |
| 1 Mg/BEA-IM 450ºC | 12.4 | 1.7 | 80 |
| 0.25 Mg/BEA-IM 800ºC | 11.8 | 0.3 | 91 |
| 0.5 Mg/BEA-IM 800ºC | 12.0 | 0.9 | 64 |
| 1 Mg/BEA-IM 800ºC | 12.4 | 1.7 | 36 |

**Table 3.7.** Structural properties of parent and cation-containing ZSM-5 zeolites prepared by impregnation.

| Zeolite ID | Si/Al (EDX) | Cation/Al (EDX) | Relative Crystallinity (%) |
|---|---|---|---|
| ZSM-5 | 32.0 | - | 100 |
| ZSM-5 450ºC | 32.1 | - | 99 |
| ZSM-5 800ºC | 31.4 | - | 90 |
| 0.25 K/ZSM-5-IM 450ºC | 33.1 | 0.2 | 100 |
| 0.5 K/ZSM-5-IM 450ºC | 32.5 | 0.4 | 101 |
| 1 K/ZSM-5-IM 450ºC | 32.6 | 1.0 | 89 |
| 0.25 K/ZSM-5-IM 800ºC | 33.1 | 0.2 | 93 |
| 0.5 K/ZSM-5-IM 800ºC | 32.5 | 0.4 | 93 |
| 1 K/ZSM-5-IM 800ºC | 32.6 | 1.0 | 89 |
| 0.25 Na/ZSM-5-IM 450ºC | 31.6 | 0.3 | 100 |
| 0.5 Na/ZSM-5-IM 450ºC | 31.6 | 0.6 | 107 |
| 1 Na/ZSM-5-IM 450ºC | 32.4 | 0.8 | 97 |
| 0.25 Na/ZSM-5-IM 800ºC | 31.6 | 0.3 | 97 |
| 0.5 Na/ZSM-5-IM 800ºC | 31.6 | 0.6 | 97 |
| 1 Na/ZSM-5-IM 800ºC | 32.4 | 0.8 | 89 |
| 0.25 Ca/ZSM-5-IM 450ºC | 35.3 | 0.3 | 100 |
| 0.5 Ca/ZSM-5-IM 450ºC | 35.3 | 0.4 | 99 |
| 1 Ca/ZSM-5-IM 450ºC | 35.2 | 0.9 | 94 |
| 0.25 Ca/ZSM-5-IM 800ºC | 35.3 | 0.3 | 93 |
| 0.5 Ca/ZSM-5-IM 800ºC | 35.3 | 0.4 | 90 |
| 1 Ca/ZSM-5-IM 800ºC | 35.2 | 0.9 | 83 |
| 0.25 Mg/ZSM-5-IM 450ºC | 31.9 | 0.2 | 100 |
| 0.25 Mg/ZSM-5-IM 800ºC | 31.2 | 0.6 | 100 |
| 0.5 Mg/ZSM-5-IM 450ºC | 31.6 | 0.8 | 100 |
| 0.25 Mg/ZSM-5-IM 800ºC | 31.9 | 0.2 | 93 |
| 0.5 Mg/ZSM-5-IM 800ºC | 31.2 | 0.6 | 92 |
| 1 Mg/ZSM-5-IM 800ºC | 31.6 | 0.8 | 91 |

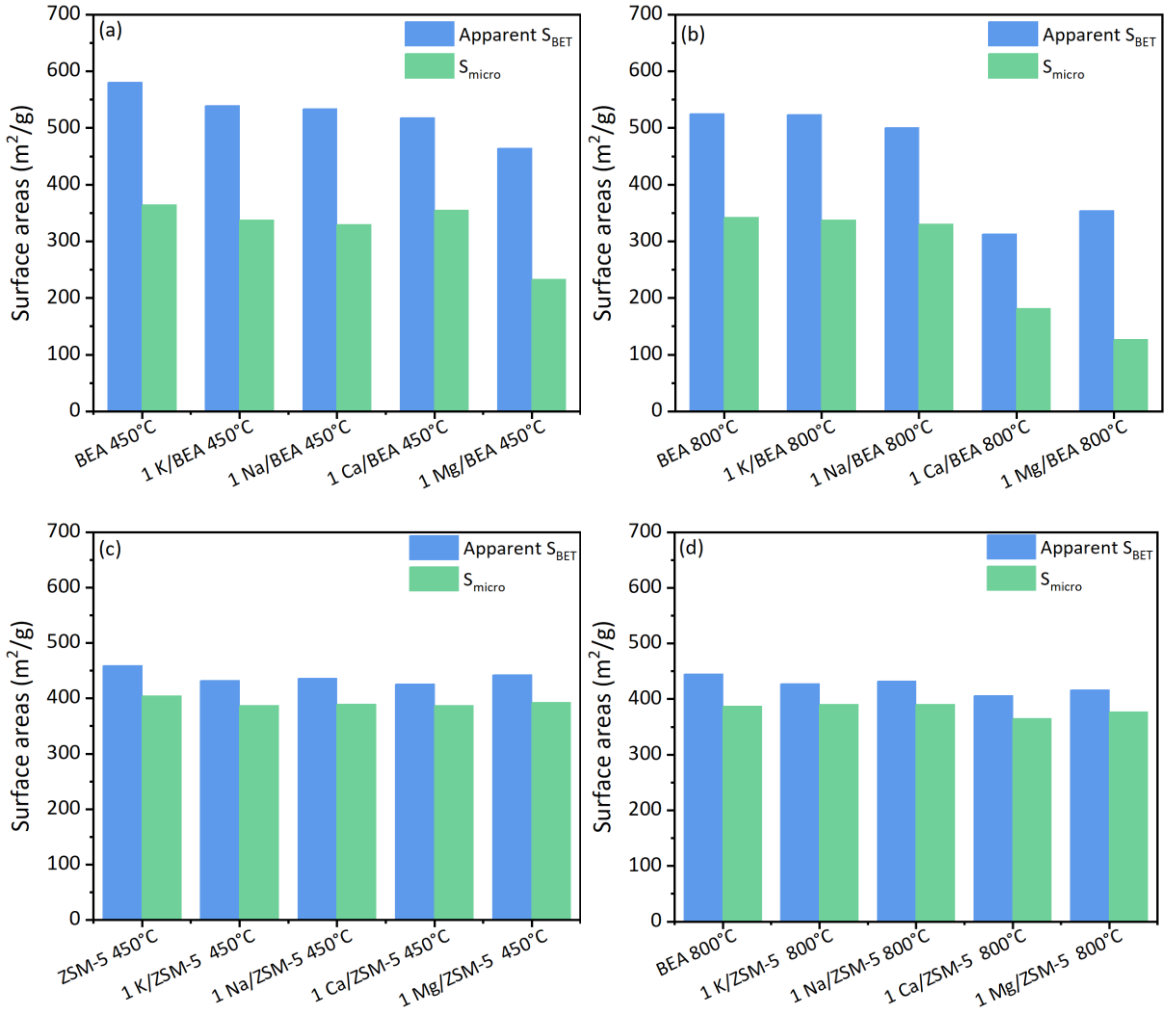


**Figure 3.13.** Textural properties of selected cation-containing zeolites. **(a)** BEA-cation containing zeolites 450°C. **(b)** BEA-cation containing zeolites 800°C. **(c)** ZSM-5-cation containing zeolites 450°C. **(b)** ZSM-5-cation containing zeolites 800°C.

Cation-containing ZSM-5 as well as Na and K/BEA zeolites show no significant differences in apparent $S_{BET}$ and $S_{micro}$ areas (Figure 3.13). In addition, all samples prepared by impregnation maintain the Si/Al ratio of their respective parent zeolite (Tables 3.6 and 3.7).

### 3.4.2 Acidic properties

Cation impregnation followed by calcination results in a variation in the OH region of the FTIR spectra of BEA and ZSM-5 zeolites (e.g. Figure 3.14). In general, the intensity of the Si-OH-Al groups peak at 3610 $cm^{-1}$ decreases gradually with increasing cation content. At high loadings of cations, most of the samples do not show the Si-OH-Al peak at 3610 $cm^{-}$

[1] (Figure 3.14 a), demonstrating a complete ion exchange of H-form with alkali and alkaline earth metal cations. The decrease in the intensities of the Si-OH-Al peak is more pronounced in the samples calcined at 800ºC (Figure 3.14 b), in agreement with the observations that higher calcination temperatures a leads to greater degree of dealumination (Section 3.3.2).

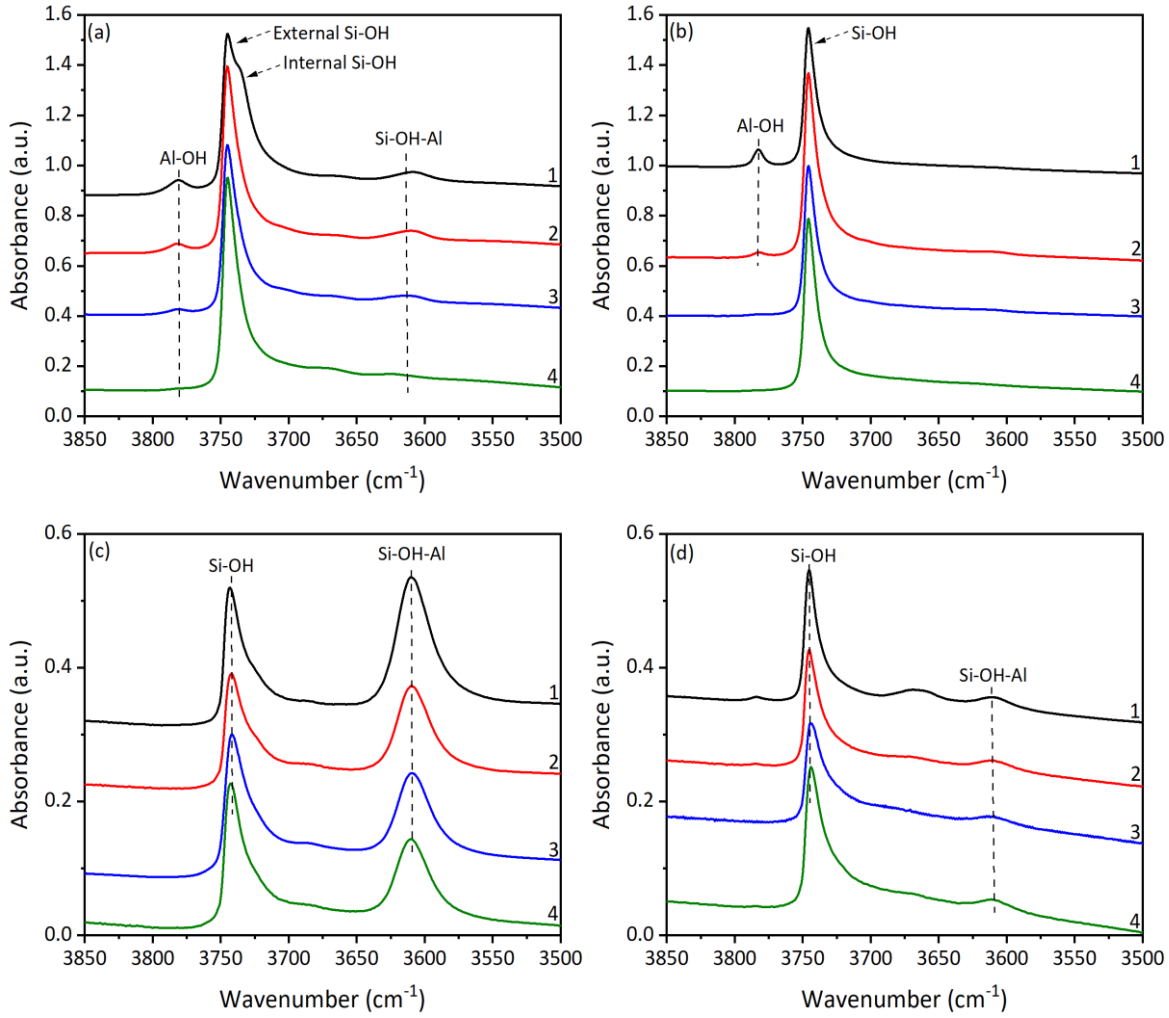


**Figure 3.14.** FTIR spectra of the hydroxyl region of **(a)** BEA K-containing zeolites calcined at 450ºC. (**1)** BEA 450ºC **(2)** 0.25 K/BEA 450ºC-IM **(3)** 0.5 K/BEA 450ºC-IM and **(4)** 1 K/BEA 450ºC-IM. **(b)** BEA K-containing zeolites calcined at 800ºC (**1)** BEA 800ºC **(2)** 0.25 K/BEA 800ºC-IM **(3)** 0.5 K/BEA 800ºC-IM **(4)** 1 K/BEA 450ºC-IM. **(c)** ZSM-5 Mg-containing zeolites calcined at 450ºC. **(1)** ZSM-5 450ºC **(2)** 0.25 Mg/ZSM-5 450ºC-IM **(3)** 0.5 Mg/ZSM-5-IM 450ºC and **(4)** 1 Mg/ZSM-5 450ºC-IM. **(d)** ZSM-5 Mg-containing zeolites calcined at 800ºC (**1)** ZSM-5 800ºC **(2)** 0.25 Mg/ZSM-5 800ºC-IM. **(3)** 0.5 Mg/ZSM-5 800ºC-IM and **(4)** 1 Mg/ZSM-5 800ºC-IM.

An incomplete exchange of H-form for $Ca^{2+}$ and $Mg^{2+}$ cations in ZSM-5 zeolite can be observed, as the peak of Si-OH-Al groups at 3610 $cm^{-1}$ is still present in the spectra (e.g

Figure 3.14 c and d). This limited exchange could be due to the degree of the hydration and the higher charge density of these ions. Hence, $Mg^{2+}$ and $Ca^{2+}$ cations cannot balance the charge of the so-called isolated Al containing tetrahedra, which are separated by a considerable distance in high-silica zeolites [52,53]. Loading low amounts of $Na^{+}$ and $K^{+}$ ions in BEA zeolite (samples 0.25 Na/BEA 450ºC and 0.25 K/BEA 800ºC) leads to an increase in the intensity of Si-OH-Al peak at the 3610 $cm^{-1}$, when compared with the BEA zeolite calcined. This could be an indication that low loadings of these ions in BEA zeolite prevents the breaking of Si-O-Al bonds and the formation of EFAl species that normally take place during thermal treatment (spectra not shown, see Figure 3.16 a and d).

The intensity in the peak at 3745 $cm^{-1}$ (Si-OH groups) is unchanged for ZSM-5 cation-containing zeolites, due to their weak acidity. These OH groups are usually not affected by the modification with cations (e.g. Figure 3.14 c and d). However, the same peak in BEA cation-containing zeolites shows considerable changes especially after impregnation of higher amounts of $Mg^{2+}$ and $Ca^{2+}$. This could be due to a neutralisation reaction between the Si-OH groups and Mg and Ca oxide particles formed during thermal treatment. The changes can also be linked to the partial destruction of BEA crystal structure, resulting in a condensation of the Si-OH groups and the formation of dense amorphous silica [16]. The Al-OH peak at 3780 $cm^{-1}$ gradually disappears with the increasing loadings of cations, indicating that these EFAl species could interact with charge-compensating cations, being able to exchange with the salts of metals [16].

After Py adsorption at 150ºC in all cation-containing zeolites, the peaks at 3610 $cm^{-1}$, 3782 $cm^{-1}$ and 3662 $cm^{-1}$ completely disappear (e.g. Figure 3.15 a and b) proving their acidic character. This decrease is accompanied by the appearance of bands at 1545 $cm^{-1}$ and 1455 $cm^{-1}$, which are ascribed to the interaction of Py with BAS and LAS, respectively. The appearance of peaks at 1441, 1443, 1445 or 1448 $cm^{-1}$ results from Py coordinated to $K^{+}$, $Na^{+}$, $Ca^{2+}$ and $Mg^{2+}$ (Py-K, Py-Na, Py-Ca and Py-Mg) and are usually associated with Lewis

acidic centres due to their extra-framework positions (e.g. Figure 3.15 c). The frequency of these bands has been widely studied and increases with cation charge/size ratio [54,55].

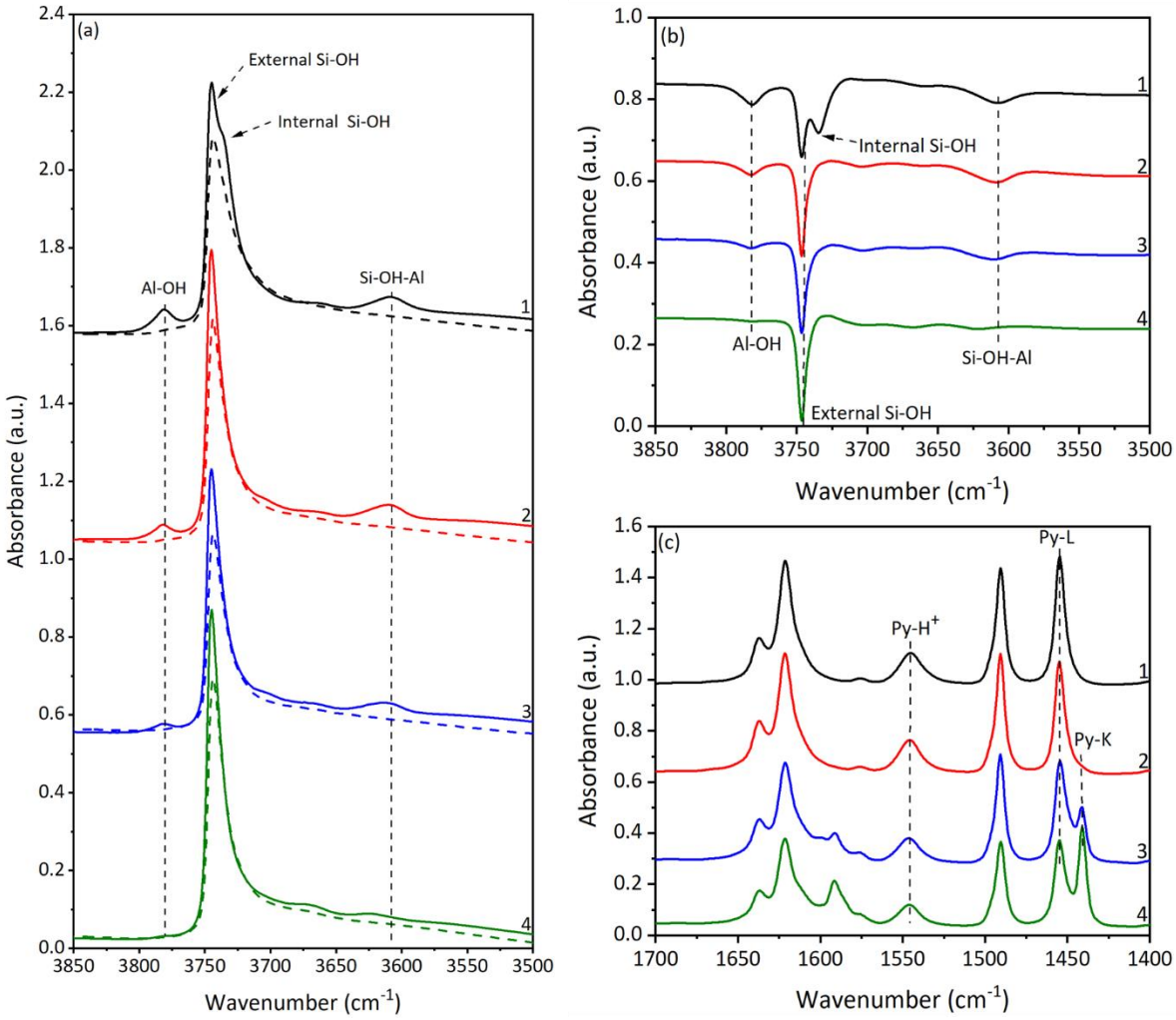


**Figure 3.15.** FTIR spectra of the hydroxyl region of BEA K-containing zeolites calcined at 450ºC prepared by impregnation **(a)** before (full lines) and after (dashed lines) Py adsorption at 150ºC. **(b)** Difference spectra of the hydroxyl region following Py adsorption at 150ºC. **(c)** Difference spectra of the Py region following Py adsorption at 150ºC: **(1)** BEA 450ºC, **(2)** 0.25 K/BEA 450ºC-IM, **(3)** 0.5 K/BEA 450ºC-IM and **(4)** 1 K/BEA 450ºC-IM.

The quantification of BAS, LAS and cationic species for each zeolite was carried out using the Py peaks in the 1400-1700 $cm^{-1}$ region and is described in the experimental section 3.2.2, using (Figures 3.16 and 3.17). The changes in the total number of BAS (peak at 1545 $cm^{-1}$, $Py\text{-}H^{+}$) are directly associated with the variations in the Si-OH-Al groups. There is a gradual decrease in the number of BAS with the increase of cation loadings (Figures 3.16 and 3.17) and calcination temperature (Figure 3.16 and 3.17 compare left and right) due to

the breaking of the Si-O-Al bonds. A few samples with higher cation content, demonstrated a complete loss of BAS associated with the complete removal of Si-OH-Al groups at 3610 $cm^{-1}$. Cation-containing BEA zeolites calcined at 800ºC still present a small number of BAS even after complete disappearance of Si-OH-Al groups (Figure 3.16 a and d). The presence of these BAS confirms that weakly acidic hydroxyl groups affected by EFAl species (e.g. Si-OH····· EFAl) contribute to the Brønsted acidity of this zeolite structure. The constant number of BAS in ZSM-5 cation-containing zeolites with alkaline earth cations is in agreement with the incomplete exchange of $H^+$ for $Ca^{2+}$ and $Mg^{2+}$ cations (Figure 3.18 a and d).

The introduction of cations also affects the number of extra-framework species detected. There is a decrease in the number of LAS and an increase in the number of cationic species (Py molecules adsorbed on the cations). The increase in the number of cationic species is in line with the increasing concentration of cations introduced in the zeolites during the modification treatment, while the decrease in the number of LAS suggests a limited formation of LAS due to the presence of these cationic species (Figures 3.16 and 3.17). Previous reports have proposed that the loss of both LAS and BAS is a consequence of steric effects caused by the introduced cations [56-58], leading to a decreased accessibility of the acid sites to Py. However, there is no evidence of decreased acid site accessibility in these samples, as all existing Si-OH-Al groups are still accessible to Py.

Py is more strongly held when the zeolite contains cations with a smaller size or with a stronger electrostatic field. The strength of the interaction changes as followed: $Mg^{2+}$ > $Ca^{2+}$ > $Na^+$ > $K^+$ (Figures 3.16 and 3.17 c and f). However, BEA containing-alkaline earth metals followed by thermal treatment at 800ºC demonstrate a reduced availability of $Mg^{2+}$ and $Ca^{2+}$ for the interaction with Py (Figure 3.16 f). This could be due to the excessive formation of oxide-like species and the partial collapse of the crystalline BEA framework. This observation can be confirmed by the decline in the relatively crystallinities, apparent $S_{BET}$ and $S_{micro}$ areas for this zeolite when calcined at 800ºC (Table 3.6 and Figure 3.14). The

damage of the zeolite lattice influences the internal channels of BEA zeolite, leading to a reduction in the micropore areas and a decrease in the potentially available cationic exchange sites.

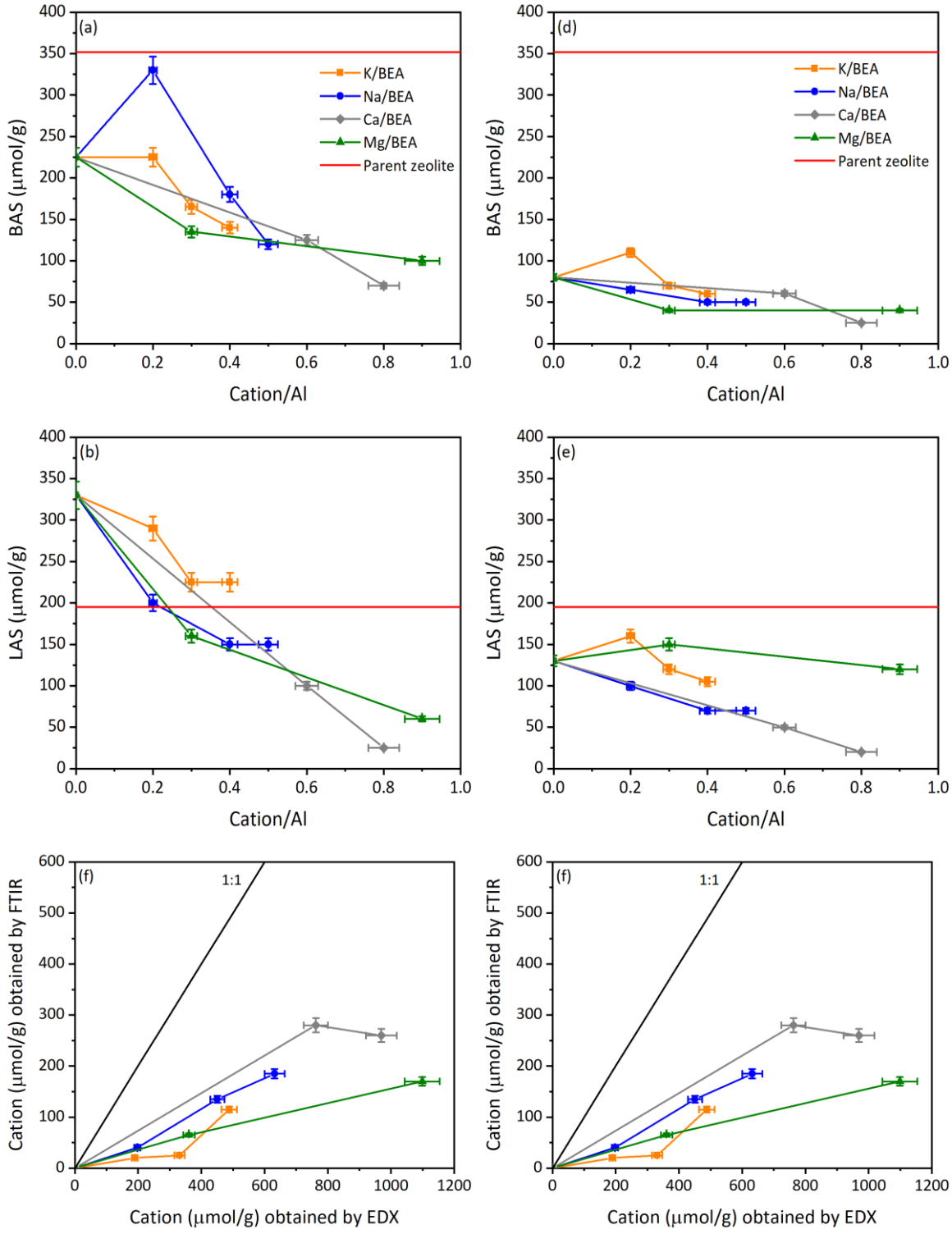


**Figure 3.16**. Relationship between number of acid sites and cation amount in cation containing BEA zeolites. **(a-c)** Cation containing BEA zeolites prepared by impregnation followed by calcination at 450ºC and **(d-f)** cation containing BEA zeolites prepared by impregnation followed by calcination at 800ºC.

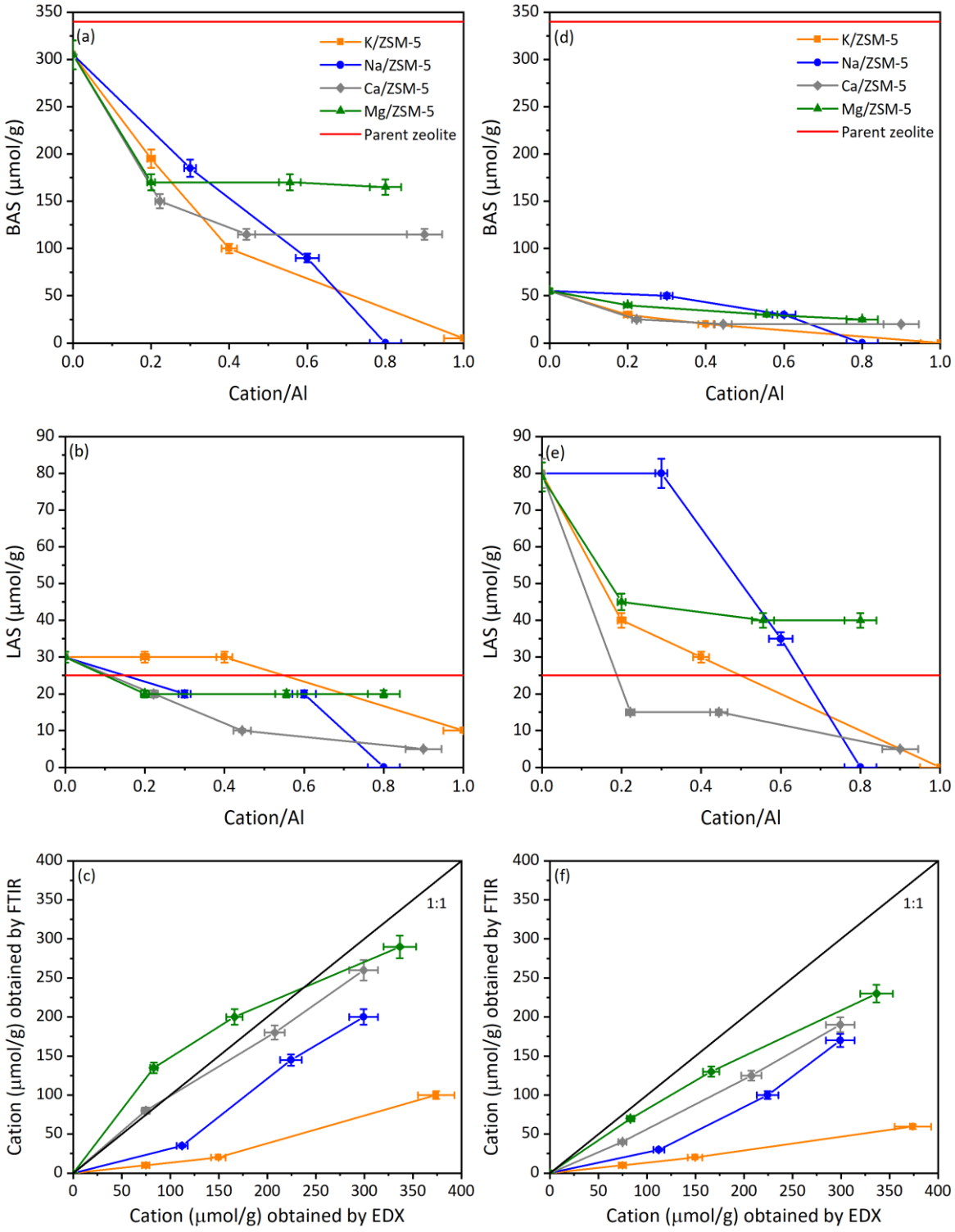


**Figure 3.17.** Relationship between number of acid sites and cation amount in cation containing ZSM-5 zeolites. **(a-c)** Cation containing ZSM-5 zeolites prepared by impregnation followed by calcination at 450ºC and **(d-f)** cation containing ZSM-5 zeolites prepared by impregnation followed by calcination at 800ºC.

Additional confirmation of partial degradation of the zeolite BEA when overloaded with $Ca^{2+}$ ions is given by the $^{27}Al$ MAS NMR spectra (Figure 3.18). The spectra show a significant decrease in the amount of tetrahedral Al species with a signal at δ~60-54 ppm; and a complete disappearance of the signal at δ~0 ppm related to EFAl species. The remaining BEA cation-containing zeolites display a decrease in the framework Al and EFAl species, which agrees with the data obtained by Py-FTIR. The broad signal of the tetrahedral Al species (δ~60-54 ppm) in all BEA cation-containing zeolites is indicative of the increasing disorder of the local Al environment caused by impregnation and thermal treatment. ZSM-5 cation-containing zeolites show no clear evidence of the formation of additional octahedral EFAl species (δ~0 ppm) or distorted tetrahedral Al species (spectra not shown).

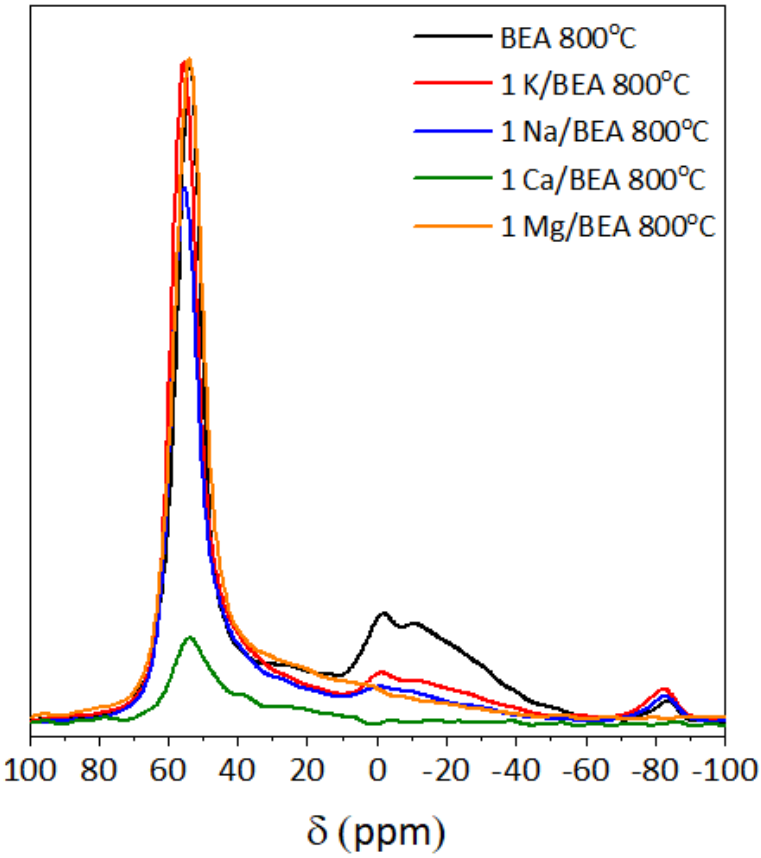


**Figure 3.18.** Normalised $^{27}Al$ solid-state MAS NMR spectra of selected zeolites. **(a)** BEA 800ºC, **(b)** 1 K/BEA 800ºC **(c)** 1 Na/BEA 800ºC **(d)** 1 Ca/BEA 800ºC **(e)** 1 Mg/BEA 800ºC.

In summary, preparation of cation-containing zeolites by impregnation followed by thermal treatments leads to three main changes in the acidic properties of both BEA and ZSM-5 zeolites:

(i) Decrease in the number of Si-OH-Al groups and BAS.

(ii) Protection of zeolite structure during thermal treatment- small amounts of $Na^+$ ions and possibly $K^+$ ions tend to prevent the breaking of the Si-OH-Al groups (BAS). Additionally, the presence of cations limits the formation of species acting as LAS.

(iii) Degradation of the zeolite structure at higher calcination temperatures- when BEA zeolite is overloaded with $Mg^{2+}$ and $Ca^{2+}$ cations.

These changes are strongly dependent on a large number of factors, such as the type of zeolitic structure, amount, size, and charge of cation incorporated and the calcination temperatures used during the modification.

## 3.5 Effect of cation incorporation by ion exchange

BEA and ZSM-5 zeolites were also ion exchanged with nitrate aqueous solutions of $K^+$, $Na^+$, $Mg^{2+}$ and $Ca^{2+}$, to compare the effect of different incorporation methods (ion exchange versus impregnation) on properties of both zeolite structures. For simplicity and due to the high volume of work only the most relevant results are described in Section 3.5.

### 3.5.1 Structural properties

The XRD patterns of selected ZSM-5-containing zeolites obtained after ion exchange with $Mg^{2+}$ and $Ca^{2+}$ are very similar to the respective parent and calcined zeolite (Figure 3.19). There is no evidence of additional peaks that could be assigned to the cations, which indicates a good dispersion of the species through the zeolitic structure.

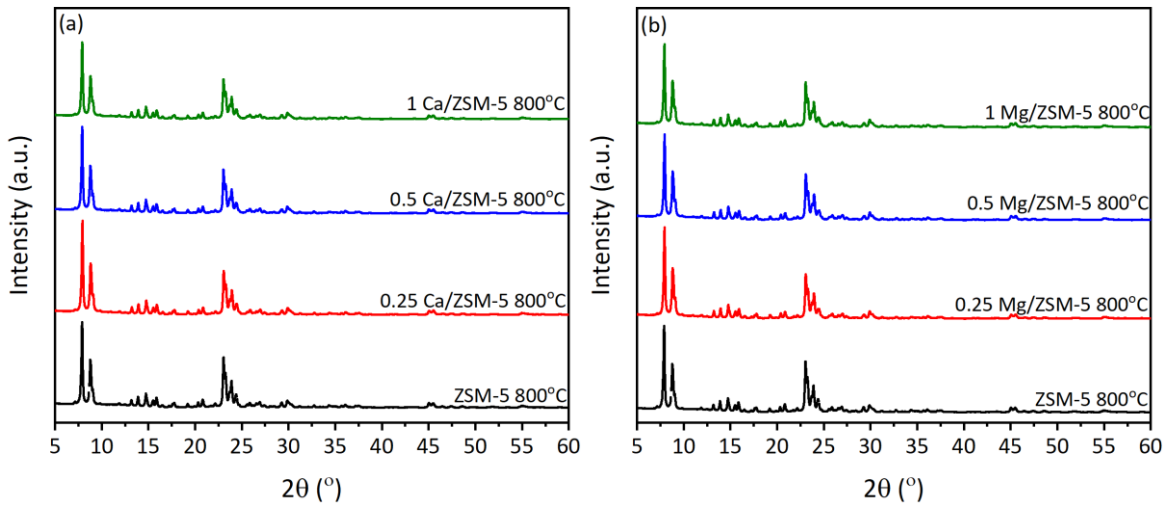


**Figure 3.19.** X-ray diffraction patterns obtained for selected zeolites **(a)** Ca/ZSM-5 800ºC **(b)** Mg/ZSM-5 800ºC.

The estimated values for the relative crystallinities slightly decrease (Table 3.8) with the presence of the cations. This decrease suggests a small loss of crystal structure associated with the high temperature at which the zeolites were calcined, in similarity with cation-containing zeolites prepared by impregnation. There are no significant changes in the Si/Al ratios after ion exchange and thermal treatment. The cation/Al ratios obtained after modification by ion exchange are very low for the selected zeolites (Table 3.8), indicating an incomplete exchange between $H^+$ and the cations.

**Table 3.8.** Structural properties of selected ZSM-5 cation-containing zeolites prepared by ion exchange.

| Zeolite ID | Si/Al (EDX) | Cation/Al (EDX) | Relative Crystallinity (%) |
|---|---|---|---|
| ZSM-5 | 32.0 | - | 100 |
| ZSM-5 800ºC | 31.4 | - | 90 |
| 0.25 Ca/ZSM-5 800ºC | 32.9 | 0.04 | 100 |
| 0.5 Ca/ZSM-5 800ºC | 32.3 | 0.05 | 97 |
| 1 Ca/ZSM-5 800ºC | 32.1 | 0.07 | 97 |
| 0.25 Mg/ZSM-5 800ºC | 32.1 | 0.03 | 100 |
| 0.5 Mg/ZSM-5 800ºC | 32.4 | 0.07 | 98 |
| 1 Mg/ZSM-5 800ºC | 32.5 | 0.09 | 99 |

### 3.5.2 Acidic properties

Ion exchange with $Mg^{2+}$ and $Ca^{2+}$ ions results in a variation in the OH region of the FTIR spectra (e.g. Figure 3.20). There is a gradual increase in the intensity of both peaks at 3610 $cm^{-1}$ and 3745 $cm^{-1}$ (bridging Si-OH-Al and Si-OH groups, respectively) with the increase of cation loadings. The increase in the intensity of the Si-OH-Al peak indicates that both $Mg^{2+}$ and $Ca^{2+}$ ions have a protective effect over the Si-OH-Al groups during thermal treatment. The more cation exchanged, less Si-O-Al bonds are broken leading to an increase in the intensity of the peak at 3610 $cm^{-1}$ when compared with ZSM-5 calcined at 800ºC (with $H^{+}$ as extra-framework cation). The changes in the intensity of the Si-OH peak could be due to a neutralisation reaction between these groups and Mg and Ca oxide particles and the creation of more defects in the structure.

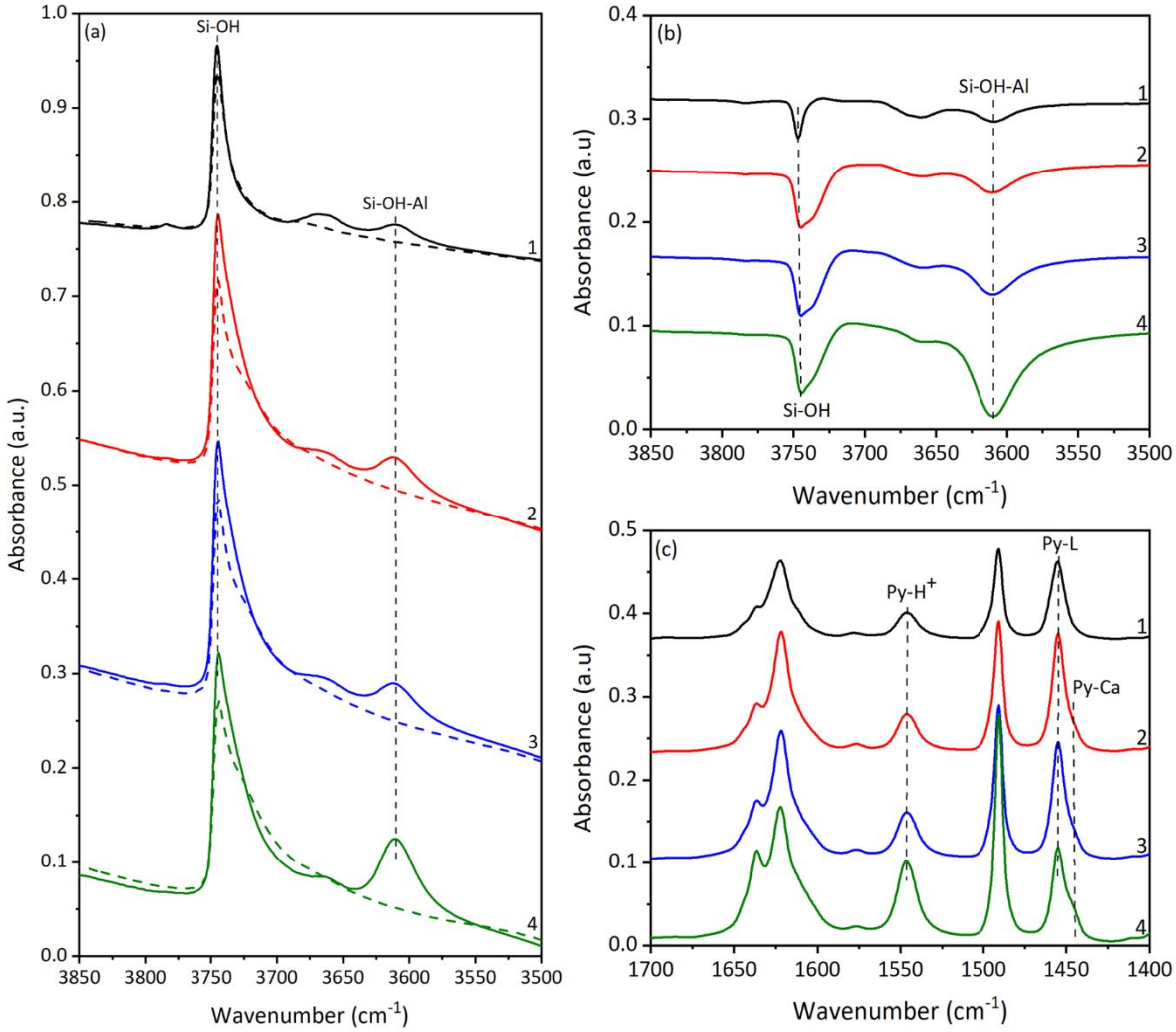


**Figure 3.20.** FTIR spectra of the hydroxyl region of ZSM-5 Ca-containing zeolites calcined at 800ºC prepared by ion exchange **(a)** before (full lines) and after (dashed lines) Py adsorption at 150ºC. **(b)** Difference spectra of the hydroxyl region following Py adsorption at 150ºC. **(c)** Difference spectra of the Py region following Py adsorption at 150ºC: **(1)** ZSM-5 800ºC, **(2)** 0.25 Ca/ZSM-5 800ºC-IE, **(3)** 0.5 Ca/ZSM-5 800ºC-IE and **(4)** 1 Ca/ZSM-5 800ºC-IE.

Adsorption of Py at 150ºC leads to the disappearance of the Si-OH-Al peak at 3610 $cm^{-1}$ and a slight decrease of the Si-OH peak at 3745 $cm^{-1}$ (Figure 3.20 a and b). From the interaction with Py, the number of BAS, LAS and cations can be obtained (in a similar way to zeolites in Section 3.3.2 and 3.4.2) using the peaks in the 1400-1700 $cm^{-1}$ region (Figure 3.20 c and 3.21). The number of BAS gradually increases with cation loadings. These changes are directly related to the Si-OH-Al groups in each zeolite, both $Mg^{2+}$ and $Ca^{2+}$ prevent the breaking of the Si-O-Al bonds due to thermal treatment. The number of LAS

slightly decreases demonstrating that the modification does not produce additional EFAl species.

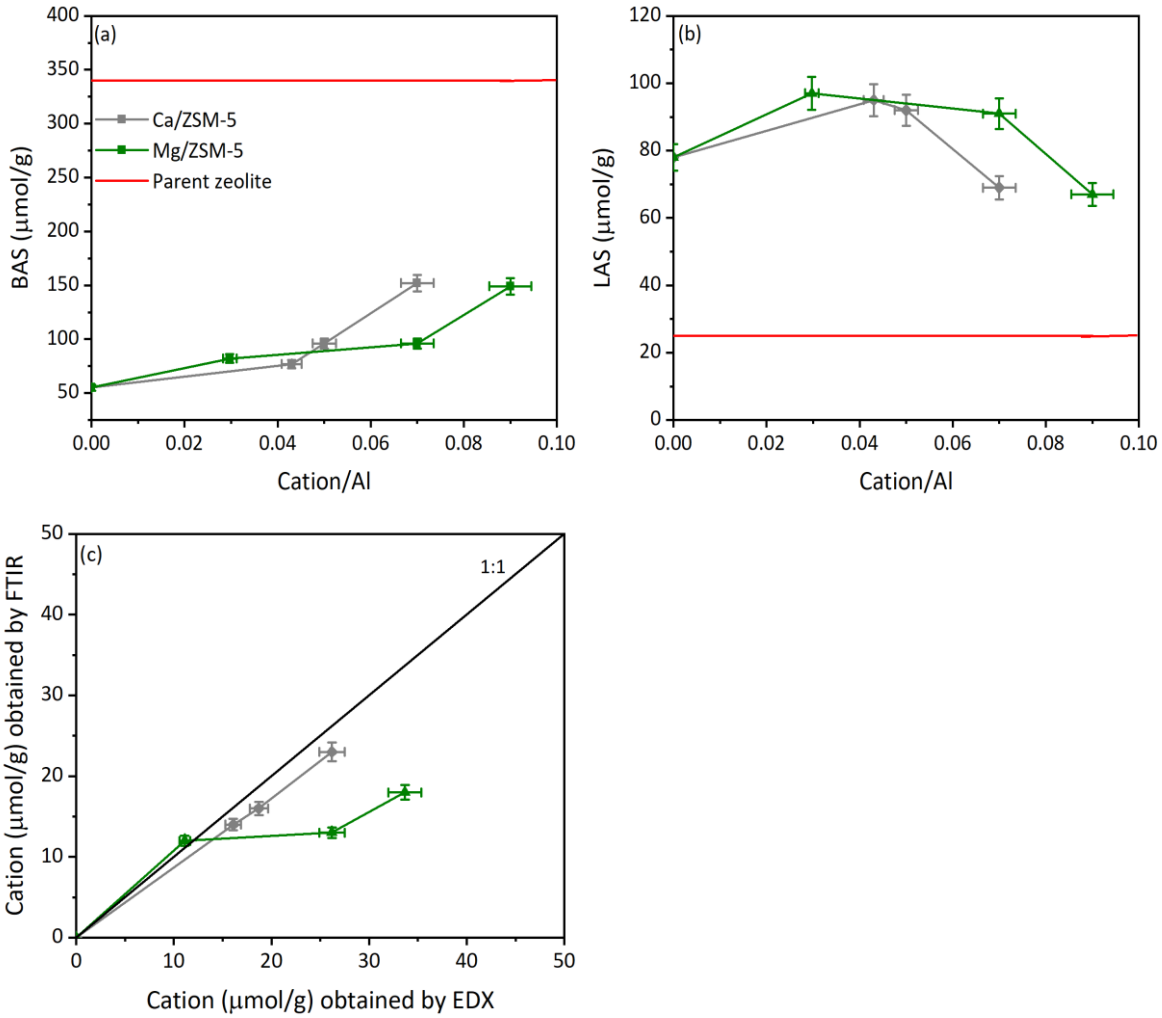


**Figure 3.21.** Relationship between number of acid sites and cation amount in ZSM-5 zeolites prepared by ion exchange followed by calcination at 800ºC.

## 3.6 Summary

An extensive characterisation of BEA and ZSM-5 zeolites was performed to evaluate the effects of thermal treatment and incorporation of alkali and alkaline earth cations on the zeolite structures. Thermal treatment leads to a decrease in the zeolite crystallinity of both zeolites and in the textural properties of BEA zeolite. The results indicate that this post-synthesis treatment causes the breaking the of Si-O-Al bonds, resulting in the reduction of strong BAS and formation of LAS (EFAl). Although no severe structural degradation is observed in both zeolites even at higher calcination temperatures, BEA zeolite is more

affected by thermal treatment in comparison with ZSM-5 zeolite, due to the flexibility in the coordination sphere of the Al atoms in the 12-MR system of this zeolite.

Both ion exchange and impregnation methods have no large effect on the crystallinity and porosity of ZSM-5 and BEA zeolites, however, they affect the hydroxyl groups and acidic properties significantly. In general, cation-containing zeolites showed a lower number of BAS when compared with the parent zeolite, due to the incorporation of the cations and thermal treatment. A limited formation of EFAl species acting as LAS and an increase of cationic species is also observed. Introduction of $Mg^{2+}$ and $Ca^{2+}$ ions by ion exchange in ZSM-5 zeolites leads to a recovery of the BAS. These cations induce a protective effect on the acidic properties of the zeolite, preventing the breaking of Si-O-Al bonds at high temperatures (800ºC). The same results were achieved for zeolite BEA, by impregnation of small amounts of $K^{+}$ followed by thermal treatment at 450ºC. Significant degradation of the structure was observed for BEA zeolite after overloading with $Mg^{2+}$ and $Ca^{2+}$ ions followed by thermal treatment at high temperatures (800ºC).

These results demonstrate that post-synthesis modifications have a great influence in the structural, textural, and acidic properties of both ZSM-5 and BEA zeolites. This work is evidence that it is possible to adapt the properties (especially acidic properties) of both structures to give selective catalysts for desired reactions.

### 3.7 References

[1] G. Busca. *Zeolites and other structurally microporous solids* in *Heterogeneous catalytic materials: Solid-state chemistry, surface chemistry, and catalytic behaviour*. Elsevier., 2014, 198-241.

[2] A. Primo and H. Garcia. *Zeolites as catalysts in oil refining.* Chem. Soc. Rev., 2014, 43, 7548-7561.

[3] J. Cejka, G. Centi, J. Pérez-Pariente and W. J. Roth. *Zeolite-based materials for novel catalytic applications: Opportunities, perspectives and open problems***.** Catal. Today., 2012, 179, 2-15.

[4] K. Shimizu and A. Satsuma. *Toward a rational control of solid acid catalysis for green synthesis and biomass conversion.* Energy Environ. Sci., 2011, 4, 3140-3153.

[5] J. Jae, E. Mahmoud, R.F. Lobo and D. G. Vlachos. *Cascade of liquid-phase catalytic transfer hydrogenation and etherification of 5-hydroxymethylfurfural to potential biodiesel components over Lewis acid zeolites*. Chem. Cat. Chem., 2014, 6, 508-513.

[6] P. Y. Dapsens, C. Mondelli and J. Pérez-Ramírez. *Design of Lewis-acid centres in zeolitic matrices for the conversion of renewables.* Chem. Soc. Rev., 2015, 44, 7025-7043.

[7] N. Brodu, M-H Manero, C. Andriantsiferana, J-S. Pic and H. Valdés. *Role of Lewis acid sites of ZSM-5 zeolite on gaseous ozone abatement*. Chem. Eng. Sci., 2013, 231, 281-286.

[8] R. Zhang, N. Liu, Z. Lei and B. Chen. *Selective transformation of various nitrogen-containing exhaust gases toward $N_2$ over zeolite catalysts*. Chem. Rev., 2016, 116, 3658-3721.

[9] D. Pietrogiacomi, M. C. Campa and M. Occhiuzzia., *Selective catalytic reduction of $N_2O$ with $CH_4$ on Ni-MOR: A comparison with Co-MOR and Fe-MOR catalysts.* Catal. Today, 2014, 227, 116-122.

[10] M. Tagliabuea, D. Farrusseng, S. Valencia, S. Aguado, U. Ravon, C, Rizzoa, A. Corma and C. Mirodatos. *Natural gas treating by selective adsorption: Material science and chemical engineering interplay*. Chem. Eng. Sci., 2009,155, 553-566.

[11] B. Sreenivasulu, P. Suresh, I. Sreedhar and K. V. Raghavan. *Development trends in porous adsorbents for carbon capture*. Environ. Sci. Technol., 2015, 49, 12641-12661.

[12] M. C. Bacariza, R. Bértolo, I. Graça, J. M. Lopes and C. Henriques. *The effect of the compensating cation on the catalytic performances of Ni/USY zeolites towards $CO_2$ methanation*. J. $CO_2$. Util, 2017, 21, 280-291.

[13] I. Graça, M. C. Bacariza, A. Fernandes and D. Chadwick. *Desilicated NaY zeolites impregnated with magnesium as catalysts for glucose isomerisation into fructose*. Appl. Catal., B., 2018, 224, 660-670.

[14] N. Kosinova, J. Gascon, F. Kapteijn and E. J. M. Hensen. *Recent developments in zeolite membranes for gas separation.* J. Membr. Sci., 2016, 499, 65-79.

[15] S. Cinar and B. Beler-Bayka. *Ion exchange with natural zeolites: an alternative for water softening?* Water Sci. Technol., 2005, 51, 71-77.

[16] C. Bisio, P. Massiani, K. Fajerwerg, L. Sordelli, L. Stievano, E. R. Silva, S. Coluccia and G. Martra. *Identification of cationic and oxidic caesium species in basic Cs-overloaded BEA zeolites*. Microporous Mesoporous Mater., 2006, 90, 175-18.

[17] H. Han, M. Liu, F. Ding, Y. Wang, X. Guo and C. Song. *Effects of caesium ions and caesium oxide in side-chain alkylation of toluene with methanol over caesium-modified zeolite X*. Ind. Eng. Chem. Res., 2016, 66, 1849-1858.

[18] W. Xu, S. Ji, W. Quan and J. Yu. *One-Post synthesis of dimethyl carbonate over basic zeolite catalysts*. Mod. Res. Catal., 2013, 2, 22-27.

[19] G. Näfe, M-A. López-Martínez, M. Dyballa, M. Hunger, Y. Traa, T. Hirth and E. Klemm. *Deactivation behavior of alkali-metal zeolites in the dehydration of lactic acid to acrylic acid*. J. Catal., 2015, 329, 413-42.

[20] C. Yuan, H. Liu, Z. Zhang, H. Lu, Q. Zhu and Y. Chen. *Alkali-metal modified ZSM-5 zeolites for improvement of catalytic dehydration of lactic acid to acrylic acid.* Chinese. J. Catal., 2015, 36, 1861-1866.

[21] O. Kikhtyanin, R. Bulánek, K. Frolich, J. Cejka and D. Kubicka. *Aldol condensation of furfural with acetone over ion-exchanged and impregnated potassium BEA zeolites*. J. Mol. Catal. A: Chem., 2016, 424, 358-368.

[22] M. Muller, G. Harvey and R. Prins. *Comparison of the dealumination of zeolites beta, mordenite, ZSM-5 and ferrierite by thermal treatment, leaching with oxalic acid and*

*treatment with $SiCl_4$ by $^{1}H$, $^{29}Si$ and $^{27}Al$ MAS NMR.* Microporous Mesoporous Mater., 34, 2000, 135-147.

[23] R. Xu, W. Pang, J. Yu, Q. Huo and J. Chen. *Preparation, Secondary Synthesis, and Modification of Zeolites* in *Structural chemistry of microporous materials* in *Chemistry of zeolites and related porous materials: synthesis and structure*. John Wiley & Sons., 2007, 345-383.

[24] G. Cruciani. *Zeolites upon heating: Factors governing their thermal stability and structural changes*. J. Phys. Chem. Solids., 67, 2006, 1973-1994.

[25] M-C. Silaghi, C, Chizallet and P. Raybaud. *Challenges on molecular aspects of dealumination and desilication of zeolites.* Microporous Mesoporous Mater., 191, 2014, 82-96.

[26] Y. Hong and J. J. Fripiat. *Microporous characteristics of H-Y, H-ZSM-5 and H-mordenite dealuminated by calcination.* Microporous Mater., 4, 1995, 323-334.

[27] H. K. Beyer. *Dealumination techniques for zeolites* in *Molecular Sieves*. Eds: H. G. Karge and J. Weitkamp. Springer-Verlag., 204-248.

[28] P. A. Wright. *The chemistry of microporous framework solids* in *Microporous framework solids*. Royal Society of Chemistry., 2007, 226-256.

[29] L. H. Ong, M. Dömök, R. Olindo, A. C. van Veen and J. A. Lercher. *Dealumination of HZSM-5 via steam-treatment.* Microporous Mesoporous Mater., 2012, 164, 9-20.

[30] J. P. Marques, I. Gener, P. Ayrault, J. C. Bordado, J. M. Lopes, R. F. Ramôa and M. Guisnet. *Infrared spectroscopic study of the acid properties of dealuminated BEA zeolites*. Microporous Mesoporous Mater., 60, 2003, 251-262.

[31] J. Datka and E. Tunik. *Infrared Spectroscopic Studies of Acid Properties of NaHZSM-5 zeolites*. J. Catal., 1986, 102, 43-51.

[32] O. Larlus, V. Valtchev, L. Delmotte and H. Kessler. *Size and morphological control of all-silica zeolite BEA.* Stud. Surf. Sci. Catal., 2004, 154, 725-730.

[33] M. M. Treacy and J. B. Higgins. *Collection of simulated XRD powder patterns for zeolites*. Elsevier. 2007.

[34] T. C. Hoff, R. Thilakaratne, D. W. Gardner, R. C. Brown and J-P. Tessonnier. *Thermal stability of aluminum-rich ZSM-5 zeolites and consequences on aromatization reactions.* J. Phys. Chem. C., 2016, 120, 20103-20113.

[35] M. Thommes, K. Kaneko, A. V. Neimark, J. P. Olivier, F. Rodriguez-Reinoso, J. Rouquerol and K. S. W. Sing. *Physisorption of gases, with special reference to the evaluation of surface area and pore size distribution (IUPAC Technical Report).* Pure Appl. Chem., 2015, 87, 1051-1069.

[36] J. Peréz-Pariente, J. Sanz, V. Fornés and A. Corma. *$^{29}$Si and $^{27}$Al MAS NMR study of zeolite β with different Si/Al ratios.* J. Catal., 1990, 124, 217-223.

[37] J. Peréz-Pariente, J. A. Martens and P. A. Jacobs. *Crystallization mechanism of zeolite beta from $(TEA)_2O$, $Na_2O$ and $K_2O$ containing aluminosilicate gels.* Appl. Catal., 1987, 31, 35-64.

[38] R. Millini, C. Perego, W. O. Parker, C. Flego and G. Girotti. *Stability upon thermal treatment of coked zeolite BEA*. Stud. Surf. Sci. Catal., 2004, 154, 1214-1221.

[39] S. B. Liu, J. F. Wu, J. L. Ma, C. T. Tsai and I. Wang. *On the thermal stability of zeolite beta.* J. Catal., 1991, 132, 432-439.

[40] V. N. Romannikov, V. M. Mastikhin, S. Hočevar and B. Držaj, *Laws observed in the synthesis of zeolites having the structure of ZSM-5 and varying chemical composition*. Zeolites.,1983, 3, 311-320.

[41] Z. Gabelica, B. Nagy, E. G. Debrouane and J. P Gilson. *The use of combined thermal analysis to study crystallization, pore structure, catalytic activity and deactivation of synthetic zeolites*. Clay Minerals., 1984, 19, 803-824.

[42] S. M. Campbell, D. M. Bibby, M. J. Coddington, R.F. Howe and R. H. Meinhold, *Dealumination of HZSM-5 zeolites I. Calcination and hydrothermal treatment.* J. Catal., 1996, 161, 338-349.

[43] Q. L. Wang, G. Giannetto, M. Torrealba, G. Perot, C. Kappenstein and M. Guisnet, *Dealumination of zeolites II. Kinetic study of the dealumination by hydrothermal treatment of a $NH_4NaY$ zeolite.* J. Catal., 1991, 130, 459-470.

[44] P. J. Kunkeler, B. J. Zuurdeeg, J. C. van der Waal, J. A. van Bokhoven, D. C. Koningsberger and H. van Bekkum. *Zeolite beta: The relationship between calcination procedure, aluminum configuration and Lewis acidity*. J. Catal., 1998, 180, 234-244.

[45] I. Kiricsi, C. Flego, G. Pazzuconi, W. O. Jr. Parker, R. Millini, C. Perego, and G. Bellussi. *Progress toward understanding zeolite ß acidity: An IR and $^{27}Al$ NMR spectroscopic study.* J. Phys. Chem., 1994, 98, 4627-4634.

[46] A. Vimont, F. Thibault-Starzyk and J. C. Lavalley. *Infrared spectroscopic study of the acidobasic properties of beta zeolite*. J. Phys. Chem. B., 2000, 104, 286-291.

[47] A. Janin, M. Maache, and J. C. Lavalley. *FTIR study of the silanol groups in dealuminated HY zeolites: Nature of the extra-framework debris.* Zeolites, 1991, 11, 391-396.

[48] K. Hadjiivanov. *Identification and characterization of surface hydroxyl groups by infrared spectroscopy.* Adv. Catal., 2014, 57, 99-318.

[49] L-E. Sandoval-Díaz, J-A. González-Amaya and C-A. Trujillo. *General aspects of zeolite acidity characterisation*. Microporous Mesoporous Mater., 2015, 215, 229-243.

[50] M. Guisnet, P. Ayrault, C. Coutanceau, M. F Alvarez and J. Datka. *Acid properties of dealuminated beta zeolites studied by IR spectroscopy.* J. Chem Soc., Faraday Trans., 1997, 93, 1661-1665.

[51] B. H. Chiche, F. Fajula and E. Garrone. *Formation of conjugated iminium ions from pyridine on dealuminated mazzite.* J Catal., 1994, 146, 460-467.

[52] A. M. McAleer, L. V. C. Rees and A. K. Nowak. *Ion exchange and aluminium distributions in ZSM-5 zeolites. Zeolites*., 1991,11. 329-336.

[53] Y. Khabzina, C. Laroche, C. Pagis and D. Farrusseng. *Monovalent and bivalent cations exchange isotherms for faujasites X and Y*. Phys. Chem. Chem. Phys., 2017, 19, 17242-17249.

[54] J. W. Ward. *The nature of active sites on zeolites: III. The alkali and alkaline earth ion-exchanged forms*. J. Catal., 1968, 10, 34-46.

[55] J. Yu, J. Luo, Y. Zhang, J. Cao, C-C. Chang, R. J. Gorte and W. Fan. *An examination of alkali-exchanged BEA zeolites as possible Lewis-acid catalysts.* Microporous Mesoporous Mater., 2016, 225, 472-481.

[56] W. Wu and E. Weitz. *Modification of acid sites in ZSM-5 by ion-exchange: An in-situ FTIR study*. Appl Surf Sci., 2014, 316, 405-415.

[57] Y. Kuwahara, K. Nishizawa, T. Nakajima, T. Kamegawa, K. Mori and H. Yamashita. *Enhanced catalytic activity on titanosilicate molecular sieves controlled by cation−π interactions.* J. Am. Chem. Soc., 2011, 133, 12462-12465.

[58] T. Yashima and N. Hara. *Infrared study of cation-exchanged mordenites and Y faujasites adsorbed with ammonia and pyridine*. J. Catal., 1972, 27, 329-331.

# Chapter 4 Accessibility and location of acid sites in zeolites with different pore sizes

## 4.1 Introduction

The microporous nature of zeolites determines some of their essential properties, such as high surface area, adsorption capacity and shape selectivity. However, the presence of micropores may lead to diffusional limitations, shorter catalyst lifetime and poor activity [1,2]. To achieve the full potential of a zeolite catalyst, it is important to maximise the accessibility of acid sites within the micropore system and the transport efficiency for feed molecules and products in catalytic reactions [3-6]. Acid sites hosted on the external surface of a zeolite are commonly accessible; the accessibility within the microporous system is dependent upon the dimensions of the pore space relative to the guest molecule [7,8]. In the last few years, hierarchical and modified zeolites have provided a method to overcome the diffusion limitations [2,3]. Therefore, the understanding of the accessibility and location of acid sites is a very important issue. For that reason, it is necessary to know the location of Brønsted acid sites (BAS) and how easy it is to access them. This chapter will provide a methodology, using IR spectroscopy to determine the distribution, location, and accessibility of BAS in a series of different zeolites structures.

The use of various probe molecules with FTIR represents one of the most important tools to give a better understanding of acid site accessibility and location in different zeolitic structures. A variety of probe molecules such as hydrocarbons, nitriles and substituted nitriles have been already utilised [9-14]. These probes, when compared with other probe molecules, interact with acid sites less effectively, creating relatively weak bonds with the Brønsted acid sites (BAS) and Lewis acid sites (LAS).

Nesterenko et al. [15,16] and Bleken et al. [17] presented a methodology based on co-adsorption of alkylpyridines and carbon oxide (CO) for the analysis of acid site distribution in dealuminated MOR and MFI zeolites. The use of these probe molecules, with increasing

kinetic diameter, allows discrimination between acid sites located on the internal and external surfaces. Both pyridine (Py) and alkylpyridines are protonated by BAS. However, due to steric hindrance produced by bulky substituents, some alkylpyridines probes do not interact with LAS [18]. Such bulky probe molecules have limited access to some micropores due to their large kinetic diameter, and therefore, can be used to indicate the distribution of BAS in a variety of zeolites [19]. It should be noted that diffusion of such molecules though the zeolite micropores can be affected by the zeolite crystallite size. Co-adsorption of CO and nonane has also been used to examine the spatial distribution of platinum in the micropores and mesopores of bi-functional PtH-MFI catalysts [20]. This method involves nonane pre-adsorption between two successive CO chemisorption experiments.

Many reports have been published on the application of alkylpyridines such as, 2,6-di-tert-butylpyridine (DTBPy) [15,21-23] 2,6-dimethylpyridine (Lut) [15,24-27] and 2,4,6-trimethylpyridine (Coll) [16,28-30] for accessibility characterisation. For instance, adsorption of Py and Lut was used to detect traces of coke in MFI catalysts and to determine which acid sites are specifically perturbed by coke molecules [31]. The authors found that coke deposits, resulting from ortho-xylene isomerisation, do not perturb BAS but perturb non-acidic silanol groups (Si-OH) inside the micropore system. Using the same approach, Barbera et al. [28] confirmed that the presence of coke could influence catalyst deactivation. Both studies clearly distinguish between internal and external Si-OH and show that silanol defects play an important role in coke formation over MFI catalysts. Corma et al. [22] used the DTBPy to investigate the external surface of many zeolitic structures. DTBPy can enter the 12-membered channels of BEA but not the 10-membered ring channels of ZSM-5 and MCM-22. Therefore, it can be used to identify acid sites situated on the external surface of medium-pore zeolites.

Coll and Lut were used in the novel approach introduced by Thibault-Starzyk et al. [32], to quantify the accessibility of acid sites in ZSM-5 samples prepared with different degrees of intracrystalline mesoporosity. This approach is based on the calculation of the

accessibility index (ACI), the ratio between the number of BAS detected by substituted pyridines and the total number of BAS in the zeolite detected by Py. The results showed that the formation of mesoporosity reduces the average length of micropores and leads to an increase in the availability of acid sites at the pore mouths of ZSM-5. This methodology has been successfully used to evaluate the accessibility of acid sites in both nanocrystalline zeolites and in materials with a relatively large crystal size [32,33]. DTBPy was used to quantify external BAS in various parent and modified zeolites indicating that the extended mesoporosity and decreased average length of micropores resulted in an enhanced accessibility of BAS [23].

Overall, the optimisation of experimental procedures and the application of a combination of probe molecules are imperative for the successful evaluation of the location and accessibility of acid sites in different zeolite-based materials. Furthermore, it is necessary to understand which probe molecule or combination of probe molecules is suitable for a specific zeolitic structure, depending on its channel size, number of acid sites and modification treatments. In this study, medium- (ZSM-5), large- (BEA) and mixed-pore (MOR and MAZ) zeolites are characterised by monitoring the interaction between the zeolite BAS and probe molecules with a range of basicity and kinetic diameters. The aim is to establish the location and accessibility of BAS in the zeolitic structures, using FTIR, and to optimise the experimental procedure for the application of different probe molecules. This study also provides examples in the application of these methodologies in medium- and large- and mixed-pore structures converted into hierarchical meso-microporous catalysts.

## 4.2 Experimental

### 4.2.1 Parent and hierarchical zeolites

Ammonium forms of zeolites BEA (CP814E, BEA framework, Si/Al=12.5), ZSM-5 (CBV8014, MFI framework, Si/Al= 40) and MOR (CBV 21A, Si/Al= 10) were obtained from *Zeolyst International*. Proton form of MAZ zeolite (Si/Al= 4.7) was prepared and

provided by Johnson Matthey PLC site in Billingham, UK. An extensive structural characterisation of BEA and ZSM-5 zeolitic structures is presented in Chapter 3.

Several hierarchical materials were prepared by Aqeel Al-Ani at Keele University from parent zeolites ZSM-5, BEA, MOR and FAU, according to [34] in order to generate an intracrystalline network of mesopores. A detail characterisation of the hierarchical zeolites used in this chapter is presented in Table 4.1 [34]. The results suggest that well-defined networks of interconnected micro- and mesopores are formed in the materials following surfactant-templating treatment. The intracrystalline nature of uniform mesopores and a degree of long-range ordering have been previously confirmed for the large-pore (12-MR) FAU and MOR zeolites. In zeolite BEA (12-MR), the formation of mesopores is complicated by the random intergrowth of polymorphs A and B, whereas the medium-pore ZSM-5 zeolite is relatively "resistant" to this treatment as the 10-MR micropores are by and large inaccessible to the surfactant species. The mesopores produced in BEA and ZSM-5 has a broader pore size distribution and show little evidence of the long-range order.

**Table 4.1.** Textural properties of the parent and hierarchical zeolites.

| Zeolite | Si/Al (SEM) | Si/Al (NMR) | Crystallinity (%) | $S_{BET}$ ($m^2g^{-1}$) | $V_{micro}$ ($cm^3g^{-1}$) | $V_{meso}$ ($cm^3g^{-1}$) |
|---|---|---|---|---|---|---|
| Y | 2.5 | 2.6 | 98 | 855 | 0.33 | 0.04 |
| M-Y | 4 | 3.1 | 65 | 830 | 0.21 | 0.28 |
| BEA (19) | 19 | 18.7 | 98 | 695 | 0.26 | 0.06 |
| MBEA (19) | 15 | 13.2 | 81 | 740 | 0.2 | 0.12 |
| MOR | 10 | 9.3 | 93 | 488 | 0.20 | 0.03 |
| MMOR | 8.5 | 6.3 | 77 | 600 | 0.14 | 0.18 |
| ZSM-5 (15) | 15 | - | 97 | 395 | 0.20 | 0.03 |
| MZSM-5 (15) | 12 | - | 90 | 430 | 0.20 | 0.20 |

### 4.2.2 Probe molecules

The selected probes to evaluate the location and accessibility of BAS were: pyridine (Acros Organics, 99.5%), 2,6-dimethylpyridine (Sigma-Aldrich, 99%), 2,4,6-trimethylpyridine (BDH reagents, 95%), 2,6-di-tert-butyl-pyridine (Sigma-Aldrich, 97%) and 1,3,5-triisopropylbenzene (TIPB, Acros Organics, 95%). The properties and chemical structure of these probe molecules are summarised in Table 4.2 and Figure 4.1.

**Table 4.2.** Probe molecules and their properties selected for this study [7].

| Probe molecule | Chemical formula | Kinetic diameter (Å) | pKa |
|---|---|---|---|
| Pyridine (Py) | $C_5H_5N$ | 5.4 | 5.4 |
| 2,6-dimethylpyridine (Lut) | $C_7H_9N$ | 6.5 | 6.7 |
| 2,4,6-trimethylpyridine (Coll) | $C_8H_{11}N$ | 7.3 | 7.4 |
| 2,6-di-tert-butylpyridine (DTBPy) | $C_{13}H_{21}N$ | 7.9 | 7.9 |
| 1,3,5-triisopropylbenzene (TIPB) | $C_{15}H_{24}$ | 8.5 | - |

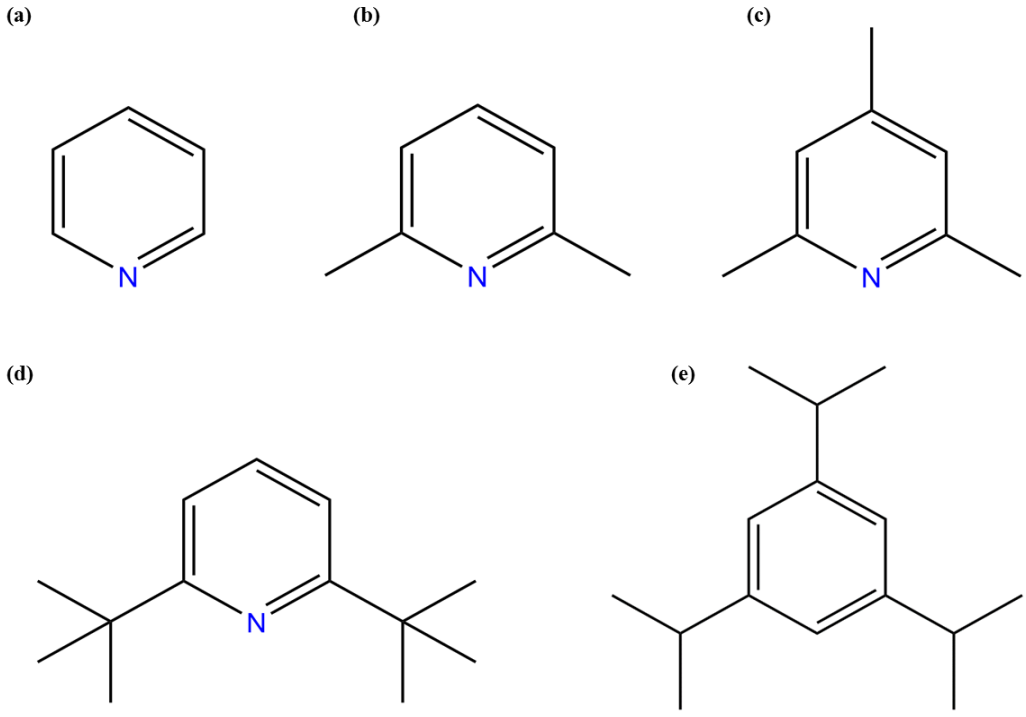


**Figure 4.1.** Chemical structure of **(a)** Pyridine (Py); **(b)** 2,6-dimethylpyridine (Lut); **(c)** 2,4,6-trimethylpyridine (Coll); **(d)** 2,6-di-tert-butylpyridine (DTBPy) and **(e)** 1,3,5-triisopropylbenzene (TIPB).

### 4.2.3 Acidity and accessibility studies

Prior to FTIR studies, the zeolites were pressed into self-supporting discs (~8-10 mg) and pre-treated in an *in situ* IR cell at 450°C under vacuum ($10^{-5}$ Torr) for 5 h. The adsorption experiments with different probe molecules were monitored by a Thermo iS10 spectrometer, equipped with a DTGS detector, at a spectral resolution of 4 $cm^{-1}$. An excess of probe molecules was introduced as 1.0 µl portions into the IR cell. Adsorption of TIPB was performed at 30°C. Py, Lut, Coll and DTBPy were adsorbed at 150-250°C. Physisorbed molecules were subsequently removed by evacuation at the adsorption temperature. The obtained infrared spectra were analysed (including integration, subtraction, and determination of peak positions) using specialised *Thermo* software, *Omnic*. Deconvolution of peaks was carried out using the Gaussian/Lorentzian function. All the spectra presented in this chapter were normalized to 10 mg sample mass and offset for clarity.

Quantification of the zeolite acidic properties was obtained by adsorption of Py and using the molar absorption coefficients values calculated on Chapter 2 Section 2.5.4. For quantification using alkylpyridines was carried out using the molar absorption coefficients for BAS from the literature [16,23,25]; ε (Lut) =6.8 cm $\mu mol^{-1}$, ε(Coll) =10.1 cm $\mu mol^{-1}$ and ε(DTBPy) =0.62 cm $\mu mol^{-1}$. The accessibility factors (AF) using alkylpyridines was calculated following the procedure described in [32] (Equation 4.1).

$$AF = \frac{n_{BAS\ external}}{n_{BAS\ total}} \times 100\% \qquad \textbf{Equation 4.1}$$

AF for TIPB was determined as the percentage of the intensity changes of the bridging OH-groups before and after adsorption of the probe molecule using difference FTIR spectra. The error margin for the acid site quantification was estimated as ±5%. $^{27}$Al solid state MAS NMR experiments were performed at Johnson Matthey PLC and a detailed description is presented in Chapter 3.

## 4.3 Preliminary studies

Preliminary studies were made with several probe molecules in order to establish which ones were suitable for location and accessibility studies on each type of zeolite structure. The first approach included co-adsorption of different linear or aromatic hydrocarbons (nonane, pentadecane, dodecane, p-xylene and 1.2-diisopropylbenzene) followed by adsorption of Py or acetonitrile. The hydrocarbons were used to block access to acid sites on the internal surface leaving only acid sites on the external surface accessible to larger probe molecules (Py or acetonitrile). However, all hydrocarbons tested were displaced by the more basic probe molecules (Py and acetonitrile) from the channels of both zeolitic structures after desorption of the probe molecules above room temperature (RT).

The second approach involved the use of bulky probe molecules, such as alkylbenzenes and alkylpyridines (with higher kinetic diameter than Py) and it is described in this chapter. These probe molecules are not able to access certain parts of the microporous system of the zeolitic structures. The analysis of the interaction of these probe molecules, along with the comparison with the results obtained from Py adsorption, allows to identify and quantify on the location of BAS.

## 4.4 Study of acid sites in medium- and large-pore zeolites

ZSM-5 zeolite is a medium-pore size zeolite (10-MR channels) characterised by straight channels with a nearly circular opening of 5.3 Å × 5.6 Å and sinusoidal channels with an elliptical opening of 5.3 Å × 5.6 Å. BEA zeolite is a large-pore size zeolite (12-MR channels) with larger pore openings of 7.5 × 5.7 Å and smaller pore openings of 5.6 Å × 5.6 Å (Figure 4.2) [35].

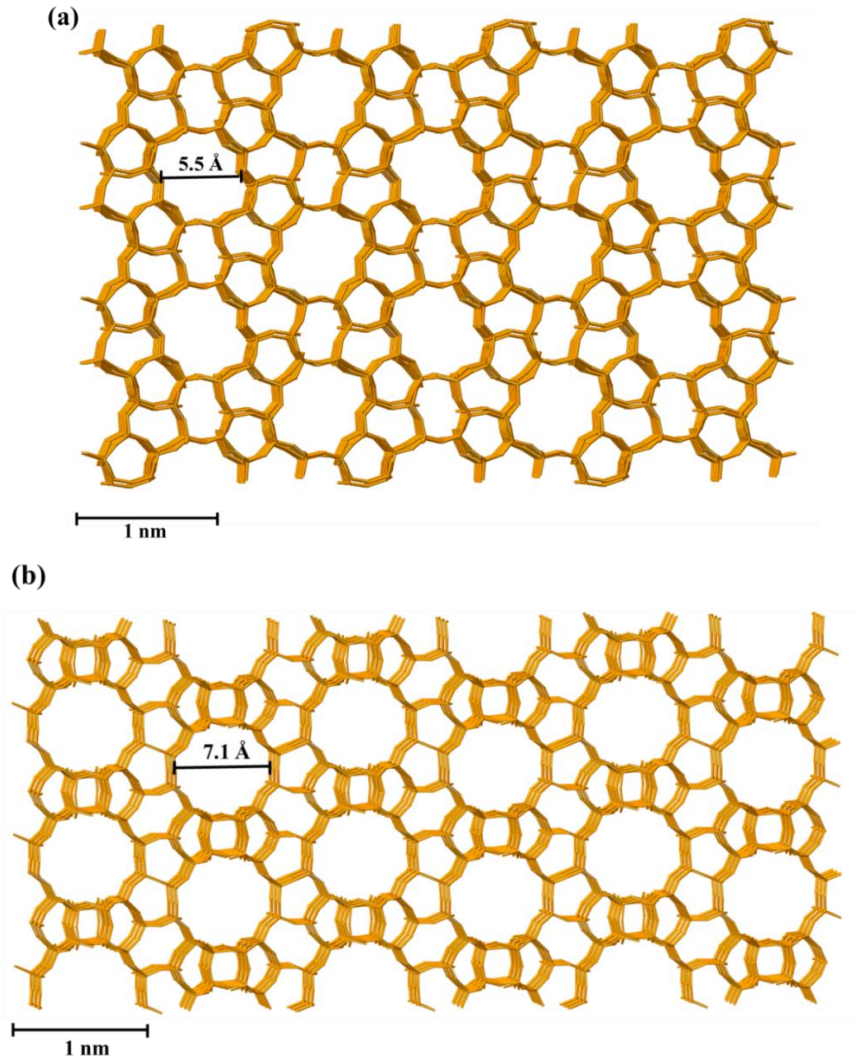


**Figure 4.2.** Structures of **(a)** ZSM-5 (10 MR channels 5.3 Å × 5.6 Å, 3D) and **(b)** BEA zeolites (12 MR channels 7.5 × 5.7 Å, 3D) viewed along [010] and [100], respectively.

### 4.4.1 Acidity measurements

FTIR spectra of BEA and ZSM-5 zeolites show two major peaks at 3745 $cm^{-1}$, with a shoulder at ~3735 $cm^{-1}$, and at 3610 $cm^{-1}$ (Figure 4.3 a). The peak at 3610 $cm^{-1}$ is assigned to acidic bridging Si-OH-Al groups and the peaks at ~3745 and ~3735 $cm^{-1}$ are attributed to the external and internal Si-OH groups, respectively. The separation of external and internal Si-OH groups is more noticeable in the BEA zeolite due to its relatively small crystal dimensions, and thus, a higher contribution from the external Si-OH groups [7] and can be distinguish by adsorption of bulky probe molecules in combination with FTIR, see Section 4.4.2. The interaction of Py with BEA and ZSM-5 zeolites (See Chapter 3, Figures 3.5 and 3.6) results in a complete disappearance of the peak at 3610 $cm^{-1}$ corresponding to bridging

Si-OH-Al groups and a decrease in the intensity of both peaks assigned to Si-OH groups (3745 $cm^{-1}$and ~3735 $cm^{-1}$). The disappearance of bridging Si-OH-Al groups means that pyridine is able to access all the acid sites of these two zeolites providing an overall concentration of acid sites. In the range of 1400-1700 $cm^{-1}$, chemisorbed Py is revealed by the following sets of peaks: two peaks at 1545 and 1637$cm^{-1}$ due to pyridinium ions ($PyH^+$), two peaks at 1456 and 1622 $cm^{-1}$assigned to Py coordinated to Lewis acid sites (PyL) and the signal at 1491 $cm^{-1}$ from Py on Lewis and Brønsted acid sites (Figure 4.3 b).

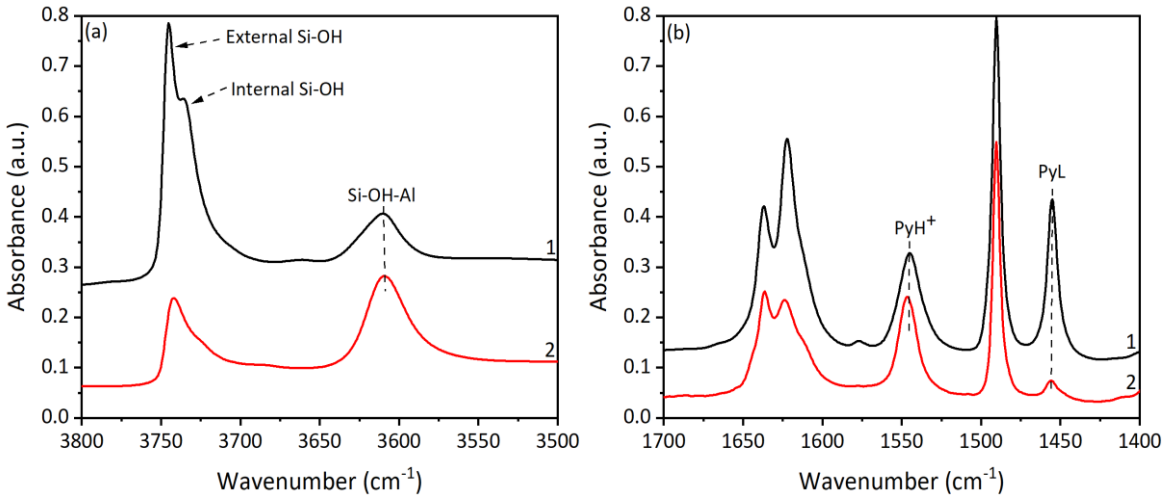


**Figure 4.3. (a)** FTIR spectra of the hydroxyl region of parent zeolites. **(b)** Difference spectra of Py region following Py adsorption at 150°C on **(1)** BEA (12.5) and **(2)** ZSM-5 (40).

**Table 4.3.** Concentration of acid sites in ZSM-5 (40) and BEA (12.5) zeolites in quantitative experiments using Py adsorption monitored by FTIR.

| Zeolite | $Al_{theoretical}$ (µmol/g) | Total amount (µmol/g) | BAS (µmol/g) | LAS (µmol/g) |
|---|---|---|---|---|
| **ZSM-5 (40)** | 340 | 363 | 338 | 25 |
| **BEA (12.5)** | 1032 | 547 | 352 | 195 |

ZSM-5 zeolite (Si/Al=40) has less Al in the structure compared to BEA (Si/Al=12.5) and consequently, a lower total concentration of acid sites. The theoretical amount of Al in zeolite BEA is considerably higher than the total amount of acid sites detected by Py (1032 versus 547 µmol/g). This is explained by the defective structure of this zeolite, BEA has a high number of LAS, which could form clusters and aggregates not fully accessible to this

probe molecule. In contract, ZSM-5 zeolite shows similar values for the theoretical amount of Al and the total concentration of acid sites, with only ~7% of LAS in the structure (Table 4.3). Further evidence for the nature of the acid sites is provided by the $^{27}$Al MAS NMR data (Figure 4.4), which displays a signal at 50 ppm characteristic of the tetrahedrally coordinated aluminium atoms in the framework ($AlO_4$) of both zeolites. Additionally, BEA zeolite shows a shoulder at ~48 ppm corresponding to distorted $AlO_4$ and a signal at 0 ppm resulting from the presence of Al in octahedral coordination ($AlO_6$) assumed to be extra-framework species [36].

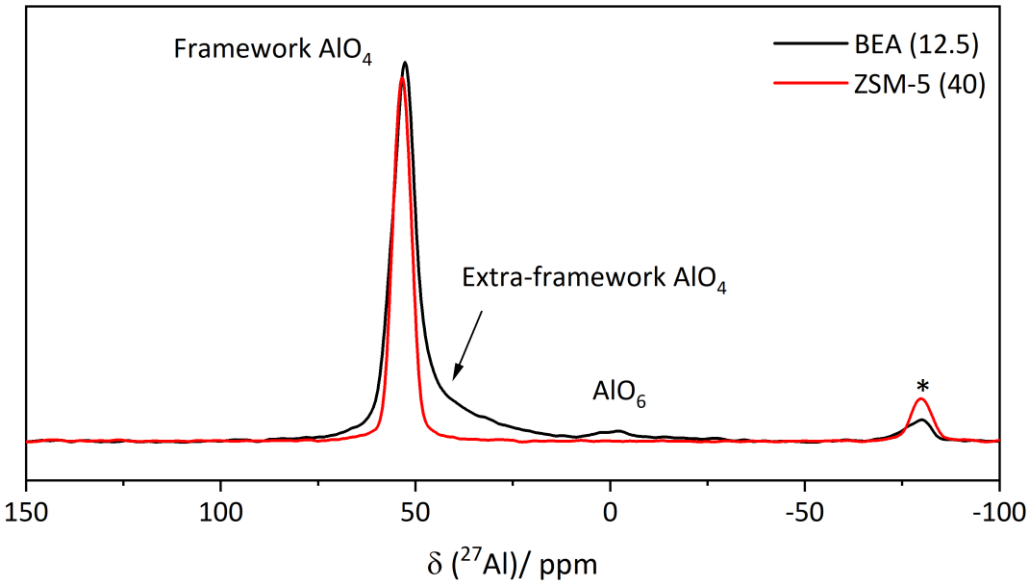


**Figure 4.4.** Normalised $^{27}$Al solid-state MAS NMR spectra of the BEA (12.5) and ZSM-5 (40) zeolites.

### 4.4.2 Accessibility and location of acid sites

Adsorption of Lut at 150°C on ZSM-5 (40) zeolite (Figure 4.5) reduces the peak at ~3610 $cm^{-1}$ assigned to bridging Si-OH-Al groups. The intensity of the Si-OH peak at 3742 $cm^{-1}$ decreases slightly and the peak seems to shift to lower wavenumbers (~3740 $cm^{-1}$). Difference spectra of the OH region after adsorption of Lut (Figure 4.5 spectrum 3) show two negative peaks at ~3610 $cm^{-1}$ and at ~3745 $cm^{-1}$. These negative peaks correspond to the portion of OH groups interacting with Lut. The reduced intensity of the bridging Si-OH-Al peak and the respective negative peak (~3610 $cm^{-1}$) confirms that Lut can access BAS

within the ZSM-5 microspore system and the negative peak at 3745 $cm^{-1}$ means that Lut is interacting with the external Si-OH groups.

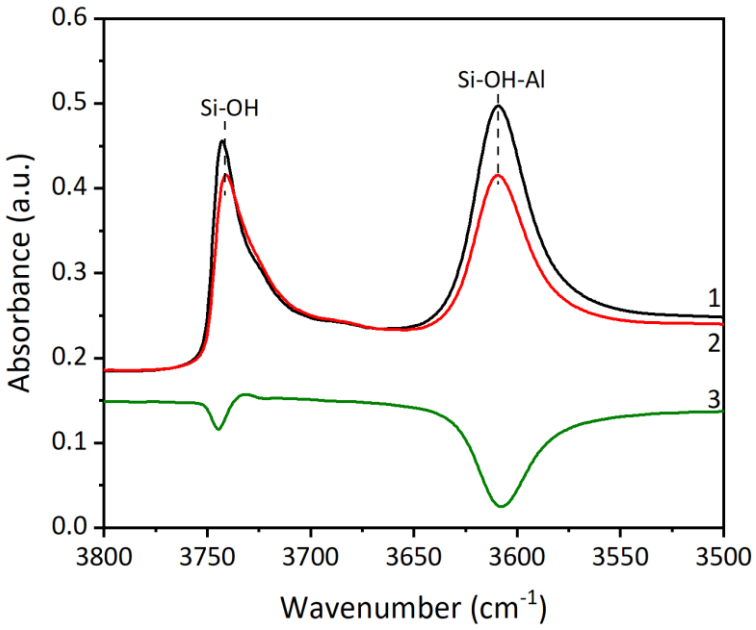


**Figure 4.5.** FTIR spectra of the hydroxyl region of ZSM-5 (40) **(1)** before and **(2)** after adsorption of Lut at 150°C, **(3)** difference spectra in the OH region after adsorption of Lut at 150°C.

The reduction of these two peaks gives rise to a range of bands around 1600-1680 $cm^{-1}$ characteristic of Lut interacting with the acidic sites (Figure 4.6). There are four main contributing peaks that can be deconvoluted: the peak at ~1616 $cm^{-1}$ due to Lut coordinated to strong LAS and the peaks at 1627, 1636 and 1647 $cm^{-1}$ characteristic of Lut protonated on BAS [37,38]. However, depending on the temperature of the experiment this probe molecule interacts differently with the acid sites in the zeolite structures (Figure 4.6).

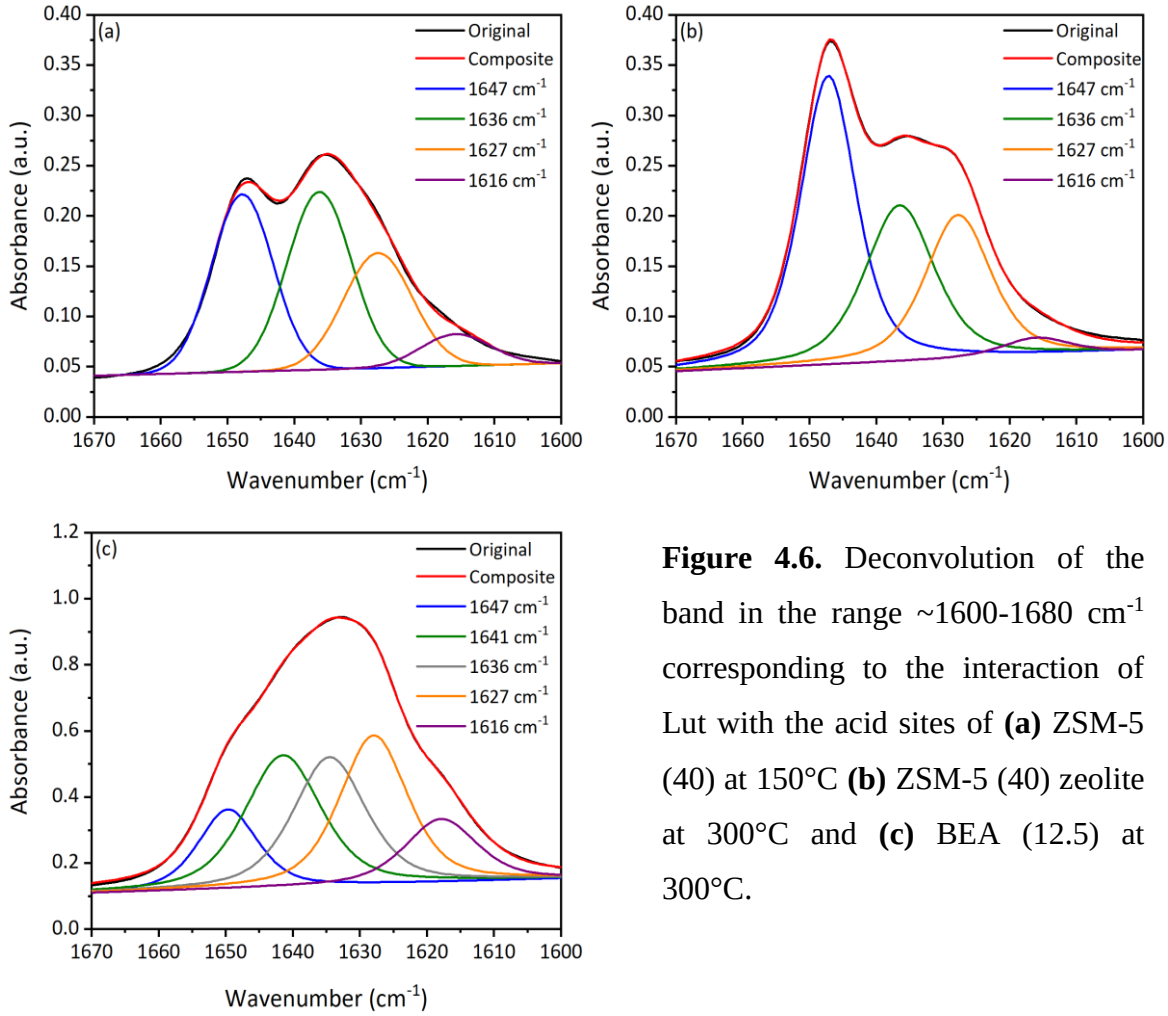


**Figure 4.6.** Deconvolution of the band in the range ~1600-1680 $cm^{-1}$ corresponding to the interaction of Lut with the acid sites of **(a)** ZSM-5 (40) at 150°C **(b)** ZSM-5 (40) zeolite at 300°C and **(c)** BEA (12.5) at 300°C.

The Lut desorption temperature effect on the Si-OH-Al, Si-OH peak intensities and peaks corresponding to adsorbed Lut species (deduced from the difference between spectra, before Lut absorption and after Lut thermodesorption) was also examined (Figure 4.7). The relative intensity of the Si-OH-Al groups at 3610 $cm^{-1}$ (black line) interacting with Lut increases up to desorption temperatures of 350°C, remaining unchanged above this temperature. This increase is directly related to the increase in the peak at 1647 $cm^{-1}$ (blue line) associated with Lut protonated on BAS, meaning that these BAS are strong acid sites related to Si-OH-Al groups. On the contrary, the relative intensity of the peaks at 3745 and 1616 $cm^{-1}$ (red and purple lines) decrease with temperatures increase. As the peak at 3745 $cm^{-1}$ corresponds to Si-OH groups, this similar behaviour in both 3745 and 1616 $cm^{-1}$ peaks suggests that Lut interacting with external Si-OH groups gives rise to the 1616 $cm^{-1}$ peak and the probe can be desorbed from these hydroxyl groups at lower temperatures. These

results confirm that Lut interaction with the different hydroxyl groups is significantly dependent on the temperature. The peaks at 1627 and 1636 $cm^{-1}$ (yellow and green lines) could be associated with weaker BAS.

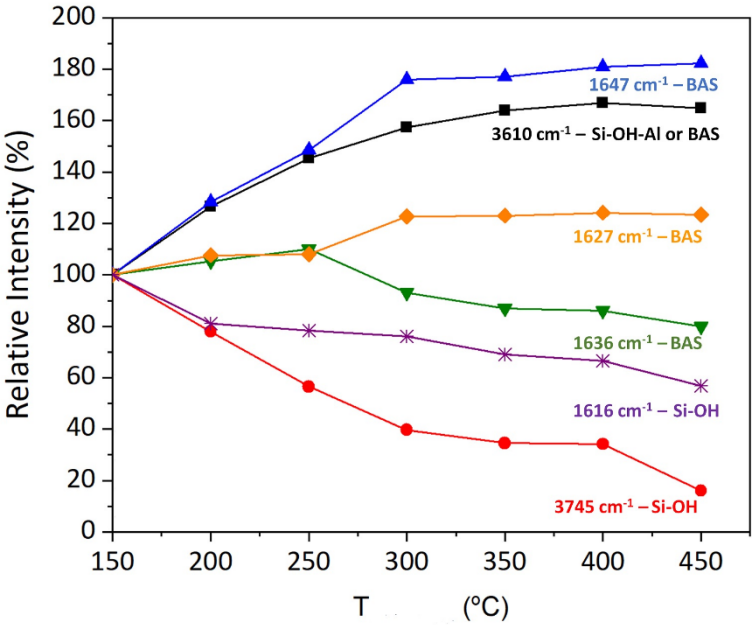


**Figure 4.7.** Evolution of intensities of the peaks of OH groups and acid sites of ZSM-5 (40) zeolite in the difference spectra at increasing temperatures (150-450°C).

At 150°C, Lut probes 26% of the total number of BAS, which means that this probe interacts with BAS located on the internal surface of ZSM-5 zeolite. At 250°C Lut can access 42% of the total number of BAS (Table 4.4). The access of this alkylpyridine to the channel spaces of ZSM-5 changes with increasing temperatures, which indicates that the diffusion of this probe is restricted and is dependent on the temperature and time of the experiment. Armaroli et al. [27] have reported similar results; Lut rapidly enters the pores of the ZSM-5 zeolite and is protonated on the bridging Si-OH-Al groups even at room temperature. Similarly, Thibault-Starzyk. [32] have shown that Lut can probe up to 50% of the acid sites in their ZSM-5 parent zeolite. These data confirm that both molecular sieving and the strength of the interaction (between the probe and the acid site) control the accessibility of the acid sites in the zeolite micropores. Also, the literature suggests that Lut still forms coordinated bonds with LAS [24,25,35] at 1616 $cm^{-1}$, however the results in this work

demonstrate that this peak could be associated with the interaction of Lut with external Si-OH groups, instead of LAS. The steric hindrance of the methyl groups, especially at high temperatures, favours the interaction of this probe with Si-OH-Al groups acting as BAS [8,39]. The results of this work suggest that this probe is not suitable to quantify BAS on the external surface of 10-MR zeolites, however it could be an adequate probe to study the enhanced accessibility in hierarchical ZSM-5 zeolites [32] and zeolites, such as FER, with pore systems smaller than ZSM-5 [27].

**Table 4.4.** Concentrations of acid sites in ZSM-5 zeolite in quantitative experiments using Lut adsorption monitored by FTIR.

| | **Py** | **Lut ads at 150°C** | **Lut ads at 250°C** |
|---|---|---|---|
| **Concentration of accessible BAS (μmol/g)** | 340 | 88 | 143 |
| **AF (%)** | 100 | 26 | 42 |

Adsorption of Coll and DTBPy at 150°C on ZSM-5 zeolite (Figure 4.8 a) reduces the intensity of the peak at 3745 $cm^{-1}$, associated with Si-OH groups on the external surface, whereas the shoulder at ∼3735-3725 $cm^{-1}$ is left unperturbed. The difference spectra provide a direct spectroscopic confirmation of the presence of external and internal Si-OH groups in ZSM-5, agreeing with recent studies [28,30]. The peak of bridging Si-OH-Al groups is virtually unaffected after Coll and DTBPy adsorption, implying that most of the corresponding sites are not accessible to these probes. However, the difference spectra in the OH region, (Figure 4.8 b) show a low intensity negative peak at ~3615 $cm^{-1}$ after adsorption of the two probes. The negative peak corresponds to a small fraction of Si-OH-Al groups interacting with the Coll and DTBPy, which are BAS located on the external surface or close to the pore mouths of this zeolite. These results agreed with reports by Thibault-Starzyk et al [31,32] demonstrating that Coll and DTBPy are not able to access BAS located in the micropore system of a medium-pore zeolite, quantifying only BAS located on the external

surface. Coll adsorption (Figure 4.8 c, spectrum 1) gives rise to the band at ~1634 with a shoulder at ~1649 $cm^{-1}$, resulting from the interaction with BAS, and two low intensity bands at 1619 $cm^{-1}$ and 1575 $cm^{-1}$, assigned to the probe adsorbed on Si-OH groups [31]. The spectra of DTBPy (Figure 4.8 c spectrum 2) show a band at 1615 $cm^{-1}$ attributed to the probe bonded to BAS [23]. Coll and DTBPy being bigger than Py (7.4 and 7.9 Å respectively, versus 5.4 Å) reach less than 10% number of BAS in the zeolite (Table 4.5). These two probes are too bulky to enter ZSM-5 micropores, accessing the small fraction of BAS located on the external surface or near the pore mouths of ZSM-5.

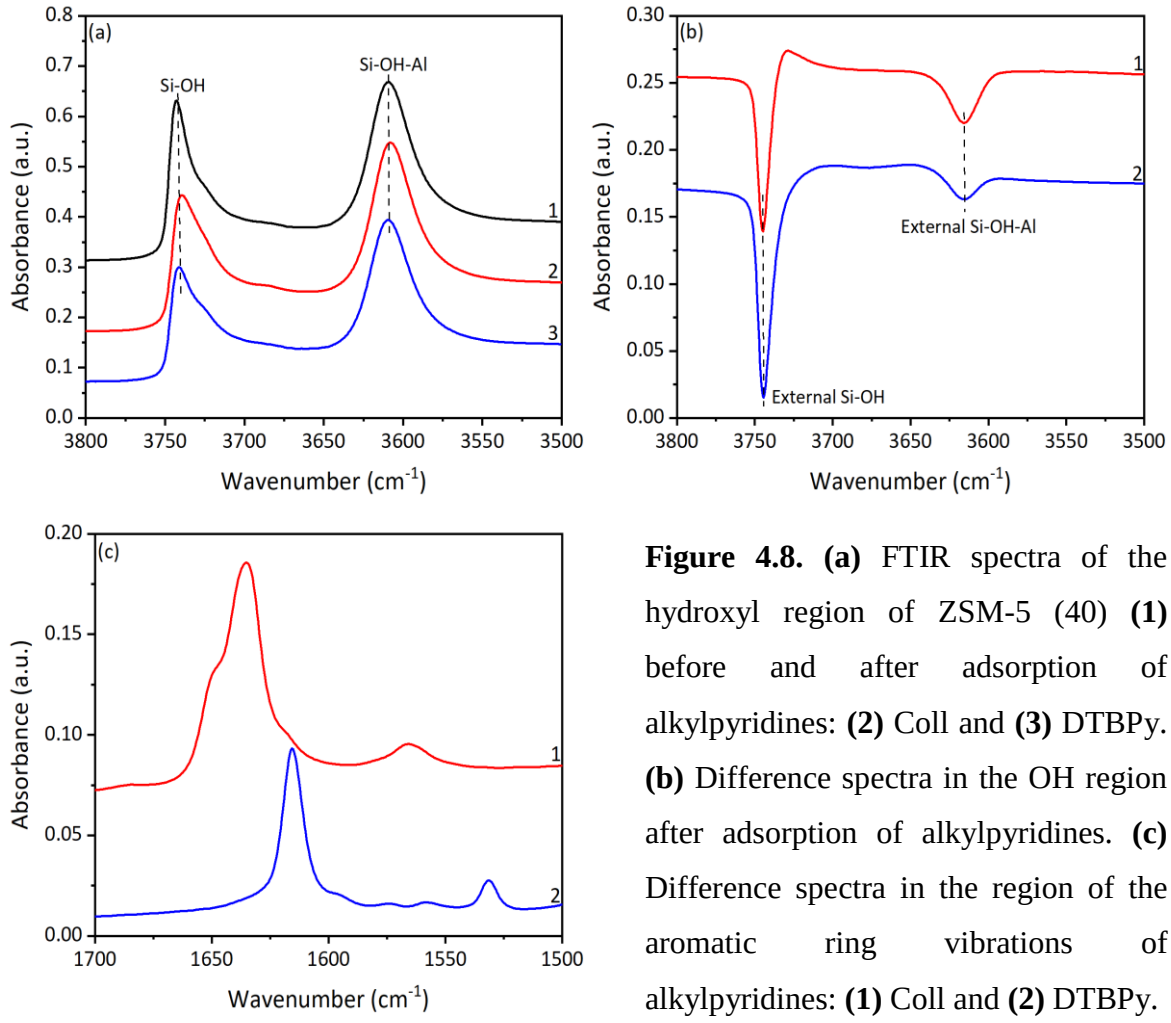


**Figure 4.8. (a)** FTIR spectra of the hydroxyl region of ZSM-5 (40) **(1)** before and after adsorption of alkylpyridines: **(2)** Coll and **(3)** DTBPy. **(b)** Difference spectra in the OH region after adsorption of alkylpyridines. **(c)** Difference spectra in the region of the aromatic ring vibrations of alkylpyridines: **(1)** Coll and **(2)** DTBPy.

**Table 4.5**. Concentration of acid sites in ZSM-5 (40) zeolite in quantitative experiments using Coll and DTBPy adsorption monitored by FTIR.

| | **Py** | **Coll** | **DTBPy** |
|---|---|---|---|
| **Concentration of accessible BAS (μmol/g)** | 340 | 25 | 15 |
| **AF (%)** | 100 | 7 | 4 |

For BEA zeolite, FTIR spectra show that all three alkylpyridines reduce the peaks at 3745 $cm^{-1}$ and ~3735 $cm^{-1}$ assigned to external and internal Si-OH groups. The peak at 3610 $cm^{-1}$ related to Si-OH-Al groups completely disappears after adsorption of the three probes. This means that all alkylpyridines interact with all of the BAS of 12-MR BEA zeolite; their behaviour during adsorption is very similar to the adsorption of Py. Indeed, the size of the substituted pyridines is similar to the dimensions of the larger pores in the BEA structure (7.7 Å × 6.6 Å) allowing their access to the BAS in the micropore system. Neither of the alkylpyridines is an ideal probe molecule to quantify BAS located on the external surface of BEA zeolite, which is in disagreement with data reported in [21] stating that only 50% of the acid sites are accessible to DTBPy in a parent zeolite BEA.

Therefore, additional experiments utilising a larger probe molecule were carried out to evaluate the changes in accessibility of BAS in large-pore zeolites. Adsorption of TIPB at 30°C on ZSM-5 and BEA zeolites (Figures 4.9) leads to a significant reduction in the intensity of the Si-OH peak at 3745 $cm^{-1}$. The changes in the intensity of the Si-OH-Al peak at ~3610 $cm^{-1}$ are best interpreted from the difference spectra (Figure 4.9 b and d). Indeed, a low intensity negative peak at ~3610 $cm^{-1}$ is observed for both zeolites, which corresponds to the external acidic Si-OH-Al groups interacting with the hydrocarbon molecules through hydrogen bonding.

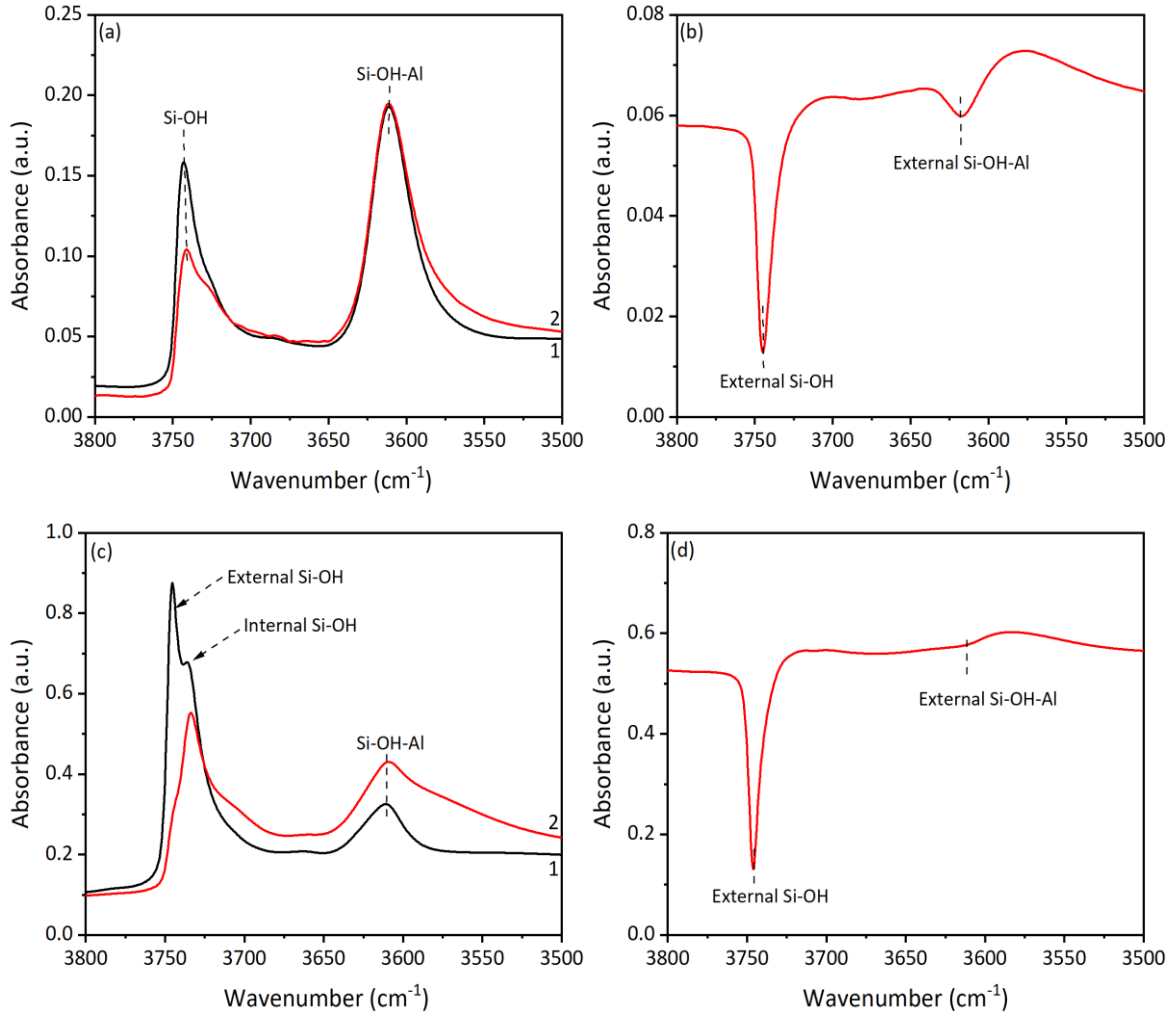


**Figure 4.9 (a)** FTIR spectra of the hydroxyl region of ZSM-5 (40) **(1)** before and **(2)** after adsorption of TIPB at 30°C. **(b)** Difference spectrum of ZSM-5 (40) after adsorption of TIPB. **(c)** FTIR spectra of the hydroxyl region of BEA (12.5) **(1)** before and **(2)** after adsorption of TIPB at 30°C. **(d)** Difference spectrum of BEA (12.5) after adsorption of TIPB. Note the differences in the absorbance scale indicated on the y-axis.

This conclusion is confirmed by the deconvolution of the 3610 $cm^{-1}$ peak in ZSM-5 after TIPB adsorption (Figure 4.10). The spectra show that the band at ~3610 $cm^{-1}$ (black-coloured) is a composite of two peaks: one due to the Si-OH-Al groups in the micropores not interacting with the probe (blue-coloured, ∿3610 $cm^{-1}$), and the other due to Si-OH groups OH-bonded to the benzene ring of TIPB (green-coloured, ∿3590 $cm^{-1}$). The same explanation applies for the results obtained for BEA zeolite. The accessibility of TIPB to BAS in both these zeolites is low, 4% for ZSM-5 and to 6% for BEA. The results demonstrate that this probe molecule, which is too large to enter the zeolite micropore

systems, can provide information about BAS on the external surface of both medium- and large-pore zeolites.

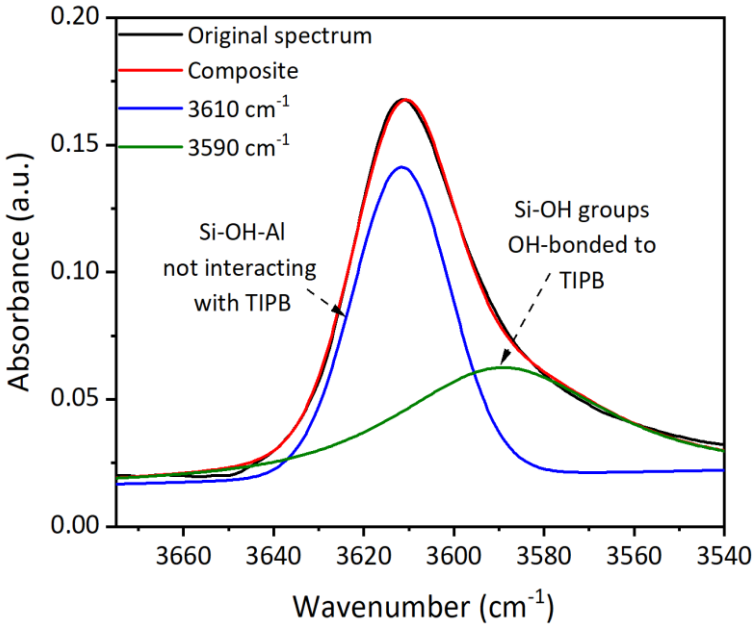


**Figure 4.10.** Deconvolution of the 3610 $cm^{-1}$ peak corresponding to Si-OH-Al groups of ZSM-5 (40) after adsorption of TIPB at 30°C.

## 4.5 Study of acid sites in mixed-pore zeolites

Both MOR and MAZ zeolites are mixed-pore size zeolites with similar structures and openings. Zeolite MOR consists of large-pore size channels (12-MR channels) with an opening of 7.0 × 6.5 Å and side pockets to the main channel composed to small-pore size channels (8-MR channels, 5.7 × 2.6 Å). MAZ zeolite has large 12-MR openings (7.4 × 7.4 Å) while the small channels measures of 3.1 × 3.1 Å [35] (Figure 4.11).

Mixed-pore zeolites are an excellent case study to highlight the relationship between the pore architecture and acidity of zeolites. BAS in these zeolites can be located in the large unidirectional channels, with little or no confinement, or in small side pockets and small channels where very little space is available for reactants or probe molecules. The goal of this section is to characterise and distinguish between BAS located in different channels and surfaces of these two mixed-pore zeolitic structures (MOR and MAZ).

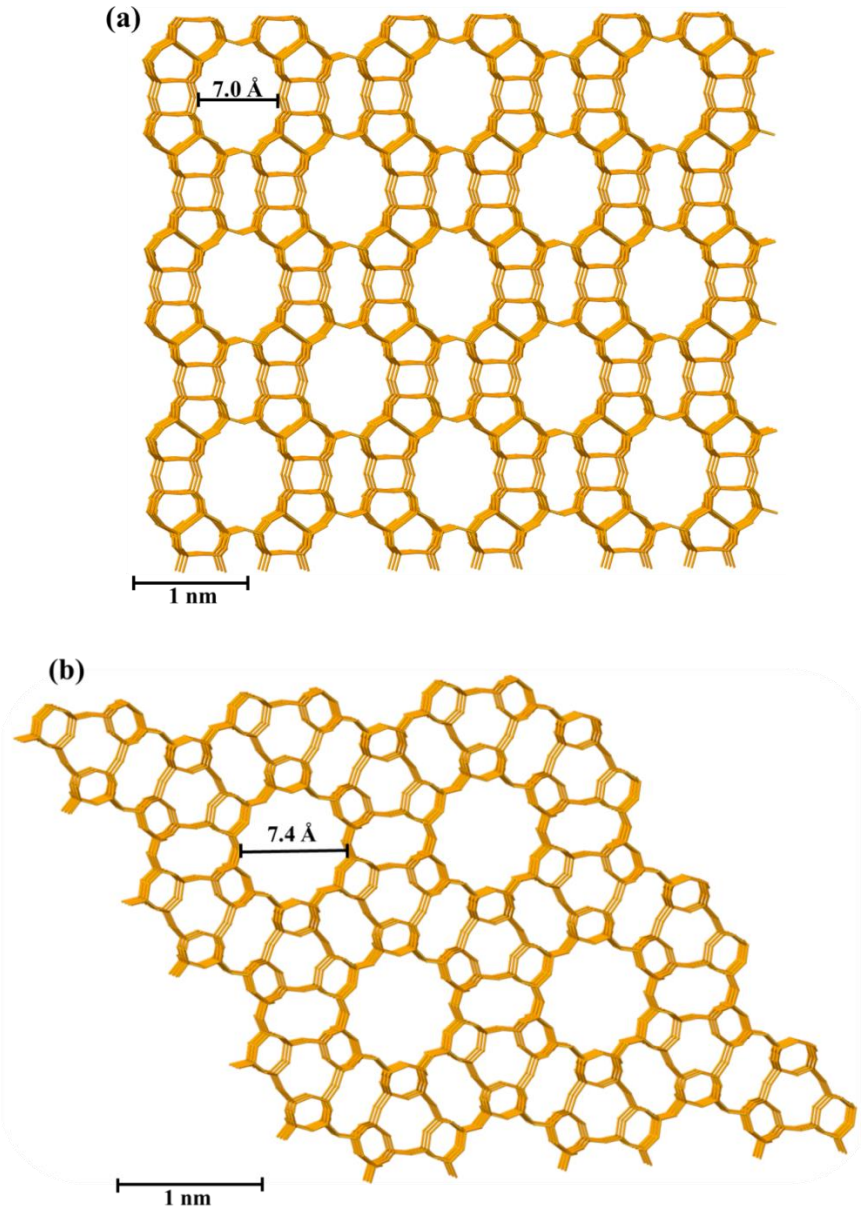


**Figure 4.11.** Structures of **(a)** MOR (12 MR channels 7.0 × 6.5 Å, 1D) and **(b)** MAZ (12 MR channels 6.0 × 6.0 Å, 1D) zeolites viewed along [001].

### 4.5.1 Acidity measurements

FTIR spectra of zeolites MOR and MAZ show two major peaks at 3745 $cm^{-1}$ and ~3600 $cm^{-1}$, assigned to Si-OH groups and acidic bridging Si-OH-Al, respectively (Figure 4.12). The asymmetric shape of the peak at ~3600 $cm^{-1}$ reveals the heterogeneity and complexity of the OH groups of both zeolites. The second derivative and deconvolution of this peak show the existence of two overlapping bands with the maxima around 3585 and 3610 $cm^{-1}$ in MOR zeolite. The low-frequency (LF) peak at 3585 $cm^{-1}$ is assigned to BAS located in the smaller 8-membered ring side pockets and the high-frequency (HF) peak at

3610 $cm^{-1}$ corresponds to BAS in the larger 12-membered ring channels (Figure 4.12 a) [7,40,41]. Additional differentiation between BAS types in MOR has been proposed 42,43]; however, there is no evidence of further OH groups in the MOR used in this study. Although the Si-OH-Al peaks in both zeolites are very similar, the deconvolution of the ~3600 $cm^{-1}$ peak in MAZ zeolite, demonstrates the presence of at least five different peaks at 3653, 3624, 3600, 3572 and 3540 $cm^{-1}$(Figure 4.12 b). The LF peaks at 3572 and 3540 $cm^{-1}$ are assigned to BAS located in smaller 8-membered ring pores while the HF peak at 3600 $cm^{-1}$ corresponds to the BAS located in the 12-membered ring channels. The peaks at 3653 and 3624 $cm^{-1}$ correspond to EFAl species and OH groups located in a non-porous phase (probably impurities), respectively. The complexity of the acidity in MAZ presented in this work have been previously reported [44,45].

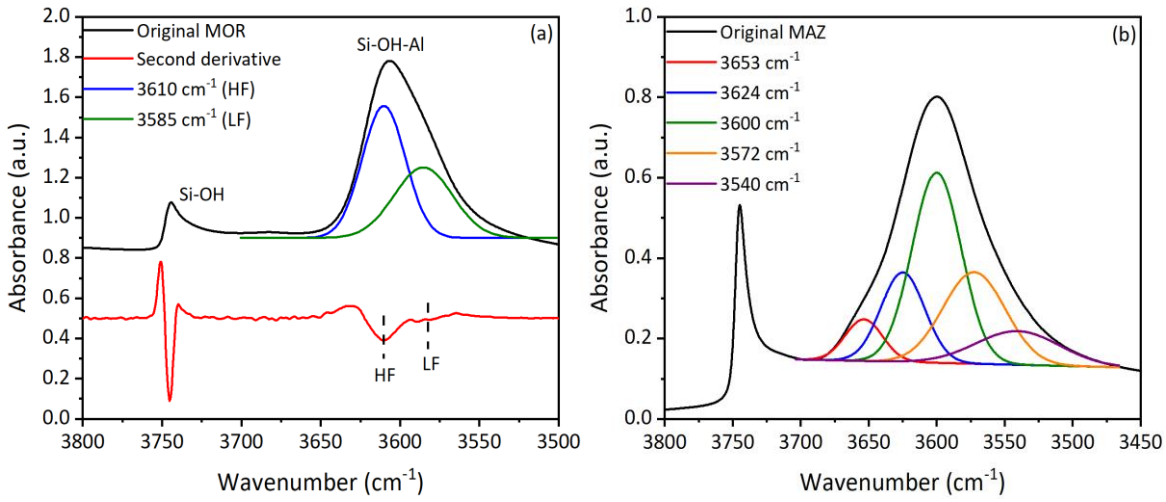


**Figure 4.12 (a)** FTIR spectra of the hydroxyl region of MOR (10). **(b)** FTIR spectra of the hydroxyl region of MAZ (4.7).

The adsorption of $NH_3$ and Py was studied in order to obtain the overall concentration of acid sites in both zeolitic structures (Figure 4.13 and Table 4.5). Adsorption of $NH_3$ at 150°C on MOR zeolite (Figure 4.13 a) leads to a decrease in the intensity of the peak at 3745 $cm^{-1}$, associated with Si-OH groups, and complete disappearance of the peak related to Si-OH-Al groups at 3606 $cm^{-1}$. The relatively small size of $NH_3$ (~2.6 Å) allows access to all BAS in this zeolitic structure (~1215 µmol/g) (Table 4.6). In contrast to $NH_3$, Py only

accesses a portion of the total number of acid sites in MOR (~864 µmol/g). This is due to diffusion limitations of the relatively bulky probe molecule inside the small 8-membered ring channels of MOR [43].

The adsorption of $NH_3$ at 150°C on MAZ zeolite (Figure 4.13 b) reduces the intensity of both peaks at 3745 $cm^{-1}$ and 3600 $cm^{-1}$ corresponding to Si-OH and bridging Si-OH-Al groups, respectively. The portion of the Si-OH-Al peak not interacting with this probe is located in the non-porous phase represented by the peak at 3624 $cm^{-1}$. The concentration of BAS in MAZ determined by Py adsorption is significantly lower than that determined by $NH_3$. These observations could be explained by (i) restricted diffusion of the probe in the small channels, as observed for MOR zeolite and (ii) blockage of access to some of the acid sites positioned in the large channels by a non-zeolitic material [45]. Although Py, as a probe molecule, does not access all acid sites in both zeolites, it allows to information to be obtained on the presence of LAS and the ratios BAS/LAS existing in these structures (Table 4.5).

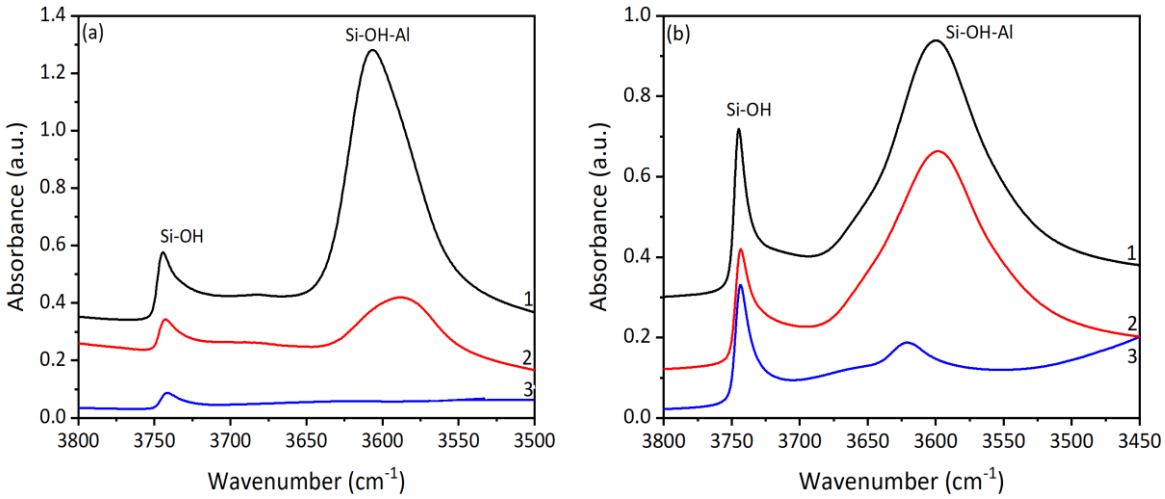


**Figure 4.13. (a)** FTIR spectra of the hydroxyl region of MOR (10). **(b)** FTIR spectra of the hydroxyl region of MAZ (4.7) **(1)** before adsorption of the probe molecules, **(2)** after adsorption of Py at 150°C and **(3)** after adsorption of $NH_3$ at 150°C.

**Table 4.6.** Concentration of acid sites in MOR (10) and MAZ (4.7) zeolites in quantitative experiments using $NH_3$ and Py adsorption monitored by FTIR.

| Zeolite | $BAS_{NH3}$ (μmol/g) | $BAS_{Py}$ (μmol/g) | $LAS_{Py}$ (μmol/g) | $BAS_{Py}/LAS_{Py}$ |
|---|---|---|---|---|
| **MOR (10)** | 1215 | 864 | 122 | 7.1 |
| **MAZ (4.7)** | 1178 | 157 | 81 | 1.9 |

### 4.5.2 Accessibility and location of acid sites

In the previous section (Section 4.5.1) it was established that $NH_3$ is a suitable probe to quantify the total concentration of BAS in both structures. Py adsorption demonstrated different acid site accessibilities in zeolites with similar structures and pore sizes. To distinguish and quantify BAS located in different channels and surfaces of MOR and MAZ zeolites, various probe molecules with different kinetic diameters were utilised (Table 4.7).

For MOR zeolite the results are straightforward and agree with a series of previous reports [40,43]. Adsorption of hexane and benzene at 30°C probe ~60% of the total amount of Si-OH-Al groups, which correspond to BAS located on the large channels of this structure. Although Coll adsorption has been used to determine the accessibility of BAS in microporous mordenites [15], the results obtained in this work demonstrate that the diffusion of this test-molecule into the micropores is dependent on the temperature and duration of the experiment. To quantify the number of BAS on the external surface of large-pore zeolites, TIPB is the most adequate probe molecule. This probe molecule access ~2% of the total number of bridging Si-OH-Al groups and these sites are located on the external surface or close to the pore mouths of MOR zeolite.

**Table 4.7.** Accessibility factor (AF) for MOR (10) and MAZ (4.7) zeolites determined using adsorption of $NH_3$, Py, hexane, benzene, Coll and TIPB.

| Zeolite | $AF_{NH3}$ (%) | $AF_{Py}$ (%) | $AF_{Hexane}$ (%) | $AF_{Benzene}$ (%) | $AF_{Coll}$ (%) | $AF_{TIPB}$ (%) |
|---|---|---|---|---|---|---|
| **MOR** | 100 | 73 | 60 | 57 | 22 | 2 |
| **MAZ** | 92 | 14 | 2 | 5 | 5 | 2 |

The accessibility of bridging Si-OH-Al groups of MAZ zeolite is very restricted. Most of the probe molecules tested are only able to access BAS located on the external surface of MAZ. These observations are explained by the restricted diffusion of the probes in the small channels and blockage of the larger channels of the zeolite.

## 4.6 Application to hierarchical zeolites

The introduction of mesoporosity in addition to the existing network of micropores in zeolites has received considerable attention in the last few years [3-6]. These hierarchical zeolites are now important for industrial applications of zeolites, due to the increased accessibility and reduction of diffusion limitations. Therefore, the comparison and quantification of this enhanced accessibility has become significant. The aim of this section is to apply the understanding obtained in the former sections to characterise the acid site accessibility for a series of mesostructured zeolites.

The spectra of the modified samples also show a decrease in the intensity of the bridging Si-OH-Al groups and a parallel increase in the intensity of the peak at 3745 $cm^{-1}$ assigned to the external Si-OH groups, confirming the removal of the framework Al and Si atoms during the formation of mesopores (e.g. Figure 4.14) [3].

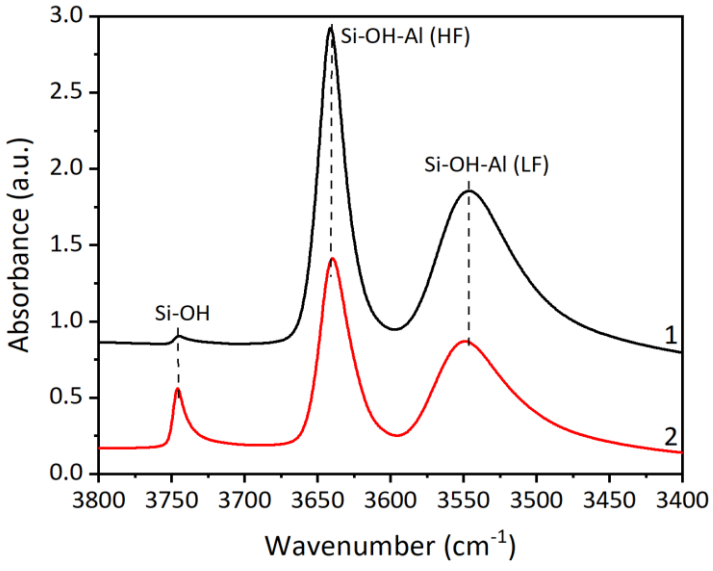


**Figure 4.14.** FTIR spectra of the hydroxyl region of **(1)** Y and **(2)** mesoporous Y zeolite. HF and LF stand for high frequency and low frequency bridging OH groups in the FAU framework, respectively.

Py has been used in this study in order to determine the number of BAS and LAS (Figure 4.15). The surfactant templating mesostructuring treatment leads to a decrease in the concentration of BAS and an increase in the concentration of LAS in all zeolitic structures. In agreement with previous studies, these changes result from partial desilication and dealumination of the modified zeolites followed by their calcination [46,47].

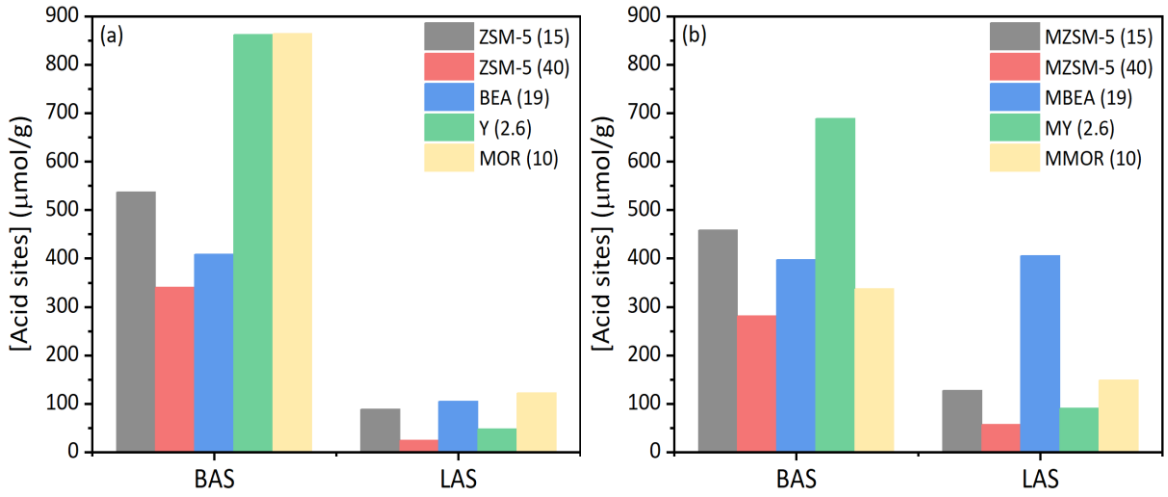


**Figure 4.15.** Concentration of acid sites in **(a)** parent **(b)** hierarchical zeolites in quantitative experiments using Py adsorption monitored by FTIR. Values in brackets refer to Si/Al ratio.

The accessibility of acid sites in both parent and mesostructured zeolites has been monitored by FTIR spectroscopy of adsorbed Py, Coll and TIPB (Table 4.7). The relatively large size of Coll molecules (7.4 Å) prevents their access to BAS in the micropores of ZSM-5 allowing the determination of the BAS accessibility of hierarchical ZSM-5 zeolites (Section 4.4). Both parent and hierarchical ZSM-5 contain a small number of BAS accessible to the bulky Coll molecules; these acid sites are located on the external surface or close to the pore mouths of the parent zeolite. Desilication, leading to the formation of a secondary system of mesopores, results in a rather modest increase in the accessibility of BAS to Coll for both ZSM-5 zeolites (Si/Al=15 and 40). As previously discussed, TIPB is the most suitable probe to study the accessibility of BAS in large pore zeolites, such as BEA and MOR (e. g. Figure 4.9 c and d), considering the low intensity negative peak at ~3610 $cm^{-1}$ assigned to the acidic Si-OH-Al groups interacting with the hydrocarbon molecules and

forming a hydrogen bond. The accessibility of the bridging OH-groups increases from 10 to 22% for BEA and from 2 to 12% for MOR following the mesostructuring treatment (Table 4.8) as there are more acid sites interacting with TIPB in the mesopores and in the pore mouths of the zeolite micropores in comparison with the parent structures [48].

**Table 4.8.** Accessibility factor (AF) for parent and hierarchical zeolites determined using adsorption of Py, Coll and TIPB. AF was calculated from the intensity of the Si-OH-Al peaks.

| Zeolite | $AF_{Py}$ (%) | $AF_{Coll}$ (%) | $AF_{TIPB}$ (%) |
|---|---|---|---|
| ZSM-5 (15) | 100 | 4(4)[a] | 3 |
| MZSM-5 (15) | 100 | 4(6)[a] | 3 |
| ZSM-5 (40) | 100 | 7(7)[a] | 4 |
| MZSM-5 (40) | 100 | 17(10)[a] | 4 |
| BEA (19) | 100 | 100 | 10 |
| MBEA (19) | 100 | 100 | 22 |
| MOR | 73 | 22[b] | 2 |
| MMOR | 63 | 25[b] | 12 |
| Y (2.6) | 100 (HF) 15 (LF) | 100 (HF) 24 (LF) | 49 (HF) 4 (LF) |
| MY (2.6) | 100 (HF) 46 (LF) | 100 (HF) 49 (LF) | 58 (HF) 6 (LF) |

[a] The data in brackets are calculated from the intensity of the Coll peak in the spectra.
[b] Depends on the time and temperature of the adsorption experiments.

Zeolite Y presents two types of hydroxyl groups, a high-frequency peak (HF, at 3650-3625 $cm^{-1}$) located in the supercages and a low-frequency peak (LF, at 3550 $cm^{-1}$) located in the sodalite cages. Several studies investigating acidity and accessibility of acid sites in Y zeolites have been already reported [49-54], but so far there is no adequate probe molecule able to distinguish between BAS located on the external and internal surfaces of this zeolitic structure. Owing to the large dimensions of the supercages (13 Å), acid sites located in the supercages are easily accessible to Coll and Py. Although the access to the supercages is restricted by the 12-MR windows (7.4 Å × 7.4 Å), the experimental FTIR spectra demonstrate that even the bulky TIPB molecules interact with ~50% of BAS in large cages (Table 4.8). In addition, some acid sites located in the smaller cages can interact with the

Coll and Py because both probes are strong bases, which can displace the acid sites from their original position. Therefore, the degree of interaction of Coll and Py with the BAS located in the smaller cages has been utilised as an indication of the acid site accessibility. Upon mesostructuring treatment, the sodalite cages of zeolite Y become more accessible to both Py and Coll probe molecules (Table 4.8). This is probably due to the opening of sodalite cages following partial dissolution of the zeolite framework

In general, the obtained hierarchical zeolites show a greater degree of interaction with bulky probe molecules due to the shorter average length of the residual micropores between the newly formed mesopores, a significantly faster diffusion in the mesopores and a greater fraction of accessible acid sites. These results demonstrate the importance of choosing the appropriate probe for quantification of accessibility of different zeolitic structures.

## 4.7 Summary

The accessibility and the number of acid sites on the internal and external surfaces of ZSM-5 and BEA zeolites have been determined using adsorption of bulky probe molecules monitored by FTIR, hence providing a clear method for the detailed examination of the acid properties of these structures. Coll and DTBPy proved to be suitable probe molecules to quantify BAS on the external surface of ZSM-5 while TIPB can be used to distinguish BAS sites located on the external and internal surfaces in the large-pore channels of BEA. These results demonstrate that it is essential to select the right probe molecule for quantification of accessibility of different zeolitic structures. The method can be further extended to include detailed characterisation of hierarchical and mixed-pore zeolites, particularly utilising a combination of several probe molecules. In addition, the experimental procedure should improve the accuracy of the quantitative analysis under *in situ* and realistic reaction conditions and help in cross validation of the data obtained from different techniques.

## 4.8 References

[1] A. Corma. *From microporous to mesoporous molecular sieve materials and their use in catalysis*. Chem. Rev., 1997, 97, (6), 2373-2419.

[2] S. van Donk, A. H. Janssen, J. H. Bitter and K. P. de Jong. *Generation, characterization, and impact of mesopores in zeolite catalysts.* Catal. Rev. Sci. Eng., 2003, 45, (2), 297-319.

[3] J. Datka, K. Tarach and K. Góra-Marek, *Acidic properties of hierarchical zeolites in nesoporous zeolites: preparation, characterization, and applications*. Eds: J. García-Martínez and K. Li. John Wiley & Sons., 2015, 461-496.

[4] J. Pérez-Ramírez, C. H. Christensen, K. Egeblad, C. H. Christensen and J. C. Groen. *Hierarchical zeolites: enhanced utilisation of microporous crystals in catalysis by advances in materials design.* Chem. Soc. Rev., 2008, 37, (11), 2530-2542.

[5] Y. Wei, T. E. Parmentier, K. P. de Jong and J. Zečević. *Tailoring and visualizing the pore architecture of hierarchical zeolites.* Chem. Soc. Rev., 2015, 44, (20), 7234-7261.

[6] M. Milina, S. Mitchell, P. Crivelli, D. Cooke and J. Pérez-Ramírez. *Mesopore quality determines the lifetime of hierarchically structured zeolite catalysts.* Nat. Commun., 2014, 5, 3922-3932.

[7] K. Hadjiivanov. *Identification and characterization of surface hydroxyl groups by infrared spectroscopy*. Adv. Catal., 2014, 57, 99-318.

[8] D. Zhai, Y. Li, H. Zheng, L. Zhao, J. Gao, C. Xu and B. Shen. *A first-principles evaluation of the stability, accessibility, and strength of Brønsted acid sites in zeolites.* J. Catal., 2017, 352, 627-637.

[9] M. Trombetta, G. Busca, M. Lenarda, L. Storaro and M. Pavan. *An investigation of the surface acidity of mesoporous Al-containing MCM-41 and of the external surface of ferrierite through pivalonitrile adsorption.* Appl. Catal., A., 1999, 182, (2), 225-235.

[10] T. Armaroli, M. Bevilacqua, M. Trombetta, F. Milella, A. G. Alejandre, J. Ramírez, B. Notari, R. J. Willey and G. Busca. *A study of the external and internal sites of MFI-type*

*zeolitic materials through the FT-IR investigation of the adsorption of nitriles.* Appl. Catal., A., 2001, 216, (1-2), 59-71.

[11] M. Trombetta, T. Armaroli, A. G. Alejandre, J. R. Solis and G. Busca. *An FT-IR study of the internal and external surfaces of HZSM5 zeolite.* Appl. Catal., A., 2000, 192, (1), 125-136.

[12] M. Bevilacqua and G. Busca. *A study of the localization and accessibility of Brønsted and Lewis acid sites of H-mordenite through the FT-IR spectroscopy of adsorbed branched nitriles.* Catal. Commum., 2002, 3, (11), 497-502.

[13] T. Montanari, M. Bevilacqua and G. Busca. *Use of nitriles as probe molecules for the accessibility of the active sites and the detection of complex interactions in zeolites through IR spectroscopy*. Appl. Catal., A., 2006, 307, (1), 21-29.

[14] D. Tzoulaki, A. Jentys, J. Pérez-Ramírez, K. Egeblad and J. A. Lercher. *On the location, strength and accessibility of Brønsted acid sites in hierarchical ZSM-5 particles.* Catal. Today, 2012, 198, (1), 3-11.

[15] N. S. Nesterenko, F. Thibault-Starzyk, V. Montouillout, V. V. Yuschenko, C. Fernandez, J-P. Gilson, F. Fajula and I. I. Ivanova. *Accessibility of the acid sites in dealuminated small-port mordenites studied by FTIR of co-adsorbed alkylpyridines and CO.* Microporous Mesoporous Mater., 2004, 71, (1-3), 157-166.

[16] N. S. Nesterenko, F. Thibault-Starzyk, V. Montouilliout, V. V. Yushchenko, C. Fernandez, J.P. Gilson, F. Fajula and I. I. Ivanova, Kinet. Katal., 2006, 47, (1), 45; translated into English. *The use of the consecutive adsorption of pyridine bases and carbon monoxide in the IR spectroscopic study of the accessibility of acid sites in microporous/mesoporous materials.* Kinet. Catal., 2006, 47, (1), 40-48.

[17] F. L. Bleken, K. Barbera, F. Bonino, U. Olsbye, K. P. Lillerud, S. Bordiga, P. Beato, T. V. W. Janssens and S. Svelle. *Catalyst deactivation by coke formation in microporous and desilicated zeolite H-ZSM-5 during the conversion of methanol to hydrocarbons*. J. Catal., 2013, 307, 62-73.

[18] P. A. Jacobs and C. F. Heylen. *Active sites in zeolites. III. Selective poisoning of Brønsted sites on synthetic Y zeolites*. J. Catal., 1974, 34, (2), 267-274.

[19] S. Bordiga, C. Lamberti, F. Bonino, A. Travert and F. Thibault-Starzyk. *Probing zeolites by vibrational spectroscopies.* Chem. Soc. Rev., 2015, 44, (20), 7262-7341.

[20] L. M. Chua, I. Hitchcock, R. S. Fletcher, E. M. Holt, J. Lowe and S. P. Rigby. *Understanding the spatial distribution of coke deposition within bimodal micro /mesoporous catalysts using a novel sorption method in combination with pulsed-gradient spin-echo NMR.* J. Catal., 2012, 286, 260-265.

[21] V. V. Ordomsky, V. Y. Murzin, Yu. V. Monakhova, Y. V. Zubavichus, E. E. Knyazeva, N. S. Nesterenko and I. I. Ivanova. *Nature, strength and accessibility of acid sites in micro/mesoporous catalysts obtained by recrystallization of zeolite BEA.* Microporous Mesoporous Mater., 2007, 105, (1-2), 101-110.

[22] A. Corma, V. Fornés, L. Forni, F. Márquez, J. Martínez-Triguero and D. Moscotti. *2,6-di-tert-butyl-pyridine as a probe molecule to measure external acidity of zeolites*. J. Catal., 1998, 179, (2), 451- 458.

[23] K. Góra-Marek, K. Tarach and M. Choi. *2,6-Di-tert-butylpyridine sorption approach to quantify the external acidity in hierarchical zeolites.* J. Phys. Chem. C, 2014, 118, (23), 12266-12274.

[24] L. Oliviero, A. Vimont, J.-C. Lavalley, F. R. Sarria, M. Gaillard and F. Maugé. *2,6-Dimethylpyridine as a probe of the strength of Brønsted acid sites: study on zeolites. Application to alumina*. Phys. Chem. Chem. Phys., 2005, 7, (8), 1861-1869.

[25] T. Onfroy, G. Clet and M. Houalla. *Quantitative IR characterization of the acidity of various oxide catalysts.* Microporous Mesoporous Mater., 2005, 82, (1-2), 99-104.

[26] A. Corma, C. Rodellas and V. Fornes. *Characterization of acid surfaces by adsorption of 2,6-Dimethylpyridine.* J. Catal., 1984, 88, (2), 374-381.

[27] T. Armaroli, M. Bevilacqua, M. Trombetta, A. G. Alejandre, J. Ramirez and G. Busca. *An FT-IR study of the adsorption of aromatic hydrocarbons and of 2,6-lutidine on H-FER and H-ZSM-5 zeolites.* Appl. Catal., A., 2001, 220, (1-2), 181-190.

[28] K. Barbera, F. Bonino, S. Bordiga, T. V. W. Janssens and P. Beato. *Structure–deactivation relationship for ZSM-5 catalysts governed by framework defects.* J. Catal., 2011, 280, (2), 196-205.

[29] S. M. T. Almutairi, B. Mezari, E. A. Pidko, P. C. M. M. Magusin and E. J. M. Hensen. *Influence of steaming on the acidity and the methanol conversion reaction of HZSM-5 zeolite.* J. Catal., 2013, 307, 194-203.

[30] M. S. Holm, S. Svelle, F. Joensen, P. Beato, C. H. Christensen, S. Bordiga and M. Bjørgen. *Assessing the acid properties of desilicated ZSM-5 by FTIR using CO and 2,4,6-trimethylpyridine (collidine) as molecular probes.* Appl. Catal., A., 2009, 356, (1), 23-30.

[31] F. Thibault-Starzyk, A. Vimont and J-P. Gilson. *2D-COS IR study of coking in xylene isomerisation on H-MFI zeolite*. Catal. Today, 2001, 70, (1-3), 227-241.

[32] F. Thibault-Starzyk, I. Stan, S. Abelló, A. Bonilla, K. Thomas, C. Fernandez, J-P. Gilson and J. Pérez-Ramírez. *Quantification of enhanced acid site accessibility in hierarchical zeolites – The accessibility index.* J. Catal., 2009, 264, (1), 11-14.

[33] K. Mlekodaj, K. Tarach, J. Datka, K. Góra-Marek and W. Makowski. *Porosity and accessibility of acid sites in desilicated ZSM-5 zeolites studied using adsorption of probe molecules.* Microporous Mesoporous Mater., 2014, 183, 54-61.

[34] A. Al-Ani, J.C. J. Haslam, N. E. Mordvinov, O. I Lebedev, A. Vicente, C. Fernandez and V. Zholobenko. *Synthesis of nanostructured catalysts by surfactant-templating of large-pore zeolites.* Nanoscale Adv., 2019,1, 2029-2039.

[35] Ch. Baerlocher, L. B. McCusker and D. H. Olson. *Atlas of zeolite framework types*. Elsevier, 2007.

[36] L-E. Sandoval-Díaz, J-A. González-Amaya and C-A. Trujillo. *General aspects of zeolite acidity characterisation*. Microporous Mesoporous Mater., 2015, 215, 229-243.

[37] F. Leydier, C. Chizallet, A. Chaumonnot, M. Digne, E. Soyer, A-A. Quoineaud, D. Costa and P. Raybaud. *Brønsted acidity of amorphous silica–alumina: The molecular rules of proton transfer.* J. Catal., 2011, 284 (2), 215-229.

[38] G. Crépeau, V. Montouillout, A. Vimont, L. Mariey, T. Cseri and F. Maugé. *Nature, structure and strength of the acidic sites of amorphous silica alumina: An IR and NMR study.* J. Phys. Chem. B., 2006, 110, 15172-15185.

[39] C. Morterra, G. Cerrato and G. Meligrana. *Revisiting the use of 2,6-dimethylpyridine adsorption as a probe for the acidic properties of metal oxides*. Langmuir., 2001, 17, 7053-7060.

[40] V. L. Zholobenko, M. A. Makarova and J. Dwyer. *Inhomogeneity of Brønsted acid sites in H-mordenite.* J. Phys. Chem., 1993, 97(22), 5962-5964.

[41] M. Bevilacqua, A. G. Alejandre, C. Resini, M. Casagrande, J. Ramirez and G. Busca. *An FTIR study of the accessibility of the protonic sites of H-mordenites*. Phys. Chem. Chem. Phys., 2002, 4, 4575-4583.

[42] D. B. Lukyanov, T. Vazhnova, N. Cherkasov, J. L. Casci and J. J. Birtill. *Insights into Brønsted acid sites in the zeolite mordenite.* J. Phys. Chem. C., 2014, 118, 23918-23929.

[43] O. Marie, P. Massiani and F. Thibault-Starzyk. *Infrared evidence of a third Brønsted site in mordenites.* J. Phys. Chem. B., 2004, 108, 5073-5081.

[44] M. Guisnet, P. Ayrault and J. Datka. *Acid properties of mazzite zeolites studied by IR spectroscopy.* Microporous Mesoporous Mater., 1998, 20, 283-291.

[45] M. Gackowski, Ł. Kuterasiński, J. Podobiński, A. Korzeniowska, B. Sulikowski and J. Datka. *Hierarchical zeolite mazzite: physicochemical properties and α-pinene isomerization.* Appl. Catal., A., 2019, 578, 53-62.

[46] K. Sadowska, K. Góra-Marek and J. Datka. *Hierarchic zeolites studied by IR spectroscopy: acid properties of zeolite ZSM-5 desilicated with NaOH and NaOH/tetrabutylamine hydroxide.* Vib. Spectrosc., 2012, 63, 418-425.

[47] K. Sadowska, K. Gora-Marek, M, Drozdek, P, Kústrowski, J. Datka, J, Martinez Triguero and F. Rey. *Desilication of highly siliceous zeolite ZSM-5 with NaOH and NaOH/tetrabutylamine hydroxide.* Microporous Mesoporous Mater., 2013, 168, 195-205.

[48] K. Sadowska, K. Góra-Marek and J. Datka. *Accessibility of acid sites in hierarchical zeolites: quantitative IR studies of pivalonitrile adsorption.* J. Phys. Chem. C, 2013, 117, 9237-9244.

[49] L. M. Parker, D. D. Bibby and G. R. Burns. *Fourier-transform infrared study of pyridine sorbed on zeolite HY.* J. Chem. Soc. Faraday. Trans., 1991, 87 (19), 3319-3323.

[50] S. Khabtou, T. Chevreau and J. C. Lavalley. *Quantitative infrared study of the distinct acidic hydroxyl groups contained in modified Y zeolites.* Microporous Mater., 1994, 3, 133-148.

[51] T. Montanari, E. Finocchio and G. Busca. *Infrared spectroscopy of heterogeneous catalysts: acidity and accessibility of acid sites of faujasite-type solid acids.* J. Phys. Chem. C., 2011, 115, 937-943.

[52] S. C. L. Dias, J. L. de Macedo and J. A. Dias. *Acidity measurements of zeolite Y by adsorption of several probes.* Phys. Chem. Chem. Phys., 2003, 5, 5574-5579.

[53] A. Corma, V. Fornés and F. Rey. *Quinoline as a probe molecule for determination of external Brønsted and Lewis acidity in zeolites.* Zeolites, 1993, 13 (1) 56-59.

[54] J. Datka. *Interaction of OH groups in NaHY zeolites with physically adsorbed alkanes.* J. Chem. Soc. Faraday Trans., 1980, 76, 705-710.

# Chapter 5 Accessibility and location of acid sites in ZSM-5 zeolites modified with phosphorous

## 5.1 Introduction

Zeolite ZSM-5 plays an important role in heterogeneous catalysis. Industrially, H-ZSM-5 is used in fluid catalytic cracking (FCC), alkylation of aromatics, methanol and dimethylether conversion to light olefins, aromatics and fuels, the dehydrogenation of paraffins, dehydration of bioalcohols, fast pyrolysis of biomass, and in photocatalytic reactions [1-8]. The successful application of this zeolite is due to the combined shape selectivity and strong acidity, however the characteristics of the zeolite structure must be adjusted during synthesis or post-synthesis treatments to achieve the catalyst's full potential. Such alterations are commonly accomplished by ion exchange, framework dealumination and the incorporation of phosphorous (P) compounds [9,10].

Phosphorous modification of H-ZSM-5 zeolite is a recognised inexpensive and simple modification utilised to change hydrothermal stability, acidity, selectivity and increase anti-coking tendency in a range of reactions. This process was reported for the first time in the late 1970s [2,11,12] and since then it has been found that P can act as a promoter [1,13,14] or as a poison [15] for zeolite-based catalysts. The introduction of P followed by calcination improves hydrothermal stability and modifies the number and strength of the acid sites in the H-ZSM-5 [13,14,16-23]. Besides, depending on the incorporation process, there is also a loss of the Si-O-Al bonds and dealumination [14,24,25]. Thermal treatment after this modification could lead to a loss of 45% of strong acid sites by dealumination depending on the treatment conditions [26-28]. P also promotes the hydrolysis of the Si-OH-Al groups, which leads to a change in the total amount of acid sites, and studies have shown that samples with P contents above 5 wt.% lack strong acid sites altogether [29,30]. Even without thermal treatment, the incorporation of P leads to a decrease in the number of acid sites. This decrease can be reversed when the samples are washed with hot water [16,27,31]. The introduction

of P also lowers the strength of the acid sites, and the effect is more pronounced at higher P loadings. Three different causes for the decrease in the overall strength of the acid sites are proposed [32]: (1) a decrease in the strength of the Si-OH-Al groups; (2) the loss of predominantly stronger acid sites and (3) the formation of new weak acid sites, such as silanol nests (Si-OH), extra-framework aluminium (EFAl) or P-OH groups.

A decrease of pore dimensions and accessibility are also found in modified ZSM-5 samples. The decrease in the surface area and micropore volume is gradual and is more pronounced at higher loadings of P. Furthermore, dealumination, partial blockage of channels and aggregation of zeolite particles are also observed [19,20,22,33-35]. These changes induce longer diffusion pathways for reactants and products, which consequently, products that diffuse quickly out of the zeolitic structure will be formed with an increased selectivity [2]. P species are mainly located on the external surface of the zeolite [11,24,36,37] and only enter the zeolite channels at higher loadings. In fact, it was suggested that P content above 5 wt.% promotes the formation of polyphosphates on or close to the external surface of the zeolite [30]. The formation of different P species in ZSM-5 depends strongly on the pre- and post-treatment of the zeolite during P modification. Some authors proposed the formation of local silicoaluminophosphate (SAPO) interfaces with the hydrolysis of Si-O-Al bonds during thermal treatment [26,38,40]. However, Damodaran et al [39] and Hendrik et al [40] showed that at higher P loadings the spectroscopic signatures of P in local SAPO interfaces became more like aluminium phosphate ($Al(PO_4)$)[1] species. This proves that with higher loadings of P more Si-O-Al bonds are broken and replaced by Al-O-P bonds [39,40]. There is a synergistic effect between the presence of P and subsequent thermal treatment, as P-containing species actively promote the dealumination of zeolites during thermal treatment and the formation of Al–O–P bonds is energetically favoured [32].

[1]Aluminium phosphate species will be referred to as $Al(PO_4)$ to avoid confusion with aluminophosphate materials which are commonly represented by $AlPO_4$.

Also, EFAl species present in the zeolite before modification can interact with P forming $Al(PO_4)$ [13,16,23] leading to a decrease in their concentration.

These changes in the catalyst can be beneficial or detrimental for catalytic reactions. For example, the control of the number and strength of the acid sites is useful in the methanol-to-hydrocarbon (MTHC), methanol-to-olefin (MTO) processes and in the production of green fuels [17,20,31,41]. Furthermore, the improvement of the hydrothermal stability and reduction of the coke formation, when P modified zeolites are used, causes a higher selectivity and activity with time-on-stream [23]. On the contrary, P treatment has a negative impact on metal ion-exchanged zeolites used in selective catalytic reduction (SCR) of exhaust gases, e.g. NOx [15].

Although there are many studies on the P modification of zeolites, further work is required to expand the understanding of the nature and effects of acidity this modification has on zeolites. This work provides details on characterisation for two sets of P/H-ZSM-5 zeolites prepared using different methods. The main goal is to evaluate the effect of P on the acidity of ZSM-5, examine the location and accessibility of acid sites following P modification and compare the two different methods of preparation. An extensive characterisation provides a better understanding of the interactions between P and the acid sites in this zeolitic structure.

## 5.2 Experimental

### 5.2.1 Materials

Two different sets of modified ZSM-5 zeolites (MFI structure, 10-MR) were studied for this part of the work (Table 5.1). The first group of zeolites was prepared and provided by the Johnson Matthey PLC site in Savannah, US. Zeolite ZSM-5 was loaded with increasing amounts of P followed by thermal treatment as a post-synthesis modification (P/ZSM-5-PS). The second group of zeolites was prepared and provided by the Johnson

Matthey PLC site in Billingham, UK; and the incorporation of P into ZSM-5 was carried out by direct one-pot synthesis (P/ZSM-5-OP).

**Table 5.1.** ZSM-5 samples loaded with different amounts of P.

| P introduction method | Zeolite ID | P wt % (XRF)[a] | Si/Al (XRF)[a] | P/Al bulk (XRF)[a] | P/Al surface (XPS)[a] |
|---|---|---|---|---|---|
| Post-synthesis | **ZSM-5** | - | 12.0 | - | - |
| | **0.7 P/ZSM-5-PS** | 0.7 | 14.5 | 0.23 | 0.50 |
| | **1.9 P/ZSM-5-PS** | 1.9 | 14.2 | 0.63 | 0.79 |
| | **3.0 P/ZSM-5-PS** | 3.0 | 15.3 | 1.10 | 1.00 |
| One-pot synthesis | **ZSM-5** | - | 15.6 | - | - |
| | **0.6 P/ZSM-5-OP** | 0.6 | 13.6 | 0.19 | < 0.06 |
| | **0.7 P/ZSM-5-OP** | 0.7 | 15.5 | 0.26 | 0.13 |
| | **0.9 P/ZSM-5-OP** | 0.9 | 13.8 | 0.29 | < 0.06 |

[a] XRF and XPS data provided by Johnson Matthey PLC. All the values were corrected for water content using TGA data.

### 5.2.2 Zeolite characterisation

A comprehensive structural and acidic characterisation of the zeolites was carried out using X-ray photoelectron spectroscopy (XPS), X-ray fluorescence (XRF), argon (Ar) physisorption, FTIR using pyridine (Py) and collidine (Coll) as probe molecules and $^{31}P$ solid state MAS NMR. A detailed description of Ar physisorption, Py- and Coll-FTIR spectroscopy and SEM-EDX analysis is available in Chapters 3 and 4. XPS, XRF, Ar physisorption and $^{31}P$ solid state MAS NMR analyses were performed and provided by Johnson Matthey PLC. Prior to the XPS analysis, all zeolites were attached to a sample stub using carbon tape and the study was carried out with a Thermo Escalab 250. Energy scales were corrected such that the silicon *2p* signal maxima were at 103.3 eV (silica). The $^{31}P$ solid-state MAS NMR spectra was acquired at a static magnetic field strength of 9.4 T ($V_o$ ($^1H$) = 400 MHz) on a Bruker Avance III console using TopSpin 3.1 software. The probe was tuned to 161.98 MHz and referenced to adenosine di phosphate (ADP) at 0.9 ppm. Prior

to the experiments, all zeolites were stored overnight in a humid environment before being packed into zirconia MAS rotors with Kel-F caps and the sample mass was recorded.

## 5.3 Effect of modification of ZSM-5 zeolite by post-synthesis

### 5.3.1 Structural and acidity properties

Ar physisorption results (Table 5.2) show that the apparent BET surface area (apparent $S_{BET}$) and micropore volume ($V_{micro}$) of the zeolites decrease with P loadings, however, this change only occurs at loadings equal to or higher than 1.9%. At low P contents there are no remarkable changes in both parameters, indicating that low loadings of P are suitable for retaining high specific surface area and pore volume of ZSM-5 zeolites, consistent with the data reported previously [14,19,34]. This decrease in apparent $S_{BET}$ and $V_{micro}$ is attributed to the formation of phosphate species at the entrance of pore channels of ZSM-5 [39].

**Table 5.2** Textural properties of parent and P/ZSM-5-PS zeolites. Experiments were performed at Johnson Matthey PLC.

| Zeolite | Apparent $S_{BET}$ ($m^2/g$) | $S_{ext}$ ($m^2/g$) | $V_{micro}$ ($cm^3/g$) |
|---|---|---|---|
| **ZSM-5** | 431 | 21 | 0.21 |
| **0.7 P/ZSM-5-PS** | 445 | 15 | 0.22 |
| **1.9 P/ZSM-5-PS** | 349 | 15 | 0.17 |
| **3.0 P/ZSM-5-PS** | 277 | 15 | 0.14 |

FTIR spectra of all ZSM-5 zeolites show four major peaks at 3782 $cm^{-1}$, 3745 $cm^{-1}$ (with a shoulder at 3722 $cm^{-1}$), 3662 $cm^{-1}$ and 3609 $cm^{-1}$ (Figure 5.1 a). The most intense peak at 3609 $cm^{-1}$ is assigned to acidic bridging Si-OH-Al groups and the peaks at 3745 and 3722 $cm^{-1}$ correspond to different silanol groups (external and internal Si-OH, respectively). The peaks at 3662 $cm^{-1}$ and 3782 $cm^{-1}$ are commonly assigned to two kinds of Al-OH groups, Al-OH from EFAl species and $Al_2O_3$-like species, respectively [42].

The intensities of the peaks of the OH groups change significantly after P modification. This indicates that P interacts with both non-acidic and acidic hydroxyl groups. The decrease

in the intensity of Si-OH-Al groups is explained by the framework dealumination and the formation of Al($PO_4$) species [25,39]. The breaking of Si-O-Al bonds often leads to the formation of new acid sites, such as Si-OH groups interacting with EFAl species [32]. The peak at ~3722 $cm^{-1}$ became more predominant in zeolites with higher P contents, this peak is due to internal Si-OH groups resulting from the breaking of Si-O-Al bonds [21,24,26]. It is important to point out that all samples have been thermally treated after modification with P, which is known to cause dealumination and breaking of Si-O-Al bonds (Chapter 3).

The interaction of Py at 150ºC (Figure 5.1 b, dashed lines) with acid sites results in a complete disappearance of the peaks at 3782 $cm^{-1}$ and 3609 $cm^{-1}$ corresponding to Al-OH and bridging Si-OH-Al groups, respectively. A small decrease in the intensity of the peaks at 3745 $cm^{-1}$ and 3662 $cm^{-1}$ assigned to Si-OH and Al-OH groups, respectively, is also observed. The disappearance of the Si-OH-Al peak at 3609 $cm^{-1}$ means that pyridine is able to access all the acid sites in the zeolites. The removal of the Al-OH peak at 3782 $cm^{-1}$ is attributed to Py interacting with Lewis acid sites (LAS) to which they are linked [37].

In the range of 1400-1700 $cm^{-1}$, chemisorbed Py is revealed by the following sets of peaks: two peaks at 1545 and 1637 $cm^{-1}$ due to pyridinium ion ($PyH^+$), two peaks at 1456 and 1622 $cm^{-1}$ assigned to Py coordinated to Lewis acid sites (PyL) and the signal at 1491 $cm^{-1}$ corresponding to Py on Lewis and Brønsted acid sites (Figure 5.1 c). The introduction of P leads to a significant decrease in the intensities of the peaks corresponding to $PyH^+$ and PyL. The total concentration of acid sites for ZSM-5 parent zeolite is ~718 μmol/g, with a BAS/LAS ratio of 2.5. The concentration of both BAS and LAS gradually decreases with increasing P loadings. In fact, the introduction of P leads to a loss of ~73% of the initial concentration of acid sites (Table 5.3). Similar changes in LAS and BAS have been observed in previous reports [21,22].

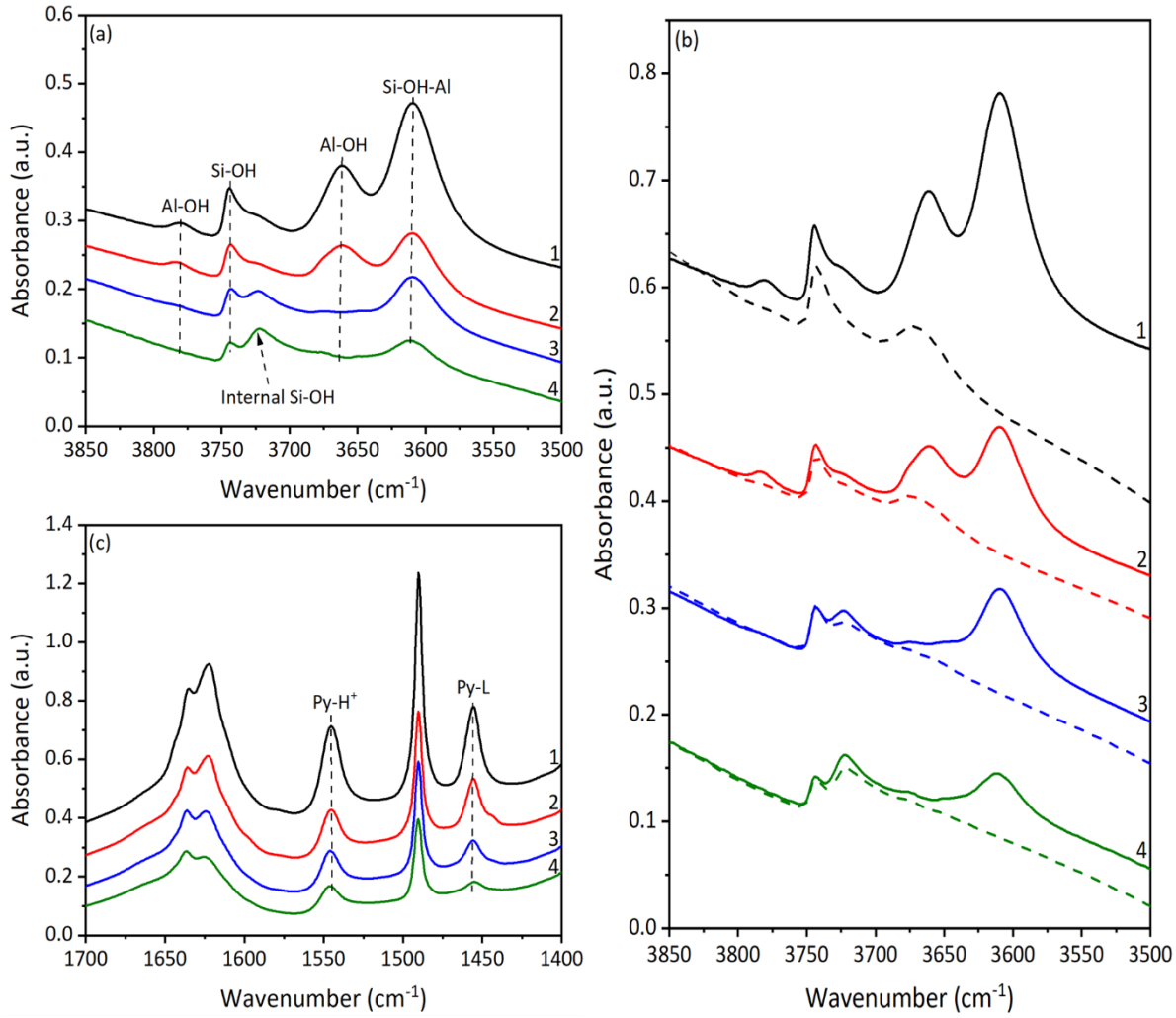


**Figure 5.1. (a)** FTIR spectra of the hydroxyl region**. (b)** FTIR spectra of the hydroxyl region before (solid lines) and after (dashed lines) adsorption of Py at 150°C. **(c)** Difference spectra Py region for: **(1)** ZSM-5 **(2)** 0.7 P/ZSM-5-PS, **(3)** 1.9 P/ZSM-5-PS and **(4)** 3.0 P/ZSM-5-PS zeolites activated at 450°C.

**Table 5.3.** Concentration of acid sites of parent and P/ZSM-5-PS zeolites in quantitative experiments using Py adsorption monitored by FTIR.

| Zeolite | P (μmol/g)[a] | BAS (μmol/g) | LAS (μmol/g) | BAS/LAS | BAS+LAS (μmol/g) |
|---|---|---|---|---|---|
| **ZSM-5** | - | 514 | 204 | 2.5 | 718 |
| **0.7 P/ZSM-5-PS** | 226 | 255 | 143 | 1.8 | 398 |
| **1.9 P/ZSM-5-PS** | 617 | 225 | 74 | 3.0 | 299 |
| **3.0 P/ZSM-5-PS** | 982 | 163 | 30 | 5.4 | 193 |

[a] These results were calculated using XRF data.

The effect of Py desorption temperature on the intensities of the Si-OH-Al peak and peaks corresponding to adsorbed pyridine species (deduced from the difference spectra, before pyridine absorption and after pyridine adsorption-desorption) was also examined (Figures 5.2 and 5.3). Figure 5.2 shows difference IR spectra of the ZSM-5 parent zeolite in the OH and Py regions whereas Figure 5.3 summarises the quantitative changes in the relative intensities of the bands corresponding to Si-OH-Al, Py-$H^+$ and Py-L species for all zeolites. The relative intensity of the Si-OH-Al peak remains constant up to 350ºC gradually decreasing at higher desorption temperatures for ZSM-5 and 0.7 P/ZSM-5-PS zeolites. Zeolites with higher P contents show a decrease in the relative peak intensity at lower temperatures, 300ºC for 1.9 P/ZSM-5 and 200ºC for 3.0 P/ZSM-5. After desorption at 450ºC a significant proportion of Si-OH-Al groups still interact with Py (e.g. 76% for the parent ZSM-5 and 72% for 0.7 P/ZSM-5-PS). In contrast, the relative intensity of the Py-$H^+$ peak decreases for all samples, following desorption above 150ºC (Figure 5.3 b). This indicates the presence of relatively weak BAS interacting with Py (weaker than Si-OH-Al, which retain Py up to desorption temperatures of ~300ºC), such as Al-OH and Si-OH groups. The data shows a considerable reduction in the apparent strength of BAS, which occurs with increasing amounts of phosphorus, as shown for zeolites with P contents above 1 wt% in agreement with data reported previously [22]. This loss in the apparent strength could be explained (i) by the formation of new weak acid sites, which are attributed in the literature to P-OH groups and internal Si-OH groups [13,30,43] observed in Figure 5.1, and (ii) by the decrease in the concentration of Si-OH-Al resulting in fewer Py desorption-readsorption cycles (‘travel’ of Py along the zeolite channels), which is observed as a lower desorption temperature required to remove Py.

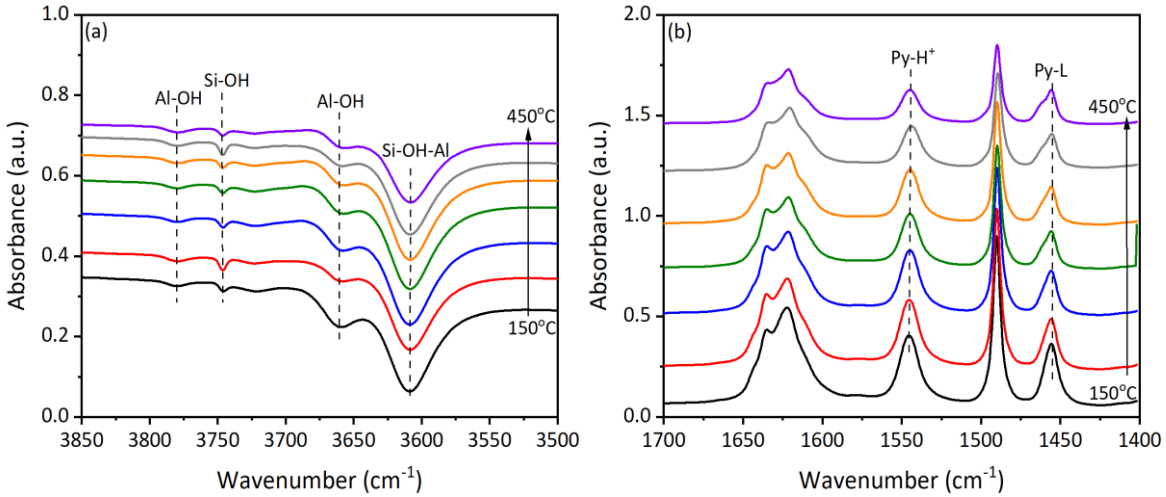


**Figure 5.2.** Difference spectra of the **(a)** hydroxyl region and **(b)** Py region of ZSM-5 parent zeolite after Py desorption at increasing temperatures (150°C- 450°C).

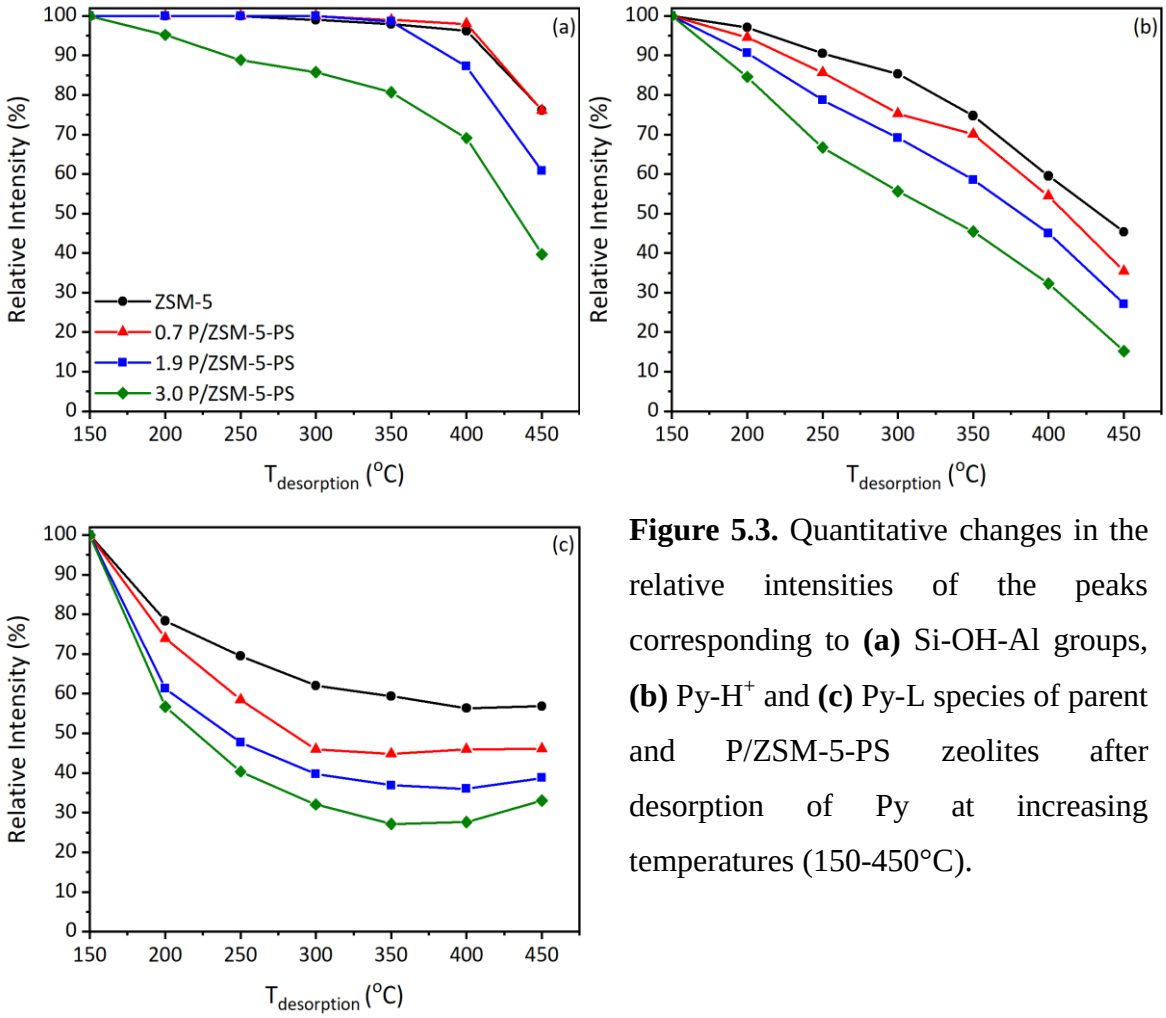


**Figure 5.3.** Quantitative changes in the relative intensities of the peaks corresponding to **(a)** Si-OH-Al groups, **(b)** Py-$H^+$ and **(c)** Py-L species of parent and P/ZSM-5-PS zeolites after desorption of Py at increasing temperatures (150-450°C).

### 5.3.2 Accessibility and location of acid sites

FTIR using Py as probe molecule has provided information about the acid strength, concentration and the presence of LAS in the samples. However, as Py is a small probe

molecule (5.4 Å), it does not give any information about the accessibility of the different acid sites in this zeolite structure. As shown in Chapter 4, the relatively large size of Coll (7.3 Å) prevents its access to BAS in the micropores of ZSM-5 (10-MR zeolite), which allows the probe to quantify acid sites on the external surface and provide a better understanding on the location of different acid sites in this zeolites.

Adsorption of Coll at 250ºC only leads to a reduction in the intensity of the peak at 3745 $cm^{-1}$ that corresponds to Si-OH groups while the other OH-species remain virtually unaffected (Figure 5.4 a spectra 1 and 2). However, the difference spectra in the OH region (e.g. Figure 5.4 a, spectrum 3) show two low intensity negative peaks at ~ 3745 and ~3610 $cm^{-1}$ after Coll adsorption. These negative peaks correspond to the fraction of Si-OH and Si-OH-Al groups located on the external surface or near the pore mouths of the zeolite, which are interacting with the probe molecule. Coll adsorption (Figure 5.4 b) also gives rise to the band at ~1634 with a shoulder at ~1649 $cm^{-1}$, resulting from the interaction with BAS, and two low intensity bands at 1619 $cm^{-1}$ and 1575 $cm^{-1}$, assigned to the probe adsorbed on Si-OH groups. This behaviour is similar for all samples studied.

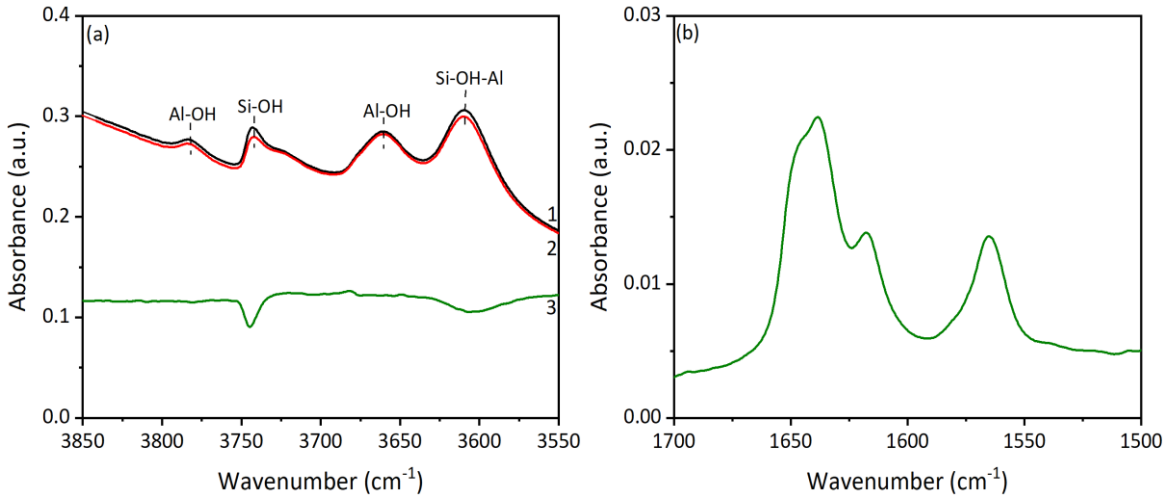


**Figure 5.4 (a)** FTIR spectra of the hydroxyl region of 0.7 P/ZSM-5-PS **(1)** before and **(2)** after Coll adsorption at 250ºC, **(3)** difference spectrum after Coll adsorption at 250ºC (spectrum was multiplied by 4 for clearer presentation). **(b)** Difference spectrum in the region of the aromatic ring vibrations after Coll adsorption at 250ºC.

Coll with a kinetic diameter of 7.4 Å, is too large to enter ZSM-5 micropores, reaching no acid sites on the internal surface and only interacting with BAS located on the external surface and in the pore mouths of the zeolite. At higher loadings of P, the accessibility values decrease gradually, however, the error margin of these data is quite high as the number of BAS detected on the external surface is very small (Table 5.4). This decrease in acid site concentration on the external surface has been previously reported in samples with P/Al above 0.6 [44], which corresponds to samples 1.9 P/ZSM-5-PS and 3.0 P/ZSM-5-PS in this work.

**Table 5.4.** Concentration of BAS and accessibility factor (AF) for parent and P/ZSM-5-PS zeolites in quantitative measurements using Py and Coll adsorption monitored by FTIR.

| **Zeolite** | **BAS $_{total}$ (µmol/g)** | **BAS $_{external}$ (µmol/g)** | **AF (%)** |
|---|---|---|---|
| **ZSM-5** | 514 | 10 | 1.9 |
| **0.7 P/ZSM-5-PS** | 255 | 6 | 2.2 |
| **1.9 P/ZSM-5-PS** | 225 | 4 | 2.0 |
| **3.0 P/ZSM-5-PS** | 163 | 2 | 1.3 |

Quantification of acid sites for the 0.7 P/ZSM-5-PS sample shows a significant reduction in the total number of BAS and a modest decrease in the number of LAS and BAS detected on the external surface of the zeolite (when compared to the parent zeolite ZSM-5) (Figure 5.5). For this 0.7 P/ZSM-5-PS sample, the amount of BAS removed and the amount of P introduced is almost the same, which could suggest that each P incorporated is interacting with one BAS from the zeolite. However, XRF data (Table 5.1) demonstrates an increase in the Si/Al ratio (from 12.0 to 14.5), which indicates that some of the Al species (BAS and LAS) in the zeolite are removed from the structure during the modification treatment (e.g. by leaching). P incorporation and Al removal cause the decrease in the total number of acid sites.

The XPS and XRF analysis (Table 5.1) show a greater P/Al ratio for the external surface than the zeolite bulk for 0.7 and 1.9 P/ZSM-5-PS samples. This suggests that P

species, in relative terms, are preferentially located on the external surface of the ZSM-5 zeolite at the initial stages of the P modification, as compared to the latter stages (0.7 P/ZSM-5-PS versus 3.0 P/ZSM-5-PS). As the number of BAS on the external surface changes very little, it is therefore impossible to conclusively state that P interacts with the BAS located on the external surface. This may be attributed to the formation of polyphosphates even at low P loadings. Further evidence of the polyphosphates formation is also observed in the $^{31}P$ NMP spectra (Figure 5.6).

At higher loadings of P, the total number of BAS, LAS, and BAS located on the external surface decrease further (Figure 5.5 a). According to the elemental analysis, the increase in the P loadings leads to a more even distribution of these species on both internal and external surfaces (Table 5.1), in agreement with other reports [11,24,36,37]. The amount of P introduced is greater than the number of BAS removed during the modification (Figure 5.5 b), which is confirmed by the increase in the polyphosphates signals evident in the $^{31}P$ NMR spectra (Figure 5.6) in samples with higher P contents. According to the literature, the distribution of these P species in the ZSM-5 structure is dependent on the P/Al ratio, crystal size, surface OH groups, Al distribution and preparation method of the sample [32].

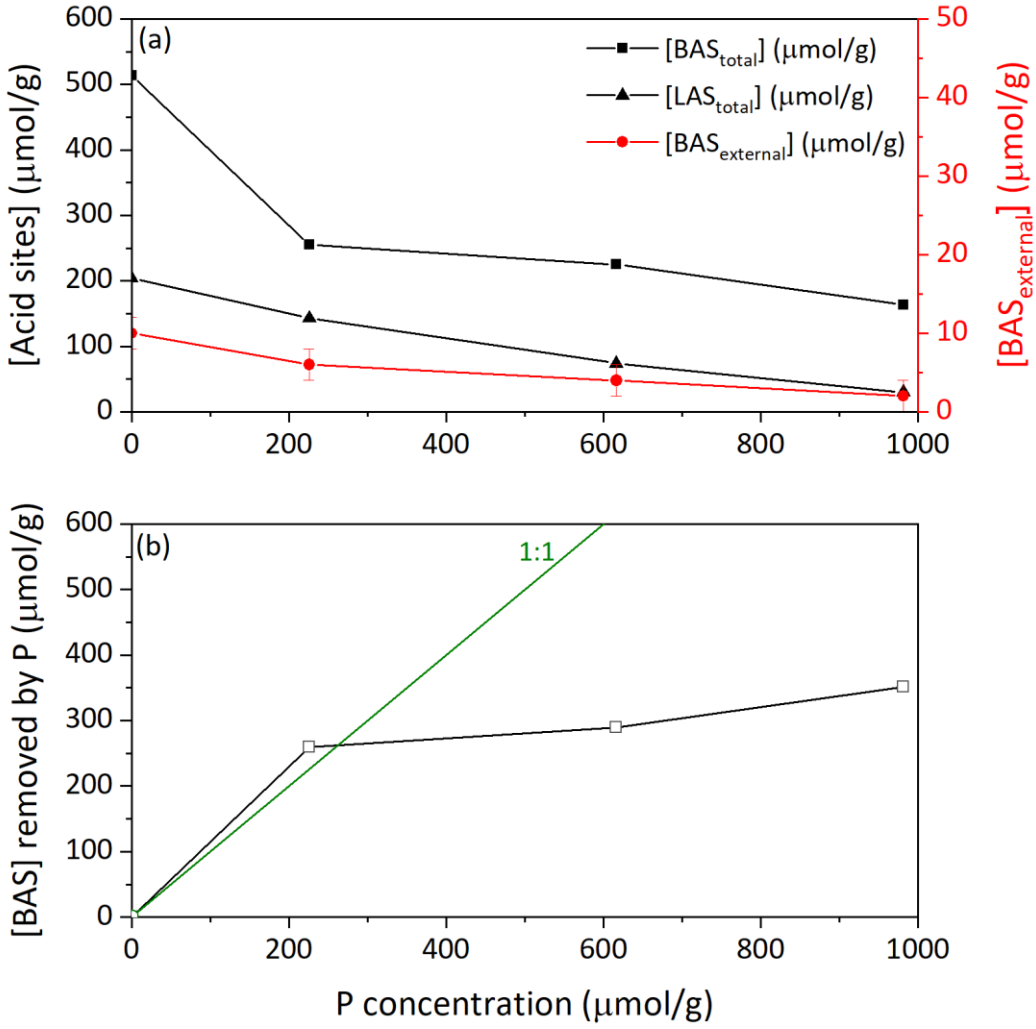


**Figure 5.5 (a)** Variation of number of acid sites with increasing P loadings. **(b)** Relationship between BAS removed and P content (µmol/g) incorporated.

Modification with P also leads to the formation of Al($PO_4$) along with polyphosphates species (Figure 5.6). These Al($PO_4$) species are mainly formed due to the interaction of P-containing species with the acid sites of zeolite and increase with P content. The polyphosphate species are mostly formed in zeolites with high P loading (above 1 wt%), demonstrating that in these samples P is less evenly distributed over the ZSM-5, increasing the possibility of the formation of clusters and pore blockage. Evidence of the formation of different P species after modification has been also reported [22,25,38-40] (Figure 5.7).

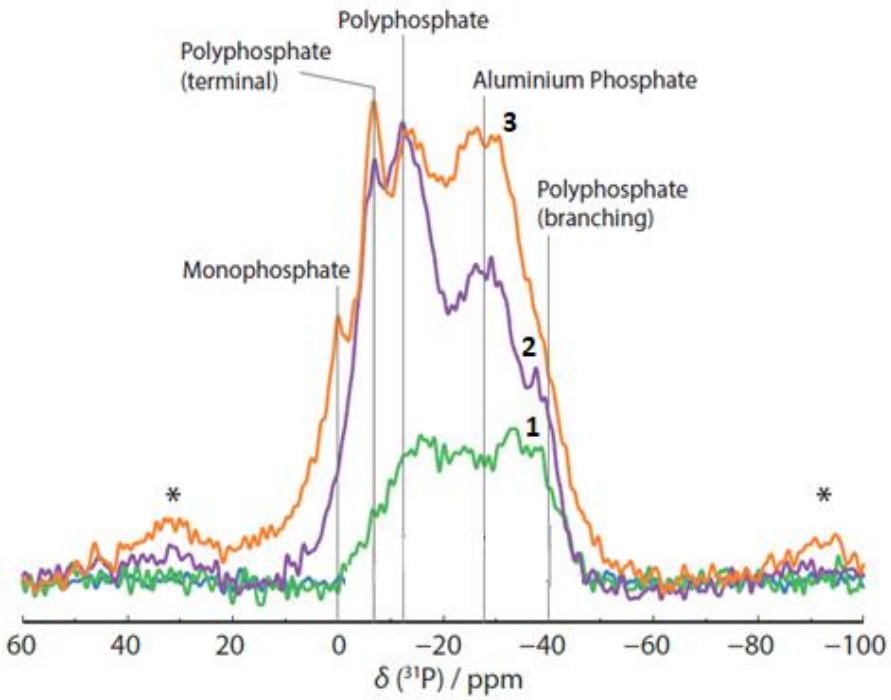


**Figure 5.6.** Normalised $^{31}$P solid-state MAS NMR spectra. **(1)** 0.7 P/ZSM-5-PS **(2)** 1.9 P/ZSM-5-PS and **(3)** 3.0 P/ZSM-5-PS. Asterisks indicate spinning sidebands.

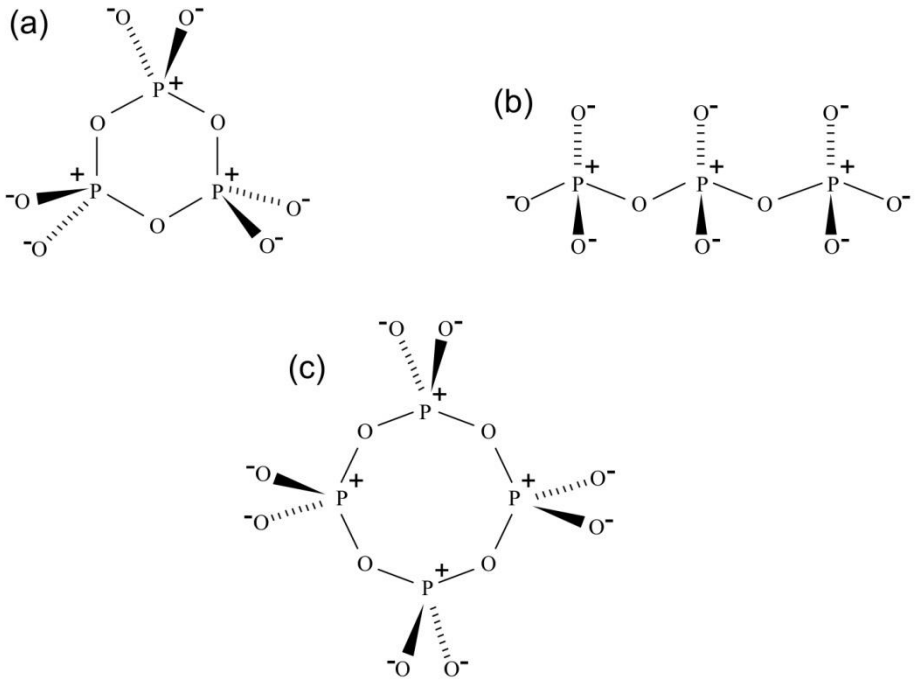


**Figure 5.7.** Schematic representation of possible polyphosphate species formed during P modification in ZSM-5 zeolite (a) $[P_3O_9]^{3-}$ (b) $[P_3O_{10}]^{5-}$ and (c) $[P_4O_{12}]^{4-}$.

Although there is no clear indication of the SAPO- or $AlPO_4$-like species, the possibility of formation of this type of species cannot be excluded. The $^{31}$P NMR overlapping

signals around -33 ppm (Figure 5.6) could also be assigned to SAPO-like species, normally present in SAPO-34 materials [45]. The increase in the Al($PO_4$) signal in the $^{31}$P MAS NMR spectra confirms that higher loadings of P favour the breaking of more Si-O-Al bonds replacing them with Al-O-P bonds [32,39,40]. Furthermore, the increase in the number of internal Si-OH groups observed by FTIR spectroscopy (Figure 5.1) agrees with this statement. The importance of controlling the amount of P incorporated can be appreciated from these results, as the formation of polyphosphate species increases with the P loadings. These polyphosphates could be responsible for the loss of pore volume and surface area (Table 5.2) as well as changes in the acidic properties of the ZSM-5 zeolite (Figures 5.3 and 5.5).

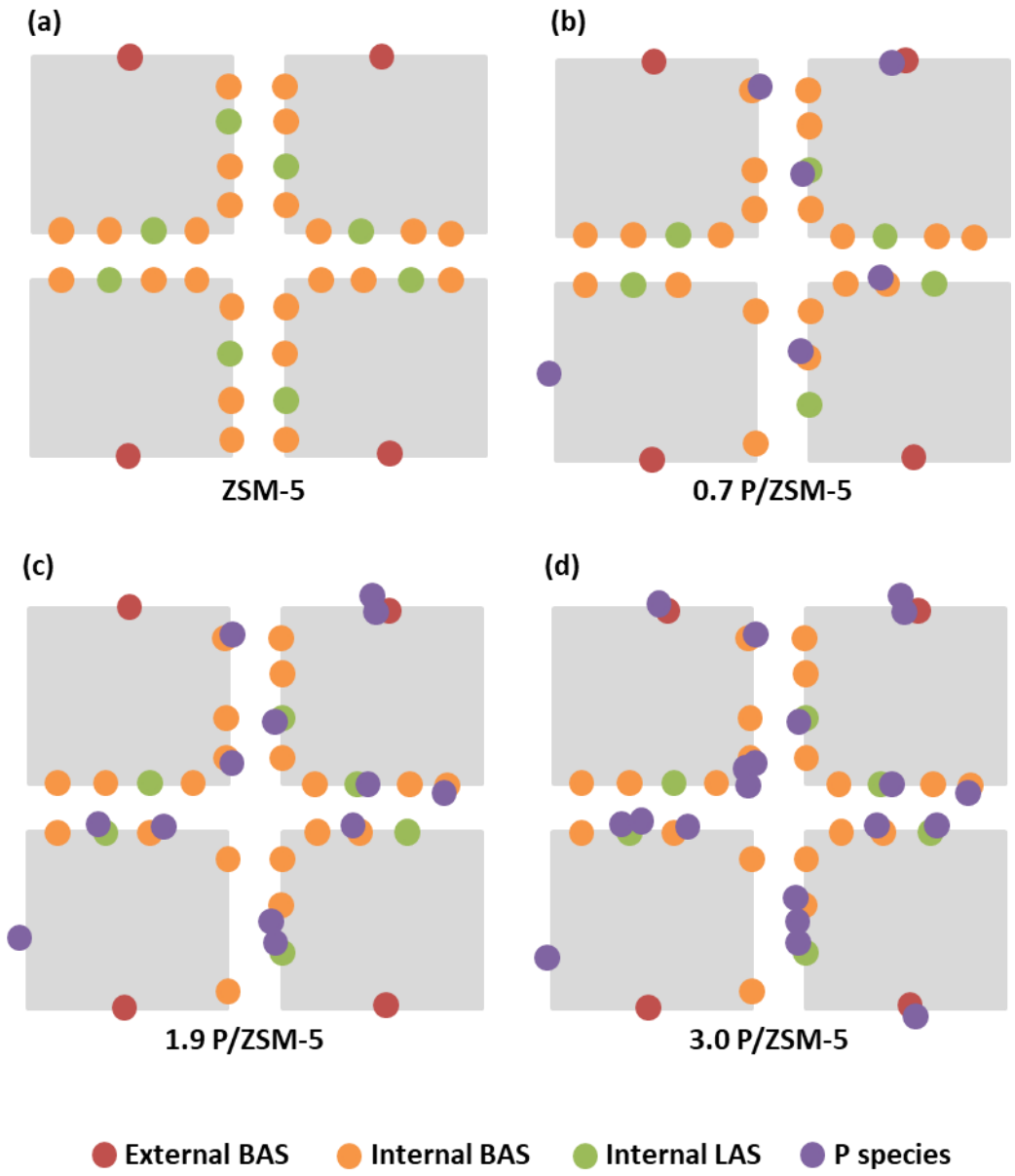


**Figure 5.8.** Simplified schematic model for the location of acid sites and P species in P/ZSM-5-PS zeolites. **(a)** Typical distribution of external and internal acid sites in parent ZSM-5. **(b)** Distribution of P in 0.7 P/ZSM-5-PS. **(c)** Distribution of P in 1.9 P/ZSM-5-PS. **(d)** Distribution of P in 3.0 P/ZSM-5-PS.

Figure 5.8 demonstrates a simplified model describing the location of P species in the set of P/ZSM-5-PS zeolites, which is based on the experimental data presented. This estimation can be made assuming (i) an approximately even distribution of Al through the zeolite and (ii) that the ratio between external and internal surface area is 1:20 (given by Ar physisorption analyses). The amount of P atoms on the external surface of the zeolites can be estimated using these assumptions and the XRF and XPS data shown in Table 5.1. For

sample 0.7 P/ZSM-5-PS, the amount of P atoms on the external surface is ~24 µmol/g and in the bulk is ~202 µmol/g (total of P atoms = 226 µmol/g, Table 5.3), which means that 1 out of ~10 P atoms are located on the external surface. For the sample with higher amounts of P (3.0 P/ZSM-5-PS), the amount of P atoms on the external surface and bulk is ~45 and 937 µmol/g (total of P atoms = 982 µmol/g, Table 5.3), respectively, indicating that 1 out of 21 P atoms are located on the external surface. Additionally, there is decrease in the overall number of acid sites, which is caused by the P introduction and additional Al removal (BAS and LAS) possibly due to leaching. In samples with higher P contents, a considerable amount of polyphosphates is formed and the overall number of acid sites decreases even further.

## 5.4 Effect of modification of ZSM-5 zeolite by direct synthesis

Ar physisorption results (Table 5.5) show that both apparent $S_{BET}$ and $V_{micro}$ of the zeolites decrease when the synthesis takes place in the presence of P. However, there are no remarkable changes in both parameters between zeolites with different amounts of P. The $S_{ext}$ is higher for the P-free ZSM-5 and 0.7 P/ZSM-5-OP zeolites, which indicates that these two samples have a smaller crystal size in comparison with the 0.6 and 0.9 P/ZSM-5-OP.

**Table 5.5**. Textural properties of P-free ZSM-5 and P/ZSM-5-OP zeolites. Experiments were performed at Johnson Matthey PLC.

| Zeolite | Apparent $S_{BET}$ ($m^2/g$) | $S_{ext}$ ($m^2/g$) | $V_{micro}$ ($cm^3/g$) |
|---|---|---|---|
| **ZSM-5** | 465 | 86 | 0.21 |
| **0.6 P/ZSM-5-OP** | 401 | 26 | 0.20 |
| **0.7 P/ZSM-5-OP** | 413 | 63 | 0.19 |
| **0.9 P/ZSM-5-OP** | 403 | 39 | 0.19 |

FTIR spectra show four major peaks at 3782 $cm^{-1}$, 3745 $cm^{-1}$ (with a shoulder at 3722 $cm^{-1}$), 3662 $cm^{-1}$ and 3609 $cm^{-1}$ (Figure 5.9 a). These peaks are assigned to Al-OH from EFAl species, Si-OH groups, acidic bridging Si-OH-Al groups and $Al_2O_3$-like species, respectively [42], which is similar to the samples described in Section 5.3.1. The four

zeolites show identical OH group signatures, with the exception of 0.6 P/ZSM-5-OP zeolite, which shows a peak at 3722 $cm^{-1}$, related to internal Si-OH groups.

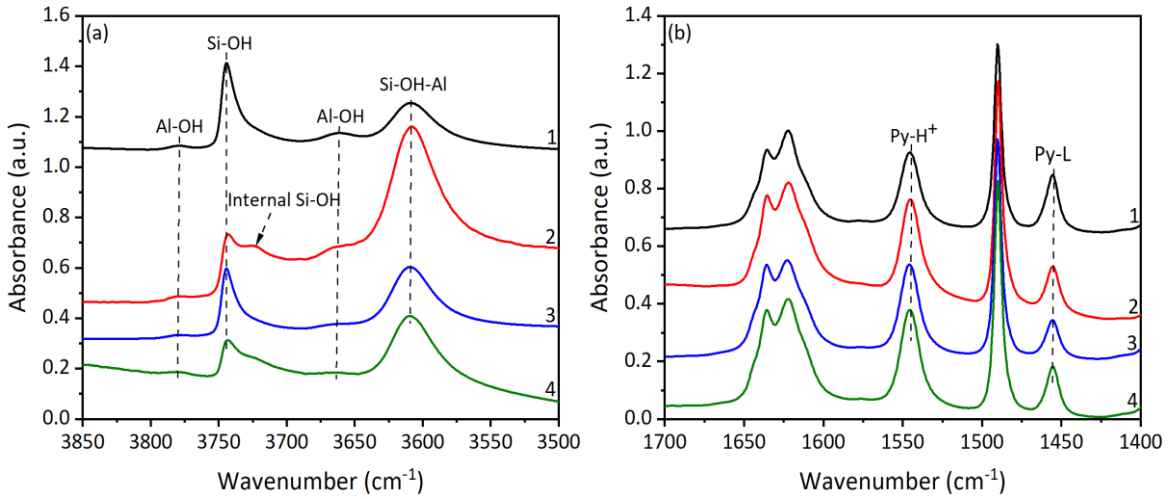


**Figure 5.9. (a)** FTIR spectra of the hydroxyl region. **(b)** Difference spectra of Py region for: **(1)** ZSM-5-OP **(2)** 0.6 P/ZSM-5-OP, **(3)** 0.7 P/ZSM-5-OP and **(4)** 0.9 P/ZSM-5-OP zeolites activated at 450°C.

Interaction of Py at 150ºC (Figure 5.9 b) allows the overall concentration of acid sites in these zeolites to be obtained (Table 5.6). The P-containing zeolites exhibit similar concentrations of BAS (within experimental error). However, with the introduction of increasing amounts of P, the number of LAS slightly decreases, when compared with P-free zeolite. The BAS/LAS ratios are found to increase from P-free ZSM-5 to P/ZSM-5 zeolites, which suggest that BAS are not as much affected by P as LAS. This indicates that the introduction of P during synthesis prevents the breaking of Si-O-Al bonds and dealumination in contrast to results demonstrated in P/ZSM-5 zeolites obtained by post-modification treatments. In this set of zeolites, P is protecting the zeolitic structure from losing strong Si-OH-Al groups related to BAS, decreasing the amount of LAS (EFAl species). Overall, the total concentration of acid sites remains similar for all P/ZSM-5-OP zeolites.

**Table 5.6.** Concentration of acid sites of P-free ZSM-5 and P/ZSM-5-OP zeolites in quantitative experiments using Py adsorption monitored by FTIR.

| Zeolite | P (µmol/g)[a] | BAS (µmol/g) | LAS (µmol/g) | BAS/LAS | BAS+LAS (µmol/g) |
|---|---|---|---|---|---|
| **ZSM-5** | - | 451 | 155 | 2.9 | 606 |
| **0.6 P/ZSM-5-OP** | 190 | 619 | 109 | 5.7 | 728 |
| **0.7 P/ZSM-5-OP** | 232 | 551 | 95 | 5.8 | 646 |
| **0.9 P/ZSM-5-OP** | 294 | 597 | 117 | 5.1 | 714 |

[a] These results were calculated using XRF data.

The effect of Py desorption temperature on the intensities of the Si-OH-Al peak and peaks corresponding to adsorbed pyridine species (deduced from the difference spectra) was also examined (Figure 5.10). Figure 5.10 summarises the quantitative changes in the relative intensities of the bands corresponding to Si-OH-Al, Py-$H^+$ and Py-L species for all of the zeolite samples. The relative intensity of the Si-OH-Al peak remains constant up to 300ºC gradually decreasing at higher desorption temperatures. After desorption at 450ºC, a significant proportion of Si-OH-Al groups still interact with Py (e.g. 74% for the P-free ZSM-5 and 69% for 0.7 P/ZSM-5-OP). In contrast, the relative intensity of the Py-$H^+$ peak decreases for all samples, following desorption above 150ºC (Figure 5.10 b). This indicates the presence of relatively weak BAS interacting with Py (weaker that Si-OH-Al, which retain Py up to desorption temperatures of 300ºC), such as Al-OH and Si-OH groups. When ZSM-5 is modified with P during synthesis, there are no considerable differences in the apparent strength of both BAS and LAS. All samples show very similar Py desorption profiles, and as a result, similar apparent strengths.

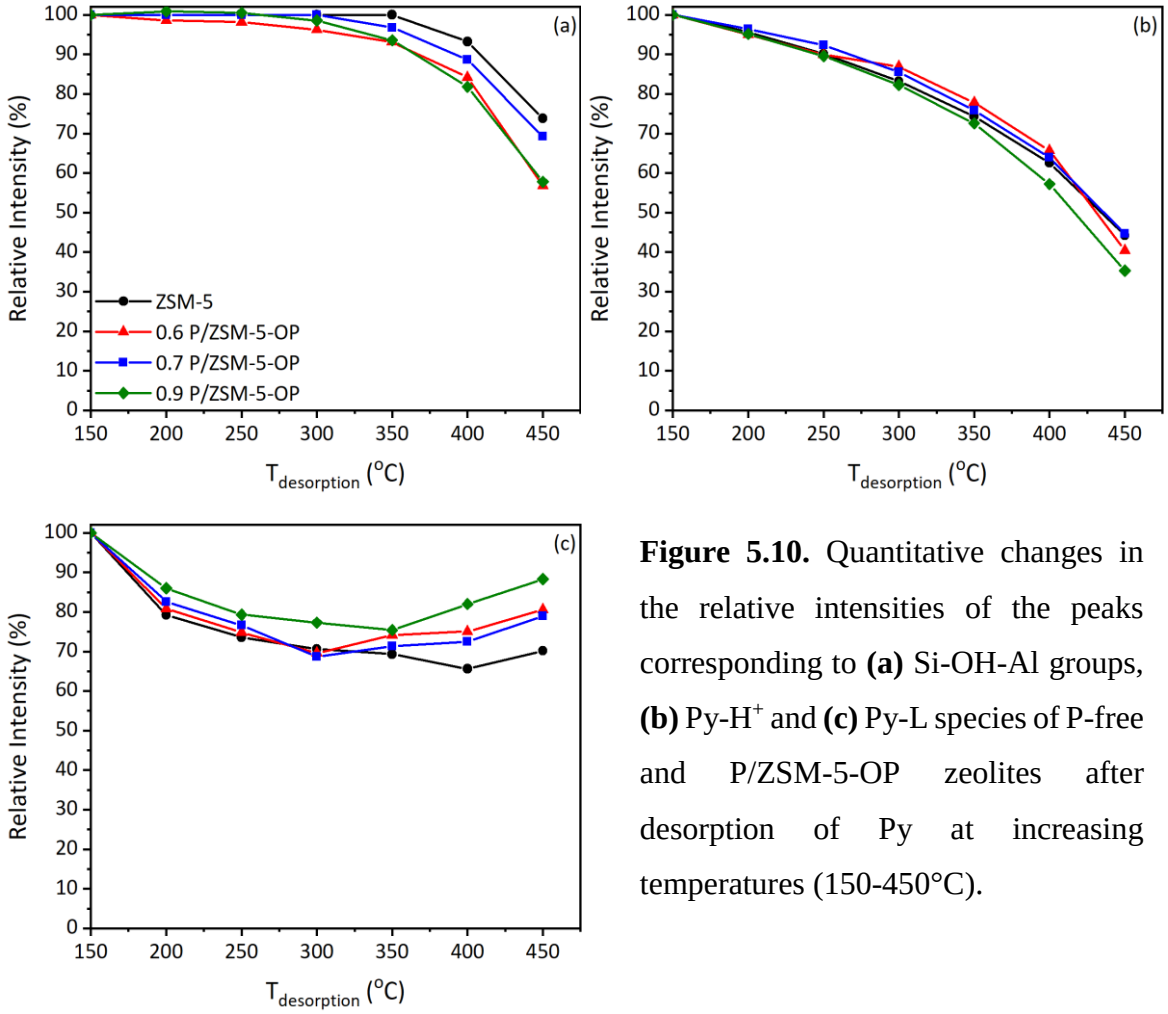


**Figure 5.10.** Quantitative changes in the relative intensities of the peaks corresponding to **(a)** Si-OH-Al groups, **(b)** Py-$H^+$ and **(c)** Py-L species of P-free and P/ZSM-5-OP zeolites after desorption of Py at increasing temperatures (150-450°C).

According to XRF and XPS data (Table 5.1), a very small amount of P species is located on the external surface of ZSM-5-OP samples, independent of the amount of P loaded. This indicates that P species when incorporated during synthesis tend to be deposited on the internal surface of the zeolites. The combination of Py- and Coll- FTIR results (Table 5.7 and Figure 5.11) shows no significant differences found within this set of samples. The only differences are due to the varying crystal sizes of these zeolites. These results are in line with Ar physisorption data presented in Table 5.5.

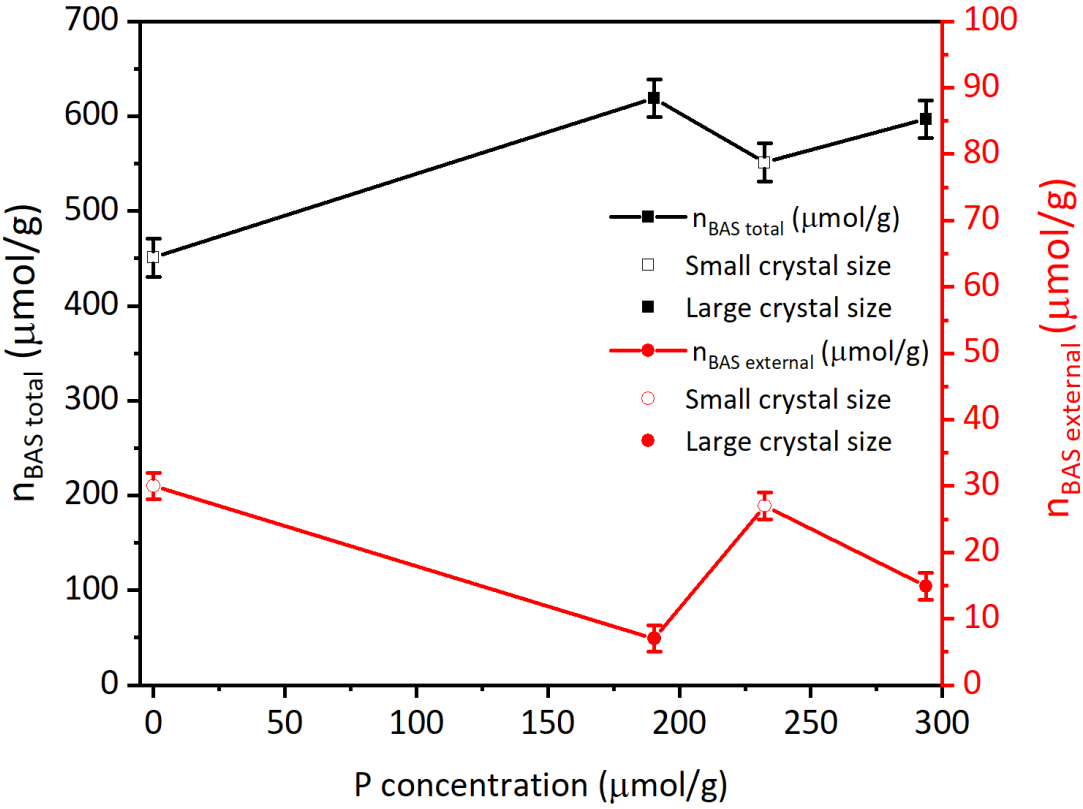


**Figure 5.11.** Variation of the number of BAS with different P contents.

**Table 5.7.** Concentration of BAS and accessibility factor (AF) for P-free ZSM-5 and P/ZSM-5-OP zeolites in quantitative measurements using Py and Coll adsorption monitored by FTIR.

| Zeolite | BAS $_{total}$ (µmol/g) | BAS $_{external}$ (µmol/g) | AF (%) |
|---|---|---|---|
| **ZSM-5** | 451 | 30 | 6.6 |
| **0.6 P/ZSM-5-OS** | 619 | 7 | 1.2 |
| **0.7 P/ZSM-5-OS** | 551 | 27 | 4.9 |
| **0.9 P/ZSM-5-OS** | 597 | 15 | 2.5 |

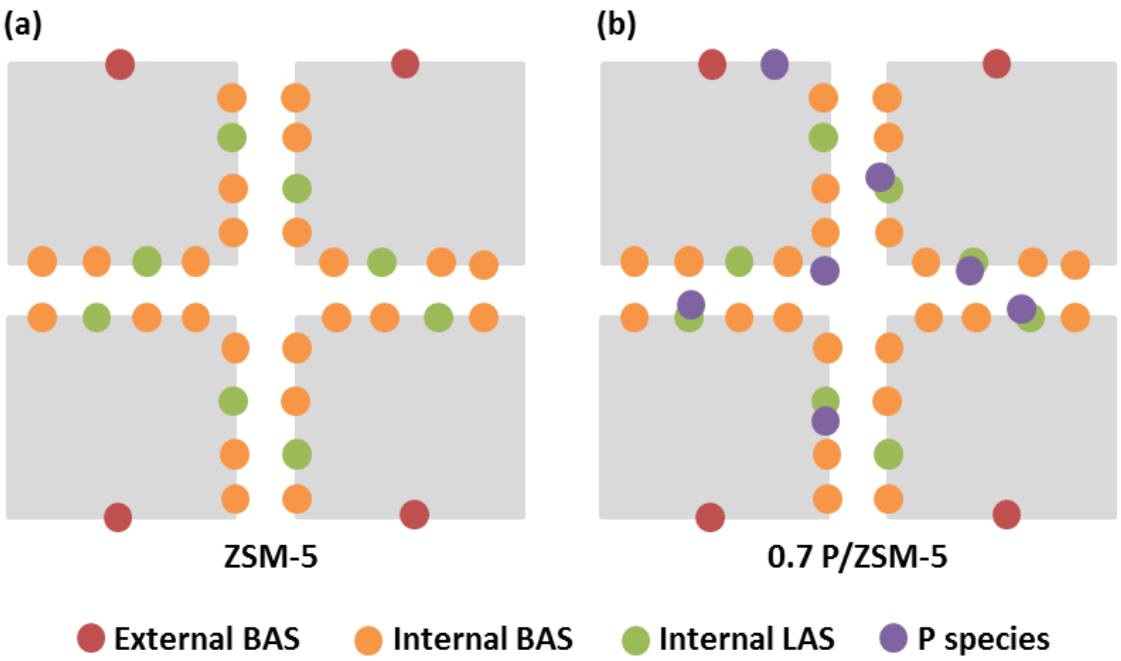


**Figure 5.12.** Simplified schematic model for the location of acid sites and P species in P/ZSM-5-OP zeolites **(a)** Typical distribution of external and internal acid sites in P-free ZSM-5. **(b)** Distribution of P in 0.7 P/ZSM-5-OP zeolite.

Based on the data presented, the model above for the distribution of P species and acid sites in P/ZSM5 zeolites can be proposed (Figure 5.12). Incorporation of P during synthesis results in the localisation of P species inside the micropore structure of ZSM-5 zeolite and these species lead to a decrease in the concentration of LAS, while the concentration of BAS remains unchanged. All P/ZSM-5-OP samples presented in this section show very similar results.

## 5.5 Summary

A detailed characterisation of the ZSM-5 zeolite porosity and acidity has been performed to evaluate the effects of P modification. One of the most important outcomes from this work is that most textural and acidic changes induced by P and their distribution are strongly dependent on the method of P incorporation.

The results indicate that the post-synthesis modified P/ZSM-5 zeolite samples show no significant pore blockage, for P contents of 0.7 wt.% or lower, while changes in the acidic properties are immediately apparent. In relative terms, P species are preferential located on

the external surface of the ZSM-5 zeolite at the initial stages of the modification, when compared with the latter stages. There is a reduction in the number of acid sites, especially those with stronger acidity and located on the internal surface of the zeolite, along with the formation of new weak acid sites.

Incorporation of P during the synthesis causes a decrease in the number of LAS from the P-free to P/ZSM-5 zeolite samples, and consequently an increase in the BAS/LAS ratio. However, when comparing zeolite samples with different P contents, there are no significant changes in the number and strength of acid sites in ZSM-5 zeolite. In P/ZSM-5 samples modified during the zeolite synthesis, P species show a preferential location on the internal surface of the structure.

## 5.6 References

[1] T. F. Degnan, G. K. Chitnis and P. H. Schipper. *History of ZSM-5 fluid catalytic cracking additive development at Mobil.* Microporous Mesoporous Mater., 2000, 35-36, 245-252.

[2] N. Y. Chen, W. W. Kaeding and F. G. Dwyer. *Para-directed aromatic reactions over shape-selective molecular sieve zeolite catalysts.* J. Am. Chem. Soc., 1979, 101, 6783-6784.

[3] M. Takeuchi, T. Kimura, M. Hidaka, D. Rakhmawaty and M. Anpo. *Photocatalytic oxidation of acetaldehyde with oxygen on $TiO_2$/ZSM-5 photocatalysts: Effect of hydrophobicity of zeolite.* J. Catal., 2007, 246, 235-240.

[4] Y. Zheng, F. Wang, X. Yang, Y. Huang, C. Liu, Z. Zheng and J. Gu. *Study on aromatics production via the catalytic pyrolysis vapor upgrading of biomass using metal-loaded modified H-ZSM-5.* J. Anal. Appl. Pyrolysis., 2017, 126, 169-179.

[5] S. S. Arora and A. Bhan. *The critical role of methanol pressure in controlling its transfer dehydrogenation and the corresponding effect on propylene-to-ethylene ratio during methanol-to-hydrocarbons catalysis on H-ZSM-5*. J. Catal., 2017, 356, 300-306.

[6] J. Jae, R. Coolman, T. J. Mountziaris and G. W. Huber. *Catalytic fast pyrolysis of lignocellulosic biomass in a process development unit with continual catalyst addition and removal.* Chem. Eng. Sci., 2014, 108, 33-46.

[7] Z. Y. Zakaria, N. A. S. Amin and J. Linnekoski. *A perspective on catalytic conversion of glycerol to olefins.* Biomass Bioenergy., 2013, 55, 370-385.

[8] R. K. Grasselli, D. L. Stern and J. G. Tsikoyiannis. *Catalytic dehydrogenation (DH) of light paraffins combined with selective hydrogen combustion (SHC) I. DH→SHC→DH catalysts in series (co-fed process mode).* Appl. Catal., A., 1999, 189, 1-8.

[9] V. Vishwanathan, K-W. Jun, J-W. Kim and H-S. Roh. *Vapour phase dehydration of crude methanol to dimethyl ether over Na-modified H-ZSM-5 catalysts.* Appl. Catal., A., 2004, 276, 251-255.

[10] L. H. Ong, M. Dömök, R. Olindo, A. C. van Veen and J. A. Lercher. *Dealumination of HZSM-5 via steam-treatment.* Microporous Mesoporous Mater., 2012, 164, 9-20.

[11] C. Védrine, A. Auroux, P. Dejaifve, V. Ducarme, H. Hoser and S. Zhou., *Catalytic and physical properties of phosphorus-modified ZSM-5 zeolite*., J. Catal., 1982, 73, 147-160.

[12] S. A. Butter and W. W. Keaedinga. U.S. Patent 3972832, 1976.

[13] T. Blasco, A. Corma and J. Martínez-Triguero. *Hydrothermal stabilization of ZSM-5 catalytic-cracking additives by phosphorus addition.* J. Catal., 2006, 237, 267-277.

[14] G. Caeiro, P. Magnoux, J.M. Lopes, F. R. Ribeiro, S. M. C. Menezes, A. F. Costa and H. S. Cerqueira. *Stabilization effect of phosphorus on steamed H-MFI zeolite.* Appl. Catal., A., 2006, 314, 160-171.

[15] I. Lezcano-Gonzalez, U. Dekaa, H. E. van der Bij, P. Paalanenb, B. Arstadc, B. M. Weckhuysenb and A. M. Beale. *Chemical deactivation of Cu-SSZ-13 ammonia selective catalytic reduction ($NH_3$-SCR) systems.* Appl. Catal., B., 2014, 154-155, 339-349.

[16] G. Lischke, R. Eckelt, H-G. Jerschkewitz, B. Parlitz, E. Schreier, W. Storek, B. Zibrowius and G. Ohlmann. *Spectroscopic and physicochemical characterization of P-modified H-ZSM-5*. J. Catal., 1991, 132, 229-24.

[17] Z. Song, A. Takahashia, I. Nakamuraa and T. Fujitani. *Phosphorus-modified ZSM-5 for conversion of ethanol to propylene*. Appl. Catal., A., 2010, 384, 201-205.

[18] A. Corma, V. Fornes, W. Kolodziejski and L. J. Martinez-Triguero. *Orthophosphoric acid interactions with ultrastable zeolite Y: Infrared and NMR studies.* J. Catal., 1994, 145, 27-36.

[19] G. Jiang, L. Zhang, Z. Zhao, X. Zhou, A. Duan, C. Xu and J. Gao. *Highly effective P-modified HZSM-5 catalyst for the cracking of $C_4$ alkanes to produce light olefins.* Appl Catal., A, 2008, 340, 176-182.

[20] Y-J. Lee, J. M. Kim, J. W. Bae, C-H. Shin and K-W. Jun, *Phosphorus induced hydrothermal stability and enhanced catalytic activity of ZSM-5 in methanol to DME conversion*. Fuel., 2009, 88, 1915-192.

[21] G. Zhao, J. Teng, Z. Xie, W. Jin, W. Yang, Q. Chen and Y. Tang. *Effect of phosphorus on HZSM-5 catalyst for $C_4$-olefin cracking reactions to produce propylene.* J. Catal., 2007, 248, 29-37.

[22] M. Göhlich, W. Reschetilowski and S. Paasch. *Spectroscopic study of phosphorus modified H-ZSM-5.* Microporous Mesoporous Mater., 2011, 142, 178-183.

[23] N. Xue, R. Olindo and J. A. Lercher. *Impact of forming and modification with phosphoric acid on the acid sites of HZSM-5*. J. Phys. Chem. C., 2010, 114, 15763-15770.

[24] A. Jentys, G. Rumplmayr and J. A. Lercher. *Hydroxyl groups in phosphorus-modified HZSM-5*. Appl Catal., 1989, 53, 299-312.

[25] J. Caro, M. Bulow, M. Derewinski, J. Haber, M. Hunger, J. Kärger, H. Pfeifer, W. Storek and B. Zibrowius. *NMR and IR studies of zeolite H-ZSM-5 modified with orthophosphoric acid.* J. Catal., 1990, 124, 367-375.

[26] H. E. van der Bij and B. M. Weckhuysen. *Local silico-aluminophosphate interfaces within phosphated H-ZSM-5 zeolites.* Phys. Chem. Chem. Phys., 2014, 16, 9892-9903.

[27] H. E. van der Bij, L. R. Aramburo, B. Arstad, J. J. Dynes, J. Wang and B. M. Weckhuysenand. *Phosphatation of zeolite H-ZSM-5: A combined, microscopy and spectroscopy study*. Chem. Phys Chem., 2014, 15, 283-292.

[28] A. Yamaguchi, D. Jin, T. Ikeda, K. Sato, N. Hiyoshi, T. Hanaoka, F. Mizukami and M. Shirai. *P-ZSM-5 pre-treated by high-temperature calcination as durable catalysts for steam cracking of n-hexane.* Catal Lett., 2014,144, 44-49.

[29] D. Zhang, R. Wang and X. Yang. *Effect of P content on the catalytic performance of P-modified HZSM-5 catalysts in dehydration of ethanol to ethylene.* Catal Lett., 2008, 124, 384-391.

[30] J. A. Lercher and G. Rumplamayr. *Controlled decrease of acid strength by orthophosphoric acid on ZSM-5.* Appl. Catalysis., 1986, 25, 215-222.

[31] M. Derewinski, P. Sarv, X. Sun, S. Müller, A. C. van Veen and J. A. Lercher. *Reversibility of the modification of HZSM-5 with phosphate anions*. J. Phys. Chem. C., 2014, 118, 6122-6131.

[32] H. E. van der Bij and B. M. Weckhuysen. *Phosphorus promotion and poisoning in zeolite-based materials: synthesis, characterisation and catalysis.* Chem. Soc. Rev., 2015, 44, 7406-7428.

[33] J. Liu, C. Zhang, Z. Shen, W. Hua, Y. Tang, W. Shen, Y. Yue and H. Xu. *Methanol to propylene: Effect of phosphorus on a high silica HZSM-5 catalyst*. Catal. Commun., 2009, 10, 1506-1509.

[34] K. Ramesh, L. M. Hui, Y-F. Han and A. Borgna. *Structure and reactivity of phosphorous modified H-ZSM-5 catalysts for ethanol dehydration.* Catal Commun., 2009, 10, 567-571.

[35] L. Janardhan, G.V. Shanbhag and A. B. Halgeri. *Shape-selective catalysis by phosphate modified ZSM-5: Generation of new acid sites with pore narrowing*. Appl Catal., A., 2014, 471, 12-18.

[36] M. Ghiaci, A. Abbaspur and R. J. Kalbasi. *Internal versus external surface active sites in ZSM-5 zeolite: Part 1. Fries rearrangement catalyzed by modified and unmodified $H_3PO_4$/ZSM-5.* Appl Catal., A., 2006, 298, 32-39.

[37] M. Ghiaci, A. Abbaspur, M. Arshadi and B. Aghabarari. *Internal versus external surface active sites in ZSM-5 zeolite Part 2: Toluene alkylation with methanol and 2-propanol catalyzed by modified and unmodified $H_3PO_4$/ZSM-5*. Appl. Catal., A., 2007, 316, 32-46.

[38] J. Zhuang, D. Ma, G. Yang, Z. Yan, X. Liu, X. Liu, X. Han, X. Bao, P. Xie and Z. Liu. *Solid-state MAS NMR studies on the hydrothermal stability of the zeolite catalysts for residual oil selective catalytic cracking.* J. Catal., 2004, 228, 234-242.

[39] K. Damodaran, J. W. Wiech and S. M. Cabral de Menezes, Y. L. Lam, J. Trebosc, J-P. Amoureux and M. Pruski. *Modification of H-ZSM-5 zeolites with phosphorus. 2. Interaction between phosphorus and aluminium studied by solid-state NMR spectroscop*y. Microporous Mesoporous Mater., 2006, 95, 296-305.

[40] H. E. van der Bij, D. Cicmil, J. Wang, F. Meirer, F. F. M. F. de Groot and B. M. Weckhuysen. *Aluminium-phosphate binder formation in zeolites as probed with X-ray absorption microscopy.,* J. Am. Chem. Soc., 2014, 136, 17774-17787.

[41] X. Wang, W. Dai, G. Wu, L. Li, N. Guan and M. Hunger. *Phosphorus modified HMCM-22: Characterization and catalytic application in methanol-to-hydrocarbons conversion.* Microporous Mesoporous Mater., 2012, 151, 99-106.

[42] K. Hadjiivanov. *Identification and characterization of surface hydroxyl groups by infrared spectroscopy*. Adv. Catal., 2014, 57, 99-318.

[43] N. Xue, X. Chen, L. Nie, X. Guo, W. Ding, Y. Chena, M. Gub and Z. Xie. *Understanding the enhancement of catalytic performance for olefin cracking: Hydrothermally stable acids in P/HZSM-5.* J. Catal., 2007, 248, 20-28.

[44] M-L. Gou, R. Wang, Q. Qiao and X. Yang. *Effect of phosphorus on acidity and performance of HZSM-5 for the isomerization of styrene oxide to phenylacetaldehyde*. Appl Catal., A., 2014, 418, 1-7.

[45] Z. Yan, B. Chen and Y. Huang. *A solid-state NMR study of the formation of molecular sieve SAPO-34.* Solid State Nucl. Magn. Reson., 2009, 35, 49-46.

# Chapter 6 Concluding remarks

The main objective of this research was the characterisation of acid sites in zeolites in terms of nature, accessibility, concentration and strength using suitably selected probe molecules in combination with FTIR. Additionally, this study aimed to improve qualitative and quantitative measurements, create new methodologies for a detailed examination of acidic properties in a great variety of zeolite structures and apply this knowledge to particularly important catalytic materials.

The first goal of this thesis was the calculation of molar absorption coefficients for more accurate quantitative analysis of acidity of zeolite based catalysts using pyridine as a probe molecule. A reliable approach to the determination of ε values has been developed based on the direct measurement of the sample weight and the IR spectra of each material. It was observed that $\varepsilon_{BAS}$ values, unlike $\varepsilon_{LAS}$, are affected by the type of zeolite structure. Other factors that affect ε calculations are the number and nature of the acid sites, experimental details of the procedure and the experimental set-up.

Quantitative and qualitative analysis of structural, textural and acidity of thermally treated and cation-containing zeolites demonstrated how the properties of medium- and large-pore zeolites can be altered by using different post-synthesis modifications. The results obtained showed that thermal treatment leads to a decrease in the acidity, crystallinity and porosity of the zeolites. Divalent cations ($Ca^{2+}$ and $Mg^{2+}$) introduced by ion exchange in ZSM-5 induce a protective effect on the Brønsted acidity of the zeolite, avoiding the decline in the number of acid sites which normally occurs during the thermal treatment. In general, the selected cations also prevent the formation of extra-framework Al species acting as LAS in cation-containing zeolites.

The accessibility studies established a clear methodology for the use of different bulky pyridine and benzene derivatives as probe molecules. These results demonstrated the importance of choosing the suitable probe molecule for the quantification of accessibility and indirect location of Brønsted acid sites. This detailed investigation showed the

significance of taking into account the dimensions of the zeolite pores, the kinetic diameter of the probe molecule and the strength of the interaction between the acid sites and the probe molecule.

Using the best approach acquired in the accessibility studies for medium-pore zeolites, the nature, location and accessibility of acid sites in ZSM-5 modified with phosphorous were investigated. The extensive characterisation performed revealed that changes in the number, nature and accessibility of acid sites and phosphorous species are dependent not only on the amount of phosphorous loaded but also on the incorporation method. For zeolites prepared by post-synthesis methods, the ratio between P species on the internal and external surfaces is greater for samples with higher P contents.

This research provides a more comprehensive FTIR characterisation of acidity in different zeolite structures and a better understanding of the zeolite properties following different treatments. This study also developed a better methodology, which provided a new insight into the interactions between different probe molecules and the acid sites of each zeolite structure under investigation. The experimental approaches obtained from this work should improve the accuracy of quantitative analysis under *in situ* and realistic reaction conditions and help in cross-validation of the data obtained from different characterisation techniques.